The role of innate immune activation in experimental glaucoma

Eirini Kokkali

A thesis submitted for the degree of Doctor of Philosophy

School of Optometry and Vision Sciences

Cardiff University

2022

Summary

Glaucoma is the leading cause of irreversible blindness worldwide. It is characterised by progressive degeneration and loss of retinal ganglion cells (RGCs) and their axons. Increasing amount of evidence indicates that neuroinflammation plays a role in glaucoma and other neurodegenerative diseases, however, its contribution in disease pathophysiology is not clear. Targeting components of the immune system, particularly the complement system, has been proposed as a potential treatment strategy for glaucoma. This thesis investigates the effect of systemic innate immune activation on RGC degeneration, in a rat experimental glaucoma model.

Ocular hypertension (OHT) is one of the main risk factors for glaucoma, so this thesis uses a model of induced OHT to mimic glaucoma, and systemic lipopolysaccharide (LPS) administration to induce innate immune activation. Morphological analysis of RGC dendrites and functional assessment of the retina, showed that OHT induced dendritic atrophy and functional deficits in the retina. However, innate immune activation did not further exacerbate RGC degeneration in this model and was associated with protection of RGC dendrites, while intravitreal inhibition of the classical pathway of the complement system did not have a significant effect on the progress of RGC degeneration. In addition, microglial activation was observed in OHT eyes and interestingly in contralateral normotensive (NT) eyes.

Overall, this thesis demonstrates the need for further research to understand the multifaceted role of immune activation in glaucoma and other neurodegenerative diseases. It also warrants for caution in the use of NT contralateral eyes as controls in ophthalmic research.

Acknowledgements

Firstly, I would like to thank my supervisors Professor James Morgan and Professor Paul Morgan for giving me the opportunity to become part of their research groups, and for their guidance and support throughout this project. I would also like to thank Fight For Sight for funding this work.

I would like to express my sincere gratitude to Associate Professor Pete Williams for welcoming me in his lab, in Karolinska Institutet, and giving me the opportunity to work with his team on a collaborative project, as well as Associate Professor James Tribble and Dr Amin Otmani for the wonderful collaboration and contributions in my results. Your enthusiasm and encouragement throughout our collaboration made this project a great experience. I would also like to thank the Cardiff Institute for Tissue Engineering & Repair for making my trip to Sweden possible with a travel award.

I am very grateful to Assistant Professor James Tribble for providing invaluable training at the beginning of my studies, on experimental techniques used throughout this thesis, as well as for all the support, encouragement, and always sound advice.

I would like to thank Associate Professor Seungsoo Rho for assisting with intraperitoneal injections.

I am thankful to all the staff in the Joint Biological Services facility at the School of Biosciences for their assistance in animal husbandry.

I would like to thank Dr Anthony Hayes and Marc Issacs for giving me access to the Imaris workstation at the Bioimaging Research Hub in the School of Biosciences, and for the technical support in relation to the software.

I am grateful to fellow PhD students and staff in the School of Optometry and Vision Sciences that I met throughout the years, with whom I shared this experience through the ups and downs.

Lastly, to my friends, family, and my partner Dimitris, thank you for your continuous support and faith through this journey.

All work presented in this thesis is my own except for the following contributions:

Chapter 3:

- Professor James E. Morgan performed 8 bead injections in the experiments presented in sections 3.2 and 3.3.1
- Assistant Professor James R. Tribble (JRT) recorded the post bead injections IOPs in section 3.3.3 (Pete Williams group, Karolinska Institutet, Sweden)

Chapter 4 and 5:

- Associate Professor Seungsoo Rho assisted with intraperitoneal LPS injections

Chapter 6 * (experiments performed in Pete Williams group, Karolinska Institutet, Sweden):

- JRT performed microbead injections on animals with bilateral OHT
- JRT did all the IOP monitoring throughout the study
- Retinal dissections were performed in collaboration with JRT and Dr Amin Otmani (AO).
- Immunofluorescent labelling was performed in collaboration with JRT and AO
- Some initial imaging was performed in collaboration with JRT and AO, but most of the imaging was performed by JRT and AO.
- Microbead injections on animals with unilateral OHT, microglial reconstructions, RGC counts, and all analysis was performed by myself

***** Tribble JR, Kokkali E, Otmani A, Plastino F, Lardner E, Vohra R, Kolko M, André H, Morgan JE, Williams PA. When Is a Control Not a Control? Reactive Microglia Occur Throughout the Control Contralateral Pathway of Retinal Ganglion Cell Projections in Experimental Glaucoma. Transl Vis Sci Technol. 2021 Jan 12;10(1):22. doi: 10.1167/tvst.10.1.22. PMID: 33510961; PMCID: PMC7804521.

Contents

List of figures

List of tables

Abbreviations

AC	anterior chamber
ACG	angle closure glaucoma
ANOVA	analysis of variance
BSS	balanced salt solution
C1-inh	C1 inhibitor
CEI	Controlled Elevation of IOP
cGMP	cyclic guanosine monophosphate
CNS	central nervous system
CR1	complement receptor 1
CRP	C-reactive protein
	complement receptor 1-related
Crry	gene/protein-y
DAF	decay accelerating factor
DAMPS	damage-associated molecular patterns
dLGN	dorsal lateral geniculate nucleus
EIU	experimentally induced uveitis
ERG	electroretinogram
FB	factor B
FD	factor D
FH	factor H
FI	factor I
GAG	glycosaminoglycan
GFAP	glial fibrillary acidic protein
GPI	glyco-phosphatidylinositol
IBA1	ionized calcium binding adaptor molecule 1
IL-4	Interleukin 4
IL-4Ra	Interleukin 4 Receptor alpha
IL-6	interleukin 6
INL	inner nuclear layer
IOP	intraocular pressure
IPL	inner plexiform layer

IQR	Interquartile Range
IsoB4	isolectin B4
LC	Lamina cribrosa
MAC	membrane attack complex
MASP	MBL-associated serine protease
MBL	manose binding lectin
MCP	membrane cofactor protein
mo	months old
NFL	nerve fibre layer
nSTR	negative scotopic threshold response
NT	normotensive
NTG	normal tension glaucoma
OAG	open angle glaucoma
OHT	ocular hypertension
ONH	optic nerve head
ONL	outer nuclear layer
ONT	optic nerve transection
OP	oscillatory potential
OPL	outer plexiform layer
PACG	primary angle closure glaucoma
PBS	phosphate buffered saline
PDE	phosphodiesterase
PERG	pattern electroretinogram
PFA	paraformaldehyde
PhNR	photopic negative response
POAG	primary open angle glaucoma
pSTR	positive scotopic threshold response
RBPMS	RNA-binding protein with multiple splicing
RGC	retinal ganglion cell
SC	superior colliculus
SD	standard deviation
SEM	standard error of the mean
TBI	traumatic brain injury

TLR-4	toll-like receptor 4
TM	trabecular meshwork

Chapter 1. Introduction

1.1 The vertebrate retina

1.1.1 Retinal layers and cell types

The retina is the neurosensory component of the eye and is a peripherally located part of the central nervous system (CNS) (Purves, Augustine and Fitzpatrick, 2001). The retina has a laminar organisation with different cell types forming distinct layers (Figure 1.1). The photoreceptors form the outermost layer of the retina, known as outer nuclear layer (ONL) (Detwiler, 1943). There are two types of photoreceptors; rods, which are mostly responsible for scotopic vision, and cones, which are mostly responsible for photopic vision, as well as colour perception. The ratio and spatial organisation of rods and cones varies between species (Curcio *et al.*, 1987; Ahnelt, 1998). Moving towards the centre of the eye globe, the outer plexiform layer (OPL) is where the photoreceptors make synaptic contact with the bipolar and horizontal cells, whose cell bodies along with the amacrine and interplexiform cell bodies form the next layer, the inner nuclear layer (INL). The inner plexiform layer (IPL) contains the synaptic contacts between the bipolar cells, the amacrine cells and the dendrites of the retinal ganglion cells (RGCs). The interplexiform cells extend dendrites in both the OPL and IPL (Boycott *et al.*, 1975). The next retinal layer is the ganglion cell layer (GCL), which is formed by the retinal ganglion cell (RGC) bodies, although in rodents amacrines are also present (Perry and Walker, 1980). The last and innermost layer of the retina is the nerve fibre layer (NFL), made up of the RGC axons. The signal is mainly transferred vertically in the retina through photoreceptors, bipolar cells and RGCs, the latter producing impulses that propagate along the optic nerve to the brain. In addition to that direct path, there is lateral feedback and modulation of the signal by the horizontal cells, which upon receiving input from the photoreceptors influence the surrounding bipolar cells, and by the amacrine cells that perform a similar task between bipolar cells and the ganglion cells (Bear, Connors and Paradiso, 2016). The retina also contains non neural cells, these are the Müller cells and the astrocytes,

which provide mechanical and metabolic support, and the microglia which are the primary immune effector cells of the retina (Ransohoff and Cardona, 2010; Chong and Martin, 2015). Astrocytes' distribution can vary between species, but they are generally found in higher numbers close to the optic nerve head (ONH) (Schnitzer, 1988).

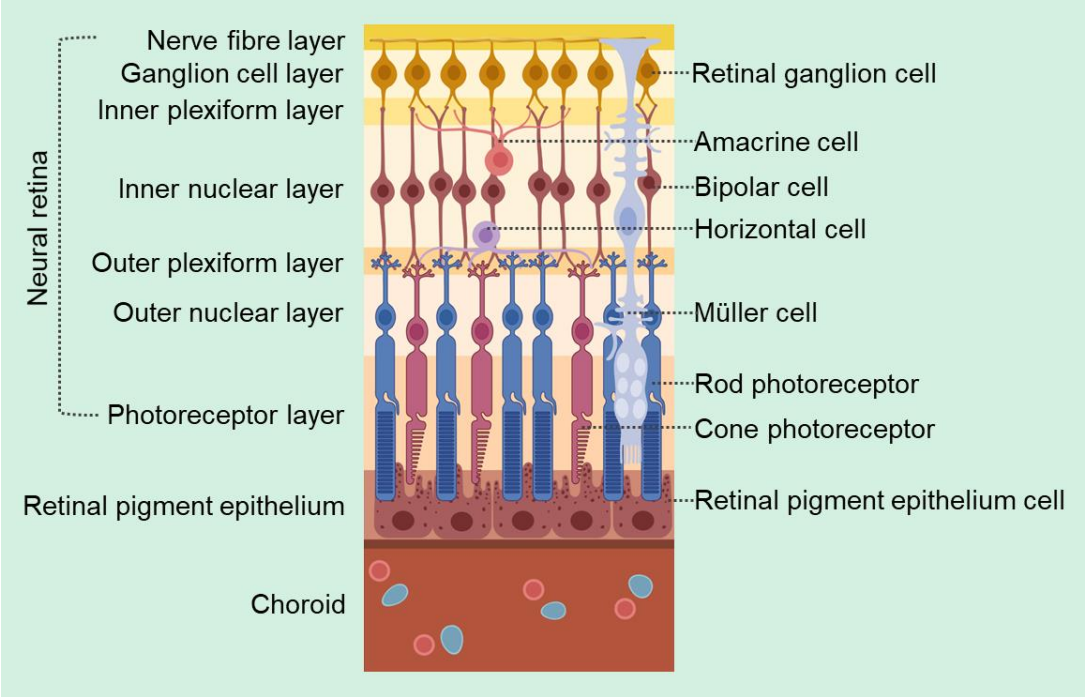

Figure 1.1 Schematic of retinal organisation. The left side shows the retinal layers as defined by the organisation of the different kinds of neurons in the retina, starting with inner retina at the top. The right side shows the respective cells in each layer. The nerve fibre layer and ganglion cell layer are defined by the axons and cell bodies of the retinal ganglion cells, respectively. The inner plexiform layer consists of the dendrites of retinal ganglion cells and the axons of the bipolar cells, while the inner nuclear layer is formed by the cell bodies of the bipolar cells. The outer plexiform layer includes the dendrites of the bipolar cells and the axons of the photoreceptors. The outer nuclear layer is defined by the cell bodies of the photoreceptors and the photoreceptor layer contains the inner and outer segments of the photoreceptors, the latter being where light absorption happens. The Müller cells span across the whole neural retina. (made with BioRender)

1.1.1.1 Retinal ganglion cells

The retinal ganglion cells are the only type of neural cells in the retina possessing an axon that projects through the optic nerve and therefore the only source of output from the retina. They are also the only retinal neurons that can fire action potentials, while all the others respond to stimulation with graded changes in their membrane potential (Dowling, 2012). Although they

all have a soma, an unmyelinated axon and dendritic processes, they demonstrate significant morphological and functional diversity.

Profiling of RGCs has been based on analyses of morphological, electrophysiological, genetic, and molecular characteristics. It is estimated that there are 20-25 distinct types of RGCs in the primate retina (Dacey, 1999). Of these, the main categories are midget and parasol cells, belonging in the parvocellular and magnocellular pathway, respectively (Polyak, 1942). Midget RGCs offer high spatial sensitivity due to their small cell bodies and dendritic fields (Perry, Oehler and Cowey, 1984), which transport signal from a single photoreceptor (Boycott and Dowling, 1969). Parasol RGCs have large cell bodies and dendritic fields, which convey signal from more photoreceptors, thus these cells provide higher contrast and temporal sensitivity. The majority of RGCs are midget cells, especially in the fovea, making up 80% of total RGCs. Parasol RGCs are primarily found in the periphery and are estimated to represent 10% of RGCs (Perry, Oehler and Cowey, 1984). This leaves only small fraction to be covered by the remaining RGC types.

In the rat, RGCs are commonly divided in three main categories based on the size of their soma and dendritic field (Fukuda, 1977; Perry, 1979; Martin, 1986; Huxlin and Goodchild, 1997). Group RG_A (also known as type I or class I) have large somata and large dendritic fields, whereas group RG_B (also known as type II or class II) have small dendritic fields and somata. Group RG_C (also known as type III or class III) have large dendritic fields, but small to medium somata. In their study of large-scale morphological classification of rat RGCs, Sun and colleagues categorised bistratified cells as group RG_D and identified a total of 12 subtypes for all groups (Sun, Li and He, 2002).

Different types of RGCs are tuned to react to specific features of the visual environment, known as “trigger features”. These can include even delicate differences in brightness, colour, shape, direction, speed of motion etc. Depending on the kind of bipolar cell they connect to, RGCs are either ON, OFF, or ON-OFF, responding to light onset, light offset, or both, respectively (Figure 1.2). Morphologically, ON cells extend their dendrites to the more proximal part of IPL, known as sublamina b, where they connect with ON

bipolar cells. OFF cells' dendritic field progresses to the distant part of IPL, sublamina a, to connect with OFF bipolar cells. ON-OFF cells arborize in both IPL zones, thus there are known as "bistratified" (Nelson, Famiglietti and Kolb, 1978; Nelson, 1995).

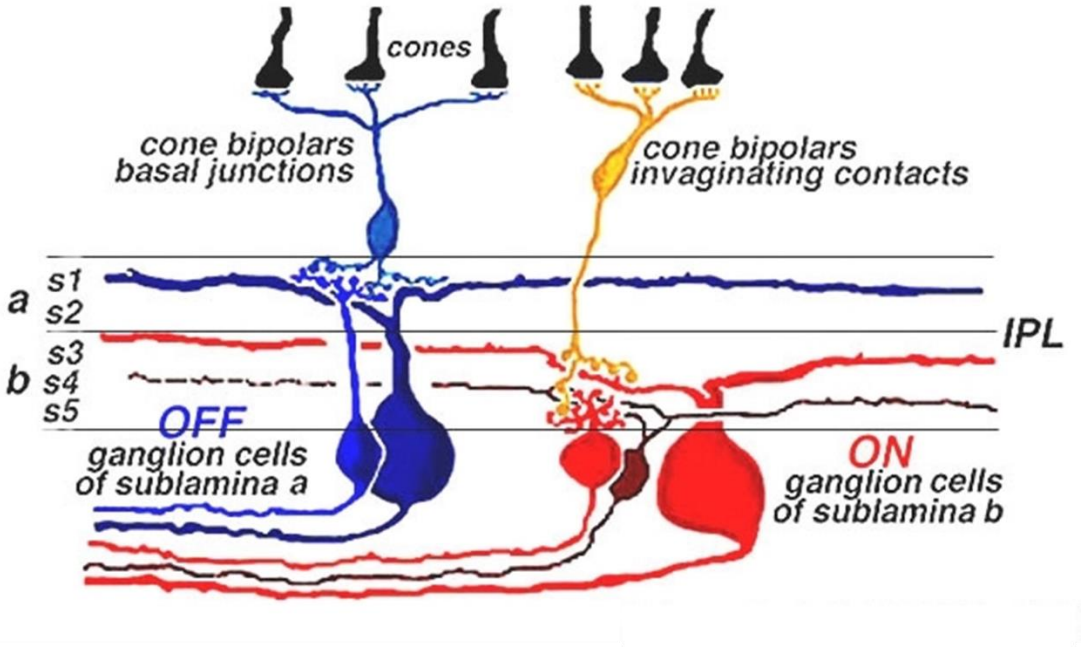

Figure 1.2 Dendritic field extension in IPL of ON and OFF RGCs. ON RGCs reach to the proximal IPL (sublamina b) and OFF RGCs spread to the distant IPL (sublamina a). (Nelson, 1995)

1.1.2 Phototransduction

Phototransduction is the process by which light is converted into neural signal through changes in the cell membrane potential of the photoreceptors. The photoreceptors have an outer segment, an inner segment, and a synaptic terminal. The outer segments are the site of initiation of the process, and are made of pigmented membranous disks that contain molecular photosensitive proteins, known as opsins, and a pre-bound cofactor called retinal, which is a derivative of vitamin A (Wald, 1935; Dowling and Wald, 1960). Opsins differ between rods and cones, as well as between different kinds of cones, the latter enabling colour perception, but the rest of the phototransduction process is virtually the same for all photoreceptors. In the human retina there are three

types of cone opsins that are maximally activated by light of different wavelengths, 420nm (blue), 530nm (green), 560(red) (Bowmaker and Dartnall, 1980). The murine retina has two types of opsins, S-opsins and M-opsins that respond maximally at about 370nm and 510nm, respectively, and as a consequence rodents' photoreceptors exhibit very little to no sensitivity in wavelengths over 600 nm (Jacobs, Neitz and Deegan, 1991; Applebury *et al.*, 2000). A typical resting neuron has a membrane potential of approximately -65 mV, but, due to a steady influx of Na+ through the outer segment's membrane, a photoreceptor's potential in complete darkness is about -30mV. Phototransduction begins when retinal's conformation changes as a response to light, which in turn activates the opsin, whose colour changes from purple to yellow, something known as bleaching. This bleaching stimulates transducin, a G-protein in the disk membrane, resulting in the activation of an effector enzyme, called phosphodiesterase (PDE). Activated PDE breaks down the intracellular messenger, responsible for keeping the Na+ channels open, called cyclic guanosine monophosphate (cGMP). As a result, Na+ channels close and the membrane hyperpolarizes. This cascade has the ability to amplify the signal, as each photopigment molecule can activate more than one G-proteins and each PDE can break down multiple cGMP molecules. As an effect of having more disks in their outer segment and higher amplification ability, rods are much more sensitive to light than cones. Respectively, rods are saturated at lower light levels than cones, thus vision under bright light conditions depends on cones (Dowling, 2012).

1.1.3 Main anatomical differences between rat and human retina

The rat eyes are placed laterally to achieve a panoramic view. Even so, it is estimated that there is a binocular overlap at 40-60° in front of the animal and above the snout (Sefton, Dreher and Harvey, 2004). A rat eye globe is much smaller than a human one, with considerable differences between the relative dimensions of the various structures. Table 1.1 compares the dimensions of some main anatomical structures of human and rat eyes. What stands out is the much greater proportion of space the rat lens occupies in the eye globe compared to human. Rats are nocturnal animals and therefore their vision is

rod-dominated, lacking a densely cone-populated region such as the macula found in primates with cones making up for only 0.85% of photoreceptors (Szel and Rohlich, 1992), as opposed to 5.35% in human retinas (Panda-Jonas *et al.*, 1993). In the human visual system, 50% of the projections of RGCs continue on the ipsilateral pathway after the chiasm (Wilks, Harvey and Rodger, 2013), but this percentage drops down to approximately 10% for pigmented rats (Jeffery, 1984) and even less for albino rats (Sefton, Dreher and Harvey, 2004). Finally, another notable difference is the lack of a well-developed lamina cribrosa (LC). The LC is located at the ONH and is made of collagen, elastin, and glial fibres. In primate eyes it has a distinct organisation, creating a mesh-like structure with pores through which the axons of the optic nerve pass in bundles to exit the eyeball. Different levels of organisation are seen in various species (Tansley, 1956). The rat LC has a collagenous composition similar to that of primates (Morrison *et al.*, 1995), but it is significantly less organised with scattered patches of connective tissue, which are thought to represent a rudimentary LC. Nevertheless, the rat ONH possesses transversely oriented astrocytes, which associate with the axon bundles in a columnar arrangement analogous to that observed in primate ONH (Morrison, Cepurna Ying Guo and Johnson, 2011).

Table 1.1 Dimensions of human and rat ocular structures. ǂ(Oyster, 1999); ɬ(Forrester *et al.*, 2016); *(Hughes, 1979)

	Human	**Rat**
Axial length (a)	ǂ24mm	*6.29mm
Diameter (b)	ǂ28mm	*6.41mm
Lens thickness (c)	ɬ4mm	*3.71mm
Lens diameter (d)	ɬ10mm	*4.23mm
Vitreous volume (e)	ǂ5.2ml	*54.4µl
Aqueous volume (f)	ǂ0.26ml	*13.6µl

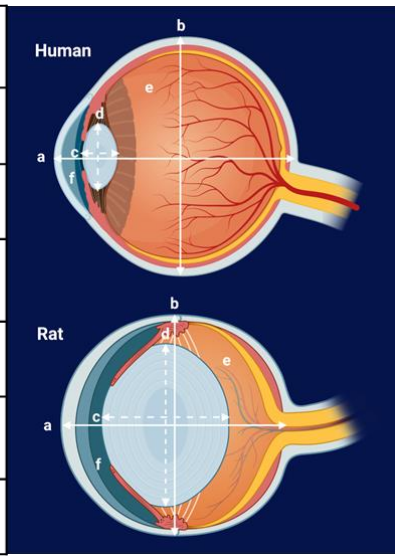

1.2 Glaucoma

1.2.1 Aetiology, classification, and clinical findings

Glaucoma refers to a group of optic neuropathies characterised by retinal ganglion cell degeneration that leads to progressive vision loss. Glaucoma is the leading cause of irreversible blindness, estimated to affect ~80 million people worldwide, which is expected to increase to 111.8 million in 2040 (Tham *et al.*, 2020). Glaucoma is a multifactorial disease (Boland and Quigley, 2007) with the most important risk factors being family history (Tielsch, 1994), ethnicity, sex, age (Leske *et al.*, 1995; Gordon *et al.*, 2002) and elevated intraocular pressure (IOP) defined as higher than 21mmHg (Dielemans *et al.*, 1994; Stewart *et al.*, 2000). Among these risk factors, IOP is the only modifiable one and is what all current treatments, pharmacological or invasive, target. There are two kinds of lowering IOP drops, those that increase the aqueous outflow, like prostaglandin analogues and miotic agents, and those that decrease aqueous humour production, like beta-blockers and carbonic anhydrase inhibitors. Glaucoma, associated with high IOP, arises either by blockage of the passageways of the trabecular meshwork (TM), in which case it is characterised as open angle glaucoma (OAG), or by structural obstruction of the iridocorneal angle, known as angle closure glaucoma (ACG) (Barkan, 1938). Nevertheless, a considerable amount of patients with OAG has IOP within the normal range (10-21mmHG), known as normal tension glaucoma (NTG). The prevalence of NTG differs between ethnic groups studied, 30-40% in white population (Klein *et al.*, 1992), raising to 52-92% in Asian populations (Cho and Kee, 2013) and 57.1% in a Zulu population in South Africa (Rotchford and Johnson, 2002). Glaucoma is also classified as primary, secondary, inflammatory, lens associated or congenital (Foster *et al.*, 2002).

Clinically, glaucoma is assessed by fundoscopy, visual fields tests and tonometry. In most cases vision loss begins with peripheral scotomas before affecting central vision, but in early stages of the disease these are often not perceived by the patient, even though structural changes in the ONH (Pederson and Anderson, 1980), the NFL (Alasil *et al.*, 2014) and the GCL (Bhagat, Deshpande and Natu, 2014) have already occurred.

1.2.2 RGC loss and structural changes

Degeneration of the RGCs and their axons, eventually resulting in RGC loss is the cornerstone of glaucomatous pathology. RGC apoptosis has been established through many studies of human (Kerrigan, 1997; Okisaka *et al.*, 1997; Cordeiro *et al.*, 2011) and experimental glaucoma (Quigley *et al.*, 1995; Guo *et al.*, 2005; Libby, Li, *et al.*, 2005; Calandrella *et al.*, 2007). In glaucoma, as in other neurodegenerative diseases, degeneration happens in a compartmentalised manner, with distinct pathways affecting axons, somata and dendrites (Whitmore, Libby and John, 2005).

1.2.2.1 Soma and axon loss

Soma loss in glaucoma has been quantified by cell counts of glaucomatous retinas (Quigley, Dunkelberger and Green, 1989; Lei *et al.*, 2009; Medeiros *et al.*, 2013). Axon loss has become evident in human eyes by both *in vivo* confirmation of NFL thinning (Bowd, 2000; Alasil *et al.*, 2014) and reduced axon counts in the optic nerve of post-mortem eyes (Quigley, Addicks and Green, 1982). Similar phenomena have been replicated in various experimental rodent and primate models (Morgan, 2000; Chauhan *et al.*, 2002; Schlamp *et al.*, 2006; Cull *et al.*, 2012; Abbott *et al.*, 2014), with studies reporting axonal degeneration before quantifiable cell loss (Buckingham *et al.*, 2008; Soto *et al.*, 2011).

1.2.2.2 Soma and dendrite atrophy

On top of the decline in the absolute number of RGC cell counts, a reduction in the size of the soma of the remaining cells is also present in glaucoma (Quigley, Dunkelberger and Green, 1989; Weber, Kaufman and Hubbard, 1998). There has been some debate regarding the interpretation of these observations. One theory suggests that these results can be attributed to selective RGC loss in the magnocellular pathway in early glaucoma (Quigley *et al.*, 1987; Glovinsky, Quigley and Dunkelberger, 1991; Glovinsky, Quigley and Pease, 1993), because this pathway includes larger cells (Silveira and Perry, 1991). However, psychophysical testing designed to assess changes in visual function mediated by the magnocellular and parvocellular pathways,

in early human glaucoma found both pathways to be similarly impaired (Swindale *et al.*, 1996). The other proposed explanation is that, prior to cell death, the volume of degenerating RGC somata decreases (Morgan, 2002), as supported by data in primate experimental glaucoma models (Weber, Kaufman and Hubbard, 1998; Morgan, 2000). Despite the numerous observations of reduced RGC soma size, it is worth noting that there have also been some contradicting reports of cell soma expansion in rat glaucoma models (Ahmed, Chaudhary and Sharma, 2001; Urcola, Hernández and Vecino, 2006). Moreover, a study on postmortem human glaucomatous retinas did not detect significant changes in the size of surviving RGCs, but did find some shape irregularities (Pavlidis *et al.*, 2003). However, this study only had 4 samples of end stage glaucoma, which is not representative of the whole range of disease stages.

Atrophy has also been extensively documented in RGC dendrites, whose length and complexity has been shown to reduce in experimental models in different species, including primates (Weber, Kaufman and Hubbard, 1998), cats (Shou *et al.*, 2003), rats (Morgan *et al.*, 2006; Williams *et al.*, 2016) and mice (Leung *et al.*, 2011; Feng *et al.*, 2013; Williams *et al.*, 2013, 2016). Moreover, a study in post-mortem human retinas of advanced glaucoma revealed similar morphologic changes in RGC dendrites (Pavlidis *et al.*, 2003). The dendritic shrinkage occurs early in glaucoma and has been documented even before detectable axon and soma loss, affecting mostly tertiary, or more distant, dendrites (Weber, Kaufman and Hubbard, 1998; Morgan *et al.*, 2006; Williams, Morgan and Votruba, 2010; Leung *et al.*, 2011).

1.3 Animal models of glaucoma

1.3.1 Introduction

Many aspects of glaucomatous pathophysiology remain a mystery, but studies on patients or post-mortem human tissue have significant study design limitations. Therefore, animal models are necessary to uncover the cellular and molecular mechanisms underlying this multifactorial neurodegenerative disease. Many species have been used for the development of animal models

of glaucoma, including large animals like primates and dogs and small animals such as rodents. Rodent models are widely used as their ocular structure and physiology is relatively comparable to human, and they have low cost, short life span and a tractable system for genetic manipulation (Johnson and Tomarev, 2010). Since the most established factor contributing to glaucoma progression is high IOP, the majority of glaucoma models are based on ocular hypertension (OHT), and they can be categorised in two broad categories of either induced IOP elevation or spontaneous IOP elevation.

1.3.2 Spontaneous IOP elevation

Spontaneous glaucomatous damage has been reported in certain strains of many species, including primates (Dawson *et al.*, 1993), dogs (Gelatt, Peiffer and Gwin, 1977), cats (Brooks, 1990; McLellan and Miller, 2011), rabbits (Kolker *et al.*, 1963), turkeys (de Kater *et al.*, 1986), rats (Heywood, 1975) and mice (John *et al.*, 1998). Feline glaucoma is usually associated with impaired aqueous outflow and in most cases is secondary to other diseases (McLellan and Miller, 2011). However, inherited congenital glaucoma, associated with specific gene mutations that affect aqueous outflow system development, has been reported in cats and proposed as a model for human primary congenital glaucoma (McLellan *et al.*, 2006; Ellinwood *et al.*, 2010). One of the most widely used and best characterised spontaneous glaucoma models is the DBA/2J mice strain, which develops a pigmentary type of glaucoma at approximately 9 months of age. Iris pigment dispersions, caused by mutations in the Gpnmb and tyrp1 genes, block the aqueous outflow through the TM, resulting in sustained IOP elevation (Anderson *et al.*, 2002). The main advantages of the DBA/2J model are that it produces chronic IOP elevation, which resembles human glaucoma, and that it offers the potential for genetic manipulation (Johnson and Tomarev, 2010). The disadvantages of the model are the high cost of ageing animals, some of which might not develop the disease phenotype, the lack of control over OHT onset, and the absence of a well-developed lamina cribrosa in mice; the latter problem applies to rats as well (Tansley, 1956).

1.3.3 Induced IOP elevation

Experimental induction of IOP elevation allows better control over the onset and duration of OHT compared to spontaneous glaucoma models, and can be achieved in both large animals like primates and small animals like rodents. These models usually involve invasive occlusion of the TM, which disrupts the aqueous outflow resulting in quick IOP elevation. The main criticism for these models is that this mechanism of acute glaucoma induction differs from the chronic human glaucoma and might involve distinct molecular pathways (Libby, Anderson, *et al.*, 2005).

The first attempt to replicate glaucoma in an experimental model dates back to 1877, when Weber produced OHT in rabbit eyes by injection of oil in the anterior chamber, or dislocation of the lens (Weber, 1877). In 1974 Gaasterland and Kupfer introduced a model using laser photocoagulation to alter the architecture of the TM in rhesus monkeys (Gaasterland and Kupfer, 1974). This is a reliable model for IOP elevation, but the dissuasive effect of the costly equipment required has prevented its extensive use. A robust rat model for IOP elevation is the Morrison model, where sustained IOP elevation is achieved by injecting episcleral veins with hypertonic saline (Morrison *et al.*, 1997). However, the limitation of this model is that it is very much dependent on the surgical skills of the person performing the procedure. A cost effective and relatively easy solution is the injection of microparticles in the anterior chamber (AC) to block the TM. This concept has existed for a long time. In 1957, Huggert, investigated the blockage of the iridocorneal angle with different sizes of microparticles, employing among others polystyrene and poly-methylmethacrylate beads (Huggert, 1957). Later Quigley and Addicks injected fixed autologous red blood cells in the anterior chamber of primates (Quigley and Addicks, 1980), but this model had significant and difficult to manage, IOP spikes, (Morgan and Tribble, 2015). An improvement to this has been the injection of latex microspheres by Weber and Zelenak (Weber and Zelenak, 2001), resulting in more moderate IOP peaks and less coverage of the anterior chamber, therefore allowing fundus imaging. However, this model required repeated injections to sustain IOP elevation as the beads tended to move away from the TM (Morgan and Tribble, 2015). Following that, many

variations of this model have been reported in rodents, using beads of different size and material, different injection volumes and techniques, as well as the addition of viscoelastic agents (Urcola, Hernández and Vecino, 2006; Smedowski *et al.*, 2014). A significant refinement has been the usage of ferromagnetic microparticles, which can be drawn in the iridocorneal angle using a small magnet (Samsel *et al.*, 2011). This results in more sustained IOP elevation reducing the need for repeated injections, reduces the injection volume, and allows *in vivo* imaging and electroretinography as the central anterior chamber remains clear. Another reported modification to this model is the employment of a magnetic ring, which is placed around the globe of the eye at the time of injection and immediately attracts the beads toward the iridocorneal angle (Bunker *et al.*, 2015). While in all these models IOP can be monitored frequently, the duration and exact level of IOP, can only be estimated, which presents a challenge in precisely determining the timing and relationship of observed changes to the injury. To address this, models of controlled elevation of IOP (CEI) have been proposed. In these models, the anterior chamber of anaesthetised animals is canulated and connected to a reservoir of saline, which is used to raise the pressure (Chrysostomou and Crowston, 2013; Morrison *et al.*, 2016). This allows complete control over the level and duration of IOP elevation. However, care must be taken to ensure blood pressure, heart and respiratory rates are kept stable throughout the procedure, which range from a few minutes to hours. In a rat model of 8 hours at 60 mmHg mild nerve damage and gene expression changes observed where comparable to changes observed in chronic IOP elevation models (Morrison *et al.*, 2016).

1.4 Electroretinography

1.4.1 Basic principles of electroretinoraphy

The electroretinogram is an electrical potential representing the summed response of all neural and glial cells in the retina to a light stimulus, in the form of extracellular currents flowing through the ocular tissue. Electroretinography (ERG) is performed non-invasively with electrodes placed on proximal surfaces, such as the cornea, and can provide useful objective information on

the functional status of the cells. ERG can be performed on dark adapted or light adapted eyes, known as scotopic and photopic ERG respectively. In dark adapted eyes the response is generated primarily by the rod photoreceptors and the circuits that transmit their signal through the retina. In most mammals, including primates and rodents, this rod-driven ERG has an initial negative wave, called a-wave that reflects mostly the rods' response, followed by a positive wave, the b-wave that largely corresponds to bipolar cells connecting with rods. The photopic ERG, on the other hand, is mostly cone-driven as the rods are suppressed by means of sufficient constant background illumination, with the a-wave representing mostly cone response, and the b-wave bipolar cells connected to cones (Frishman and Wang, 2011). Although it has long been thought that electrical activity of the RGCs is not reflected in ERGs (Riggs, 1986), it has now become evident that certain ERG components can give information specific to the inner retina, corresponding to amacrine and ganglion cells. Those ERG components are, the pattern ERG (PERG), the positive scotopic threshold response (pSTR), negative scotopic threshold response (nSTR), photopic negative response (PhNR) and oscillatory potentials (OP) of the flash ERG, and the multifocal ERG (Porciatti, 2015).

1.4.2 PERG in glaucoma

The PERG stimulus is a contrast-reversing checkerboard or grating pattern with steady mean luminance (Frishman and Wang, 2011). Multiple studies have shown RGC related alterations in the PERG response in glaucoma. Initially, reductions in PERG were recorded in primates with TM laser photocoagulation-induced glaucoma, in some case even before detectable ONH cupping (Marx *et al.*, 1986, 1988; Johnson *et al.*, 1989). Reduction of PERG, up to 85%, has also been reported in the DBA/2J mouse model (Saleh, Nagaraju and Porciatti, 2007; Howell *et al.*, 2012), with changes appearing even before detectable axon loss (Howell *et al.*, 2007). Finally, changes in PERG have also been recorded in glaucomatous rats, using a model of episcleral vein injection with hypertonic saline (Husain, Abdul and Crosson, 2012; Abdul, Akhter and Husain, 2013).

1.4.3 PhNR in glaucoma

The PhNR is a negative component of the photopic flash electroretinogram following the positive b-wave. It was first identified and associated with glaucomatous damage in a primate laser-induced glaucoma model, in which PhNR was selectively affected in eyes with mild visual field defects (Viswanathan *et al.*, 1999). The association of PhNR with the effects of glaucomatous damage in inner retina, has been confirmed by comparison of recordings from glaucomatous primate eyes with healthy controls, in which inner retina spiking was suppressed by pharmacologic manipulation (Viswanathan, Frishman and Robson, 2000), as well as numerous human studies of different stages of glaucoma (Colotto *et al.*, 2000; Viswanathan *et al.*, 2001; Drasdo *et al.*, 2002; Preiser *et al.*, 2013; Kirkiewicz, Lubiński and Penkala, 2016) and other optic neuropathies (Gotoh, Machida and Tazawa, 2004; Rangaswamy *et al.*, 2004; Miyata *et al.*, 2007). Interestingly, a study on glaucoma patients found that PhNR amplitude can be increased following significant IOP reduction, suggesting it can be used as a measure of restoration of retinal function (Niyadurupola *et al.*, 2013). The PhNR is also gaining ground on studies using rodent models. Following optic nerve transection (ONT) on rats, the PhNR was progressively reduced in various time points, as opposed to the b-wave that was not significantly affected (Li, Barnes and Holt, 2005), and so was in a study using a rabbit model of induced glaucoma (ElGohary and Elshazly, 2015). Finally, a specific reduction to the PhNR has also been reported in mouse models of acute, short-term, elevation of IOP (Chrysostomou and Crowston, 2013; Crowston *et al.*, 2015).

1.5 Neuroinflammation

Neuroinflammation is the term describing the molecular and cellular changes that involve components of the innate immune system, occurring in response to stress or injury of the CNS. Those components are mainly the glial cells (astrocytes, oligodendrocytes, microglia and Müller cells) and components of immune signaling pathways involving the complement system and cytokines.

There is strong evidence that neuroinflammation plays a role in neurodegenerative diseases, such as Alzheimer's disease (Hong *et al.*, 2016; Morgan, 2018). However, it is not clear under which circumstances the observed neuroinflammation has a negative effect. The main reason why there is not a straightforward answer to this question lies in the complex nature of glial cells and the molecular pathways they communicate with. Collectively, glia perform an array of functions ranging from metabolic and structural support, regulation of extracellular ion concentration, regulation of synaptic activity, immune surveillance, to primary inflammatory response and phagocytosis (Križaj, 2019). It is considered likely that the immune responses at the early stages of the disease represent the body's attempt to minimize the damage and repair, but chronicity possibly tips the scale towards a detrimental effect (Soto and Howell, 2014).

1.5.1 Glial cells in glaucoma

Retinal glia constitute a highly versatile population that plays an important role in maintaining homeostasis in the retina. Glaucomatous insults result in a glial response, as do traumatic injuries in the CNS and neurodegenerating diseases. Glial cells have mechanisms to recognise cellular signals of stress or damage from the host organism, called damage-associated molecular patterns (DAMPs) (Zhang *et al.*, 2010). Such molecules could possibly be released by compromised RGC axons in the ONH (Soto and Howell, 2014). Indeed, it has been shown that heat shock proteins, which belong in the DAMP family, are upregulated in response to high IOP in glaucoma (Tezel, Yang and Wax, 2004; Luo *et al.*, 2010). Glaucomatous glia demonstrate many signs of an activated phenotype including altered morphology and gene expression, gliotransmitter release, and immune and reactive oxygen species (ROS)-related signaling (Križaj, 2019).

1.5.1.1 Müller cells

Müller cells span through the entire retina (Figure 1.1) ensheathing every neuron and performing a wide range of functions to maintain retinal homeostasis and structure. They regulate ion, water and neurotransmitter

concentration in the extracellular space, provide metabolic support, regulate retinal blood flow and release neurotrophic factors and antioxidants. In retinal disease, Müller cells enter a reactive state known as gliosis, which eventually can lead to a dysregulation of their neuron-supportive functions (Bringmann *et al.*, 2006). Müller cell reactivity, but not proliferation, as confirmed by glial fibrillary acidic protein (GFAP) upregulation, is observed as an early response to IOP elevation in experimental glaucoma (Wang, Tay and Ng, 2000; Woldemussie, Wijono and Ruiz, 2004; Inman and Horner, 2007). Glutamate, a neurotransmitter that is toxic to neurons when present in high concentrations and whose concentration is regulated by Müller cells, is increased in the extracellular space of glaucomatous retinas (Dreyer, 1996). Increased immunoreactivity for glutamine, the product of glutamate uptake by Müller cells and a precursor of glutamate, is also increased in Müller cells from glaucomatous retinas in a laser primate model (Carter-Dawson *et al.*, 1998). In addition, Müller cells in the presence of activated microglia, *in vitro*, demonstrate increased production of pro-inflammatory factors, which in turn enhance microglial activation. They also attract and adhere to microglia, possibly offering a path for microglia to migrate in retinal regions (Wang *et al.*, 2011).

1.5.1.2 Astrocytes

Astrocytes are located in the NFL (Schnitzer, 1988) and support neuronal function via maintaining a homeostatic environment. They play an important role in maintaining the neurovascular unit, dysregulation of which has been found in glaucoma (Kur, Newman and Chan-Ling, 2012). In most mammals, astrocytes are the main glial cells of the ONH and provide axonal support. In response to injury, astrocytes can enter a reactive state, known as astrocytocis, which is characterised by a range of changes, from increased expression of GFAP, to thickening of their processes, to proliferation and migration to sites of injury and the formation of glial scars (Hernandez, Miao and Lukas, 2008; Williams *et al.*, 2017). The presence of reactive astrocytes particularly in the ONH is widely acknowledged as a feature of human glaucoma and signs of astrocyte reactivity have also been found in animal

models (Schneider and Fuchshofer, 2015), where they have been proposed to be involved in initial glaucomatous damage (Dai *et al.*, 2012).

1.5.1.3 Microglia

Microglia are the resident macrophage-like cells of the CNS. They are myeloid derived cells that reside the CNS during early development (Ginhoux *et al.*, 2010). They are highly plastic cells that use their motile processes to constantly surveil their surroundings in an effort to maintain homeostasis. “Resting” microglia typically have a ramified morphology with a small soma and fine long processes. Upon detection of signals of disruption of homeostasis, microglia become activated, which is manifested with rapid and profound changes in their morphology, gene expression and function. Figure 1.3 shows the morphological changes occurring in activated microglia as their long, ramified processes are retracted and become shorter and thicker. Maximally activated microglia take an amoeboid shape and exhibit phagocytic activity (Kettenmann *et al.*, 2011).

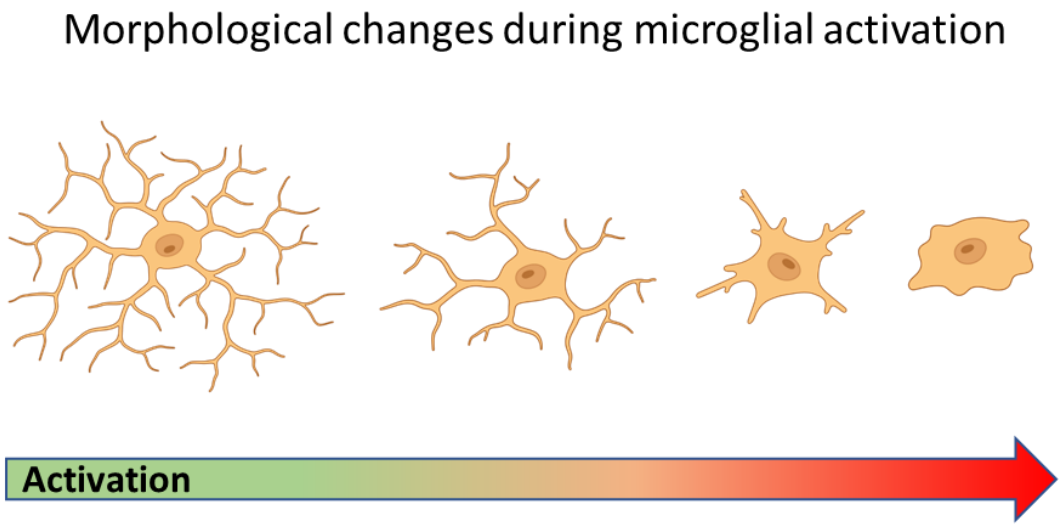

Figure 1.3 Morphological changes during microglial activation. Resting microglia have ramified process. When microglia are activated their processed become shorter and thicker. (Made with BioRender)

Activated microglia have been detected in human glaucomatous retina and particularly the OHT, as well as in various animal models (Neufeld, 1999; Naskar, Wissing and Thanos, 2002). In the DBA/2J model, microglial

activation has been shown to occur in the early stages of the disease before detectable RGC loss (Bosco, Steele and Vetter, 2011). In the same model reduction of microglial activation via minocycline increased RGC axonal transport and decoupled RGC axon loss from increased IOP (Bosco *et al.*, 2008), however, the role of microglia in glaucoma still remains largely unclear.

1.5.2 Systemic inflammation in neurodegenerative diseases

There has been evidence that systemic inflammation, originating outside of the CNS, can have an impact on cognitive abilities and even exacerbate the progression of neurodegenerative diseases such as Alzheimer's disease, in both human and animal studies (Teeling *et al.*, 2007; Holmes *et al.*, 2009; Püntener *et al.*, 2012). Periodontitis in particular has been associated with increased cognitive decline in Alzheimer's disease (Ide *et al.*, 2016) as well as increased risk of developing primary open angle glaucoma (POAG) (Sun *et al.*, 2020); and analysis of the oral microbiome of glaucoma patients has revealed higher bacterial counts compared to control subjects (Astafurov, Elhawy, *et al.*, 2014). In the same study, administration of LPS increased axonal degeneration and neuronal loss in DBA/2J mice. Moreover, recently, systemic inflammation has been linked to POAG, but not primary angle-closure glaucoma (PACG) progression (Li *et al.*, 2021).

Lipopolysaccharides (LPS) are large molecules found on the wall of gram-negative bacteria. They consist of a distal polysaccharide, also known as O-antigen, a non-repeating oligosaccharide and a hydrophobic domain known as lipid A. When LPS are detected in the body, mainly by the toll-like receptor 4 (TLR-4), a plasma membrane protein that belongs to the family of pattern recognition receptors, they elicit an immune reaction (Raetz and Whitfield, 2002). This responsiveness of the immune system to LPS, has made their administration a commonly used method for immune priming to study the effect of systemic inflammation on animal models of neurodegenerative diseases (Teeling *et al.*, 2007; Püntener *et al.*, 2012; Orihuela, McPherson and Harry, 2016).

1.6 The complement system

Complement was first introduced in the late 1890's by Paul Ehrlich, as a blood component enhancing the bactericidal function of the adaptive immune system. Later it became apparent that complement can act independently and today it is considered part of the innate immune system, necessary for host defense against pathogens. Complement also provides an important link between adaptive and innate immunity and helps maintain homeostasis via cell debris clearance (Ricklin and Lambris, 2007). During the last decades, a wider range of complement activities has been revealed. These include complement involvement in synaptic pruning during the developmental phase of the CNS (Stevens *et al.*, 2007), complement upregulation in the aging brain (Stephan *et al.*, 2013), and involvement in cognitive decline and neurodegenerative diseases such as Alzheimer's disease (Hong *et al.*, 2016; Morgan, 2018) and multiple sclerosis (Ingram *et al.*, 2008).

1.6.1 Complement activation

The complement system consists of more than 30 proteins, either soluble or surface expressed, which participate in a cascade of enzymatic reactions that results in chemoattraction of immune cells, cell opsonisation and cell lysis (Sarma and Ward, 2011). Many of the complement proteins are zymogens that turn into active enzymes when they are cleaved. There are three pathways for complement activation, the classical, the lectin and the alternative pathways (Figure 1.4). All of them aim towards forming C3 convertases in order to break down C3 to C3a and C3b. The main activator of the classical pathway is the C1q molecule, which together with two C1r serine proteases and two C1s serine proteases form the C1 complex. C1q has a flower-like shape with a "stalk" consisting of six heterotrimeric collagen-like tails, each ending to a divergent C-terminal globular head (Bally *et al.*, 2009). Recognition of antibody-antigen complexes by C1q results in activation of C1r, which then cleaves and activates C1s. Activated C1s cleaves C4 to C4a and C4b, and C2 to C2a and C2b. The C4b and C2a fragments form the C3 convertase C4b2a. The lectin pathway can be triggered by three different oligomeric lectins, mannose binding lectin (MBL), L-ficolin or H-ficolin, which

bind to microbe related carbohydrate moieties, such as mannose. Those lectins have similar structure to C1q and can form a complex with MBL-associated serine proteases (MASP), whose structure is homologous to C1r and C1s and can cleave C4 and C2 resulting in the formation of the C4b2a C3 convertase, as in the classical pathway (Sarma and Ward, 2011). The alternative pathway is always active at a low level, due to spontaneous hydrolysis of a C3 thioester bond resulting in the formation of C3(H_2O). The latter binds factor B (FB) allowing it to be cleaved by factor D (FD) and broken down to Ba and Bb, forming the initial alternative pathway C3 convertase C3Bb, which converts C3 to C3a and C3b. When C3b binds on a foreign surface it associates with FB, which is then cleaved and activated by FD, yielding another C3 convertase, C3bBb, which is further stabilised by properdin. This process of constantly using C3b to form C3 convertases, which results in even more C3 conversion is called the amplification loop and, regardless of the initial complement activation, it always happens through the alternative pathway (Dunkelberger and Song, 2010).

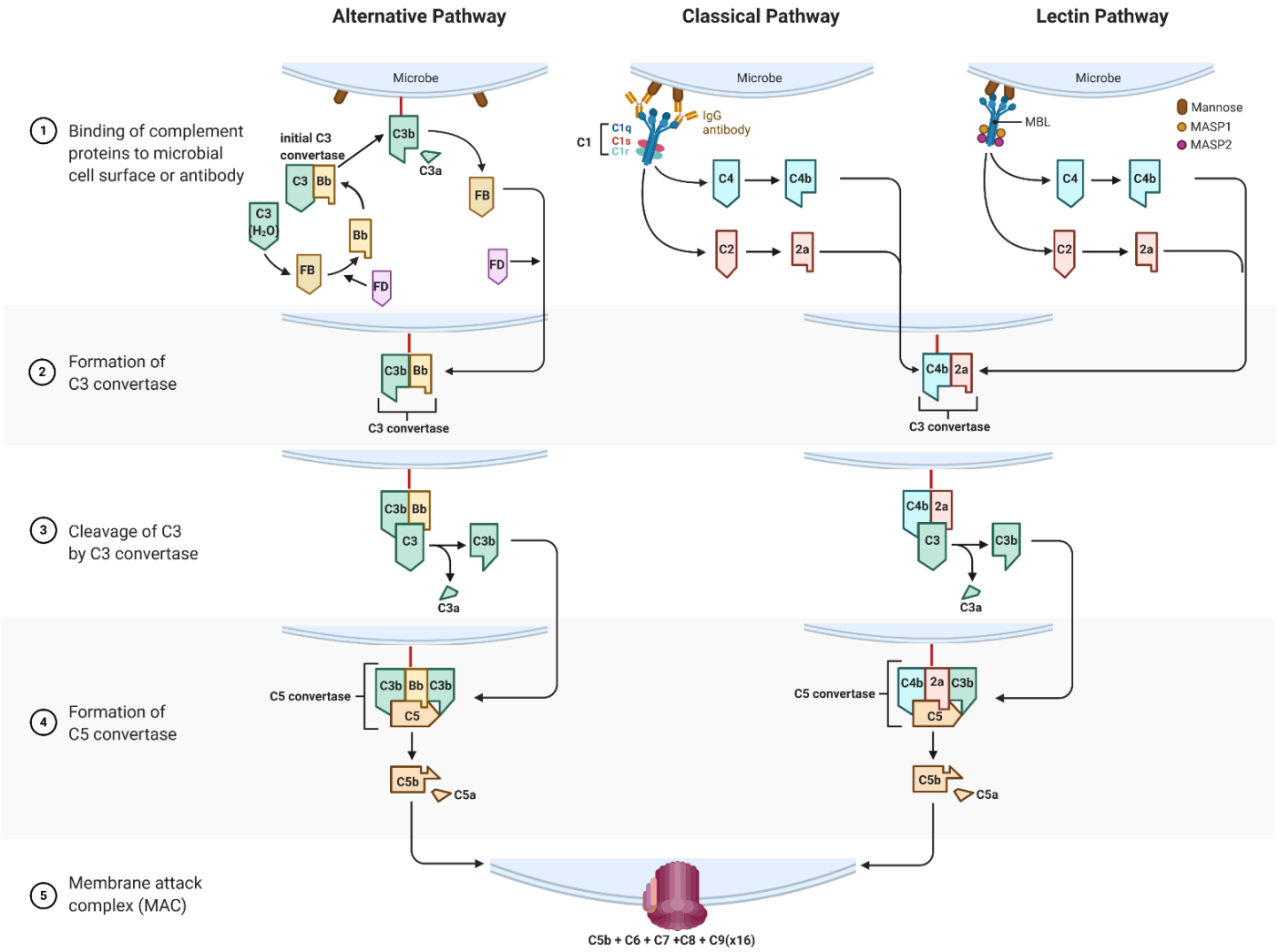
Alternative Pathway
Classical Pathway
Lectin Pathway
1 Binding of complement proteins to microbial cell surface or antibody
2 Formation of C3 convertase
3 Cleavage of C3 by C3 convertase
4 Formation of C5 convertase
5 Membrane attack complex (MAC)
Microbe
initial C3 convertase
C3b
C3a
C3
Bb
FB
FD
C3 (H2O)
C1
C1q
C1s
C1r
IgG antibody
C4
C4b
C2
2a
MBL
Mannose
MASP1
MASP2
C3 convertase
C5 convertase
C5
C5b
C5a
C5b + C6 + C7 +C8 + C9(x16)

Figure 1.4 Complement cascade pathways. Classical pathway: C1q binds antigen-antibody complexes and together with C1r and C1s form the C1 complex, which cleaves C4 and C2 to create the C3 convertase C4b2a, which in turn cleaves C3 to C3a and C3b. This leads to the formation of the C5 convertase C4b2aC3b. Lectin pathway activation: MBL binds to oligosaccharides (Mannose) and together with MASP1 and MASP2 form a complex homologous to C1 complex, resulting in formation of C3 convertase and C5 convertase, via the same process as in the classical pathway. Alternative pathway activation: this pathway is constantly active at a low level through spontaneous hydrolysis of C3 ($C3H_2O$). FB binds $C3H_2O$ and is cleaved by FD, resulting in the formation of the initial alternative pathway C3 convertase, C3Bb, which can cleave C3 to C3a and C3b. When C3b binds on a foreign surface, it gets bound by FB, which in turn is cleaved by FD, forming an amplification loop, which creates another C3 convertase, C3bBb, resulting in even more production of C3b and the formation of the C5 convertase C3bBbC3b. C5 convertases cleave C5 to C5b and C5a, initiating the final phase of the complement system. Sequential binding of proteins C5b, C6, C7, C8 and C9 (x16) forms the membrane attack complex, which lyses target cells by creating pores on their cell membranes (made with BioRender).

1.6.2 Effector mechanisms

The terminal pathway of the complement system leads to the formation of the membrane attack complex (MAC), which promotes cell lysis of non-nucleated cells by forming pores on cell membranes and cellular activation and/or tissue damage on nucleic host cells. The central molecule of the terminal pathway is C5. There are two C5 convertases C4b2aC3b and C3bBbC3b that cleave C5 to C5a and C5b, each formed by the association of additional C3b molecules with the C3 convertases C4b2a and C3bBb, respectively. C5b binds to C6 and the complex binds C7, then C8 and finally recruit sixteen C9 molecules to form the MAC (Figure 1.4) (Serna *et al.*, 2016). C3a and C5a, the smaller fragments derived from cleavage of C3 and C5, are known as the complement anaphylatoxins and have potent proinflammatory functions. Among others, they can cause smooth muscle contraction, increased vascular permeability and histamine release from mast cells, and they exhibit chemoattractant properties for neutrophils and other leucocytes, reviewed in (Klos *et al.*, 2009).

1.6.3 Complement regulation

To prevent host tissue damage from complement activation, complement is regulated at many different steps of the cascade. Decay accelerating factor (DAF; CD55), regulates the classical and alternative pathway C3 and C5 convertases. It is a glyco-phosphatidylinositol (GPI)-anchored protein found on endothelial cells, erythrocytes, platelets, neutrophils, lymphocytes and monocytes, which rapidly dissociates C2a and Bb from C4b and C3b, respectively (Fujita *et al.*, 1987). Another complement regulator is factor I (FI), a serine protease, which, with the help of some other proteins that serve as cofactors, proteolytically cleaves C3b and C4b, preventing the amplification loop from constantly generating C3 convertases when not needed (Lachmann and Müller-Eberhard, 1968; Roversi *et al.*, 2011). One of those cofactors is membrane cofactor protein (MCP), also known as CD46, a cell surface protein which binds to C3b and C4b and allows their inactivation by FI (Liszewski, Post and Atkinson, 1991). In rodents, DAF and MCP are replaced by a single regulatory protein, complement receptor 1-related gene/protein-y (Crry), which exhibits both decay accelerating activity for the C3 convertases and

cofactor activity for FI cleavage of C3b and C4b (Kim *et al.*, 1995). The blood borne protein factor H (FH) is a complement regulator of the alternative pathway. FH binds on host surfaces, including extracellular matrices, mainly via glycosaminoglycan (GAG) recognition, where it competes FB for binding of C3b, and when it binds C3b it attracts FI, which cleaves and inactivates it. FH also accelerates C3bBb decay into C3b and Bb and obstructs formation of the initial alternative pathway convertase C3Bb (Makou, Herbert and Barlow, 2013). At the level of MAC, complement is regulated by CD59, a small GPI-anchored glycoprotein, which inhibits the association of C9 to the C5b-8 complex, thus not allowing pore formation (Rollins and Sims, 1990; Farkas *et al.*, 2002; Kimberley, Sivasankar and Paul Morgan, 2007). The mouse analogues of CD59 are, the cell surface and organ-distributed mCD59a and, the testes-restricted, mCD59b; both of which are equally efficient in inhibiting complement (Harris *et al.*, 2003). Surface-expressed complement receptor 1 (CR1) regulates the formation of the classical and alternative convertases, by having both decay-accelerating activity and co-factor activity for FI (Java *et al.*, 2015). Activation of the classical and lectin pathway is regulated by C1 inhibitor (C1-inh), a serpin that binds and inactivates C1r, C1s and MASP-2 (Singer and Jones, 2011). Complement anaphylatoxins C3a and C5a are regulated by plasma carboxypeptidases that cleave their C-terminal arginine, resulting in a significant reduction of their inflammatory activity, although C5a maintains some of its functions (Noris and Remuzzi, 2013).

1.6.4 Complement in glaucoma

During the last fifteen years many studies have highlighted the role of the complement system, especially of the classical pathway, in glaucoma. Complement was first shown to be involved in glaucoma in a 2003 study, using a model of glaucoma in cynomolgus monkeys, where elevated gene transcription of retinal C4 and properdin genes was found in both severe and mild glaucoma, and of C3 and C1q gene in severe glaucoma (Miyahara *et al.*, 2003). Raised transcription levels of C1q and C3 was reported again, in rat OHT models (Ahmed *et al.*, 2004) and human eyes with OHT, together with C1q and C3 localization in the RGC layer and RNFL, and MAC formation in

both rat and human eyes (Kuehn *et al.*, 2006). Studies on the DBA/2J mouse have identified complement upregulation as an early feature in glaucoma. Stasi and colleagues reported C1q upregulation before the appearance of extensive RGC cell death, as well as C1q upregulation in glaucomatous monkey and human eyes (Stasi *et al.*, 2006). Molecular clustering in DBA/J2 retinae has also identified complement upregulation before the appearance of detectable optic nerve damage (Howell *et al.*, 2011). On top of increased expression of complement proteins of the classical pathway, changes in the lectin pathway and MAC, as well as an oxidative stress-related reduction of FH expression have also been reported in glaucomatous human retina (Tezel *et al.*, 2010).

Since it became apparent that complement is upregulated in glaucomatous eyes, many studies have reported neuroprotective properties of complement inhibition. Complement depletion with cobra venom was shown to result in less RGC loss, reduced apoptosis markers, decreased MAC deposition and reduced GFAP expression in a rat model of chronic ocular hypertension (Jha *et al.*, 2011). In a study that compared glaucoma severity between DBA/2J mice, which are naturally deficient in C5, and DBA/2J mice backcrossed with a functional C5 gene for at least ten generations, it was shown that the latter group developed more severe glaucoma and at an earlier age, indicating that C5 inhibition can be considered as a therapeutic target for glaucoma (Howell *et al.*, 2013). As proteins of the classical pathway have repeatedly been highlighted in glaucoma, studies investigating complement involvement have proposed targeting the classical pathway as a therapeutic strategy. Williams and colleagues showed that knocking out the C1qa gene in DBA/2J mice, or pharmacologically inhibiting the C1 complex in rats with induced glaucoma, prevented dendritic and synaptic loss occurring before RGC death (Williams *et al.*, 2016). A combinational treatment targeting both the endothelin system and the complement system has also been suggested, as simultaneous inhibition of the endothelin system and the classical pathway of the complement system in DBA/2J mice, exhibited more profound neuroprotective effects than targeting each pathway alone (Howell *et al.*, 2014).

It is still not clear whether complement over-expression is caused by RGC degeneration or directly by IOP increase. A study using *in vitro* and *in vivo* models of short-term IOP elevation, from 24 hours to 7 days, reported no statistically significant difference in complement expression levels (Astafurov, Dong, *et al.*, 2014). On the contrary, a study using DBA/2J mice, a strain that spontaneously develops chronic age-related glaucoma, and DBA/2J.Wlds mice, which similarly to DBA/2J mice develop high IOP, but have an allele that protects RGCs, found complement upregulation in both strains, suggesting that early immune responses involving complement might be driven by IOP elevation even at the absence of RGC dysfunction (Harder *et al.*, 2017). In the second study the eyes were exposed to elevated IOP for at least 2 months, the findings from these studies suggest that while high IOP might be driving complement overexpression, a certain level of exposure might be necessary for the effect to take place.

Although many studies point towards the harmful properties of complement upregulation in glaucoma, there is also some evidence of a dual role of complement that includes neuroprotective properties as well. While C1q inhibition (Williams *et al.*, 2016) and C5 deficiency (Howell *et al.*, 2013) prevent RGC degeneration in rodent models, Harder and colleagues (Harder *et al.*, 2017) reported that global complement inhibition in a C3 knockout model increased glaucomatous damage in DBA/2J mice, with the authors highlighting the need for treatments that will target specific parts of complement. On the other hand, a recent study using retinal gene therapy of a complement C3-targetting regulator, CR2-crry, reported a neuroprotective effect on RGCs despite the maintenance of elevated IOP in DBA/2J mice (Bosco *et al.*, 2018). While these might seem like contradicting results, it is worth noting that C3 deficiency via gene knock out, as in the Harder et al. 2017 study, would completely eliminate C3 systemically, while intravitreal CR2-crry delivery would inhibit C3 activation locally. These findings further emphasize the complex, yet still unclear, role of complement in the pathophysiology of glaucoma.

1.7 Aims and Hypothesis

Current treatments for glaucoma are focused on reducing intraocular pressure, the principal modifiable risk factor, with little regard to the general health of the patient. Increasing amount of evidence indicates that systemic inflammation can adversely affect cognitive abilities and even exacerbate the progression of neurodegenerative diseases, (Teeling *et al.*, 2007; Püntener *et al.*, 2012). In addition, periodontitis has been associated with increased cognitive decline in Alzheimer's disease (Ide *et al.*, 2016) and analysis of the oral microbiome of glaucoma patients has revealed higher bacterial counts compared to control subjects (Astafurov, Elhawy, *et al.*, 2014). As discussed in 1.5.1.3 and 1.6.4 components of the immune system, such as the microglia and the complement system are activated in glaucomatous retina, and have been shown to mediate retinal ganglion (RGC) damage in experimental glaucoma (Bosco *et al.*, 2008; Howell *et al.*, 2013; Williams *et al.*, 2016). Using a rat magnetic bead model, this thesis aims to test the hypothesis that background inflammation from systemic immune activation may exacerbate RGC degeneration in glaucoma, and that complement inhibition may provide a protective benefit.

Therefore, this thesis addresses 4 main aims, each of which is presented as an experimental chapter:

1. The basis of all experiments in this thesis is the experimental glaucoma model. A robust glaucoma model that produces reliable IOP elevation with limited invasiveness is essential for achieving the aims of the studies in this thesis. Therefore, the first chapter is dedicated to optimising the magnetic bead model.
2. LPS is commonly used to induce systemic inflammation in various disease models. To investigate whether systemic inflammation plays a role in glaucomatous RGC degeneration, LPS is used to induce immune activation in rats with experimental glaucoma, and the effect of this on RGC structure and function will be assessed.
3. Complement inhibition has been proven to be neuroprotective in a rat magnetic bead model (Williams *et al.*, 2016). To investigate whether

this neuroprotective effect is maintained in the presence of systemic immune activation, complement inhibition will be added as an additional layer to the model.

4. Microglia are the resident macrophages of the CNS and, in response to signals received from their environment, they play an important and diverse role in immune processes in the CNS, which manifests with constant changes in their morphology. Microglial activation occurs in glaucoma, and any effect of systemic inflammation on glaucomatous neurodegeneration will likely involve the microglia. Interestingly, studies have reported signs of microglial activation in both retinas in unilateral glaucoma models, including the unoperated eye with normal IOP. Given the significance of those cells for understanding the role of the immune system in glaucoma, this chapter aims to investigate the effect of unilateral OHT on the microglial population of the contralateral eye, via a detailed morphological characterization.

Chapter 2. General Methods

2.1 Animal husbandry

All experiments were conducted in accordance with the regulations of the Animals (Scientific Procedures) Act 1986 (ASPA). Experiments in Cardiff University were conducted under the following project licences: 30/3084, PB89BF24D. Adult, male Brown Norway rats were housed under continuous light of 60-90lux or under a 12 hours light/12 hours dark cycle (the light conditions for each cohort are indicated in each chapter). Food and water were always available *ad libitum*. All animals were allowed to acclimatize for at least 2 weeks before being included in any experiments.

2.2 Intraocular pressure monitoring

IOP was measured using a Tonolab rebound tonometer (iCare), calibrated for the rat eye. Recordings were performed on awake animals, using gentle hand restraint (Figure 2.1). A total of 3 measurements per eye were taken, each of which was the average of 6 rebounds. The baseline intraocular pressure (IOP) was established before OHT induction and monitored every 1 to 4 days until the end of the experiment. The recordings were taken on the same hour of the day each time (~9am) to minimise the effect of diurnal variation.

Figure 2.1 Tonometry on awake rats. Using a rebound tonometer calibrated for the rat eye, recordings of intraocular pressure were taken on awake animals using gentle hand restraint. The animal was placed on a flat surface and the tonometer was held vertically with the probe having an approximately perpendicular position against the corneal apex. (made with BioRender)

2.3 Electroretinography

To investigate changes in visual function, non-invasive electroretinography (ERG) was conducted in both OHT and control eyes, before and after OHT induction. Both photopic and scotopic ERGs were acquired using an Image-Guided Focal ERG system (Phoenix research labs). Prior to measurement the animals were left to dark adapt for 2 hours and from that point all the procedures were conducted in the dark using a table lamp covered with a red filter, the pc monitor was covered with the same filter. Animals in earlier experiments were anaesthetised with a ketamine (Anaestamine, Animalcare), 75 mg per kg of body weight, and medetomidine (Domitor, Orion Pharma), 0.5 mg per kg of body weight) mixture. However, in subsequent experiments the protocol was refined so that animals were only sedated with medetomidine (0.2mg per kg of body weight). The change was induced in consultation with the Named Veterinary Surgeon due to observations of mild skin reactions to

ketamine. A nonsteroidal anti-inflammatory substance with analgesic properties, meloxicam (Metacam, Boehringer Ingelheim), was also administered subcutaneously prior to the beginning of the procedure, at 1mg per kg of body weight. For experiments involving immune priming with LPS, to avoid any interference from meloxicam with the experiment, the analgesic substance was changed to buprenorphrine (Buprecare, Animalcare) at 0.01mg per kg of body weight, which is a partial opiate agonist. ERGs from the OHT eye were always recorded first and always starting from the scotopic ERG. To record, the animal was placed on a platform with a heat pad and the pupils were dilated with tropicamide 0.5% w/v (Bausch & Lomb) drops. Topical anaesthetic cream containing 5% Lidocaine (Teva Pharmaceutical Industries) was applied at the sites of electrode insertion, a drop of Oxybuprocaine 0.4% w/v anaesthetic eye drops (Bausch & Lomb) was instilled in both eyes and then both eyes were covered with Viscotears gel (Bausch & Lomb). The ground electrode was inserted subcutaneously at the base of the tail, the reference electrode at the scalp between the eyes, and the recording electrode/camera attached on the ocular surface (Figure 2.2). To ensure a good view of the ONH and the temporal retina, the Discover 2.2 software was used to locate the ONH, and a reference image of the focal area was captured using red light to ensure the retina was not stimulated. The signal to noise ratio was tested and if acceptable the red filter was removed and the ERG recording acquired using the LabscribeERG3 software. Acceptable noise was considered anything with a noise wave peak of up to 50μV at the raw ERG. The LabscribeERG software used to capture the recording, performs a signal filtering of each recording, which further reduced the noise to about 10μV. The scotopic response to a flash stimulus of 2.2 log cd sec/m^2 was recorded 10 times with 1.5 sec intervals between flashes. Then, following 15 minutes of exposure to a background light of 3.5 log cd/m2 to supress the photoreceptor response, the photopic responses to 6 stimuli of gradually increasing intensities of 0.7, 1, 1.3, 1.6, 1.9 and 2.2 log cd sec/m^2 were recorded. Each of the 6 different stimuli of the photopic ERG was recorded 25 times, with 3 sec intervals. All the flashes (scotopic & photopic) had a duration of 8 msec and the retinal response was recorded for 300 msec after the flash. When the recordings were completed, sedation was reversed with subcutaneous

injections of 1mg per kg of body weight of atipamezole (Antisedan, Zoetis). The animals were monitored and kept warm to recover from sedation, before being returned to their cages.

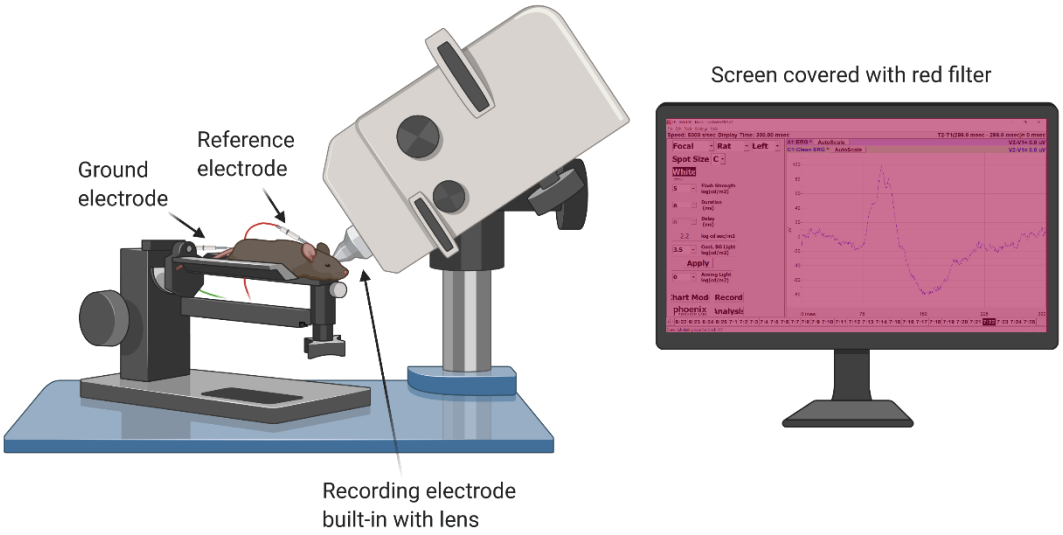

Figure 2.2 ERG recording on sedated rats. The sedated animal is placed on a heated platform. A red-light torch or a desktop lamp covered with red filter are used as the only light source in the room. The pc monitor is also covered with a red filter. The ground electrode is inserted subcutaneously at the top of the tale, the reference electrode is inserted subcutaneously in the scalp (between the eyes), and the recording electrode, which is built in the lens, gently touches the corneal surface. (made with BioRender)

2.4 Ocular hypertension model

2.4.1 Microbead solution preparation

The solutions of paramagnetic microbeads in sterile balanced salt solution (BSS) were prepared as described in this paragraph. There was a model optimisation process which involved trying different kinds of beads and final concentrations. This is detailed in the following chapter and the specific solution concentration for the cohorts are indicated in each chapter. The process was performed under aseptic conditions, using sterile tips and tubes. The beads were separated from the aqueous solution in which they were supplied, using a small bench top centrifuge for 3 minutes, at 6000 rpm. To give them a thorough BSS wash they were resuspended in sterile BSS and

centrifuged again as above, twice. Finally, they were resuspended in sterile BSS to the desired final concentration.

2.4.2 Induction of ocular hypertension

The procedure was performed unilaterally, under general anaesthesia, which was induced by exposure to 5% isoflurane and maintained by 2.5% isoflurane. Topical anaesthetic drops of oxybuprocaine hydrochloride 0.4% w/v were instilled in the eye to be operated while the contralateral eye was covered with viscotear gel to prevent corneal dryness. All surgical instruments were sterilised with 70% ethanol, followed by a thorough wash in sterile balanced salt solution (BSS). Using a 100µl NanoFil syringe (World Precision Instruments) and a 33G tribevelled needle (World Precision Instruments), and looking through a surgical microscope, a few µl of the bead solution were injected in the anterior chamber (AC) through the peripheral cornea. Different volumes were tried during the model optimisation process. The exact volume for each cohort is indicated at the respective chapters. To minimise fluid loss and facilitate corneal healing, the needle was inserted almost parallel to the iris and was allowed to proceed through the corneal stroma for ~1 to 2mm, before exiting through the corneal endothelium. As soon as the solution was released in the AC, and with the needle still in place, the beads were drawn to the periphery and distributed evenly around the iridocorneal angle, using a small hand-held magnet (Figure 2.3). Then the needle was gently withdrawn and topical antibiotic drops of chloramphenicol 0.5% w/v (Bausch & Lomb) were instilled. The animals were monitored until consciousness was restored, and then returned to their cages.

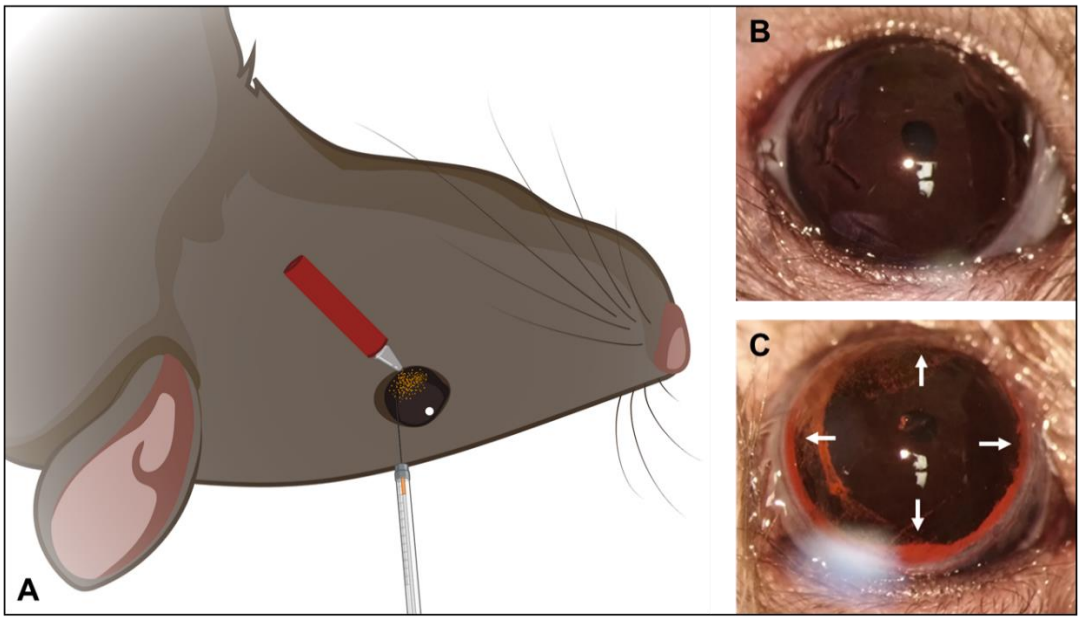

Figure 2.3 Intracameral magnetic microbead injections. (A) Schematic of the injection technique, a tunnel incision is done on the cornea and as the magnetic microbeads are released the magnet is brought to the other side of the eye to quickly draw them towards the iridocorneal angle. (B) A naïve rat eye before the injection. (C) A rat eye following a microbead injection. The beads have been distributed all around the iridocorneal angle, achieving a 360° occlusion of the trabecular meshwork. The arrows are pointing towards the beads. (made with BioRender)

2.5 Lipopolysaccharide-induced immune priming

2.5.1 Lipopolysaccharide solution preparation

LPS from Salmonella enterica serotype abortus equi (Sigma, L5886) was reconstituted in sterile normal saline (Baxter Sterile Saline, 0.9%) to prepare a stock concentration of 5 mg/ml and aliquoted in sterile 1.5ml eppendorf tubes under aseptic conditions. A further diluted solution of 500 µg/ml in sterile saline was prepared fresh before each round of injections, under aseptic conditions.

2.5.2 LPS injection

Awake rats were injected with 500 µg per kg of bodyweight of LPS via a subcutaneous or an intraperitoneal injection. The route chosen will be detailed and discussed for each cohort in following chapters. To deliver 500 µg per kg of weight, the weight of the rats was recorded immediately prior to the injection. As the dilution of the solution was 500 µg/ml, animals received as

many µl of either the LPS solution or plain saline (for the control group) as their weight in grams. For example, a rat weighing 300g would receive a 300µl of either the LPS solution or saline.

2.5.3 Clinical evaluation of inflammation

The health of the rats was closely monitored following the LPS injections. The appearance, behaviour and weight of the rats was recorded every 24 hours for 3 days following the injections and on day 7, using a health score sheet with specified endpoints (see appendix A).

2.6 Blood sample collection and serum preparation

Blood collection was performed under anaesthesia, which was induced and maintained with 5% and 2.5 % isoflurane, respectively. The tail was prepared with 70% ethanol and a sterile surgical scalpel (Swann Morton, UK) was used to cut 1 to 2 mm of the tip of the tail. The tail was gently massaged to induce blood flow through the cut and the blood was collected in sterile 1.5ml Eppendorf tubes. When ~0.3 ml was collected, finger pressure was applied to the tip of the tail until bleeding stopped and the animals were returned to their cages. The blood was allowed to clot in room temperature for 15 minutes and then placed on ice for 1 hour. To separate the serum, the samples were centrifuged at 4000 x g, at 4℃, for 15 minutes, and the supernatant was collected and stored at -80℃.

2.7 Intravitreal injections

To examine the effect of C1 inhibition on glaucomatous progression, C1 inhibitor 100 Units/ml (C1 esterase inhibitor; CINRYZE; Shire), or vehicle only (PBS) for controls, were administered via intravitreal injections. The procedure was performed unilaterally, under general anaesthesia, which was induced by inhalation of 5% isoflurane and maintained by 2.5% isoflurane. To perform intravitreal injections, the pupil of the eye to be injected was dilated with 0.5% w/v tropicamide. The control eye was covered with viscotear gel to prevent corneal dryness, and the eye to be injected was prepared with anaesthetic drops of oxybuprocaine hydrochloride 0.4% w/v and antibiotic drops

chloramphenicol 0.5% w/v. All instruments were cleaned in 70% ethanol, followed by a thorough wash in sterile BSS. To neutralise the corneal refractive power and be able to view the retina through the surgical microscope, a drop of viscotear gel was placed on the apex of the cornea and on top of it a glass coverslip. Using a 33G tri-bevelled needle, 5 µl of the injectable solution were drawn in a NanoFil 10µl syringe (World Precision Instruments). A tunnel through the hard tissue of the sclera was made using a 26G needle taking care not to go through the retina, and then the 33G needle was inserted through the peripheral retina in the vitreous, with a steep angle, in order to avoid the lens. The solution was released as close to the ONH as possible. The needle was carefully withdrawn, antibiotic drops were instilled, and once awaken from anaesthesia the animal was taken back to its cage.

2.8 DiOlistic labelling of retinal ganglion cells

2.8.1 Microparticle preparation for labelling

To prepare the bullets, 2mg of 1,1'-Dioctadecyl-3,3,3',3'-Tetramethylindocarbocyanine Perchlorate (DiI, Life Technologies) and 4mg of 3,3'-Dioctadecyloxacarbocyanine Perchlorate (DiO, Life Technologies) were dissolved in 300µl methylene chloride (Sigma). To ensure multicolour labelling, each of the solutions was separately poured over 40mg of tungsten microcarriers M25 (1.7µm diameter) (BioRad), on a glass surface. When the mixture dried any clumps were dispersed with a razor blade and the coated particles were mixed and transferred in a transparent Ethylene tetrafluoroethylene (ETFE) tubing (BioRad). Both sides of the tubing were sealed with para-film and the tubing was shaken so that it was entirely covered by the dyed microparticles. Any excess particles not adhering to the tubing walls were removed and bullets ~12mm long were cut. The bullets were either used immediately or kept away from light until use for up to two months.

2.8.2 Eye dissection

A previously described protocol was followed with small modifications (Williams, Morgan and Votruba, 2010). The animals were euthanised by increasing concentration of CO_2, which was confirmed by cervical dislocation.

The eyes were quickly enucleated and placed in ice cold Hank's Balanced Salt Solution (HBSS) (ThermoFisher). Starting from the OHT eye, they were dissected to flat retinal whole mounts, RGC side up, under a microscope. To isolate the retina, a puncture was made close to the limbus using a needle, and a peripheral cut just behind the ora serrata was performed to remove the anterior chamber and lens. The retina was gently detached from the sclera and the optic nerve was cut away.

2.8.3 DiOlistic labelling

The isolated retina was transferred on a slide, flattened RGC side up, and the vitreous was removed as much as possible using a small pair of scissors and pierse notched forceps (Duckworth & Kent). Any excess fluid was removed and retinas were immediately shot using a Helios Gene Gun system (BioRad) at ~120psi through a falcon cell culture insert of 3μm pores (BD Biosciences) to filter out aggregated tungsten-dye microparticles. The retinas were then incubated in Neurobasal-A medium (Life Technologies) for 30 minutes, at 37° and 5% CO2. Finally, they were fixed in 4% Paraformaldehyde solution for 30 minutes, nuclear stained with 1:1000 Hoechst 33342 (ThermoFisher) for 15 minutes, mounted with FluorSave (MerckMilipore) and covered with a coverslip, and imaged. Figure 2.4 shows how DiOlistic labelling allows to image a whole RGC.

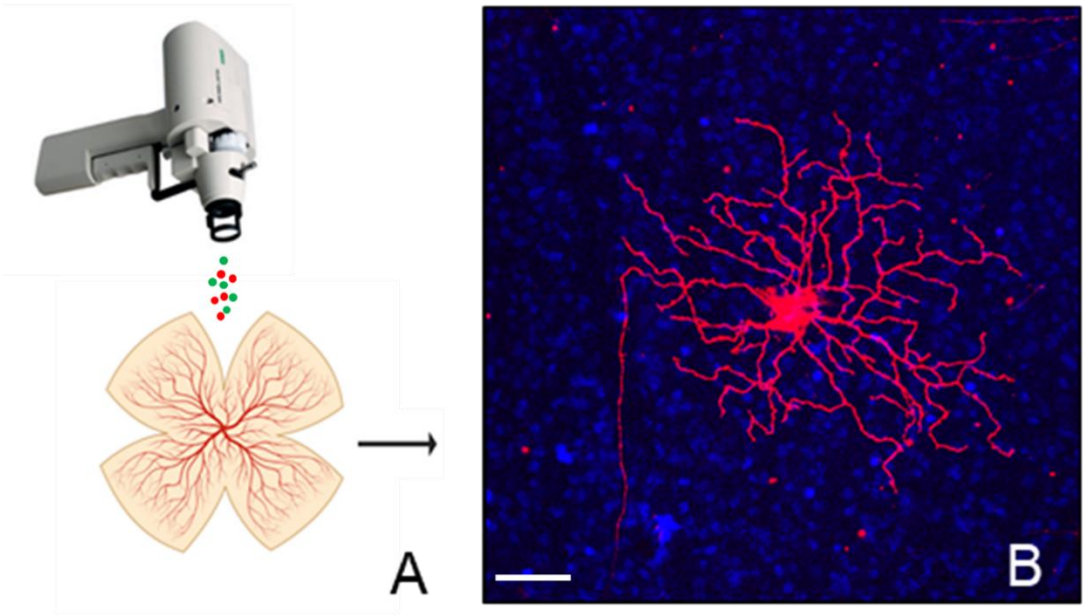

Figure 2.4 DiOlistic labelling. (A) Retinas are dissected flat, RGC-side up, and tungsten microparticles covered with lipophilic fluorescent dyes are delivered in the tissue using a Helios gene gun. (B) High definition, z-stack images of labelled RGCs are captured using a confocal microscope. Scale bar = 10μm.

2.8.4 DiOlistic Imaging

Labelled RGCs were imaged on a Leica SP8 confocal microscope. Identified as RGC cells, were the cells with a soma in the GCL, dendrites protruding towards the IPL layer and an axon projecting towards the ONH. Images were collected using a HC PL APO CS2 20x/0.75 dry objective. The microscope was set at resonant imaging with a scan speed of 8,000 Hz. Z-stack images were collected, with 1μm intervals and each section was 1024 x 1024 pixels. Three channels were set in accordance with the wavelength profile of the dyes. Hoechst 33342 and DiO were collected by a Photomultiplier tube (PMT) detector at (410nm - 495nm) and (495nm - 556nm), respectively, and DiI was collected via a HyD detector at 557-757nm (Figure 2.5). Line averaging between 2 to 4 was used to improve the signal to noise ratio. DiOlistic labelling follows a random pattern and the amount of dye delivered to each cell might differ. Therefore, the gain and laser intensity would be slightly adjusted between images to get the best possible image for each cell that would allow accurate reconstruction.

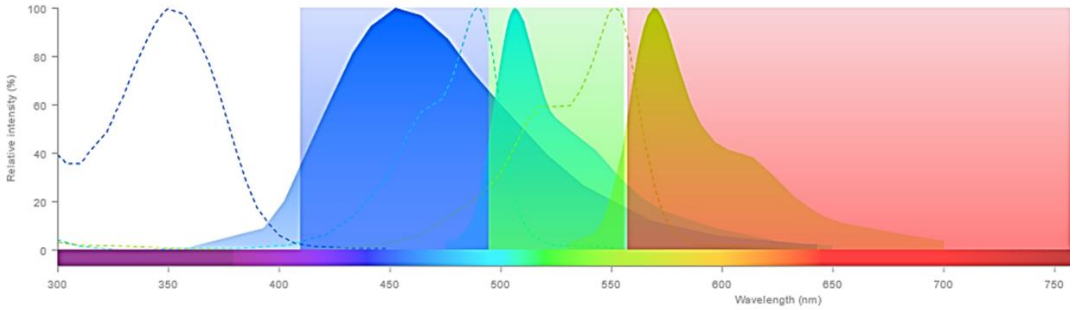

Figure 2.5 DiOlistic labelling excitation and emission profiles. From left to right: Hoechst 33342, DiO and DiI. The dashed and solid lines correspond to excitation and emission spectrums, respectively. The coloured areas correspond to the detection bandwidth. Created with ThermoFisher Fluorescence SpectraViewer.

2.8.5 RGC 3D reconstructions

Retinal ganglion cells were 3D reconstructed semi-automatically using the Filament Tracer tool of Imaris (Bitplane). Semi-automatic tracing is performed using a wizard-like user interface which consists of 5 main steps:

1. Selection of algorithm (Figure 2.6)
2. Selection of region of Interest
3. Selection of source channel
4. Reconstruction by the software
5. Export of data

During this process the software detects the cell body, which is confirmed by the user, and this is set as the starting point for branching. From there, the reconstruction is expanded to the cell dendrites using thresholds determined by the user. While the settings were kept as consistent as possible, manual intervention was necessary to ensure accurate reconstruction of RGCs.

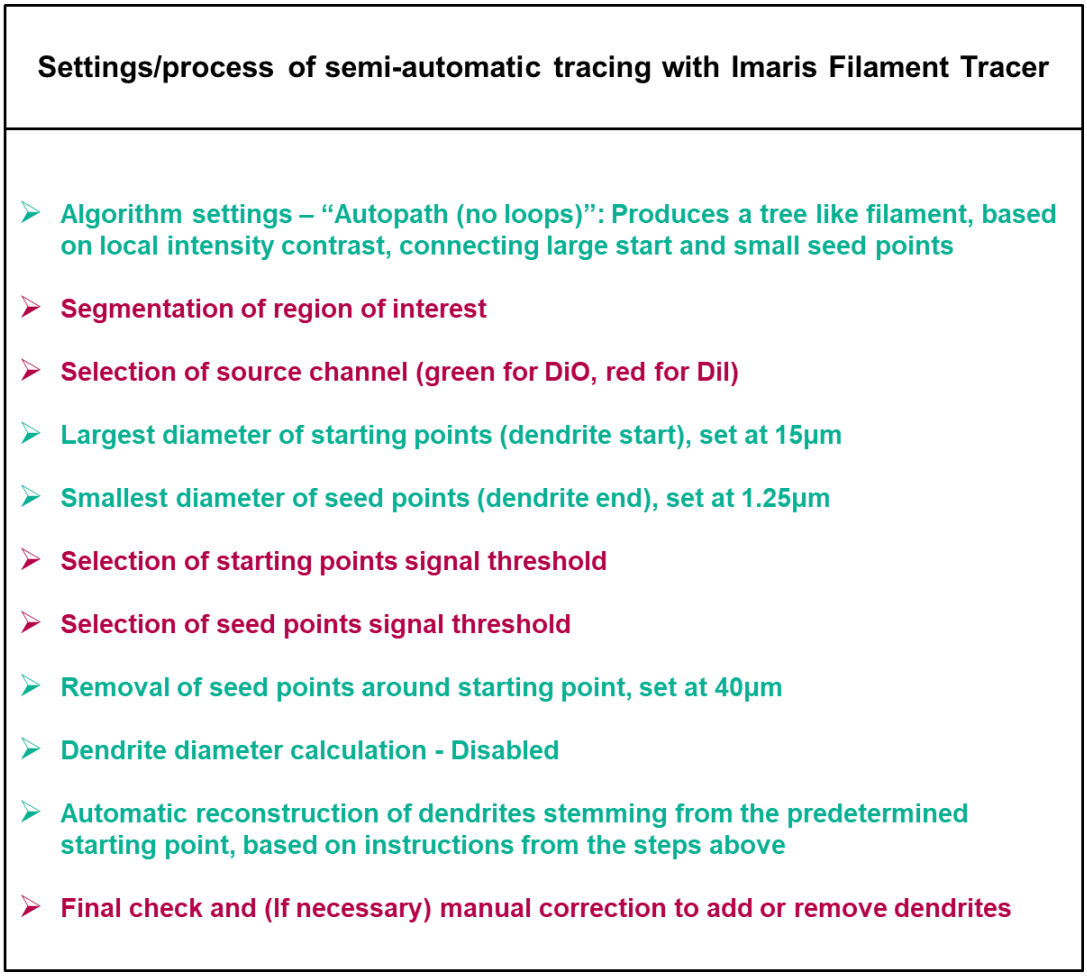

Figure 2.6 Process and outline of settings for semi-automatic tracing of labelled RGCs using predetermined parameters. Automated steps are coloured green and steps requiring manual intervention are coloured red.

Once the cell were reconstructed a Sholl analysis (Sholl, 1953) was conducted to assess the cell's dendritic complexity. Sholl analysis measures the number of dendritic intersections to concentric circles originating from the soma as shown in Figure 2.7. For RGCs the intervals were set 10µm. The counted intersections can be plotted as the Sholl curve. The larger and more complex the arborisation of the cell, the larger the area under the curve (AUC) of the Sholl profile. Neurodegeneration results in loss of the dendritic complexity and this is indicated by a reduction in the Sholl AUC.

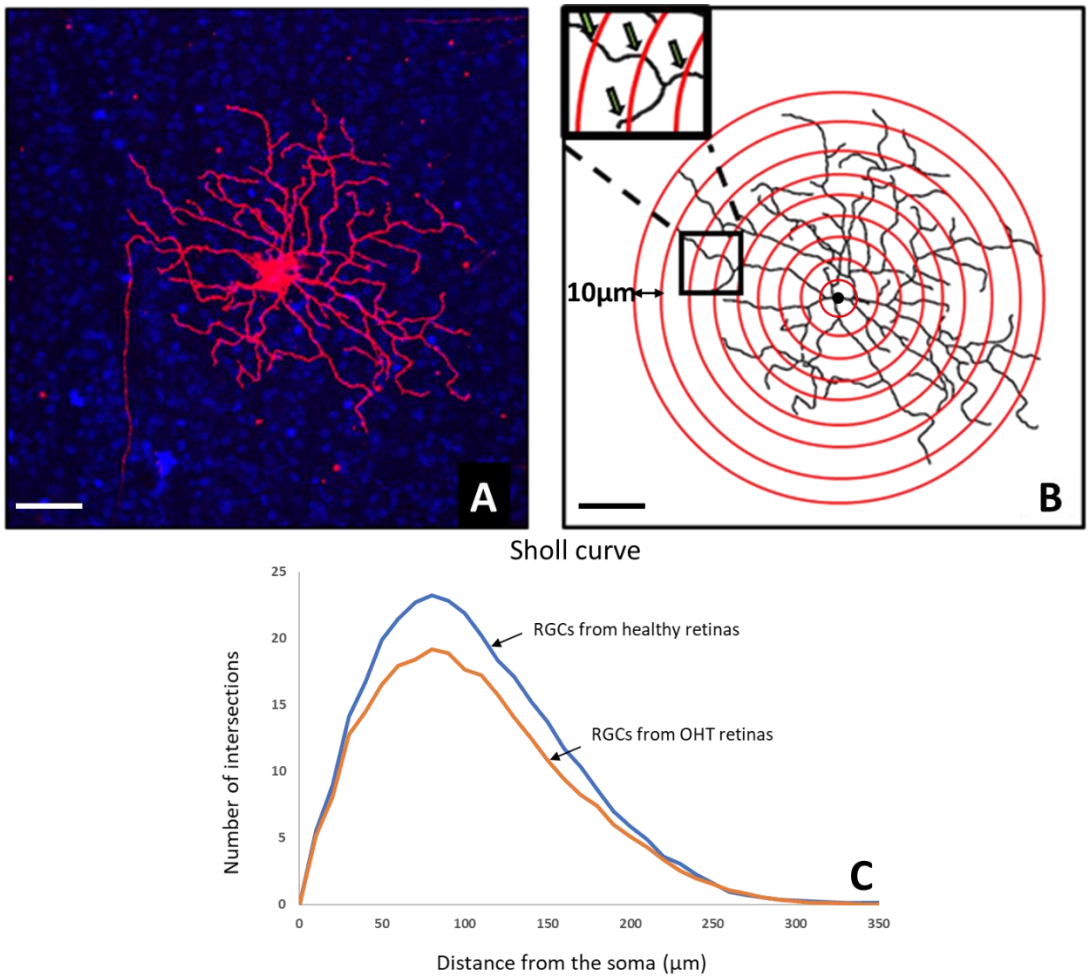

Figure 2.7 RGC reconstruction and Sholl analysis. (A) High definition, z-stack image of a labelled RGC. (B) The RCG is reconstructed using the filament tracer of Imaris (Bitplane) and the reconstructed cell is used to conduct a Sholl analysis of the cell's arborisation. The Sholl analysis measures the number of dendrite intersections to concentric circles in 10µm intervals. The black bullet placed on the soma indicates the starting point of reconstruction and Sholl analysis. The arrows indicate what constitutes a dendrite intersection. (C) The number of intersections is plotted to generate the Sholl curve. The Sholl curve is an indicator of the cell's health state. In degenerating cells dendritic complexity decreases and by extent so does the Sholl AUC. In this Sholl curve example RGCs from healthy rat retina are in blue and RGCs from OHT retina are in orange. Scale bars = 50µm.

2.9 Immunofluorescent labelling

2.9.1 Tissue preparation

Eyes allocated for flat mount immunofluorescent labelling were immersed in 4% Paraformaldehyde (PFA) in 1 x phosphate buffered saline (PBS) solution immediately after enucleation, and fixed for 2 hours at 4°C. Subsequently, they were dissected as described in 2.8.2 and they were post-fixed in 4% PFA for

another hour. After fixation, they were kept in 1 x PBS, for labelling up to 7 days later, or in 0.4% PFA in 1 x PBS for labelling up to 6 months later. Some samples were half retinas of eyes that the other half retina was used for DiOlistic labelling. These retinas were dissected before fixation and cut in half, with one part being immediately used for DiOlistics and one part being immediately placed in 4% PFA for 2 hours at 4°C. Following fixation, these samples were also stored in either 1 x PBS or 0.4% PFA in 1x PBS depending on the expected time of processing as described above.

2.9.2 Retinal flat mounts immunofluorescent labelling

RNA-binding protein with multiple splicing (RBPMS) and ionized calcium binding adaptor molecule 1 (IBA1) antibodies were used to label RGCs and microglia, respectively. RBPMS is an RGC specific marker that identifies the soma of RGCs without labelling any other retinal neurons (Rodriguez, de Sevilla Müller and Brecha, 2014). IBA1 is a microglial and macrophage-specific calcium-binding protein that is commonly used as a marker of microglial activation.

Stored retinas were permeabilised in 0.1% Triton in PBS for 1 hour in room temperature, followed by 30 minutes heat-induced antigen retrieval in sodium citrate buffer (10mM sodium citrate, 0.05% Tween 20, pH 6.0). The samples were blocked in 5% normal horse serum, in room temperature, on a rocker. From this stage onward all steps were conducted on a rocker for improved staining. After blocking, the samples were incubated in primary antibodies RBPMS (host: rabbit (Novus)) at 1:1000 and IBA1 (host: goat (Abcam)) at 1:500 overnight, in room temperature. Following a thorough wash in PBS, a conjugated donkey anti-goat Alexa Fluor 488 (Abcam) antibody was added first, at a 1:500 concentration, for 3 hours in room temperature. To avoid any cross reactivity between the detection antibodies, the samples were thoroughly washed again, and then a goat anti-rabbit antibody Alexa Fluor 594 (Abcam) was added at 1:500 concentration for another 3 hours. The samples were washed, nuclei stained with Hoechst 33342 and mounted in FluorSave. The sections were kept in the dark and imaged on a Leica SP8 confocal.

2.9.3 Imaging of Immunofluorescence

The samples were imaged on a Leica SP8 confocal microscope using a HC PL APO CS2 20x/0.75 dry objective. Z-stack images of 0.5µm intervals, 1024 x 1024 pixels (pixel size = 0.568µm) were taken. Three channels were set in accordance with the wavelength profile of the secondary antibodies, and the acquisition settings were kept constant for all images as per Table 2.1. To improve the signal to noise ratio line averaging, set at 2, was used.

Table 2.1 Microscope settings

Channel	Detection wavelength (nm)	Gain	Laser Line Intensity (%)
Hoechst 33342	410 - 495	859	15%
Alexa Fluor 488	495 - 586	600	5%
Alexa Fluor 594	586 - 751	20	7%

2.10 RGC cell counts

To ensure RGC counts were specific, cells labelled with RBPMS following the protocol described in 2.9.2 were identified using a semi-automated method. Using the Spots tool of Imaris, RGC cells in a 300 µm x 300 µm region were first counted automatically. For this automatic count the estimated diameter was set to 10 µm and background subtraction was activated. This count was able to pick up accurately most cells, however, to improve the accuracy rate, the counts were checked manually to delete surplus counts or add any missed cells. To calculate the RGC density per retina, RGCs were counted in 4 or 3 areas in the mid-peripheral area (as shown in Figure 2.8), depending on whether the tissue sample was a whole retina or half a retina.

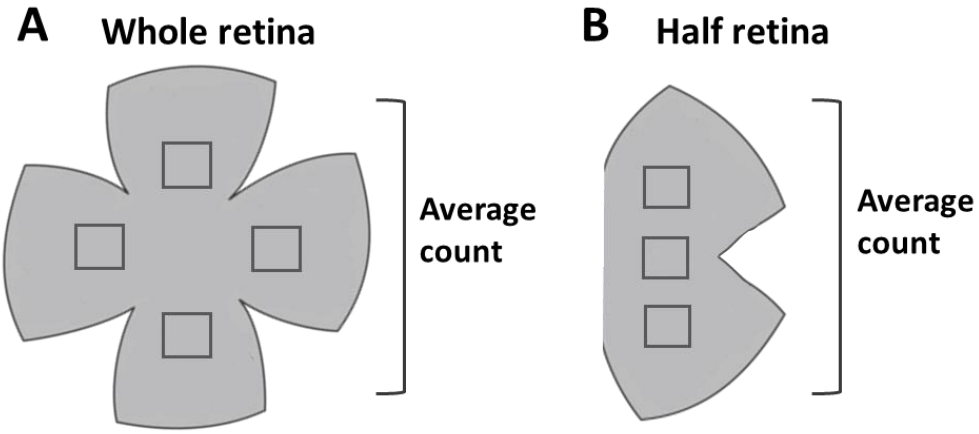

Figure 2.8 RGC counts on whole and half retinas. RGCs were counted in 4 or 3 regions (each 300 µm x 300 µm) in the mid-peripheral area, depending on whether the tissue sample was a whole retina or half a retina. The average count per retina was used to calculate the RGC density.

2.11 Microglia 3D reconstructions

Retinal microglia were reconstructed manually on Imaris using the Filament tracer tool. Reconstructions were done manually because due to the large number of microglia in some images it was found that the software was not always able to distinguish the cells and a lot of manual intervention was needed. To enable 3 dimensional reconstructions, the automatic depth estimation was enabled. Automatic volume filling was also used to provide information on the thickness of the processes.

2.12 Detection of inflammation markers

To assess the level of inflammation in rats injected with LPS, interleukin 6 (IL-6), which is a pro-inflammatory cytokine, was detected in the serum of animals collected 2 hours post LPS injection. This time was chosen because it has been shown that in adult rats administered with LPS via intraperitoneal injection, IL-6 levels peak after 2 hours (Gomez *et al.*, 2008).

IL-6 was detected using a sandwich enzyme-linked immunosorbent assay (ELISA) for measuring rat IL-6 (DY506-05, R&D Systems), following the manufacturer's protocol. All reagents were supplied by R&D Systems. Briefly,

after bringing all the reagents to room temperature, a 96-well microplate was coated with 100 µl per well of the rat IL-6 capture antibody diluted in PBS. The plate was sealed and incubated overnight at room temperature. The plate was washed 3 times with wash buffer (0.05% Tween 20 in PBS, pH 7.2 to 7.4) and then blocked with 300 µl of reagent diluent (1% BSA in PBS, pH 7.2 to 7.4, 0.2 µm, filtered) in each well, for 1 hour at room temperature. The plate was washed again and then incubated for 2 hours with 100µl of the standards and samples in reagent diluent per well, at room temperature. The assay was optimised to ensure the concentration range of the standards and the dilution of the samples would allow optimal detection within the assay's sensitivity range. For the standards, recombinant rat Il-6 was added in 2-fold serial dilutions ranging from 8000 pg/ml to 62.5 pg/ml, and the samples were added in 1:2 concentration. The plate was washed and incubated for another 2 hours at room temperature with 100 µl of the detection antibody diluted in reagent diluent with 2% normal goat serum. Following another wash, 100 µl of the working dilution of Streptavidin-HRP B were added per well and the plate incubated for 20 minutes at room temperature, away from light. The plate was washed again and incubated with 100 µl of substrate solution (1:1 mixture of Color Reagent A (H_2O_2) and Color Reagent B (Tetramethylbenzidine) in each well, for 20 minutes at room temperature and away from light, after which 50µl of stop solution (2 N H_2SO_4) were added to each well. Finally, the optical density of each well was immediately detected using a microplate reader set to 450 nm. Following the manufacturer's protocol, to correct for optical imperfections of the plate, readings were also taken at 570nm and subtracted from readings at 450nm when the data was analysed.

To determine the concentration of IL-6 in the samples, a Four Parameter Logistic Regression (4PL) was fitted to the standard values to create a standard curve using GraphPad Prism, which was used to interpolate the unknown values of the samples.

2.13 Statistical analysis

Normality of data distribution was tested using the Shapiro Wilk test. Normally distributed data were analysed with two-tailed Student's t-test to compare the

means of two groups, or one-way analysis of variance (ANOVA) to compare the means of three or more groups. ANOVA indicating statistically significant changes between the groups was followed by Tukey's HSD post hoc for multiple comparisons. Non-normally distributed data were analysed with Welch's t-test to compare two groups, or with a Kruskal Wallis test to compare more than two groups. If Kruskal Wallis rejected the null hypothesis, Dunn's test with Benjamini and Hochberg correction was used for multiple comparisons. For all statistical tests, alpha level was set at .05. All statistical analysis and graphical presentation of data was performed in R (R Core Team, 2019), with the exception of data analysis and graphs in 3.2 and 3.3, which was done in GraphPad Prism.

Chapter 3. Experimental glaucoma model optimisation

3.1 Introduction

The magnetic microparticle occlusion model is a robust and widely used model for the induction of ocular hypertension in glaucoma studies, but often repeated injections are required to achieve sustained OHT (see 1.3.3), which can compromise the stability of the IOP and risk ocular inflammation. To address this issue, experiments were conducted to refine methods for experimental induction of OHT, using paramagnetic microbeads that would improve the success rate and minimize the number of injections required for induction and maintenance of OHT.

3.2 Polystyrene paramagnetic beads

A cohort of 6 adult male Brown Norway rats (retired breeders), housed under continuous light of 60-90lux to reduce diurnal IOP variation (Morrison *et al.*, 2005), received unilateral injections of 5μm diameter plain polystyrene paramagnetic beads (Sigma, 39689) following the protocol described in 2.4.2. To find the optimal combination of concentration and total volume, different combinations were tested. After the 1st round of injections (see Table 3.1 for detailed parameters of each injection) most animals did not develop OHT, or only developed OHT for 3 to 4 days (see Figure 3.1), after which IOP returned to normal (i.e. to the same level as the contralateral non-injected eye). Subsequent injections were required to sustain an increase in IOP. To explore whether iris dilation would enhance the adherence of the beads to the structures of the iridocorneal angle by pushing them to the periphery, some injections were followed by instillation of dilating drops (Cyclopentolate Hydrochloride 1% w/v, Tropicamide 0.5% w/v, Bausch & Lomb) Table 3.1 shows the details of the injections performed on each animal and Figure 3.1 shows the IOP profiles of each animal in the cohort.

Table 3.1 Details of intracameral injections performed using plain magnetic polystyrene beads.

Animal ID	Injection order	Injected volume (µl)	Concentration (mg/ml)	Dilating drops after injection
1260	1	20	15	-
1261	1	10	30	-
1262	1	10	30	-
1263	1	10	30	-
1264	1	10	20	-
1265	1	10	20	-
1260	2	10	20	-
1261	2	10	20	Tropicamide
1263	2	10	20	Cyclopentolate
1264	2	10	20	-
1265	2	10	30	-
1260	3	10	20	Tropicamide
1261	3	10	30	Cyclopentolate
1264	3	15	20	Tropicamide
1265	3	10	20	Tropicamide

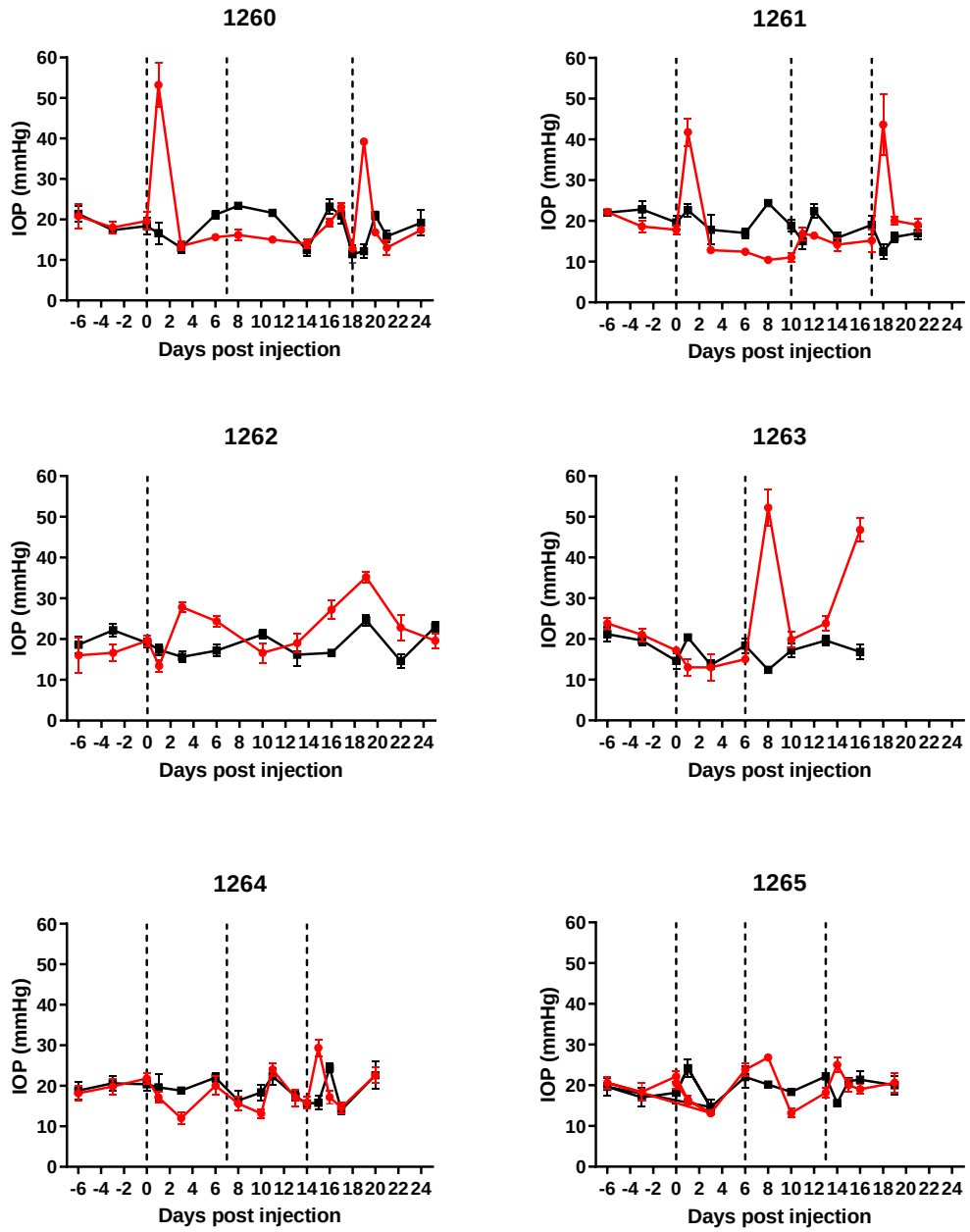

Figure 3.1 Individual IOP profiles of the cohort that received intracameral injection of plain polystyrene magnetic beads to induce OHT. Red = injected eye, black = contralateral control eye, dashed line = bead injection, error bars = SD.

Macroscopic evaluation of the injected eyes revealed that the beads had the tendency to move away from the iridocorneal angle towards the centre, lying on the lens within the anterior chamber. The bead distribution was further assessed microscopically at the end of the experiment. When animals were euthanised, the eyes were enucleated, fixed in 4% PFA in PBS and cryo-embedded in optimal cutting temperature compound (OCT) (Fisher Scientific).

Sagittal sections of the anterior chamber, 12 to 16 μm thick, were collected using a Leica CM3050S Cryostat and stained with Hematoxylin and Eosin. The sections were imaged on a Leica DMRA2 bright-field microscope using a x20 lens. In most of the images the beads were shown to have moved away from the iridocorneal angle and/or not providing sufficient blockage, as shown in the representative images below (Figure 3.2).

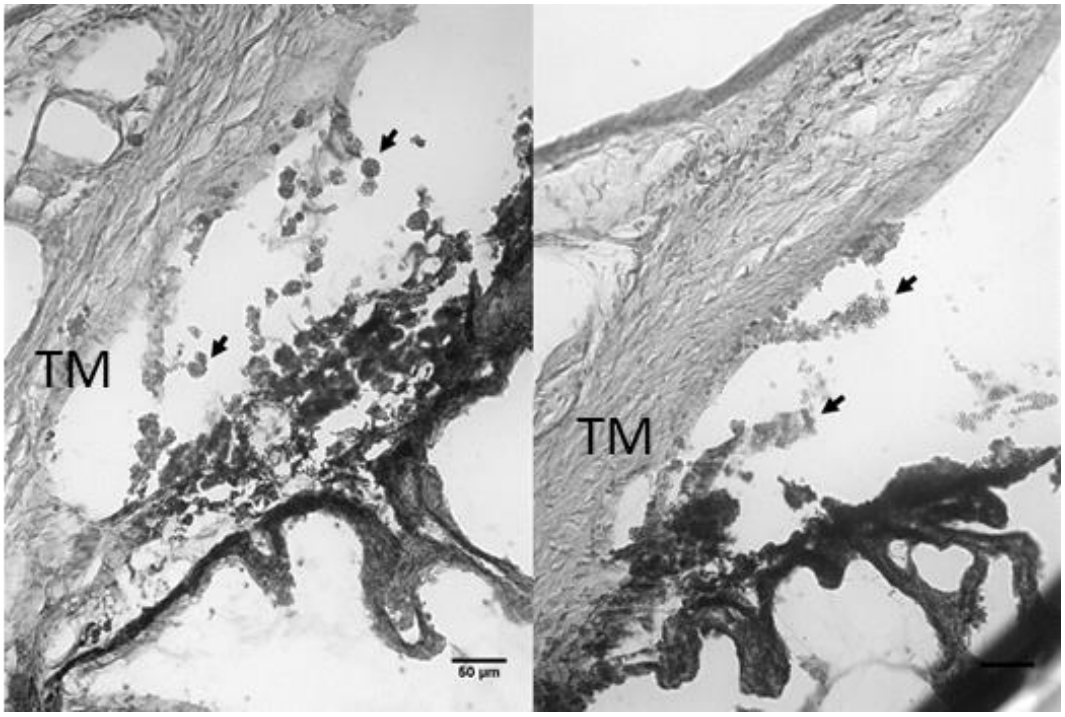

Figure 3.2 Representative sagittal sections of the iridocorneal angle showing the bead position in post-mortem injected eyes. The arrows point towards some of the imaged beads, TM indicates the trabecular meshwork. The beads are only partially blocking the iridocorneal angle. Scale bar = 50μm.

3.3 Coated beads

Since plain polystyrene paramagnetic beads did not adhere to the iridocorneal angle in a robust fashion, the next step was to explore whether beads coated with reactive molecular tags could improve adherence to the structures of the iridocorneal angle and induce sustained OHT.

3.3.1 Carboxyl and amine coated beads

Adult male lister hooded rats were injected with 4.5μm and 8.5μm diameter paramagnetic beads coated with carboxyl and amine functional groups, respectively (Spherotech Inc). Lister hooded rats were used for initial tests with these beads as an alternative strain that is tractable and has pigmented eyes, due to limitations in obtaining Brown Norway rats. These beads were chosen as it was expected that these functional groups would react with tissue structures and with each other. The goal was to explore whether beads injected sequentially in the anterior chamber would form peptide bonds that would create a relatively rigid ring-like structure around the iridocorneal angle. The injections were performed using the protocol described in 2.4.2. To avoid formation of bead clumps within the syringe that would block the solution outflow, a separate syringe was used for each bead type. Either the amine coated, or the carboxyl coated beads were injected first and drawn towards the iridocorneal angle. Immediately after, the other beads were released in the anterior chamber through the same corneal incision. It became apparent from the first two injections performed with that method that directing the second group of beads without disturbing the previously injected one was not possible since bead clumps formed within the AC before beads were directed towards the angle. The amine coated beads were easier to handle during the procedure, so the next step was to inject only the amine coated beads; two pilot injections were therefore performed using different volumes. The injections are summarised in Table 3.2. One of the amine-only injections resulted to a promising IOP profile, with OHT lasting for two weeks (Figure 3.3). These beads were taken forward to optimise further and explore whether it was possible to achieve sustained IOP elevation, such as in LH004, but of a more moderate level (i.e. less than 50 mmHg).

Table 3.2 Details of intracameral injections of beads coated with functional groups.

Animal ID	Injected volume (µl)	Concentration (mg/ml)
LH001	10 (AB) + 5 (CB)	30
LH002	8 (CB) + 8 (AB)	30
LH003	8 (AB)	50
LH004	12 (AB)	50
Notes: AB = amine coated beads (bead-NH2) CB = carboxyl coated beads: (bead-COOH)		

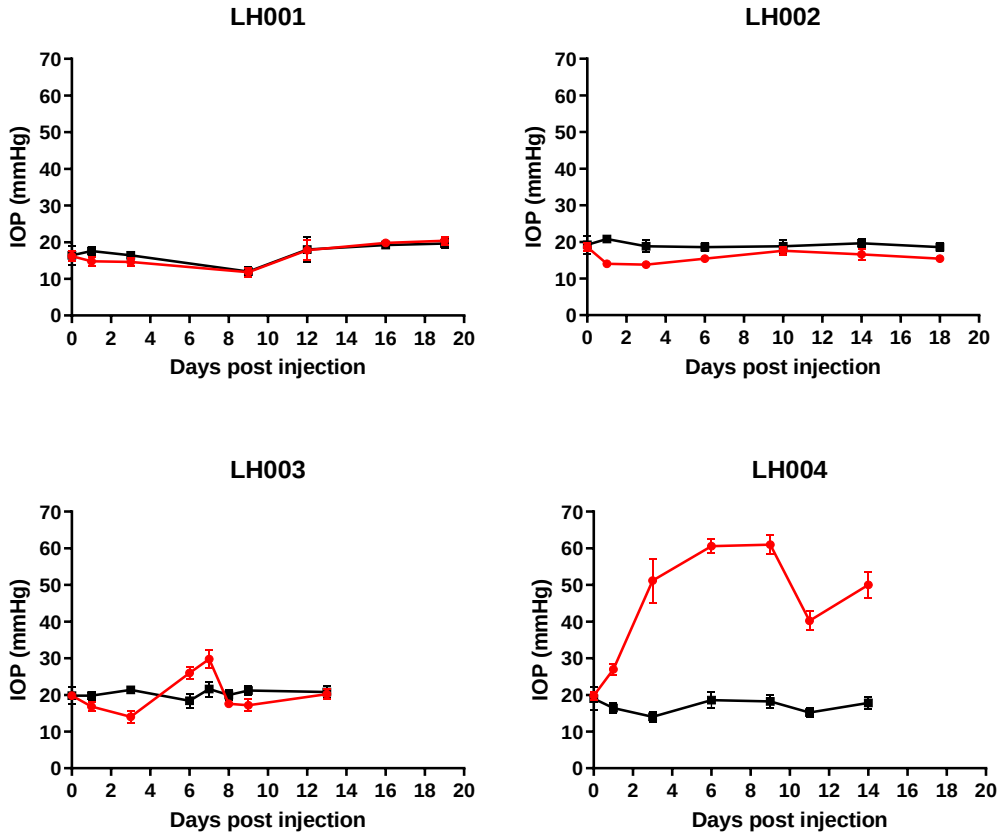

Figure 3.3 Individual IOP profiles of eyes injected with amine and carboxyl coated beads. (Top) combination of both beads. (Bottom) Amine coated beads only. Red line = injected eye, black line = contralateral control eye. Error bars = SD.

3.3.2 Amine coated beads

3.3.2.1 Partial *vs* full iridocorneal angle blockage

In the first round of injections with coated beads, the animal that was injected with 12µl of the amine coated beads solution, at a concentration of 50mg/ml, developed sustained OHT for 2 weeks, but IOP was elevated to almost 60mmHg. To explore whether more moderate OHT could be achieved with partial angle blockage, in a small cohort of 5 male adult Brown Norway rats (retired breeders), 2 eyes were injected with beads around the iridocorneal angle (360°) and 3 eyes were injected so that part of the angle remained unobstructed. Table 3.3 lists the details of the injections performed on each animal and Figure 3.4 shows the individual IOP profiles. In two animals (1266 and 1267) the needle was clogged by the beads during the procedure, preventing bead delivery, and the injections were repeated a few days later. Animal 1268 did not develop OHT after the 1st injection, so another injection was performed a few days later. Animals 1269 and 1270, where the beads occluded the iridocorneal angle over 360°, showed sustained IOP elevation, but with high peaks. Occlusions that did not cover the entire angle did not result in moderate sustained OHT. Either they did not elevate IOP or resulted in short (1 to 2 day) IOP spikes. Therefore, the approach of partial occlusion was not taken forward.

Table 3.3 Details of intracameral injections with amine coated beads in pilot cohort with partial vs full blockage.

Animal ID	Injection order	Volume (µl)	Concentration (mg/ml)	Coverage (˚)
1266	1	0*	NA	NA
1267	1	0*	NA	NA
1266	2	9	50	~300
1267	2	9	50	~330
1268	1	9	50	~270
1269	1	10	50	360
1270	1	10	50	360
1268	2	6	50	360
Notes: * = during the first attempt the beads settled and the syringe was clogged				

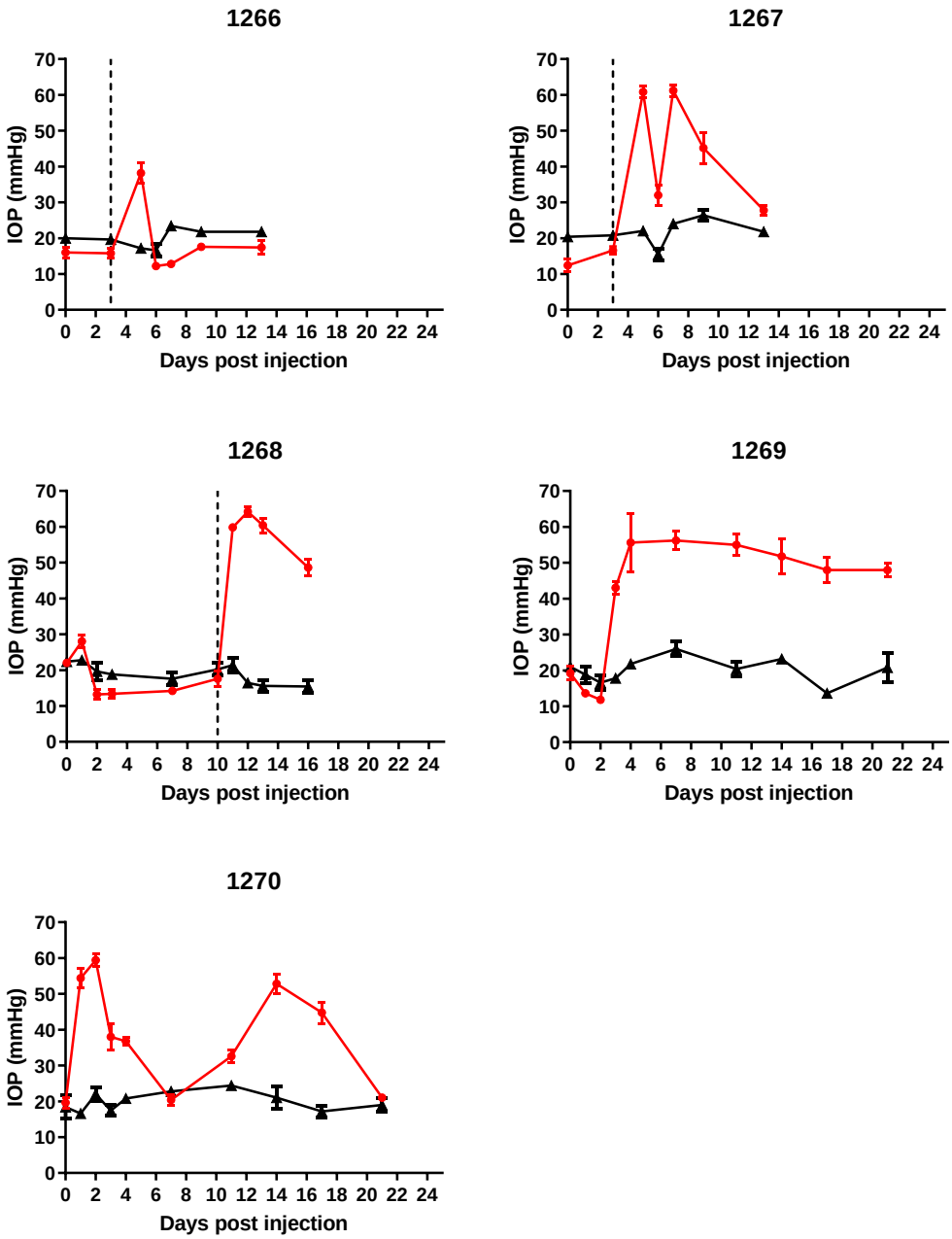

Figure 3.4 Individual IOP profiles in pilot cohort with partial vs full blockage. The details of coverage are as summarised in table 3.3. Red line = injected eye, black line = contralateral control eye. Error bars = SD.

3.3.2.2 Concentration optimisation

Since occlusion of the iridocorneal angle over 360° was required for sustained OHT. The next step was to address the factors that influenced the level of IOP increase. The principal variable to be adjusted was the bead concentration,

evaluated in the range of 40 to 25 mg/ml (Table 3.4), tested on a cohort of 9 adult male Brown Norway rats (retired breeders).

Table 3.4 Details of intracameral injections with amine coated beads covering the full periphery iridocorneal angle.

Animal ID	Injection order	Volume(µl)	Concentration (mg/ml)	Coverage (°)
1271	1	10	40	360
1272	1	10	30	360
1273	1	10	30	360
1274	1	10	30	360
1275	1	10	30	360
1276	1	9	25	360
1277	1	9	25	360
1278	1	9	25	360
1279	1	9	25	360

Lowering the concentration resulted in a small reduction of the level of IOP elevation and for most animals sustained OHT could be achieved with a single injection. However, most animals had IOP peaks over 50 mmHg and lowering the concentration further would result in having insufficient coverage of the iridocorneal angle, a critical requirement for the elevation of IOP. Figure 3.5 shows the individual IOP profiles for each animal in this cohort.

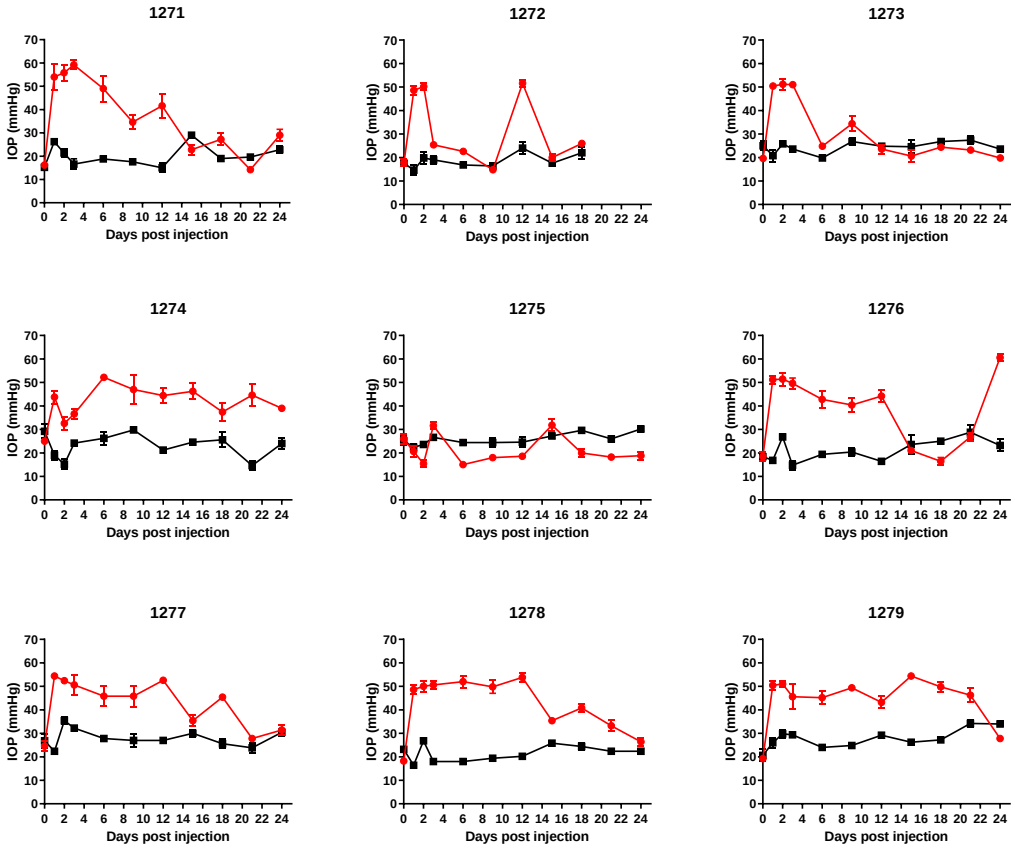

Figure 3.5 IOP profiles in the cohort of single intracameral injections with amine coated beads. IOP measurements for animal 1272 were limited due to animal health (not related to the procedures). Red = experimental eye, black = contralateral control eye, error bars = SD.

3.3.3 Epoxy coated beads

The next step was to evaluate the efficacy of beads coated with other molecular tags, in particular epoxy groups. These beads were evaluated in collaboration with Associate Professor Pete Williams and Assistant Professor James Tribble, in the Pete Williams lab in Karolinska Institutet, Stockholm. This study was conducted under protocols approved by Stockholm's Committee for Ethical Animal Research (10389-2018). A cohort of 12 adult male adult Brown Norway rats, 3 to 4 months old, received uniocular injections of 6 to 8 µl (~1.6 × 106 beads/µL) magnetic epoxy coated beads of 4.5µm diameter (Dynabeads M-450, ThermoFisher). The injection protocol used was the same as described in 2.4.2. The animals were kept in 12 hours light - 12 dark housing conditions. Until that point the cohorts of previous experiments

conducted in Cardiff University were housed under continuous light of 60-90lux. All animals received one intracameral injection and IOP was monitored for 2 weeks following OHT induction. Ocular hypertension was achieved in most animals after a single injection. Figure 3.6 shows all individual IOP profiles of this cohort.

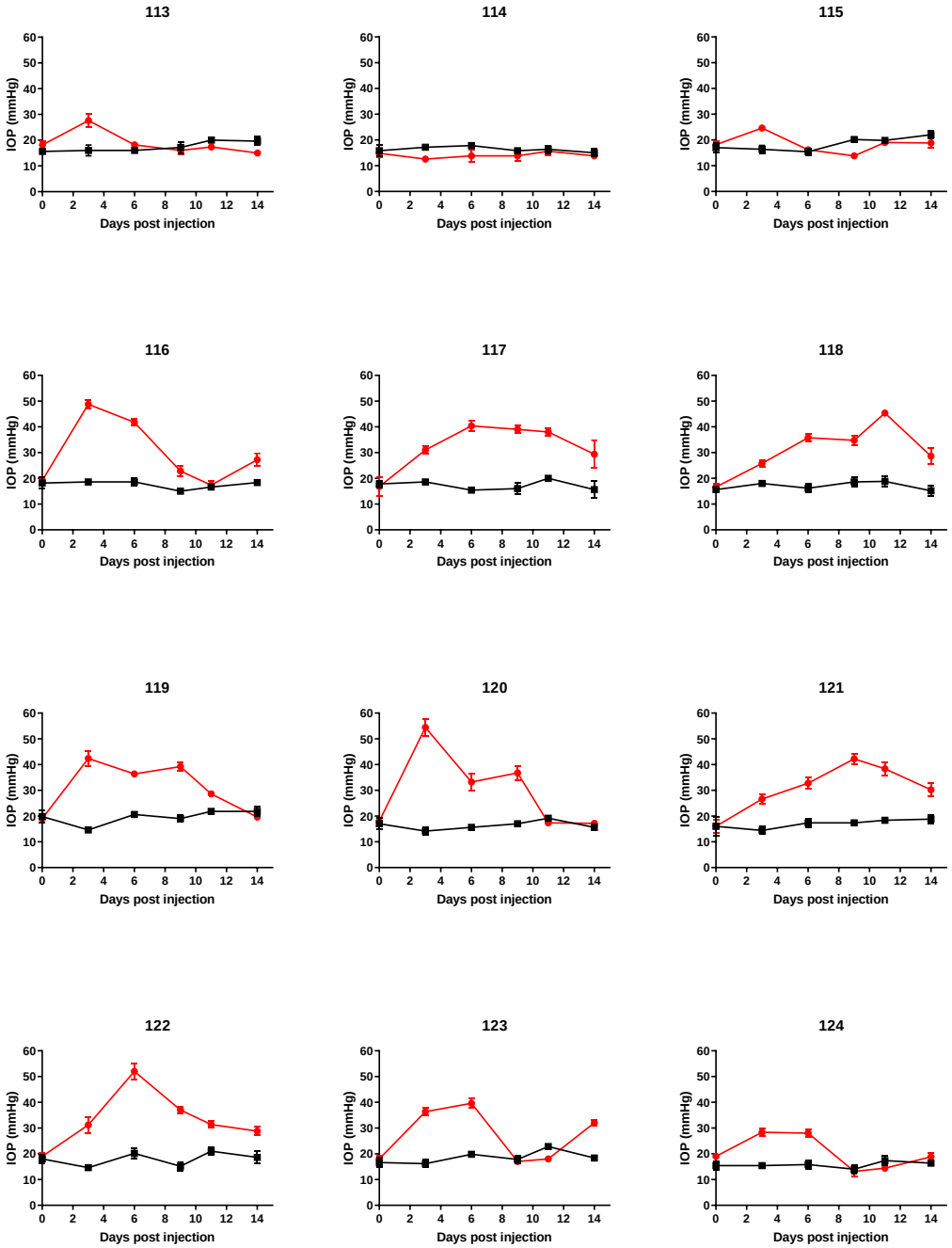

Figure 3.6 Individual IOP profiles of the cohort injected with epoxy coated beads. Red = experimental eye, black = contralateral control eye, error bars = SD.

3.3.4 Amine vs epoxy bead injections

To assess which of the two methods produced an experimental glaucoma model with more desirable properties, IOP profiles of animals 1271 to 1279 from the amine cohort were compared to IOP profiles of the epoxy cohort. To allow a balanced comparison, given than the epoxy cohort experiment lasted two weeks, only the first two weeks of the amine cohort experiment were used in this analysis. Moreover, IOP measurements from the 1st and 2nd day post injection of the amine cohort were excluded as in the epoxy cohort IOP measurements were collected from the 3rd day post injection. Injections that did not result in IOP elevation of at least 2 standard deviations (SD) of the control mean, were considered as not having a significant effect on the IOP of the eye.

Table 3.5 shows maximum difference of IOP between the injected eyes and the contralateral control eye for each animal in the amine and epoxy cohorts, as well as the IOP peak per animal. The percentage of animals per cohort, who at any point after OHT induction had an IOP measurement of at least 2 SD of the control was 88.9% (n = 8/9) for the amine group and 91.7% (n = 11/12) for the epoxy group. Recorded IOP of more than 50 mmHg was noted in 77.8% of the amine group and 16.7% of the epoxy group.

Table 3.5 Comparison of IOP elevation achieved by amine and epoxy bead injections and frequency of peak IOP above 50mmHg.

	ID	ΔMax OHT - Control	OHT peak (mmHg)	ΔMax ≥ 2SD from control mean = (%)	Peak > 50mmHg (%)
Amine beads	1271	**42.6**	**59.2**	**88.9**	**77.8**
	1272	**27.6**	**51.6**		
	1273	**27.4**	**51**		
	1274	**26**	**52.2**		
	1275	5	31.8		
	1276	**34.8**	49.6		
	1277	**25.6**	**52.6**		
	1278	**34**	**53.8**		
	1279	**28.2**	**54.4**		
Epoxy beads	113	**11.6**	27.6	**91.7**	**16.7**
	114	-0.8	15.6		
	115	**8.2**	24.6		
	116	**30.2**	48.8		
	117	**25**	40.4		
	118	**26.6**	45.4		
	119	**27.8**	42.4		
	120	**40.2**	**54.4**		
	121	**24.8**	42.2		
	122	**31.8**	**52**		
	123	**20.2**	39.6		
	124	**13**	28.4		

Notes:
Amine contralateral control IOP 2*SD = ±9.72
Epoxy contralateral control IOP 2*SD = ±4.16

For a more detailed comparison of IOP, the AUC of the IOP profiles per animal was calculated using the trapezoidal rule, and used to compare the IOP profiles between groups. Figure 3.7 shows the average IOP profile per cohort as well as the comparison of AUC among the OHT and NT eyes of the amine cohort and the OHT and NT eyes of the epoxy cohort. This comparison does not include animals 1275 and 114 of the amine and epoxy cohorts, respectively, because the injections did not induce OHT in either. The mean and SD of AUCs were 593.1 ± 107.1, and 403.9 ± 86.76 for the OHT eyes of the amine and epoxy group respectively, and 336.5 ± 61.65 for the amine NT controls and 244.8 ± 14.15 for the epoxy NT controls. Although the mean AUC

of the OHT eyes of the amine cohort was higher than the mean AUC of the epoxy cohort, there was no statistically significant difference between the two groups. Similarly, the mean AUC of the NT controls was higher in the amine cohort, but the difference was not statistically significant. The difference of the mean AUC of IOP between the OHT and NT eyes in the amine cohort was statistically significant, $p = 0.047$, as was the difference between the OHT and NT eyes in the epoxy cohort, $p < 0.001$. The difference between the OHT eyes of the amine cohort and the NT eyes of the epoxy cohort was statistically significant, $p < 0.001$, as opposed to the difference between the OHT eyes of the epoxy cohort and the NT eyes of the amine cohort ($p > 0.05$).

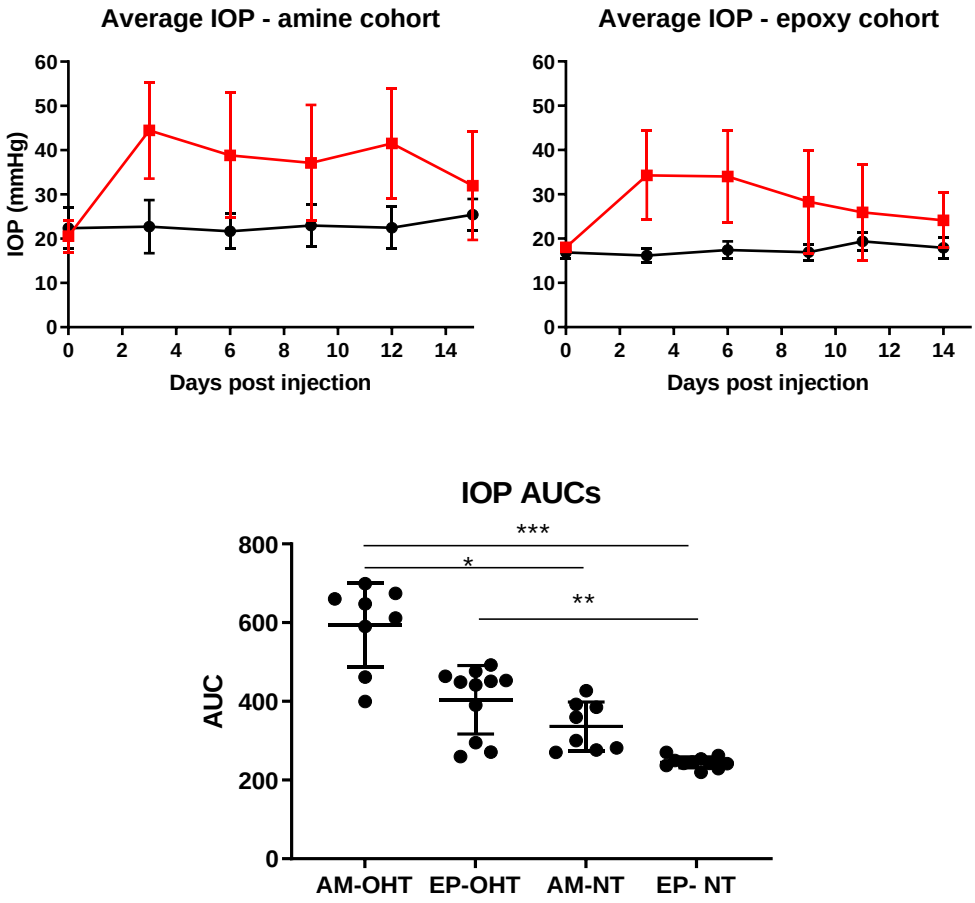

Figure 3.7 Comparison of IOPs in the amine and epoxy cohorts. (Top) Average IOP profile of OHT eyes (red) and NT eyes (black). Error bars = SD. (Bottom) Comparison of the AUCs of the IOP profiles of OHT eyes in the amine (AM-OHT) and epoxy (EP-OHT) group, and NT eyes in the amine (AM-NT) and epoxy (EP-NT) group. AM-OHT mean AUC = 593.1 ± 107.1, EP-OHT mean AUC = 403.9 ± 86.76, AM-NT mean AUC = 336.5 ± 61.65, EP-NT mean AUC = 244.8± 14.15. Kruskal Wallis test $p < 0.001$, Dunn's post hoc with multiple comparisons corrections * $p < 0.05$, ** $p < 0.01$, *** $p < 0.001$, error bas = SD.

3.3.5 Model optimisation discussion

3.3.5.1 High success rate with coated beads

Through this series of experiments, it was shown that using magnetic microparticles coated with functional groups increases the success rate of induction of ocular hypertension with a single injection. It was observed that plain polystyrene magnetic beads have the tendency to move away from the iridocorneal angle soon after the procedure, as first observed by clinical examination and confirmed by sagittal sections of the anterior chamber.

Amine and epoxy coated magnetic polystyrene beads allowed induction of ocular hypertension with a single injection in 89% and 92% of animals in each cohort, respectively. These types of beads are commonly used for cell separation due to their ability to bind ligands on cell surfaces, which is likely what immobilised them in the angle.

3.3.5.2 Higher IOPs for OHT and NT eyes in the cohort injected with amine coated beads

Comparison of the two methods, amine vs epoxy coated beads, shows that both had good success rates of induction of OHT, but the epoxy coated beads resulted in fewer high spikes over 50mmHg, 17% vs 78% in the amine cohort. Moreover, the mean IOP AUC of the OHT eyes of the amine cohort was higher than the mean IOP AUC of the epoxy cohort although the difference was not statistically significant. An interesting observation was that the mean IOP AUC was higher in the NT controls of the amine group than NT controls of the epoxy group, although this difference was not statistically significant. A factor that could have affected the IOP in unoperated eyes could be the housing conditions. The rats in the amine cohort were housed singly (to avoid fights that sometimes occurred in retired breeders that were initially used in this thesis) under continuous dim light, while the rats in the epoxy cohort were housed in pairs under a 12:12 light:dark cycle. Both single housing and continuous light conditions could gradually generate some level of stress to the animals and stress has been shown to result in increased intraocular pressure measurements (Prashar *et al.*, 2007). Therefore, although the continuous light is a choice that has been made to dampen the circadian rhythm and prevent IOP spikes (Morrison *et al.*, 2005), it is possible that it constitutes a chronic stressor that may affect baseline IOP measurements.

3.3.5.3 Conclusions from model optimisation

Using coated beads, it was possible to achieve a high success rate of OHT induction with a single injection and prolonged duration. The epoxy coated beads were shown to produce more moderate IOP elevation with fewer instances of high spikes over 50mmHg. It is possible that one of the factors

contributing to this could be the different housing conditions, as the rats housed in Karolinska were kept under a 12:12 hours light:dark cycle, while the rats housed in Cardiff were kept under continuous light conditions. The continuous light could be a possible source of stress for the animals that may also be contributing to higher IOP recordings. As a next step, the model using epoxy coated beads was replicated in Cardiff University for further characterisation and to ensure reproducibility of results. As a refinement to animal welfare all further experiments in Cardiff University were conducted under a 12:12 hours light:dark cycle and the animals were housed in pairs.

3.4 Epoxy model

The epoxy model, which was first tried on a cohort of Brown Norway rats in Professor Pete William's lab in Karolinska Institutet, over a 2-week experiment, was further evaluated in Professor James Morgan's lab in Cardiff University, by the author, in 4-week experiments. A cohort of 8 male Brown Norway rats, 4 to 8 months old, was injected unilaterally with epoxy coated beads as described in 3.3.3. All animals received just one injection and IOPs were monitored for 4 weeks. At the end of the experiment, the effect of OHT to RGC dendrites was assessed with DiOlistic labelling, as described in 2.8. The effect of the model on retinal function was also assessed on some animals, via ERG recordings acquired prior to induction of OHT and after approximately 3.5 to 4 weeks.

3.4.1 IOP profiles

The injections produced OHT in all animals in this cohort (8/8), which lasted for about 2 weeks, after which IOP gradually returned to normal. The average IOP peak in the OHT group was 42.5 (± 18.3) mmHg. Figure 3.8 shows the individual IOP profiles of the animals in this cohort as well as the average IOP profile of the NT and OHT eyes grouped.

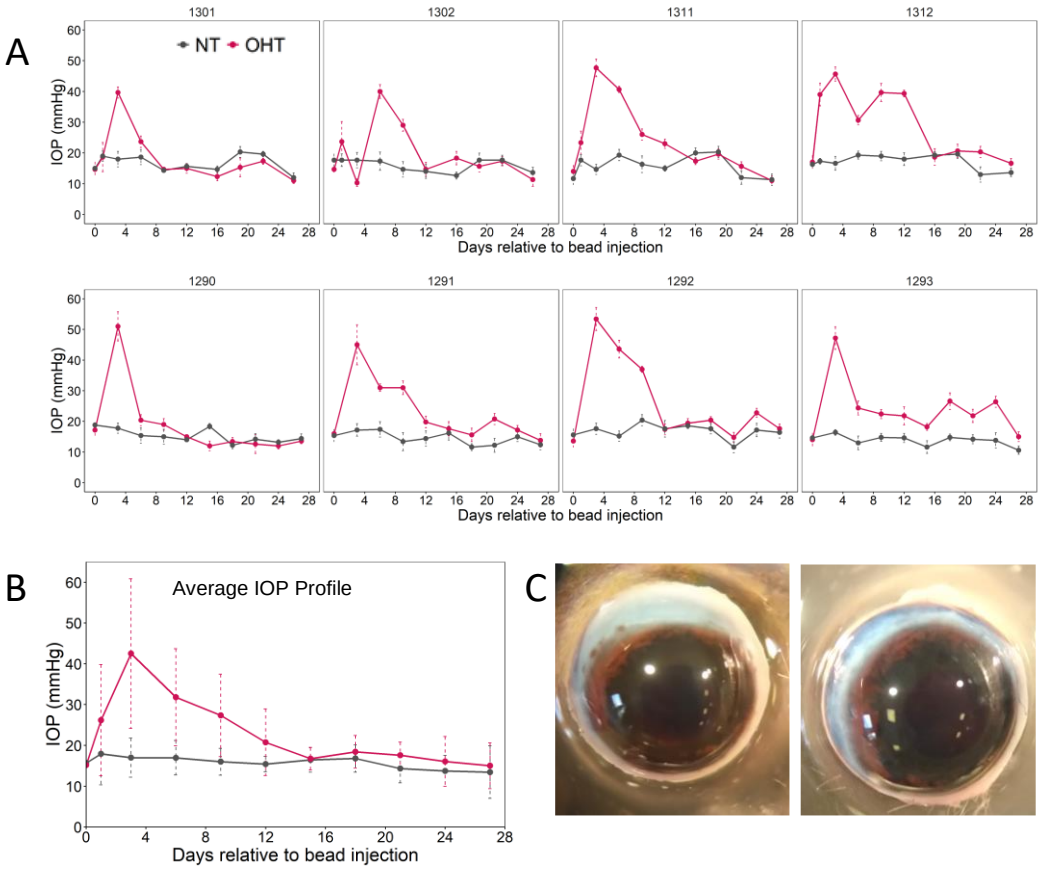

Figure 3.8 IOP profiles using the epoxy coated beads to induce OHT over 4 weeks. (A) Individual IOP profiles of each animal. (B) Average IOP profile of all animals in this cohort (n=8). (C) Two enucleated bead injected eyes at 4 weeks after bead injection, where the beads can still be seen in the iridocorneal angle. Error bars = SD

3.4.2 Sholl analysis of RGC dendrites

To assess the effect of the model on RGC dendrites, 4 weeks after OHT induction the retinas were harvested and RGCs were labelled using DiOlistics. RGCs were reconstructed as described in 2.8.5 and a Sholl analysis was performed on the RGCs dendrites (Figure 3.9). 80 RGCs were reconstructed, 31 in the NT group and 49 in the OHT group. Dendritic retraction was observed in the OHT group between 20 to 130µm from the cell soma, however between 140 to 300µm the OHT group had slightly more dendritic intersections than the NT group. Overall, the mean Sholl AUC ± SD of the OHT group was lower than the control group; 2,473 ± 1,169 *vs* 2,658 ± 1,131. However, the difference was not statistically significant (p = 0.5).

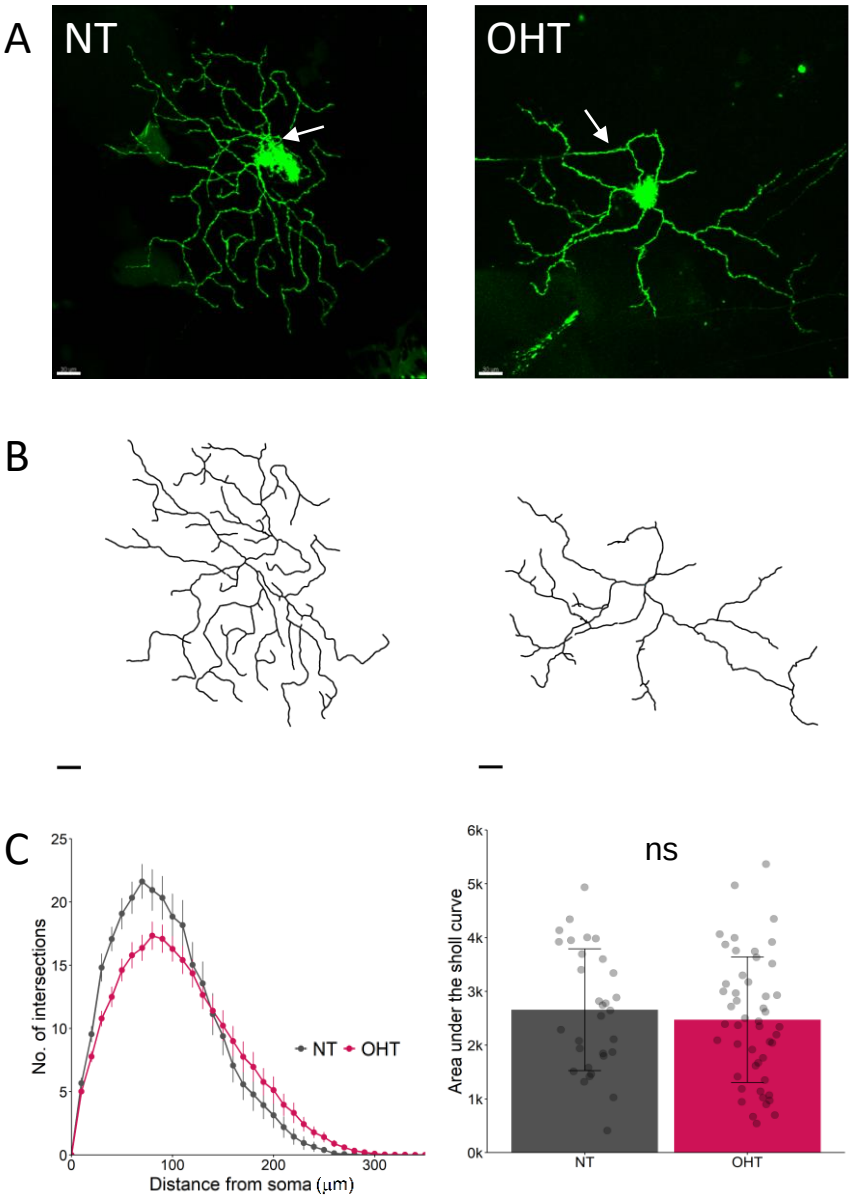

Figure 3.9 Sholl analysis of cells labelled using DiOlistics in the epoxy cohort. (A) Left a healthy cell from an NT retina, and right a degenerated cell from an OHT retina. Arrows point to the axons. (B) Cell reconstructions. Scale bar = 30µm. (C) Average Sholl profile of cells from OHT (fuchsia, cell n =49) and NT retinas (grey, cell n=31), error bars = SEM. (D) AUC of Sholl profiles. NT mean = 2, 658 ± 1,131, OHT mean 2,473 ± 1,169. NT vs OHT p > 0.05 (Two Sample t-test). Error bars = SD**.**

3.4.3 Assessment of retinal function – electroretinography

The effect of the OHT model on retinal function was evaluated via scotopic and photopic ERG following the protocol described in 2.3. To establish the basal retinal response, ERGs were recorded before OHT induction and repeated after ~3.5 to 4 weeks. The amplitude of the b-wave and the PhNR,

determined as the distance between the peak of the wave and non-stimulated state (Figure 3.10), was compared between the two recordings. Baseline recordings were obtained in 8 eyes from 4 rats. However, it was not possible to obtain final recordings from 2 eyes, due to excessive electrical noise in the ERG signal. To achieve a more accurate assessment only the 6 eyes (from n = 3 rats) with a full set of recordings were included in the analysis.

Figure 3.10 shows the average ERG wave for OHT and NT eyes at the baseline and after ~4 weeks from OHT induction. The a-wave, reflecting the rods' response, can be seen as an initial negative wave in the scotopic ERG, while at the photopic ERG the a-wave is diminished, indicating the protocol successfully suppressed the rod response. At the photopic ERG at 0.7 log cd sec/m2, there was essentially no response following a flash equal to the background illumination used for light adaptation, but with increasing intensity of the flash a gradient response was seen. The most notable difference between baseline and post injury response can be seen in the PhNR of the photopic response following the 2.2 log cd sec/m^2 stimulus. The median percentage change (Figure 3.11) of PhNR amplitude between the first and the second recording in OHT retinas was -29% vs +1.4% in NT ($p = 0.2$). In the b-wave the median change was -6% for OHT and +28% for NT ($p = 0.4$).

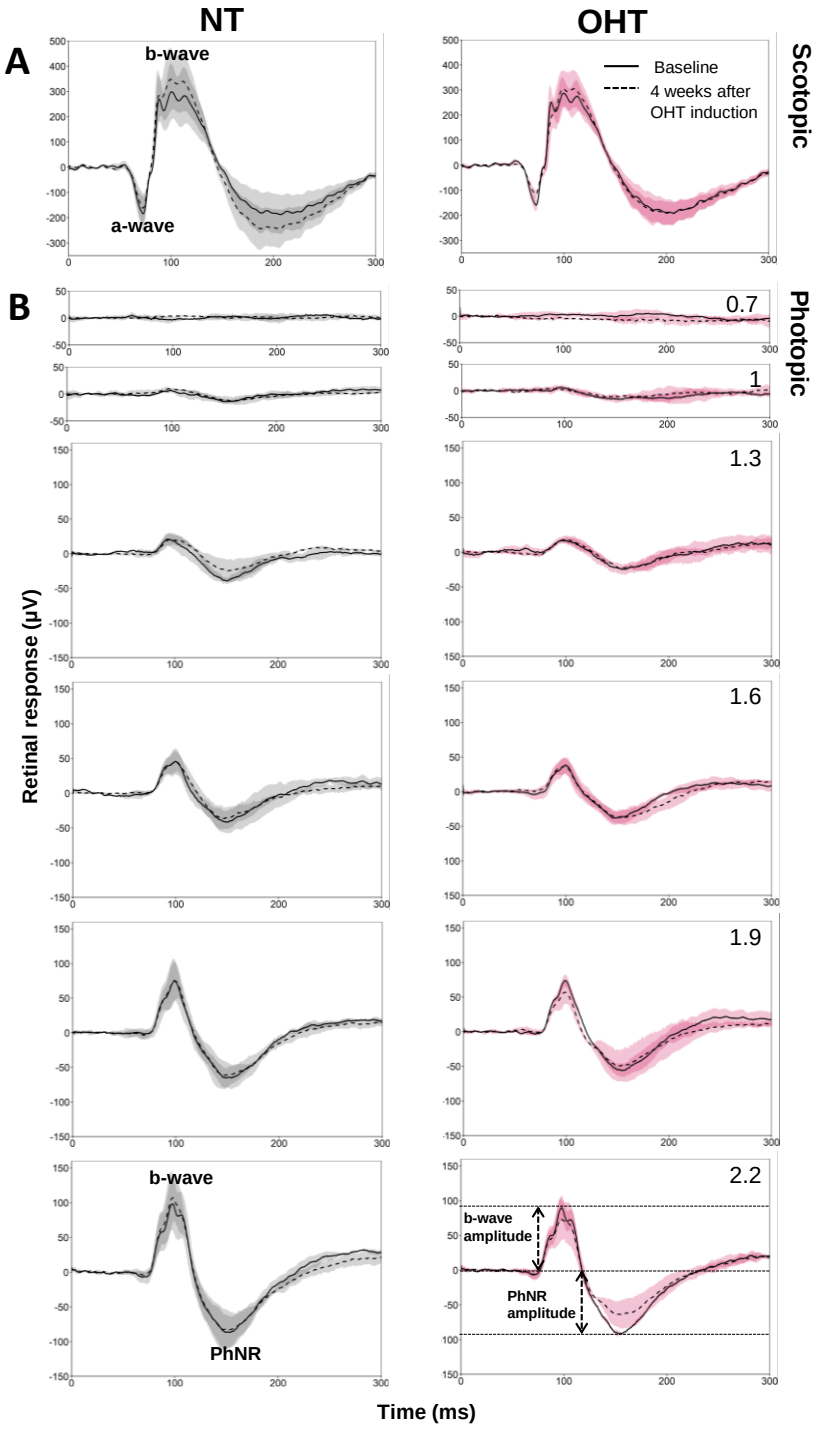

Figure 3.10 Retinal response 4 weeks after OHT induction. Average response waves from n = 3 OHT and n = 3 NT eyes before OHT induction (solid lines) and after OHT induction (dashed lines). (A) Scotopic ERG: the rod response (a-wave) is evident as an initial negative wave. (B) Photopic ERG at 0.7, 1, 1.3, 1.6, 1.9, 2.2 log cd sec/m^2. The a-wave is supressed, and a gradient response is seen with increasing stimuli. There is no response at 0.7 log cd sec/m^2 because this stimulus is the same as the constant background illumination. The OHT PhNR at 2.2 log cd sec/m^2 shows the most noteworthy reduction between the baseline and post injury response. Arrows indicate B-wave and PhNR amplitude.

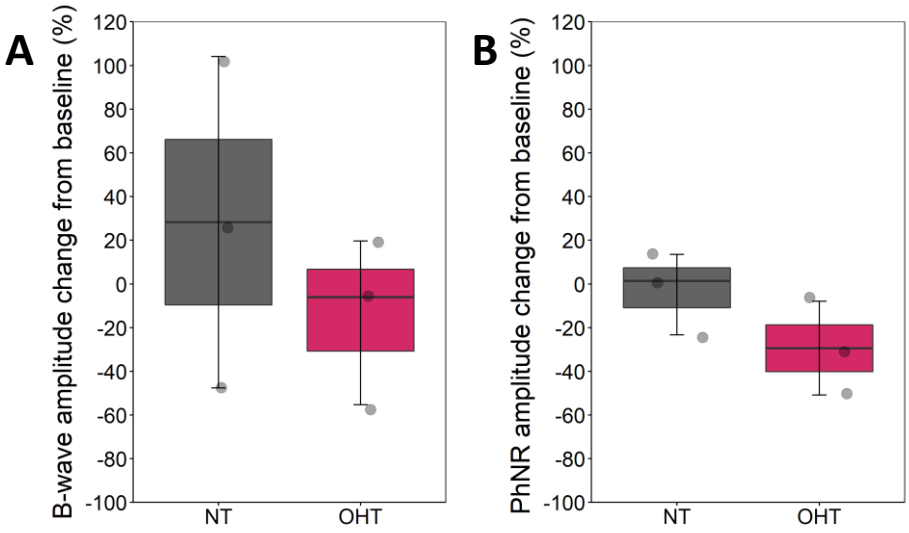

Figure 3.11 B-wave and PhNR amplitude changes 4 weeks after OHT induction with epoxy microbeads (n = 3 rats). (A) Percentage change in b-wave's amplitude from baseline, $p > 0.05$ (Welch t-test). (B) Percentage change in PhNR's amplitude, $p > 0.05$ (Welch t-test).

3.4.4 Epoxy model discussion

OHT induction with epoxy coated beads provided a reliable way to induce OHT with a single injection. Over the course of 4 weeks, OHT elevation was more marked in the first two weeks and then gradually returned to basal values by the end of the fourth week. At the end of the experiment the beads could still be seen around the iridocorneal angle, the cornea and lens were clear with no detectable signs of inflammation in the anterior chamber. Two weeks of elevated IOP with this model produce RGC degeneration and clinically relevant disease features (Tribble, Otmani, *et al.*, 2021). At the same time there is some initial evidence that injured RGCs may be able to recover some of their function and structure if stress is relieved (Fry *et al.*, 2018). The approximately two-week window of close to normal IOP prior to termination of experiments and tissue analysis, could present an opportunity for this to occur. Although examining this was not in the scope of the studies in this thesis, it is a factor worth considering and further studies assessing the state of RGCs at different time points following IOP induced injury could provide useful information.

Sholl analysis of RGC dendritic complexity produced inconclusive findings, as proximally to the soma (within 130μm from the soma) the RGCs from the OHT group had reduced dendritic complexity but at the more distal area (after 130μm) this was reversed. For this cohort of rats, the Sholl AUC was not significantly different between NT and OHT. Dendritic atrophy is an established feature of experimental glaucoma and has been reproduced in many studies (Weber, Kaufman and Hubbard, 1998; Shou *et al.*, 2003; Morgan *et al.*, 2006; Leung *et al.*, 2011; Williams *et al.*, 2013, 2016). However, the morphological diversity that RGCs naturally exhibit, as discussed in 1.1.1.1, induces significant variability in the data and often larger datasets than those available for this analysis are required to reach conclusive results. ERG results, although based on a small sample of 3 animals, were in agreement with the published literature (see 1.4.3) identifying the PhNR as a useful metric for assessment of RGC function in glaucoma.

Overall, among the models tested in this chapter, the model using epoxy coated beads was shown to have the most desirable properties, in terms of reliably producing high success rates of sustained IOP elevation with a single injection and moderate spikes. Four weeks after OHT induction the beads could still be seen retained in the iridocorneal angle, possibly due to the ability of epoxy groups to bind amino and hydroxyl groups, which are present on many cell surfaces. Based on those findings, this model was taken forward and used in subsequent experiments in this thesis.

Chapter 4. Effect of systemic inflammation on RGC degeneration

4.1 Introduction

Evidence has shown that systemic inflammation can have an adverse impact on cognitive abilities and even exacerbate the progression of neurodegenerative diseases, (Teeling *et al.*, 2007; Püntener *et al.*, 2012). Periodontitis has been associated with increased cognitive decline in Alzheimer's disease (Ide *et al.*, 2016) and analysis of the oral microbiome of glaucoma patients has revealed higher bacterial counts compared to control subjects (Astafurov, Elhawy, *et al.*, 2014). In light of these findings, this chapter uses a model of systemic immune priming via LPS, to investigate the effect of systemic inflammation on RGC degeneration in the experimental model of induced OHT via intracameral injections of epoxy coated magnetic microbeads, developed in Chapter 3.

4.2 LPS – subcutaneous delivery model

4.2.1 Experimental design

A cohort of 11 male Brown Norway rats 4 to 6 months old was injected with epoxy coated magnetic microbeads in the anterior chamber to induce ocular hypertension following the protocol described in 2.4.2. The bead injections were unilateral, always performed on the left eye, with the contralateral eye serving as control. The animals also received systemic, subcutaneous injections of either normal saline, n = 4, or 500 µg per kg of body weight LPS, n = 7, as described in 2.5.2. Each animal received 3 weekly injections. The 1st injection was given 3 days prior to induction of OHT to prime the immune system. Four weeks after the induction of OHT the retinas were harvested for DiOlistic labelling of RGCs. Figure 4.1 shows a schematic outline of the experiment. The experiment originally allowed for the assessment of the effects of inflammation on retinal function using ERG as described in 2.3. Unfortunately, technical issues with the subcutaneous electrodes prevented the reliable collection of ERG data in this cohort

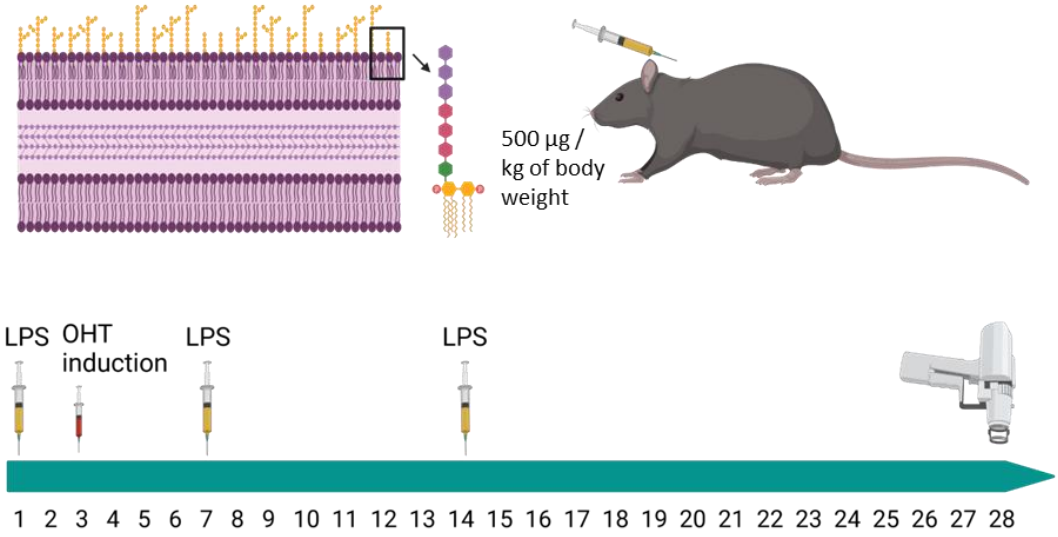

Figure 4.1 Experimental setup for immune priming via subcutaneous LPS delivery. A cohort of 11 adult male Brown Norway rats received subcutaneous injections of 500 µg of LPS per kg of body weight to prime their immune system, or saline for control. After three days OHT was induced unilaterally via intracameral injections of epoxy coated magnetic microbeads. Four days after OHT induction and seven days after the first LPS injection, the animals received one more round of subcutaneous LPS injection, followed by a third round one week later. Four weeks after OHT induction retinas were harvested for DiOlistic RGC labelling.

4.2.2 Results

4.2.2.1 IOP analysis

IOP was monitored following the protocol described in 2.2. IOP was increased in all animals to different degrees (individual IOP profiles for all experimental eyes are included in *Appendix B: Intraocular pressure profiles*). The hypertensive eyes injected with magnetic microbeads are named LPS-OHT and Saline-OHT depending on whether the animal received LPS or Saline injections, and similarly the contralateral normotensive control eyes are named LPS-NT and Saline-NT. Figure 4.2 Shows the average IOP profile per group during the course of the experiment, as well as the peak IOP, the IOP AUC and the mean IOP. For most animals the IOP peaked 3 days following induction of OHT and then gradually dropped, over 2 to 3 weeks, returning to similar levels as the contralateral controls towards the end of the experiment. The mean IOP ± SD (mmHg) per group was: LPS-NT = 16.36 ± 1.88, Saline-NT = 17.23±1.25, LPS-OHT = 20.93 ± 3.67, Saline-OHT = 23.12 ± 4.22. The

difference between OHT and NT was statistically significant within both the LPS and Saline groups, LPS-OHT vs LPS-NT p = 0.025 and Saline-OHT vs Saline-NT p = 0.003. However, there was no statistically significant difference between LPS and Saline OHT groups, LPS-OHT vs Saline-OHT p = 0.48, nor between the LPS and Saline NT groups, LPS-NT vs Saline-NT p = 0.94 (ANOVA followed by Tukey's HSD). The mean AUCs of the IOP profile per group showed a similar pattern with group means of: LPS-NT = 425.4 ± 48.9, Saline-NT = 452.25 ± 32.8, LPS-OHT = 550.5 ± 109.6, Saline-OHT = 622.5 ± 135.3. The statistical comparison results were: LPS-OHT vs LPS-NT p = 0.05, Saline-OHT vs Saline-NT p = 0.005, LPS-OHT vs Saline-OHT p = 0.41, LPS-NT vs Saline-NT p = 0.94. The mean IOP peak (maximum IOP recorded per animal) for each group was LPS-NT = 19.42 ± 1.49, Saline-NT = 20.38 ± 0.9, LPS-OHT = 36.5 ± 7.04, Saline-OHT = 41.13 ± 5.26. The difference between LPS-OHT and LPS-NT, and Saline-OHT and Saline-NT was statistically significant in both cases, $p<0.001$ and $p<0.001$, respectively. The difference between the peaks across the OHT groups and NT groups was again not statistically significant, LPS-OHT vs Saline-OHT p = 0.19 and LPS-NT vs Saline-NT p = 0.97.

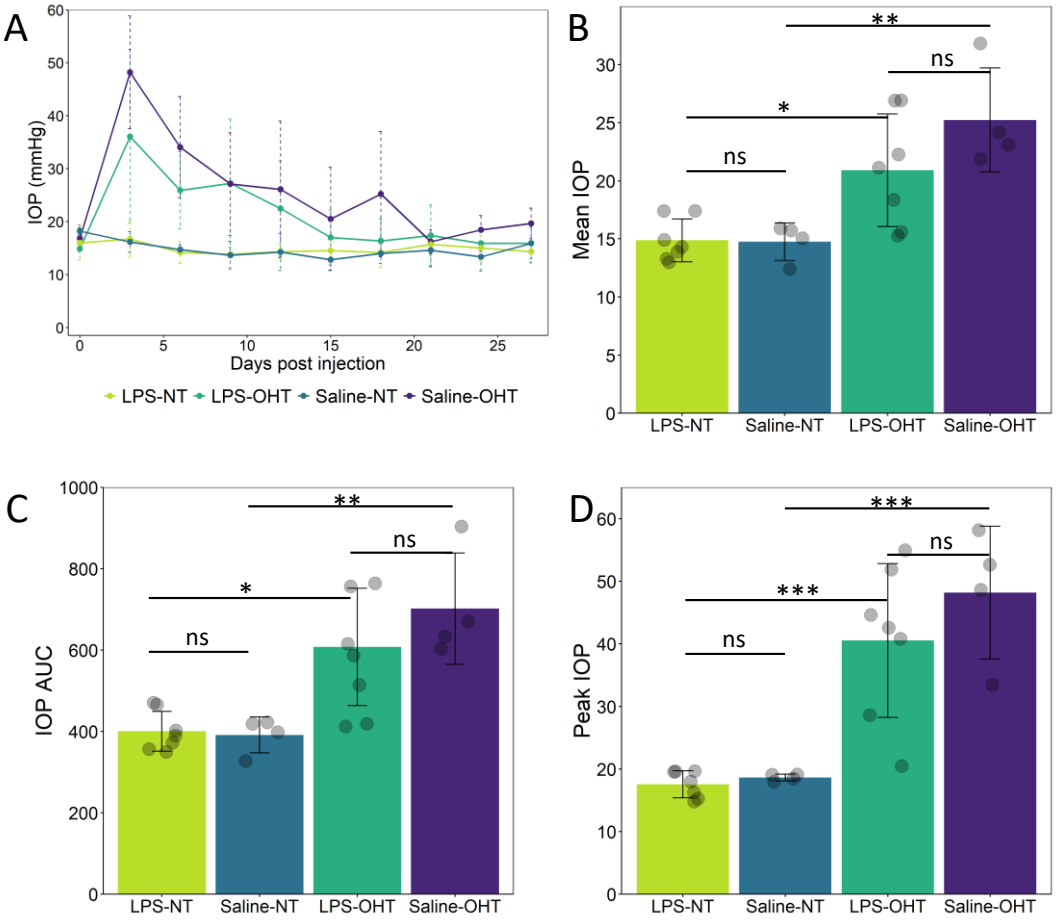

Figure 4.2 IOP analysis of the cohort injected with LPS or Saline via the subcutaneous route. LPS-NT n = 7, LPS-OHT n = 7, Saline-NT n = 4, Saline-OHT n = 4. (A) Average IOP profile. (B,C,D) Mean IOP, AUC of the IOP, and Peak IOP. Error bars = SD, one-way ANOVA with Tukey's HSD ns $p>0.05$, * $p<0.05$, ** $p<0.01$, *** $p<0.001$.

4.2.2.2 Weight monitoring

The change in animal weight provides a useful estimate of animal health during the experiments. Animals were weighed before the LPS or saline injections and 24 hrs, 48 hrs, 72 hrs, and 7 days after each injection. Figure 4.3 shows the changes in average weight in each group following the injections, as well as the percentage of weight change in 24 hours following each injection, as this was shown to be the time point where weight loss peaked following exposure to LPS. The animals demonstrated moderate weight loss of -5% at 24 hours following the first LPS injection, however subsequent LPS injections did not produce the same effect. There was essentially no weight loss triggered by the saline injections. In detail, the

weight loss recorded 24 hours following the first LPS injection was -4.7(±1.8)%, and was significantly different from the weight loss observed after the other LPS injections and all saline injections. All other comparisons were not significant ($p > 0.05$). As a conclusion the weight monitoring, and general monitoring of the animals' behaviour and appearance, showed that the first exposure to LPS had a mild to moderate effect on the animals, without at any point resulting in severe ill health, and the animals appeared to recover quickly and fully. Subsequent weekly exposure to LPS did not produce any response detectable via weight monitoring.

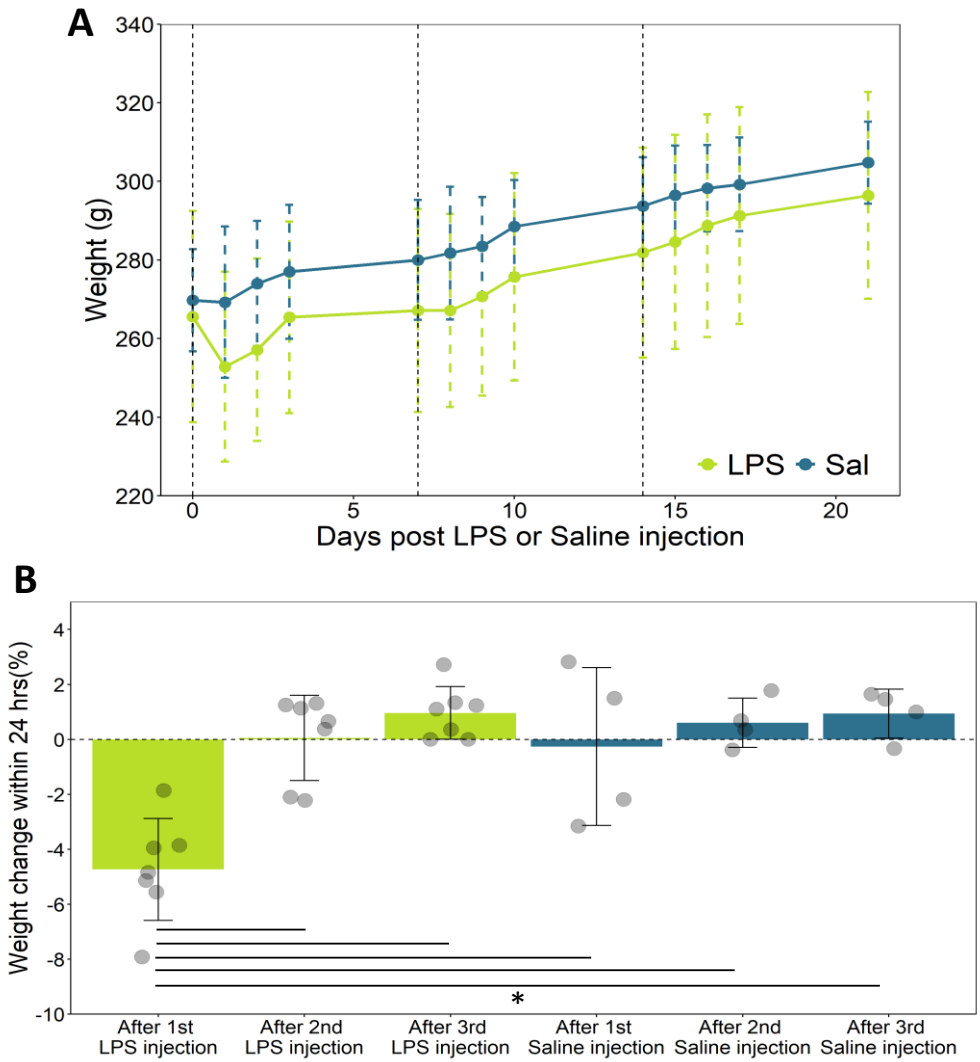

Figure 4.3 Weight monitoring following subcutaneous LPS and saline injections. (A) Average body weight of rats throughout the course of repeated LPS (green) or saline injections (blue). The vertical dashed lines indicate the injection days (0, 7 and 14). On those days the weight was measured before the injection. Error bars = SD. (B) Average weight change in 24 hours following each injection, from the weight measured before the injection. The asterisk indicates significant difference in weight change ($p<0.05$) between the recorded weight 24 hours after the 1st LPS injection and all other injections. All other comparisons are not statistically significant (Kruskal Wallis with Dunn's post hoc).

4.2.2.3 Assessment of dendritic changes

At the end of the experiment, animals were euthanised and retinas collected for DiOlistic labelling following the protocol described in 2.8. A total of 104 RGCs from 11 retinas were analysed (average per group n=26). Figure 4.4

shows the Sholl analysis, AUC of the Sholl analysis, number of segments per order of dendrites, and total dendritic length for each group. The cells from the OHT retinas had lower number of intersections in the Sholl analysis, demonstrated with a decreased Sholl AUC, as well as decreased total dendritic length, without notable differences between the two groups. The Saline OHT group showed a slight reduction of dendritic segments across the three grouped orders, while the LPS OHT group demonstrated a more targeted loss at the tertiary and higher order dendrites (noted as tertiary+). The AUC and total dendritic length were in descending order Saline-NT 3,796 ± 1,678 > LPS-NT 3,231 ± 1,304> Saline-OHT 2,870 ± 1,066 > LPS-OHT 2,739 ± 1,346, and Saline-NT 5,508 ± 2,442 µm > LPS-NT 4,796 ± 1,945 µm > Saline-OHT 4,257 ± 1,593 µm > LPS-OHT 4,094 ± 1,915 µm, respectively. There was a trend for reduced dendritic complexity in RGCs from OHT retinas, however, the statistical analysis (Kruskal Wallis test) did not confirm any statistically significant differences.

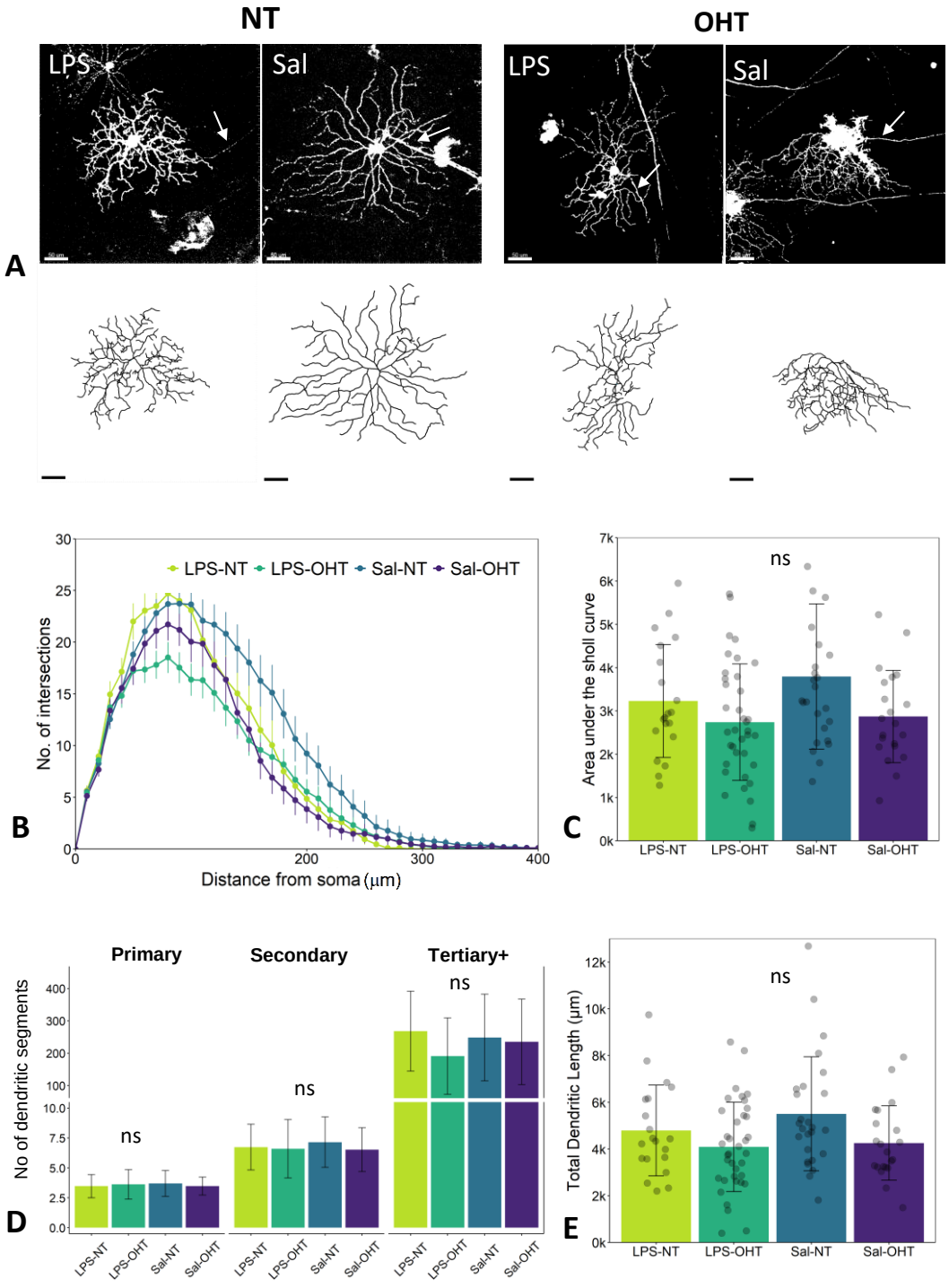

Figure 4.4 RGC dendritic morphology analysis following induced OHT and subcutaneous LPS. (A) Representative RGCs and their dendritic reconstructions. The arrows indicate the axons. Scale bars = 50 µm. (B) Sholl analysis showing the number of dendritic intersections to concentric circles as a function of distance form the soma. (C) AUC of the Sholl profile. (D) Number of primary, secondary and tertiary+ dendrites (i.e. tertiary and higher). (E) Total dendritic length in µm. (B-E) Cells per group: LPS-NT n = 20, LPS-OHT n = 37, Sal-NT n = 26, Sal-OHT n = 21. (B) Error bars = SEM. (C,D,E) Error bars = SD. Statistical test = Kruskal Wallis, ns $p > 0.05$

4.2.3 IL-6 detection

Having observed a decreased response following the 2nd and 3rd LPS injections, as manifested through the lack of any weight loss or behavioural signs of ill health, the next step was to assess the response of IL-6, an acute phase pro-inflammatory cytokine. 6 male Brown Norway rats aged 5 to 6 months old received 3 subcutaneous injections at weekly intervals, of either saline (n = 3) or 500µg of LPS per kg of body weight (n = 3). Blood was collected and serum samples were prepared following the protocol described in 2.6. IL-6 was quantified as described in 2.12.

Within the sensitivity range of the assay (125 - 8,000 pg/mL) IL-6 was detectable in the samples following the 1st LPS injection, but not in the samples collected after the 2nd and 3rd LPS injections, or any baseline or post saline samples. Table 4.1 Shows the amount of IL-6 in each sample. The average IL-6 concentration after the 1st LPS injection was 1,406 (±836) pg/ml.

Table 4.1 IL-6 quantification via ELISA – summary of results

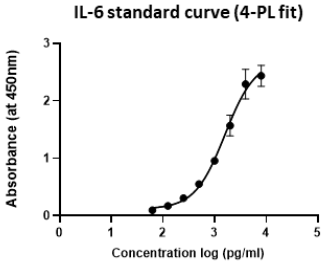

Sample ID	IL-6 baseline (pg/ml)	IL-6 after 1st injection (pg/ml)	IL-6 after 2nd injection (pg/ml)	IL-6 after 3rd injection (pg/ml)
Saline (Rat1)	Undetectable	Undetectable	Undetectable	Undetectable
Saline (Rat2)	Undetectable	Undetectable	Undetectable	Undetectable
Saline (Rat3)	Undetectable	Undetectable	Undetectable	Undetectable
LPS (Rat4)	Undetectable	**1641**	Undetectable	Undetectable
LPS (Rat5)	Undetectable	**478**	Undetectable	Undetectable
LPS (Rat6)	Undetectable	**2100**	Undetectable	NA*

*sample not available

4.3 LPS – intraperitoneal delivery model

With subcutaneous LPS delivery, it was possible to establish that the LPS dose of 500µg/kg of body weight was sufficient to produce a mild-to moderate response, confirmed by temporary weight loss and increased concentration of IL-6 in blood serum. However, the response was limited to the 1st LPS injection, in that subsequent injections at the same dose did not induce any weight loss or detectable increase in IL-6. In addition, the yield of RGC cells

through DiOlistic labelling was insufficient to reach definitive conclusions with regard to the effect of LPS on glaucomatous dendritic loss. Therefore, the experiment was repeated using a modified model and with a bigger cohort.

4.3.1 Experimental design

A cohort of 20 male Brown Norway rats 7 to 8 months old were injected with either saline or 500µg per kg of body weight LPS (n =10 per group). The aim was to achieve higher response to repeated LPS exposure. In rats, LPS tolerance has been shown to last 2 to 3 weeks (Sanchez-Cantu, Rode and Christou, 1989; Ziegler-Heitbrock, 1995). Therefore, the time between LPS injections was increased to 2 weeks. In addition, the intraperitoneal (IP) route was chosen for LPS (or saline) delivery, as it has been shown that IP injections usually result in faster and more complete absorption of molecules compared to subcutaneous injections (Al Shoyaib, Archie and Karamyan, 2020). To mitigate the possibility that tolerance to LPS might still occur even with this additional time between injections, it was decided that the 1st LPS injection would not be given before OHT induction, but 3 days after, which would ensure at least one time point during the experiment where a systemic inflammatory response would occur while the animals had OHT (usually within the 1st week following bead injections). As shown in the experimental timeline in Figure 4.5, the 2-week interval and later onset of LPS injections meant that up to 2 doses could be given in the course of the 4-week experiment.

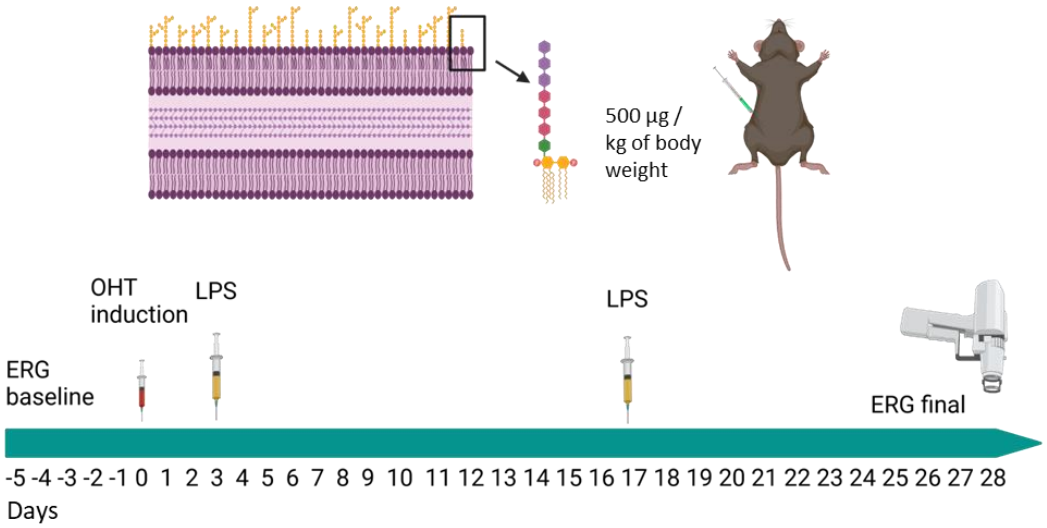

Figure 4.5 Experimental setup for immune priming via intraperitoneal LPS delivery. Baseline ERGs were collected before OHT induction. The first LPS injection was given 3 days after OHT induction and the second LPS injection was given after a 14-day interval. ERGs were collected approximately 3.5 to 4 weeks after OHT induction.

4.3.2 Results

4.3.2.1 Weight monitoring

The weight was recorded before each injection and then daily for 3 days (i.e. 24, 48 and 72 hours after the injection) and after 1 week. Weight loss peaked 24 hours after the injections and the animals gradually regained their weight in the following days. Figure 4.6 (A-B) shows the average recorded weight per group throughout the days and the percentage weight loss in 24 hours after each injection. Figure 4.6 C compares the weight changes seen 24 hours after IP and subcutaneous LPS. The average weight loss following the 1st LPS IP injection was -4.7(±0.6)%, the same as the weight loss observed following the 1st subcutaneous LPS in the previous experiment ($p = 0.99$). The average weight loss following the 1st saline injection was -0.15(±0.9)% (weight loss 24hrs post 1st IP LPS vs 1st IP Saline injection $p < 0.001$). Using this amended experimental design, -2.9(±1.1)% weight loss was seen 24hrs after the 2nd IP LPS injection (weight loss 24hrs post 1st IP LPS vs 2nd IP LPS, $p = 0.003$). Some weight loss, -1(±1.3)%, was also observed after the 2nd IP saline

injection, however it was still significantly less compared to the 2nd LPS injection (p = 0.001), and not statistically significant compared to weight loss after the 1st saline injection (p = 0.25). This could have been related to stress from repeated handling or irritation from the injection itself. Comparison of the weight loss triggered by the LPS injections delivered 2 weeks apart vs the weight loss observed in the cohort where LPS was delivered weekly (Figure 4.6, C), indicated the 2-week interval resulted in significantly more weight loss. 2nd IP LPS (2-week interval) vs 2nd subcutaneous LPS (1-week interval) p < 0.001, 2nd IP LPS (2-week interval) vs: 3rd subcutaneous LPS (1-week interval) p < 0.001).

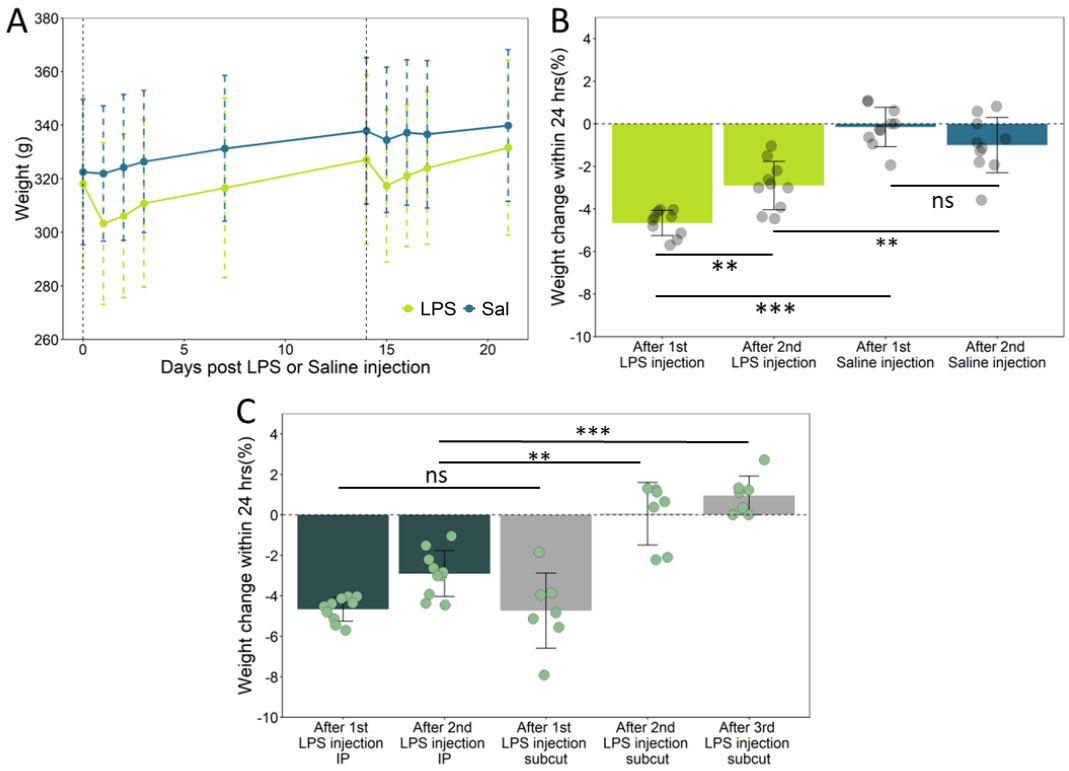

Figure 4.6 Weight loss triggered by intraperitoneal LPS delivery. (A) Average weight profile per group (LPS or Saline) following the injections. The timepoints of injections are indicated by the dashed lines. (B) Percentage weight change in 24 hours following each injection. (C) Comparison of % weight change observed in 24 hours after IP and subcutaneous LPS injections. Error bars = SD, one-way ANOVA followed by Tukey's HSD, ns p>0.05, * p<0.05, ** p<0.01, *** p<0.001

4.3.2.2 IL-6 detection

IL-6 levels were determined in serum samples from 6 rats that received IP LPS or Saline. Since previous work indicated that IL-6 was not detectable in samples collected prior to injections or after saline injections (see 4.2.3), baseline samples were not analysed in this assay and samples were obtained from 2 animals from the saline group. IL-6 upregulation was detected in 3/4 samples after the 1st LPS dose. The average concentration was 1,436 ± 1,244 (pg/ml). However, an increase in IL-6 was not observed in any samples from the saline group, nor following the 2nd LPS injection, despite the weight loss observed (see 4.3.2.1). Out of four LPS samples one had undetectable levels of IL-6 and one had a markedly lower concentration (24.97 pg/ml). This raises the question of what could have caused this inconsistency between the samples, raising the possibility of variation in the biological activity of LPS preparation. However, this is considered unlikely, because animals were housed in pairs, 1303 with 1304, and 1305 with 1306, with the same vial of LPS used per pair. Therefore, 1303 and 1304 were injected with the same LPS preparation, but the IL-6 levels in their sera samples vary significantly. Similarly, 1305 and 1306 received the same LPS preparation, but IL-6 level in their sera samples are again very different. No technical issues were encountered in the delivery of the LPS (i.e. no haemorrhage or leakage).

Table 4.2 IL-6 quantification via ELISA – summary of results

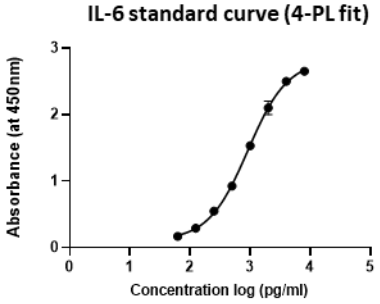

Sample ID	IL-6 after 1st injection (pg/ml)	IL-6 after 2nd injection (pg/ml)
LPS (1303)	**2372.21**	undetectable
LPS (1304)	**24.97**	undetectable
LPS (1305)	**1911.36**	undetectable
LPS (1306)	undetectable	undetectable
Saline (1307)	undetectable	undetectable
Saline (1308)	undetectable	undetectable

4.3.2.3 IOP analysis

OHT was induced unilaterally (left eye) as described in 2.4.2, and IOP was monitored as described in 2.2. IOP increased in all injected eyes to a varying

extent. Individual IOP profiles can be found in *Appendix B: Intraocular pressure profiles.* Figure 4.7 Shows the average IOP profile per group of eyes (LPS NT, LPS OHT, Saline NT, Saline OHT) throughout the experiment, and the peak IOP, IOP AUC and IOP mean. Consistently with previous experiments, for most animals IOP peaked at about 3 days following OHT induction, and then gradually dropped. The mean ± SD IOP (mmHg) per group was: LPS-NT = 16.6 ± 1.8, Saline-NT = 17.8 ± 1.6, LPS-OHT = 21.5 ± 3.9, Saline-OHT = 24.6 ± 4.9. The IOP increase was statistically significant in both the LPS and Saline groups, LPS-OHT vs LPS-NT $p = 0.01$ and Saline-OHT vs Saline-NT $p < 0.001$. Similarly, the IOP AUCs were significantly increased in both OHT groups compared to their respective NT controls. IOP AUC: LPS-NT = 435.2 ± 49, Saline-NT = 469.8 ± 47, LPS-OHT = 574.5 ± 119.4, Saline-OHT = 671.6 ± 158.3; LPS-OHT vs LPS-NT $p = 0.03$ and Saline-OHT vs Saline-NT $p < 0.001$. The average peak of IOP per group was close to 40 mmHg for the OHT groups: LPS-NT = 19.8 ± 1.6, Saline-NT = 20.8 ± 1.2, LPS-OHT = 38.8 ± 7.9, Saline-OHT = 42.4 ± 5.4 (LPS-OHT vs LPS-NT $p < 0.001$, Saline-OHT vs Saline-NT $p < 0.001$). For all metrics (mean IOP, IOP AUC, Peak IOP) the average values of both LPS-NT and LPS-OHT eyes were lower compared to the respective Saline-NT and Saline-OHT eyes, with the difference being more notable between the OHT groups. However, those differences were not statistically significant ($p > 0.05$).

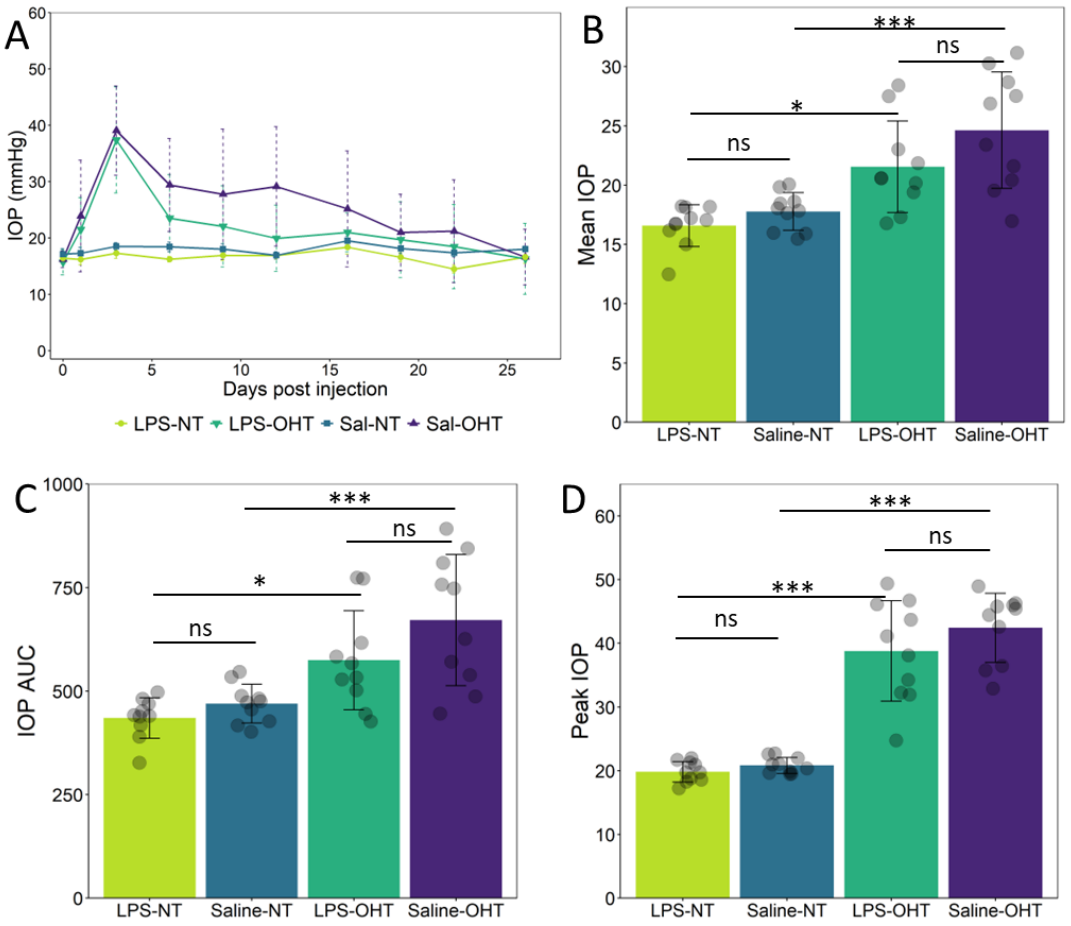

Figure 4.7 IOP analysis of the cohort injected with LPS or Saline via the intraperitoneal route. LPS-NT n = 10, LPS-OHT n = 10, Saline-NT n = 10, Saline-OHT n = 10. (A) Average IOP profile. (B,C,D) Mean IOP, AUC of the IOP, Peak IOP. Error bars = SD, one-way ANOVA with Tukey's HSD ns $p>0.05$, * $p<0.05$, ** $p<0.01$, *** $p<0.001$.

4.3.2.4 Assessment of dendritic changes

Whole retinas from 16 rats (n = 8 LPS group, n = 8 Saline group) were harvested using the protocol described in 2.8.2 and labelled using the DiOlistic labelling protocol described in 2.8.3. A total of 197 RGCs were reconstructed (LPS NT n = 50, LPS OHT n = 45, Sal NT n = 50, Sal OHT = 52) as described in 2.8.5. Dendritic complexity, as assessed by Sholl analysis, the total dendritic length and number of primary, secondary and tertiary dendrites are summarised in Figure 4.8. Sholl AUC and total dendritic length, were similar

in the NT groups, Interestingly, while the Saline OHT group demonstrated notable dendritic atrophy in all those metrics, the LPS OHT group showed only moderate differences compared to NT control. The AUC was: LPS-NT = 2,835 ± 1,280, LPS-OHT = 2,626 ± 1,563, Saline-NT = 2,776 ± 1,143, Saline-OHT = 1,796 ± 1,072; LPS-NT vs Saline-NT $p = 0.88$, LPS-OHT vs LPS-NT $p = 0.36$, Saline-OHT vs Saline-NT $p < 0.001$, LPS-OHT vs Saline-OHT $p = 0.008$. The total dendritic length ± SD in µm was: LPS-NT = 4,107 ± 1,804, LPS-OHT= 3,784 ± 2,241, Saline-NT= 4,002 ± 1,629, Saline-OHT= 2,567 ± 1,512; LPS-NT vs Saline-NT $p > 0.84$, LPS-OHT vs LPS-NT $p = 0.32$, Saline-OHT vs Saline-NT $p < 0.001$, LPS-OHT vs Saline-OHT $p = 0.006$. At the primary and secondary dendrite level there are no significant differences ($p = 0.29$ and 0.36) in the number of dendrites across the groups, although the Sal-OHT group had slightly lower dendrite counts (Primary: LPS-NT = 3.6 ± 1.1, LPS-OHT = 3.8 ± 1, Saline-NT = 3.8 ± 1.3, Saline-OHT = 3.4 ± 1; Secondary: LPS-NT = 6.5 ± 2.2, LPS-OHT = 7 ± 2, Saline-NT = 7.1 ± 2.3, Saline-OHT = 6.4 ± 1.8). At the tertiary+ (i.e. tertiary and higher) dendrite level there was significant dendritic loss in both OHT groups compared to their respective controls (LPS-OHT vs LPS-NT $p = 0.04$, Saline-OHT vs Saline-NT $p = 0.001$), which was more severe in the Saline group (Tertiary: LPS-NT = 231 ± 135.7, LPS-OHT = 177.2 ± 136.6, Saline-NT = 214.4 ± 134.5, Saline-OHT = 132 ± 104.4), however this difference was not statistically significant (LPS-OHT vs Sal-OHT $p = 0.11$).

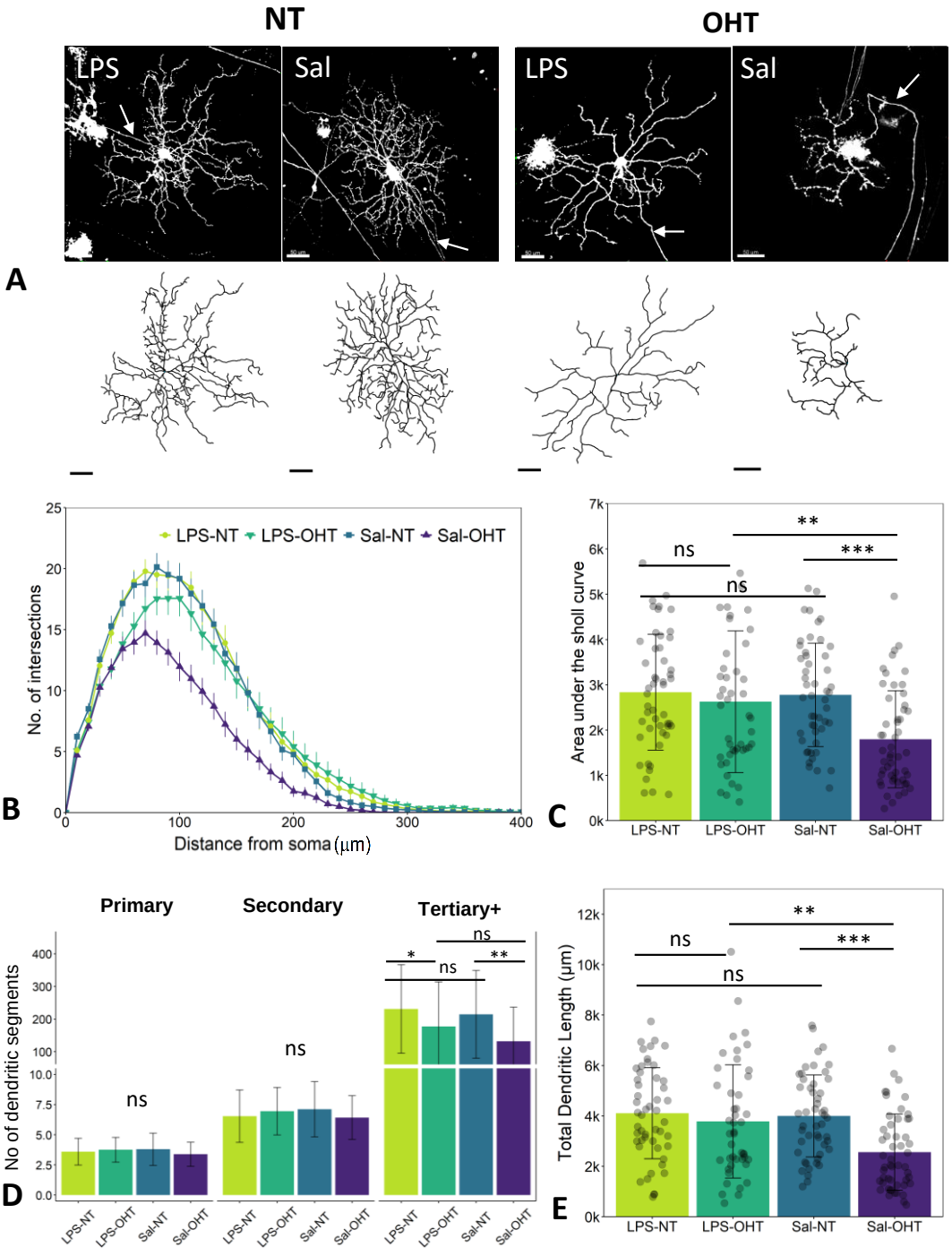

Figure 4.8 RGC dendritic morphology analysis following induced OHT and intraperitoneal LPS. (A) Representative RGCs and their dendritic reconstructions. The arrows indicate the axons. Scale bars = 50 µm. (B) Sholl analysis showing the number of dendritic intersections to concentric circles as a function of distance from the soma. (C) AUC of the Sholl profile. (D) Number of primary, secondary and tertiary+ dendrites. (E) Total dendritic length in µm. (B-E) Cells per group: LPS NT n=50, LPS OHT n=45, Sal NT n=50, Sal OHT=52. (B) Error bars = SEM. (C,D,E) Error bars = SD. Test = Kruskal Wallis followed by Dunn's test for multiple comparisons, ns p>0.05, * p<0.05, ** p<0.01, *** p<0.001.

4.3.2.5 Electroretinography

The retinal response to light stimuli was examined with non-invasive ERG following the protocol described in 2.3. ERGs were recorded before the induction of OHT and again during the last 2 to 3 days of the experiment (~3.5 to 4 weeks post bead injection). Although baseline recordings could be obtained from all eyes (n = 40), it was not possible to obtain final recordings from 8 eyes, due to excessive electrical noise in the ERG signal. To achieve a more accurate assessment of the change, only eyes where a full set of recordings was available (n = 32 (LPS-NT = 10, LPS-OHT = 8, Sal-NT = 7, Sal-OHT = 6)) where included in the analysis. The photopic response at 2.2 log cd sec/m^2 is shown in Figure 4.9. Those particular recording were analysed because as shown in Figure 3.10, this is where it was most likely to detect any changes. A and B in Figure 4.9 show the change in amplitude of response, measured at the peaks of the B-wave and PhNR, and C-D show the average waves at the baseline and after 4 weeks of OHT per group. The median B-wave amplitude of the NT eyes at the second recording was similar to baseline (median B-wave change: -1.8% for LPS-NT and -2% for Sal-NT, p = 0.84). For the OHT eyes there was notable loss of amplitude of the B-wave (LPS-OHT -34.2%, Sal-OHT -42.6%, p = 0.93). Comparable changes were seen in the PhNR amplitude, where the median difference in the LPS-NT and Sal-NT groups was -0.93% and -16.6%, respectively and -35.1% for LPS-OHT and -34.6% for Saline-OHT. However, these differences were not statistically significant (p > 0.05). In contrast to what was observed in the dendritic analysis, where dendritic retraction was much more moderate in the LPS-OHT group, the reduction in ERG amplitude was similar across the OHT groups, with the most significant changes observed in the B-wave (LPS-NT vs LPS-OHT p=0.03, Sal-NT vs Sal-OHT p=0.04).

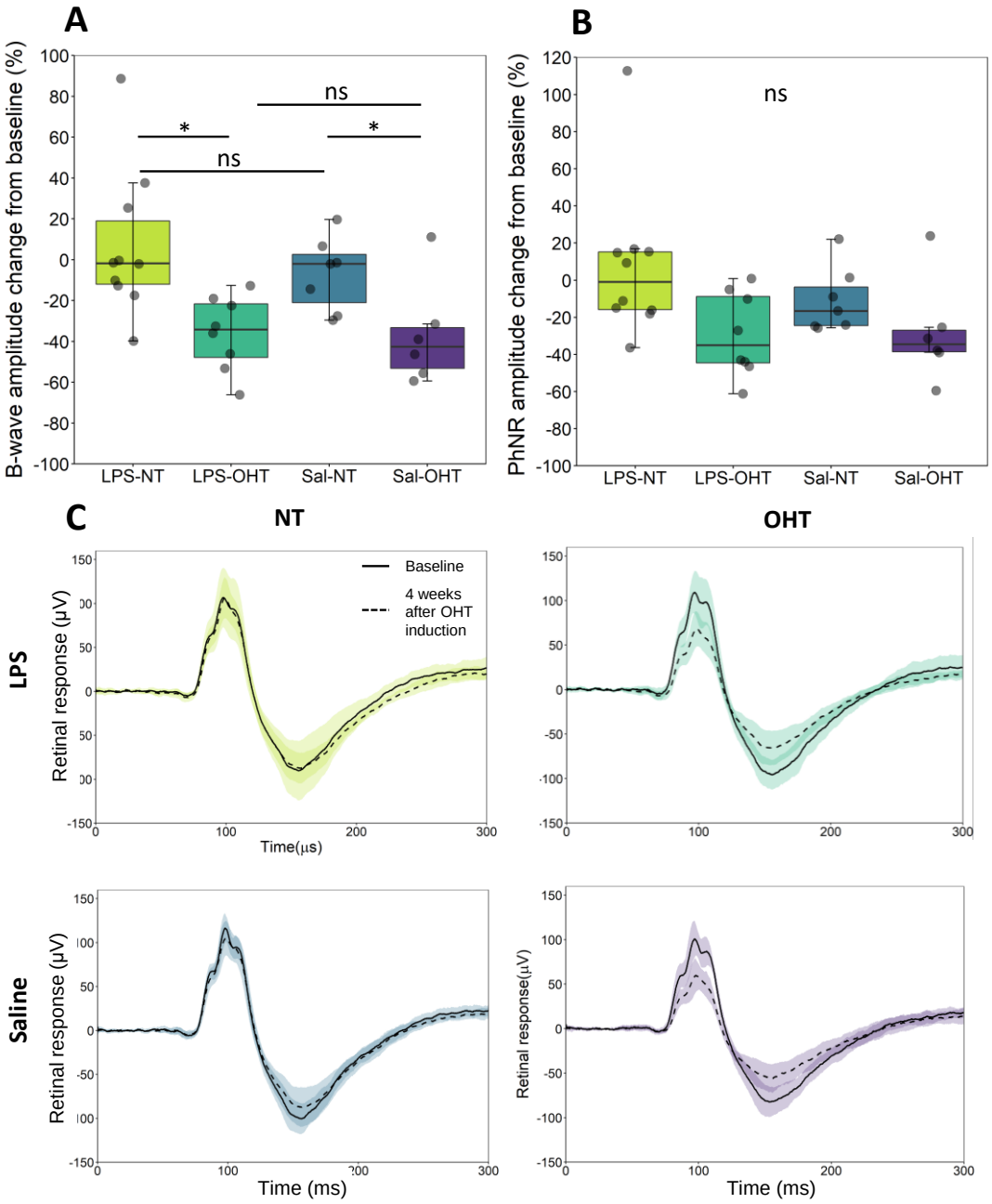

Figure 4.9 Changes in retinal response (B-wave and PhNR) after 4 weeks of OHT and LPS induced systemic inflammation. (A-B) Percentage of amplitude change of B-wave and PhNR between baseline recording and recording obtained at the end of the experiment. Boxplot middle line = median, lower hinge = 25% quartile, upper hinge =75% quartile, lower whisker = smallest observation greater than or equal to lower hinge -1.5 * IQR, upper whisker = largest observation less than or equal to upper hinge + 1.5 * IQR, Kruskal Wallis followed by Dunn's Test * $p<0.05$, ns $p>0.05$. (C) Average retinal response per group before the onset of experiments and at the end of the experiment. The solid line indicates the baseline response and the dashed line the final response.

4.3.2.6 RGC density

RGC density in retinas, after 4 weeks in this experimental protocol, was calculated via immunofluorescent labelling with an RGC specific marker, RBPMS. 8 retinas from 4 animals (LPS n = 2, Saline n = 2) were labelled and imaged using the protocol described in 2.9. For every retina, RGC density was calculated as the average count from a total of 4 images (1 per retinal quadrant), taken from the mid-peripheral area of the retina as shown in Figure 2.8. RBPMS+ cells were counted as described in 2.10. Figure 4.10 shows the average density of RBPMS+ cells per group. Cell counts across all NT retinas yielded similar results with small variability (Average ± SD per mm^2: LPS-NT 2,507±29, Sal-NT 2,568±88). In the OHT eyes, the average RBPMS+ density from the two retinas from animals in the LPS group was 1,265 ± 862/mm^2 (-50% compared to LPS-NT), while in the Saline group it was 525±67/mm^2 (-80% compared to Saline-NT). While there is a substantial difference between the OHT groups, it is worth noting the small sample size of all groups, and high variability in the LPS-OHT retinas. As evident in Figure 4.10, the difference between LPS-OHT and Saline-OHT in this dataset is mainly driven by one datapoint in the LPS-OHT group, which corresponds to the OHT retina with the lowest IOP increase as shown in Figure 4.10 C. Although RGC density in OHT retinas was decreased in both groups compared to their respective controls with the effect being more marked in Saline-OHT retinas, due to the small sample size no statistical significance test were conducted for this dataset.

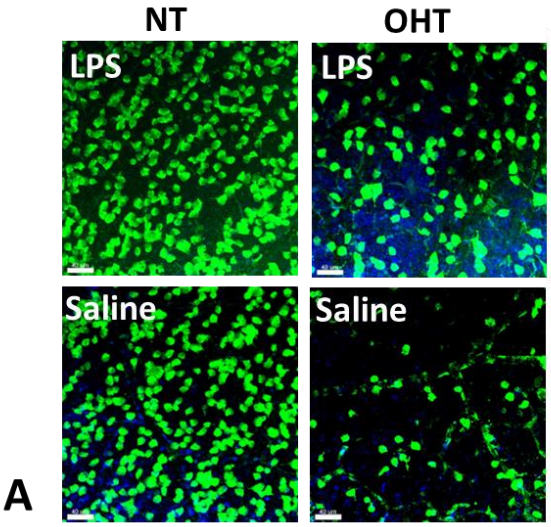

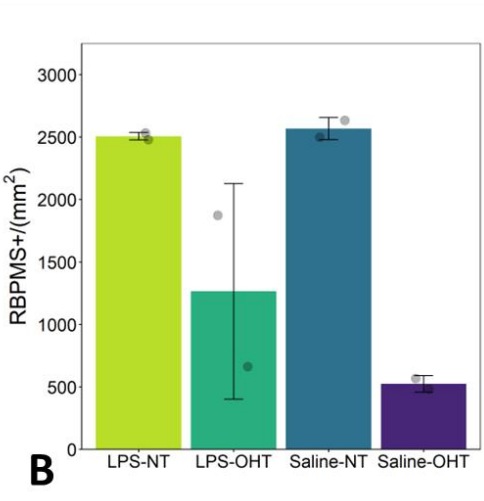

C

Retina	IOP AUC	RGC density / mm²
LPS-NT (1321)	451	2,528
LPS-NT (1322)	497	2,486
Sal-NT (1323)	534	2,506
Sal-NT (1324)	546	2,631
LPS-OHT (1321)	**774**	**656**
LPS-OHT (1322)	**567**	**1,875**
Sal-OHT (1323)	**892**	**572**
Sal-OHT (1324)	**844**	**478**

Figure 4.10 RGC density in OHT and NT retinas after 4 weeks of experimental glaucoma and LPS or saline injections. (A) Representative images of RBPMS labelling of RGCs (green labelled cells). Scale bars = 40µm (B) Density of RBPMS labelled cells per mm^2. Reduced density was observed in OHT retinas. The average density in Saline-OHT retinas was notably lower than LPS-OHT retinas. However, as seen in (C) the datapoint driving this difference (highlighted in yellow) corresponds to the retina with significantly less IOP increase as summarised by the IOP AUC value.

4.3.2.7 Microglial morphology

Microglial process retraction is a sign of microglial activation. Therefore, in order to assess the microglial response, the complexity of microglial processes was analysed. Microglia from 8 retinas (n= 4 rats, 2 per group) were labelled with IBA1 as described in 2.9. A total of 4 images, 1 per retinal quadrant, were obtained from the mid-peripheral region of each retina. From each image, 4 to 5 microglia were reconstructed following the protocol

described in 2.11. Figure 4.11 (A) shows examples from NT and OHT retinas in which resting microglia have elongated processed and activated microglia retracted processes. Figure 4.11 (B) Shows the results of Sholl analysis (3μm intervals) and total process length analysis from microglial reconstructions. Microglial processes were significantly retracted in both OHT groups but there were no significant differences between the LPS and Saline groups in neither NT nor OHT retinas. The microglial Sholl AUCs (±SD) were: LPS-NT 185 ± 58, LPS-OHT 73 ± 27, Sal-NT 198 ± 41, Sal-OHT 82 ± 33 (LPS-NT vs LPS-OHT $p < 0.001$, Sal-NT vs Sal-OHT $p < 0.001$, LPS-NT vs Sal-NT $p = 0.45$, LPS-OHT vs Sal-OHT $p = 0.43$). The total process length (μm) (±SD) was: LPS-NT 294 ± 96, LPS-OHT 104 ± 48, Sal-NT 326 ± 63, Sal-OHT 116 ± 50 (LPS-NT vs LPS-OHT $p < 0.001$, Sal-NT vs Sal-OHT $p < 0.001$, LPS-NT vs Sal-NT $p = 0.35$, LPS-OHT vs Sal-OHT $p = 0.48$).

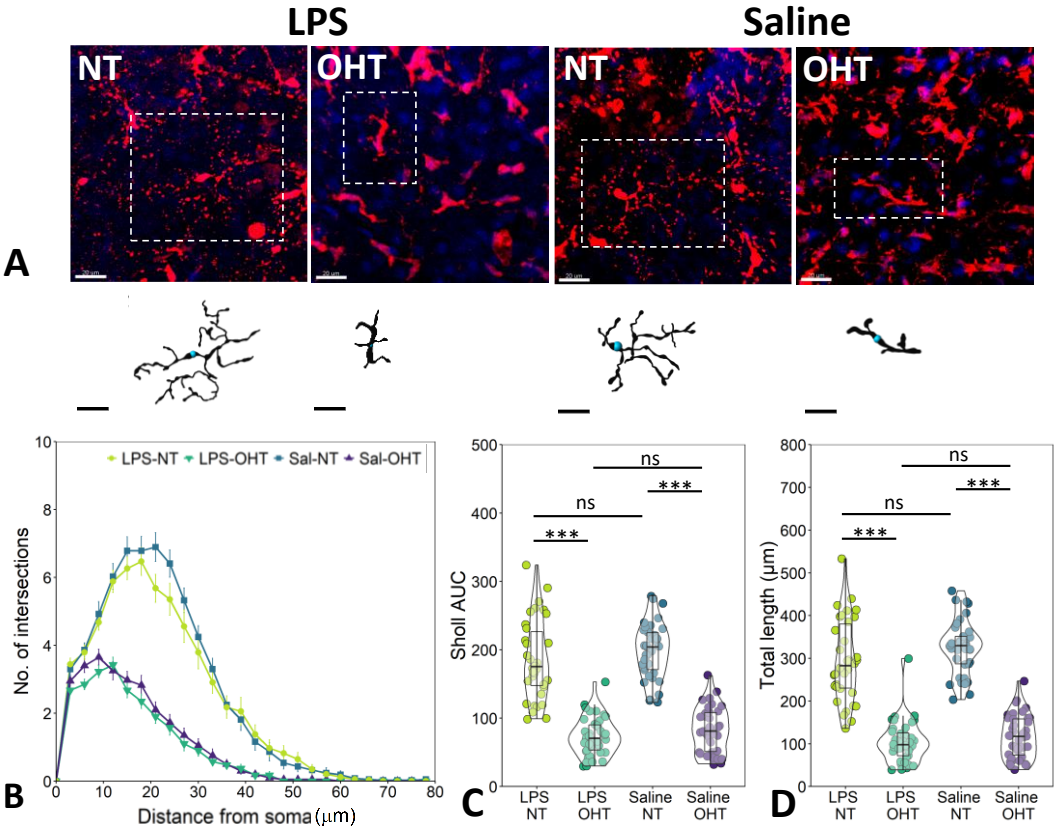

Figure 4.11 Analysis of microglial morphology after induced OHT and immune priming by LPS. Microglia from 8 retinas, n = 2 retinas in each group (microglia n = 34 in LPS-NT, 40 in LPS-OHT, 38 in Saline-NT, 40 in Saline-OHT) were reconstructed, and the complexity and length of their processes were analysed. (A) Representative resting microglia from NT retinas, and activated microglia from OHT retinas with their reconstructions. Scale bar = 20μm. (B,C) Average Sholl profile and Sholl AUC per group. Sholl profile error bars = SEM. (D)Total process length (μm) per group. Kruskal Wallis with Dunn's post hoc *** $p<0.001$, ns $p>0.05$.

4.3.3 Estimation of the effect of IOP increase and immune activation on dendritic morphology and retinal response

RGC dendritic retraction was more moderate in animals under the LPS protocol in this experiment. The IOP increase was also more moderate in that group though the difference comparing to the Saline group was not as significant. Since an increase in IOP is an established factor driving dendritic loss and decreasing functional retinal response, it is important to consider whether the reduced RGC damage in the LPS treated animals is related to reduced IOP or to a protective effect of repeated LPS injections. To examine

these interactions the relationship of two predictors, either IOP AUC or IOP Peak and the group the animal was in (LPS, Saline), with Sholl AUC, B-wave and PhNR was examined via multiple linear regression. The model is described by the following equation:

$$Y = b_0 + b_1X_1 + b_2X_2 + b_3X_1X_2$$

Where Y is the dependent variable Sholl AUC, B-wave, or PhNR; b_0 is the intercept; b_1 is the regression coefficient of X_1, which corresponds to IOP AUC or IOP peak; b_2 is the regression coefficient of X_2, which corresponds to the experimental group (LPS, Saline); and b_3 is the regression coefficient of the interaction between X_1 and X_2 (X_1X_2).

To assess the effect of IOP in the whole cohort, regardless of experimental group, simple linear regressions were also conducted. These models are described by the following equation, which again includes Sholl AUC, B-wave, or PhNR as the dependent variable Y, and IOP AUC or IOP peak as the independent variable X1:

$$Y = b_0 + b_1X_1$$

As shown in Figure 4.12, both the IOP AUC and IOP peak had a negative linear relationship with Sholl AUC (simple linear regression: $R^2 = 0.51$ for IOP AUC and $R^2 = 0.45$ for IOP peak) and were shown to be significant predictors of the value of Sholl AUC in both simple linear regression ($p < 0.001$) and multiple regression models ($p < 0.05$). On the other hand, the interaction with the experimental group Saline or LPS was not shown to be a significant predictor in the multiple regression models ($p > 0.05$), even though the Saline group slopes were slightly steeper indicating a trend for more reduced Sholl AUC in the Saline group than the LPS group with the same level of IOP increase. In relation to changes in b-wave amplitude, increased IOP AUC showed some association with more amplitude reduction from baseline (more negative percentage change from baseline) ($R^2 = 0.16$), which was significant in the single linear regression ($p < 0.05$) but not the multiple linear regression ($p > 0.05$). The interaction of IOP AUC and group was not significant in the multiple linear regression ($p > 0.05$). A similar but more reduced trend was seen in the relationship between IOP AUC and PhNR percentage change from

baseline (R^2 = 0.11), however the effect was not statistically significant, neither was the interaction with treatment group. Similar relationships were seen between the IOP Peak and b-wave percentage change from baseline (R^2 = 0.28, where higher IOP peaks were significantly associated with more severe b-wave amplitude reduction in both simple and multiple linear regression ($p < 0.05$). The interaction between IOP Peak and treatment group, LPS or Saline, did not come up as a significant predictor ($p > 0.05$). In relation to the PhNR, higher IOP peaks were slightly associated with more amplitude loss (R^2 = 0.12) but in this case the effect of IOP Peak was not significant in any of the regressions ($p > 0.05$), neither was the interaction between IOP Peak and treatment group ($p > 0.05$).

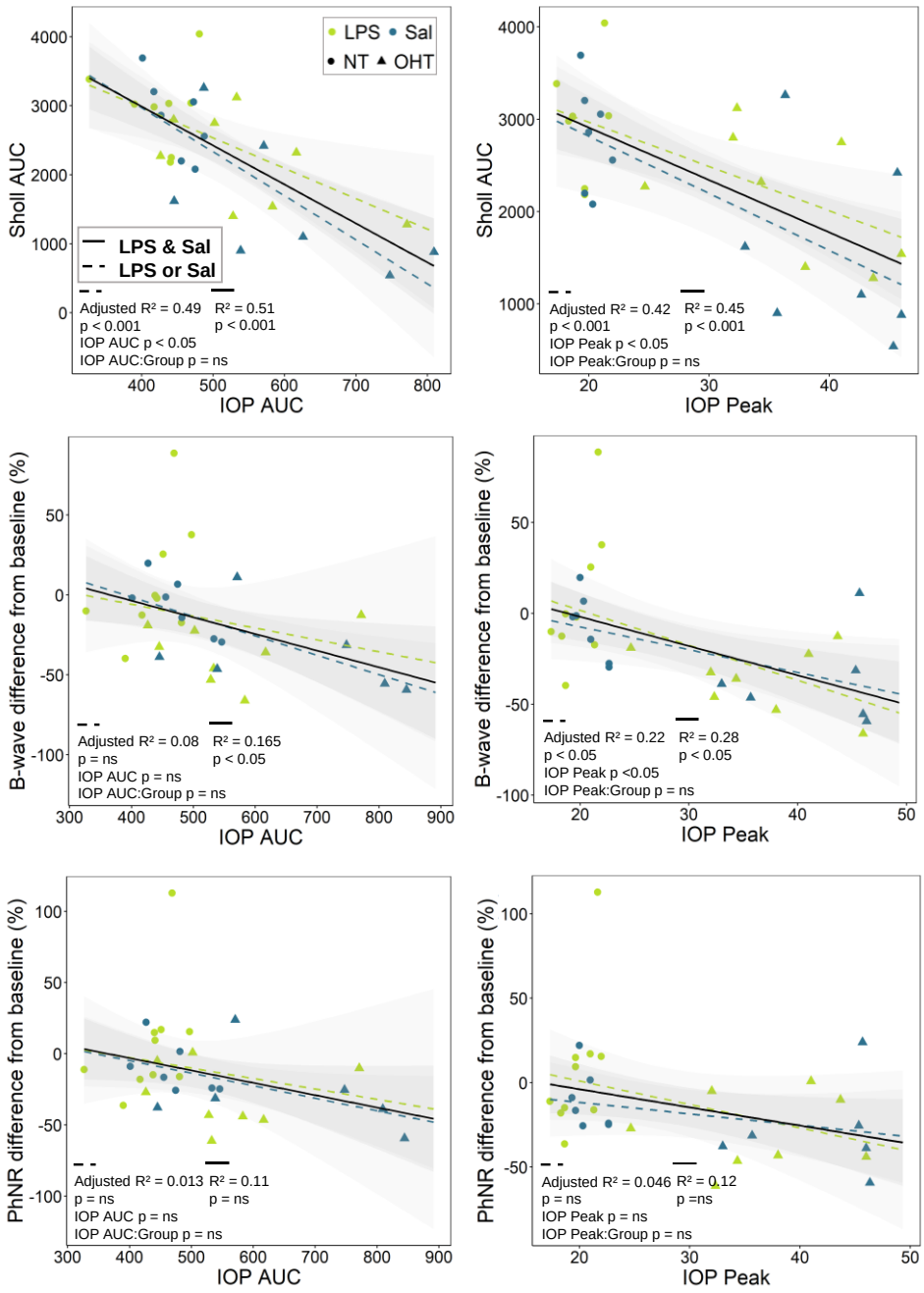

Figure 4.12 Simple linear regression of the relationship of IOP with Sholl AUC (as average per retina) and ERG amplitude, and multiple linear regression examining the interaction of IOP and LPS/Saline. The shape of datapoints indicates whether it corresponds to NT (circle) or OHT (triangle) eye, and the colour shows the experimental group, LPS (green) or Saline (blue). The solid line corresponds to the slope of simple linear regression (LPS and Saline pooled) and the dashed lines to the multiple regression slopes when group = LPS (green) or group = Saline (blue). For the multiple regression, the adjusted R^2, p value of the model, p value of IOP, and p value of the interaction of IOP with group are shown at the lower left corner of each graph, under the dashed line. The R^2 and p value of simple regressions are shown at the central lower part of the graph, under the solid line. The significance level is at $p < 0.05$.

4.4 Discussion

The aim of this chapter was to use a model of induced OHT in combination with LPS-induced systemic inflammation to investigate whether the latter would exacerbate retinal ganglion cell damage in experimental glaucoma. The first exposure to LPS triggered an inflammatory response as evidenced by IL-6 upregulation and 5% weight loss, resulting from inflammation-induced appetite suppression. IL-6 concentration in blood serum 2 hours after LPS administration was approximately 1,400pg/ml, which is comparable with previous studies quantifying IL-6 in rat sera 2 to 4 hours following LPS administration at 2 mg to 50 µg per kg of body weight (Gomez *et al.*, 2008; Dokladny *et al.*, 2010). However, subsequent weekly injections did not produce the same effect, with no apparent symptoms of inflammatory response as assessed via weight monitoring and IL-6 quantification. The reduced response to repeated exposure to bacterial LPS has been reported elsewhere, including rats and humans and is associated with reduced pro-inflammatory cytokine expression, including IL-6 (West and Heagy, 2002). In rats, LPS tolerance has been shown to last 2 to 3 weeks (Sanchez-Cantu, Rode and Christou, 1989; Ziegler-Heitbrock, 1995). Therefore, to limit the effect of LPS tolerance, the protocol was amended to allow a longer interval of 14 days between the first and second LPS challenge. In addition, the 1st LPS dose was given 3 days after OHT induction to ensure that in case LPS tolerance persisted, there would be at least one time point of concurring systemic inflammation and OHT, which in this model is typically more marked during the first week. The second LPS injection administered after a 14-day interval induced greater weight loss (3%) compared to no loss after the 2nd injections administered after a 7-day interval, but this was not associated with IL-6 upregulation. Nevertheless, the weight loss was a promising indication that the increased interval between injections limited the tolerance effect. Systemically delivered LPS can induce uveitis and is used in rat models of experimentally induced uveitis (EIU) (Forrester, Worgul and Merriam, 1980; Rosenbaum *et al.*, 1980). However, the susceptibility of different rat strains to LPS-induced EIU varies vastly between rat strains, likely due to genetic differences. Lewis rats are very susceptible, while Brown Norway rats are

resistant (Herbort, Chan and Nussenblatt, 1990; Hoekzema *et al.*, 1992; de Kozak *et al.*, 1994). Hoekzema and colleagues detected no signs of uveitis in Brown Norway rats receiving similar amounts of systemic LPS as used in this thesis, despite still producing a systemic IL-6 response. In agreement with those findings, in the experiments in this thesis there were no detectable signs of uveitis. These observations emphasise the importance of selecting an appropriate rat strain and highlights the suitability of the Brown Norway rat. The protocol developed in this chapter produced measurable inflammation related changes (weight loss and IL-6 upregulation), from which the animals recovered fully without demonstrating signs of severe ill health at any point throughout the experiments. Acknowledging the limitation of not achieving an equal response following repeated LPS administration, but given that some response was seen after the second dose when administered in a 2-week interval, the model described in the second part of this chapter 4.3.1 was maintained in the next experiment of this thesis to ensure consistency.

Systemic inflammation did not exacerbate dendritic loss in this model. In the first experiment (3 weekly LPS doses) there was an underlying trend for decreased dendritic complexity in the RGCs from OHT retinas, which did not reach statistical significance. The dendritic loss was at a similar level across OHT eyes of both LPS and saline injected animals, however the number of cells was relatively small (~30 cells per group). In the second experiment (two fortnightly LPS doses), dendritic analysis is of particular interest as it showed that in RGCs from OHT eyes of the LPS group there was no significant loss of dendritic arborisation comparing to NT eyes, as opposed to RGCs from OHT eyes of the Saline group that had significantly more dendritic loss. At the same time, IOP increase in the LPS OHT group was lower than in the Saline OHT group. The difference was not statistically significant, but this trend was observed in both experiments in this chapter. In most mammals, including rats, prostaglandin is released following exposure to LPS as part of the inflammatory response (Ueno, Narumiya and Ogorochi, 1982; Fu *et al.*, 1990). Prostaglandins can decrease IOP via binding to receptors in the ciliary muscle, which results in ciliary muscle relaxation and disrupts the extracellular matrix turnover to increase scleral permeability and facilitate aqueous outflow

(Winkler and Fautsch, 2014). Although prostaglandin release and its effect on IOP was not assessed in this study, it might have played a role in the lower IOP trend observed in the LPS groups in both experiments in this chapter. By consequence the lower IOP could have moderated the OHT challenge on RGCs. Multiple linear regression with both IOP and treatment group (LPS or saline control) as interacting predictors showed that the level of IOP increase was a significant predictor of dendritic complexity, but the administration of LPS did not provide a significant additional effect, even though the Saline slope of the regression was steeper, indicating that for the same amount of IOP increase, dendritic loss was more severe in the saline group. Preliminary analysis of RGC loss in OHT retinas was more severe in the Saline group compared to the LPS group, but this analysis is limited by the small sample size per group (n=2), and the fact that in one of the LPS-OHT samples IOP increase was lower comparing to the rest of the samples, which could have skewed the results.

Although RGC morphological changes were evident in the Saline group but limited in the LPS, functional loss was similar in both OHT groups. Reduction of amplitude was observed in the photopic b-wave (LPS-OHT -34.2%, Sal-OHT -42.6%) and PhNR (LPS-OHT -35.1%, Saline-OHT -34.6%). The PhNR has been established as an inner retina specific component of the ERG that is sensitive to both human glaucoma (Colotto *et al.*, 2000; Viswanathan *et al.*, 2001; Drasdo *et al.*, 2002) and experimental OHT damage in primates (Viswanathan *et al.*, 1999), rabbits (ElGohary and Elshazly, 2015), rats (Huang *et al.*, 2018) and mice (Chrysostomou and Crowston, 2013; Crowston *et al.*, 2015). Many of those studies report minimal changes to the b-wave. However, it has been shown that the b-wave is reduced in s-cone specific ERGs in human Primary Open Angle Glaucoma (Drasdo *et al.*, 2002). In addition, in a chronic OHT rat model, the b-wave amplitude was significantly reduced after four weeks and partly recovered by week 8, when IOP returned to basal values (Grozdanic *et al.*, 2003). In an optic nerve transection (ONT) rat model the b-wave was also significantly affected with the authors noting that the findings indicate RGCs contribute to the rat photopic b-wave (Bui and Fortune, 2004). The b-wave is an ERG component sensitive to ischemia

(Block, Schwarz and Sontag, 1992; Block and Schwarz, 1998). It has been shown that in mice retinal perfusion is not affected by IOP reaching 50mmHg or even 70mmHg (Kong *et al.*, 2012). IOP levels reported in the study by Grozdanic *et al.*, were below 50mmHg, and in the study by Bui and Fortune, it is unlikely that the ONT model would obstruct retinal perfusion. In the present study, IOP generally peaked between 30-50mmHg, suggesting that impaired perfusion is unlikely to be a significant factor. However, the possibility of transient undetected spikes resulting in temporary ischemic events cannot be excluded. Comparing the structural and functional findings, the loss of ERG amplitude in the Saline OHT group indicated a notable loss of function, which is in agreement with the dendritic atrophy observed via Sholl analysis. Notable functional deficits were also seen in the LPS OHT group despite dendritic atrophy being quite minimal in the same group. Further studies are required to determine the precise relationship between structural RGC changes and functional measurements. It has been suggested before that structural changes are detectable prior to functional changes in glaucoma (Kerrigan-Baumrind *et al.*, 2000; Keltner *et al.*, 2006). However, these studies used patients' visual field test to assess retinal function. In a study using PERG to assess retinal function, it was indicated that changes in PERG precede RNFL thickness loss (Banitt *et al.*, 2013). These comparisons are complex and likely to relate more to the precision of measurements.

Signs of systemic inflammation have been associated with cognitive decline in animal models and in Alzheimer's disease (Teeling *et al.*, 2007; Holmes *et al.*, 2009; Püntener *et al.*, 2012; Ide *et al.*, 2016) Moreover, increased bacterial counts have been found in mouthwash specimens from patients with glaucoma (Astafurov, Elhawy, *et al.*, 2014). In the experiments in this chapter, systemic inflammation did not result in more severe outcomes in terms of both RGC structure and function in a chronic OHT model. In addition, there was a trend for lower IOP in the OHT eyes of the LPS groups. A discussion of these findings, as well as findings of the next chapter (Chapter 5) that investigated the effect of complement inhibition on the model developed here, are further discussed in context with relevant literature in Chapter 7.

Chapter 5. Classical complement pathway inhibition in experimental glaucoma with LPS induced inflammation

5.1 Introduction

The complement system and in particular the classical pathway have been implicated in glaucoma via numerous studies reporting upregulation of complement proteins in both experimental glaucoma and human glaucomatous eyes, as detailed 1.6.4. The role of complement in glaucoma is not clear, nevertheless complement inhibition in experimental models has shown promise as a neuroprotective strategy. Inhibiting the classical pathway protected RGCs in experimental glaucoma (Williams *et al.*, 2016), and backcrossing the DBA/2J mice strain with a functional C5 allele aggravated glaucomatous progression (Howell *et al.*, 2013). In addition, retinal gene therapy using a complement C3-targetting regulator was shown to have a neuroprotective effect on DBA/2J mice (Bosco *et al.*, 2018). However, interestingly, systemic complement inhibition using a C3 knockout model increased glaucomatous damage in DBA/2J mice (Harder *et al.*, 2017).

As inhibition of the classical pathway of the complement system, via intravitreal C1inhibitor administration, was shown to be neuroprotective in a similar experimental glaucoma model, the scope of the experiment in this chapter was to see what effect C1 inhibition would have on glaucomatous progression in the presence of moderate to low level systemic inflammation. C1 inhibition delivered via intravitreal injections was added as an extra layer to the model used in the second part of Chapter 4.

5.2 Experimental design

Following the protocol in (Williams *et al.*, 2016) with small modifications, 5µl of C1 inhibitor 100 Units/ml (n=8) (C1 esterase inhibitor; CINRYZE; Shire) or vehicle only, PBS (n=8), was administered 24 hours before OHT induction unilaterally, via intravitreal injections. A total of 5 doses were given in 4-5-day intervals. All animals received IP LPS injections (500µg per kg of body weight) to prime the immune system 3 days after OHT induction and again after 14

days. Figure 5.1 is a schematic overview of the timepoints of the interventions. In this cohort it was necessary to repeat bead injections in order to achieve OHT. Animals received either 1 or 2 additional bead injections on days 3 and/or 10 after initial OHT induction (this will be further discussed in the IOP results part of this chapter). Prior to the beginning of the experiment and during the last 2-3 days ERG recordings were obtained following the protocol in 2.3. At the end of the experiment retinas were harvested and most of the tissue was assigned for DiOlistic labelling, using the protocol described in 2.8. The retinas from half of the animals were split in two, with one part being used for DiOlistics and one part being used for immunofluorescent labelling with RBPMS and IBA1, as described in 2.9.

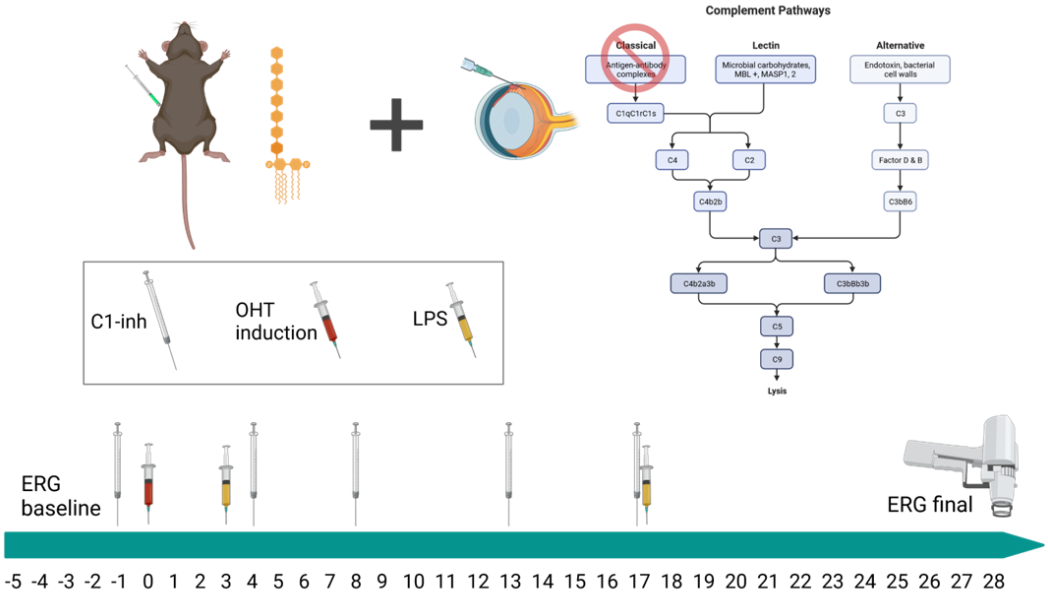

Figure 5.1 Experimental setup for investigating the effect of C1 inhibitor on immune primed animals with OHT. A cohort of 16 male BN rats was administered either 5µl of C1 inhibitor (n=8) or PBS (n=8) via intravitreal injections in one eye. After 24 hours OHT was induced at the same eye. A total of five C1 inhibitor/PBS doses were given in 4 to 5-day intervals. All rats in this cohort received IP LPS injections (500µg per kg of body weight) to prime the immune system 3 days after OHT induction and again after 14 days. Prior to the beginning of the experiment and during the last 2 to 3 days ERG recordings were obtained, and at the end of the experiment retinas were harvested and processed via DiOlistic or immunofluorescent labelling.

5.3 Results

The results are presented per eye group. The OHT eyes and contralateral control NT eyes of the C1 inhibitor group are labelled as C1inh-OHT and C1inh-NT, respectively. Similarly, the OHT eyes in the PBS group are labelled PBS-OHT and their contralateral NT controls are labelled PBS-NT.

5.3.1 Weight monitoring

All animals in this cohort received IP LPS injections for immune system priming. Their weight was recorded prior to LPS administration and every day for the following 3 days as well as after 1 week. The percentage weight change in 24 hours following each injection as well as the weight throughout the monitored period are shown in Figure 5.2. Weight loss was observed after both injections, with the effect being more notable after the first injection, and animals gradually regained their weight in agreement with previous experiments in this thesis. The percentage change following each injection was at a slightly lower level than in 4.3 but comparable. Across the whole cohort weight loss after the 1st and 2nd LPS injection was -3.7 ± 1.2% and -1.6 ± 1.4%, respectively. The effect was evenly distributed across the C1 inhibitor and PBS groups, without any significant differences (C1 inhibitor: 24 hours after 1st LPS -3.5 ± 1% and 2nd LPS -1.8 ± 1.3% (p=0.06); PBS: 24 hours after 1st LPS -4 ± 1.3% and 2nd LPS -1.3 ± 1.5% (p = 0.04); 1st LPS: C1inh vs PBS p = 0.9, 2nd LPS C1inh vs PBS p = 1).

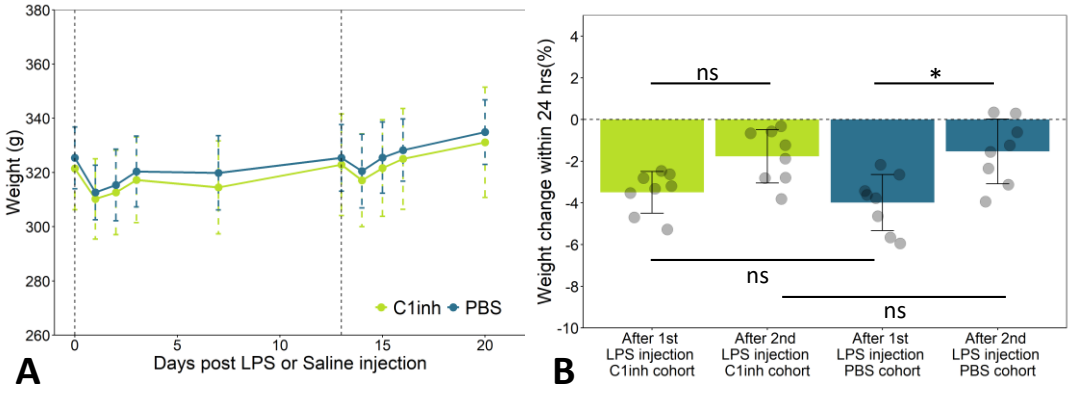

Figure 5.2 Weight loss triggered by LPS induced inflammation. The effect of LPS on body weight was similar across both groups (C1 inhibitor in green and PBS in blue). (A) Average weight profile per group following LPS administration. The timepoints of injections are indicated by the dashed lines. (B) Percentage weight change in 24 hours following each injection. Error bars = SD, one-way ANOVA followed by Tukey's HSD, ns $p > 0.05$, * $p < 0.05$.

5.3.2 IOP analysis

OHT was induced unilaterally following the protocol described in 2.4. One day before the bead injections, the same eyes had undergone intravitreal injections of either C1 inhibitor or PBS. As a result, some eyes were hypotonic and the low pressure in the eye globe made it challenging to distribute the beads well. This lowered the rate of OHT achieved in this cohort by the 3rd day following the injections, by which timepoint IOP was expected to have increased in this model. Therefore, additional bead injections were performed at that point to 7 eyes from the C1 inhibitor group and 5 eyes from the PBS group. As more intravitreal injections were given, 5 eyes in the C1inh group and 5 eyes in the PBS needed one more additional bead injection at day 10. In total, 4/8 eyes received 2 bead injections and 4/8 eyes received 3 bead injections in the C1 inhibitor group, and in the PBS group 6/8 and 2/8 eyes received 2 and 3 bead injections, respectively. The individual IOP profiles and time points of repeated injections can be found in *Appendix B: Intraocular pressure profiles,* and average IOP profiles as well as mean IOP, IOP AUC and Peak IOP are summarised in Figure 5.3 Eventually it was possible to achieve sufficient IOP increase in all experimental eyes. The mean IOP in

mmHg per group was: C1inh-NT= 19.9 ± 1.33, PBS-NT= 19.6 ± 1.6, C1inh-OHT= 25.7 ± 4.3, PBS-OHT= 24.7 ± 4.5. The difference between OHT and the contralateral controls was statistically significant within both the C1inh and PBS groups, C1inh-OHT vs C1inh-NT $p = 0.008$, and PBS-OHT vs PBS-NT $p = 0.02$. Between C1inh and PBS OHT groups, as well as C1inh and PBS NT groups there were no statistically significant differences ($p > 0.05$). The IOP AUC results showed a similar pattern: C1inh-NT = 571.4 ± 35.7, PBS-NT = 565.4 ± 43.6, C1inh-OHT = 785.7 ± 155.8, PBS-OHT = 744.8 ± 166.8. The statistical significance results were: C1inh-OHT vs C1inh-NT $p = 0.006$, PBS-OHT vs PBS-NT $p = 0.02$, C1inh-OHT vs PBS-OHT $p = 0.9$, C1inh-NT vs PBS-NT $p = 1$. As an average IOP peaked at 46.5 ± 6.6 for C1inh-OHT and 45 ± 9.7 for PBS-OHT ($p = 0.9$). Among the NT eyes, the average IOP peak was 24.4 ± 1.3 and 24.7 ± 1.8 for C1inh and PBS, respectively ($p = 1$). The difference of C1inh-OHT vs C1inh-NT, and PBS-OHT vs PBS-NT was statistically significant in both cases, $p < 0.001$and $p < 0.001$, respectively.

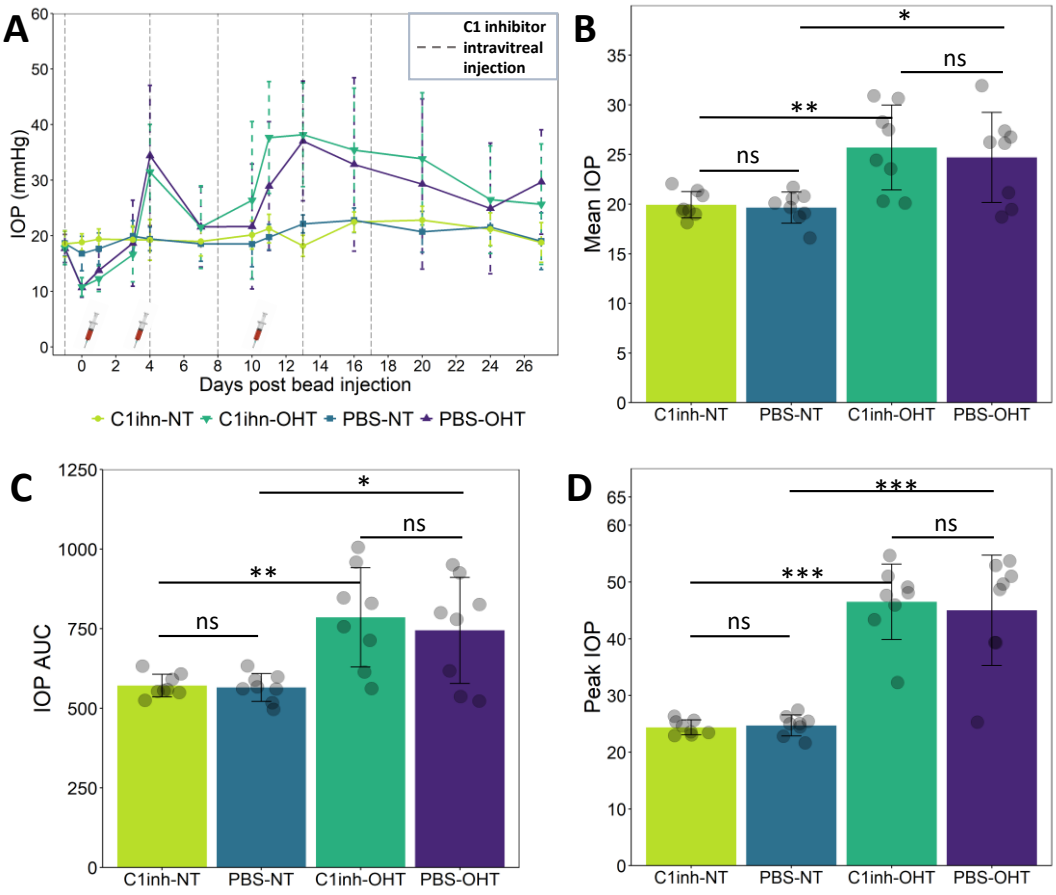

Figure 5.3 IOP analysis of the cohort administered with intravitreal C1 inhibitor or PBS unilaterally, while having OHT at the same eye, and LPS induced low level systemic inflammation. C1inh-NT n = 8, C1inh-OHT n = 8, PBS-NT n = 8, PBS-OHT n = 8 (n refers to eyes). (A) Average IOP profile per group. The dashed lines indicate the time points of C1 inhibitor or PBS intravitreal administration, and the injection symbols indicate the time points of bead injections. Error bars = SD, (B, C, D) Mean IOP, AUC of the IOP, Peak IOP. Error bars = SD, One-Way ANOVA with Tukey's HSD ns $p > 0.05$, * $p < 0.05$, ** $p < 0.01$, *** $p < 0.001$.

5.3.3 Dendritic analysis

5.3.3.1 Assessment of C1 inhibition on OHT related dendritic loss

Whole or half retinas from 16 rats (n = 8 C1 inhibitor group, n = 8 PBS group) were labelled using DiOlistic labelling following the protocol described in 2.8. A total of 119 RGC cells were reconstructed (C1inh-NT n = 33, C1inh-OHT n = 28, PBS-NT n = 27, PBS-OHT n = 31) as described in 2.8.5. Figure 5.4 summarises the dendritic morphology of the cells as assessed by Sholl

analysis, the total dendritic length, and the number of primary, secondary and tertiary+ dendrites. There was some loss in dendritic complexity across the OHT groups, but overall differences between the Sholl AUCs were quite moderate. The mean ± SD Sholl AUC in the C1inh group was: NT = 3,263 ± 1,118, OHT = 2,603 ± 1,237 ($p = 0.06$), and in the PBS group: NT = 2,801 ± 1,305, OHT = 2,470 ± 1,117 ($p = 0.7$); C1inh NT vs PBS-NT $p = 0.2$; C1inh-OHT vs PBS-OHT $p = 0.7$. The total dendritic length followed the same pattern. The total length in μm for the C1inh group was: NT = 4,623 ± 1,545, OHT = 3,662 ± 1,607 ($p = 0.07$); and for the PBS group it was: NT = 4,108 ± 1,852, OHT = 3,552 ± 1,627 ($p = 0.5$); C1inh NT vs PBS-NT $p = 0.2$; C1inh-OHT vs PBS-OHT $p = 0.7$. At the primary dendrite level all groups had very similar numbers of dendrites. The mean number of primary dendrites was: C1inh-NT = 3.7 ± 0.8, C1inh-OHT = 3.3 ± 1.1, PBS-NT = 3.5 ± 1.2, PBS-OHT = 3.4 ± 0.8 ($p > 0.05$). At the secondary level some reduction across both OHT groups started to appear, which was slightly more notable in C1inh-OHT. Average number of secondary dendrites in the C1inh group: NT = 7.1 ± 1.9, OHT = 5.6 ± 2.1 ($p = 0.03$), in the PBS group NT = 7 ± 2.6, OHT = 6.5 ± 1.5 ($p = 0.7$); C1inh NT vs PBS-NT $p = 0.7$; C1inh-OHT vs PBS-OHT $p = 0.1$. The same trend was also seen at the tertiary+ dendrite level, where the average number of dendrites in the C1inh group was: NT = 258.3 ± 103.5, OHT = 185.2 ± 100.6 ($p = 0.03$), and in the PBS group: NT = 247 ± 124.8, OHT = 189.2 ± 119.3 ($p = 0.1$); C1inh NT vs PBS-NT $p = 0.6$; C1inh-OHT vs PBS-OHT $p = 0.9$.

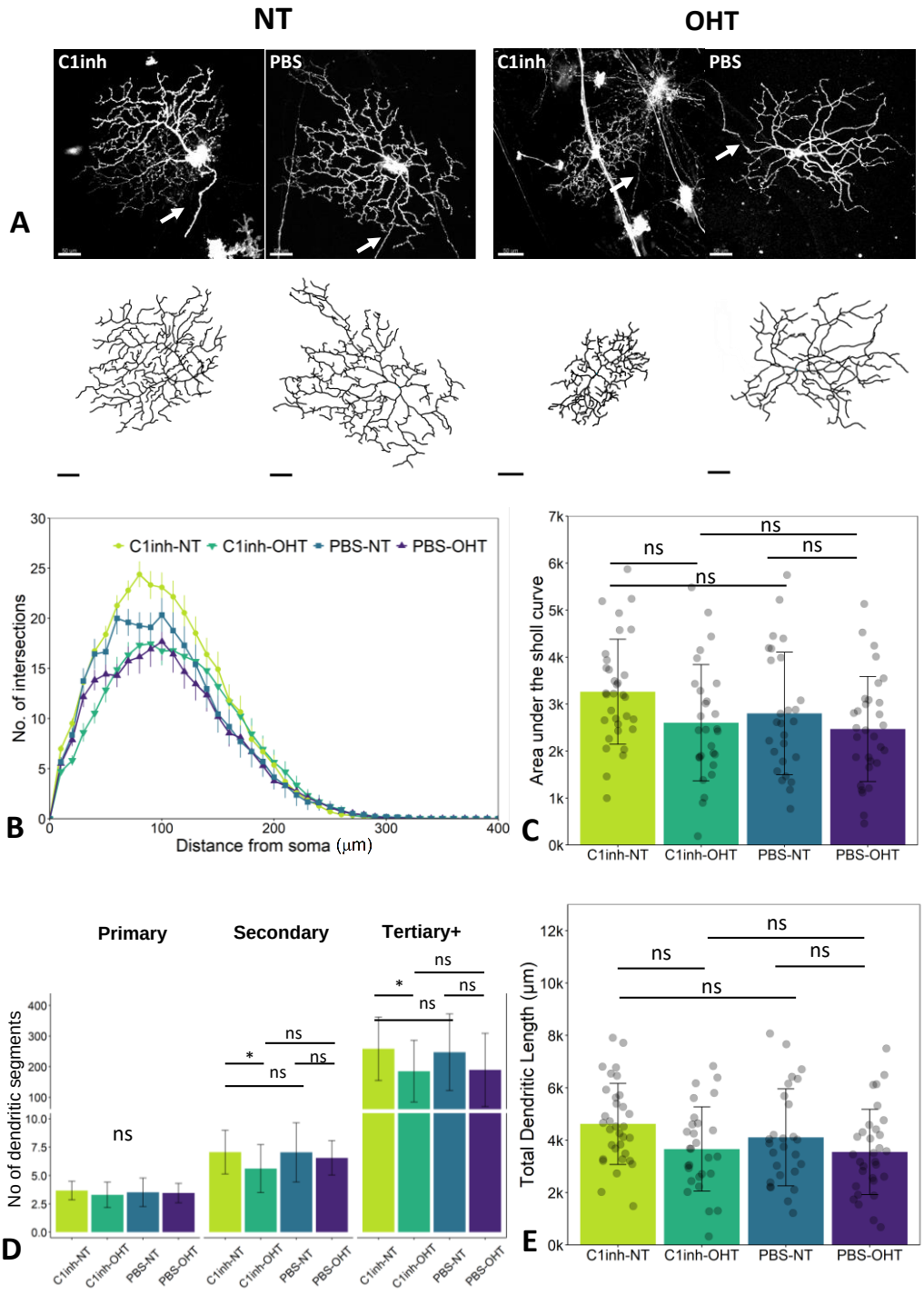

Figure 5.4 RGC dendritic morphology in the cohort with induced OHT, LPS-induced inflammation and intravitreal injections of C1 inhibitor. (A) Representative RGCs and their dendritic reconstructions. The arrows indicate the axons. Scale bars = 50 µm. (B) Sholl analysis showing the number of dendritic intersections to concentric circles as a function of distance from the soma. (C) AUC of the Sholl profile. (D) Number of primary, secondary and tertiary+ dendrites. (E) Total dendritic length in µm. (B-E) Cells per group: C1inh-NT n=33, C1inh-OHT n=28, PBS-NT n=27, PBS-OHT=31. (B) Error bars = SEM. (C,D,E) Error bars = SD. Test = Kruskal Wallis followed by Dunn's test.

5.3.3.2 IOP and Sholl analysis results across the LPS receiving groups

In Chapter 4 there was a repeated, but non-statistically significant, trend for lower IOP in the OHT eyes of LPS receiving animals compared to Saline receiving animals. Examining IOP results across all the OHT groups in this chapter and Chapter 4, which includes three LPS treated groups (plain LPS (LPS), LPS + intravitreal C1inhibitor (LPS(C1inh)), LPS + intravitreal PBS (LPS(PBS))) and the control OHT group treated with saline, it is shown that IOP AUC in the LPS groups that received intravitreal injections of C1inhibitor or PBS was higher than in the LPS group that did not receive intravitreal injections. The difference was significant between the LPS and LPS(C1inh) ($p = 0.03$), but not between LPS and LPS(PBS) ($p = 0.09$). In addition, there was no statistical difference between any of the LPS groups compared to the Saline group (Saline vs LPS $p = 0.5$, Saline vs LPS (C1inh) $p = 0.4$, Saline vs LPS(PBS) $p = 0.7$. There was also no statistical significance between the LPS(C1inh) and LPS(PBS) groups ($p = 0.9$). The mean IOP followed a similar pattern but there were no statistical differences between any groups ($p = 0.2$). However, as shown in Figure 5.5, even though there were no significant differences between the Saline and any of the LPS groups in terms of IOP increase, the Saline Sholl AUC was significantly lower compared to all LPS groups (Saline vs LPS $p = 0.01$, Saline vs LPS(C1inh) $p = 0.02$, Saline vs LPS (PBS) $p = 0.02$), and the Saline Sholl profile demonstrated a left shift compared to LPS Sholl profiles. Contrary, there were no significant differences between the LPS groups, which as shown in Figure 5.5 all had very similar Sholl profiles.

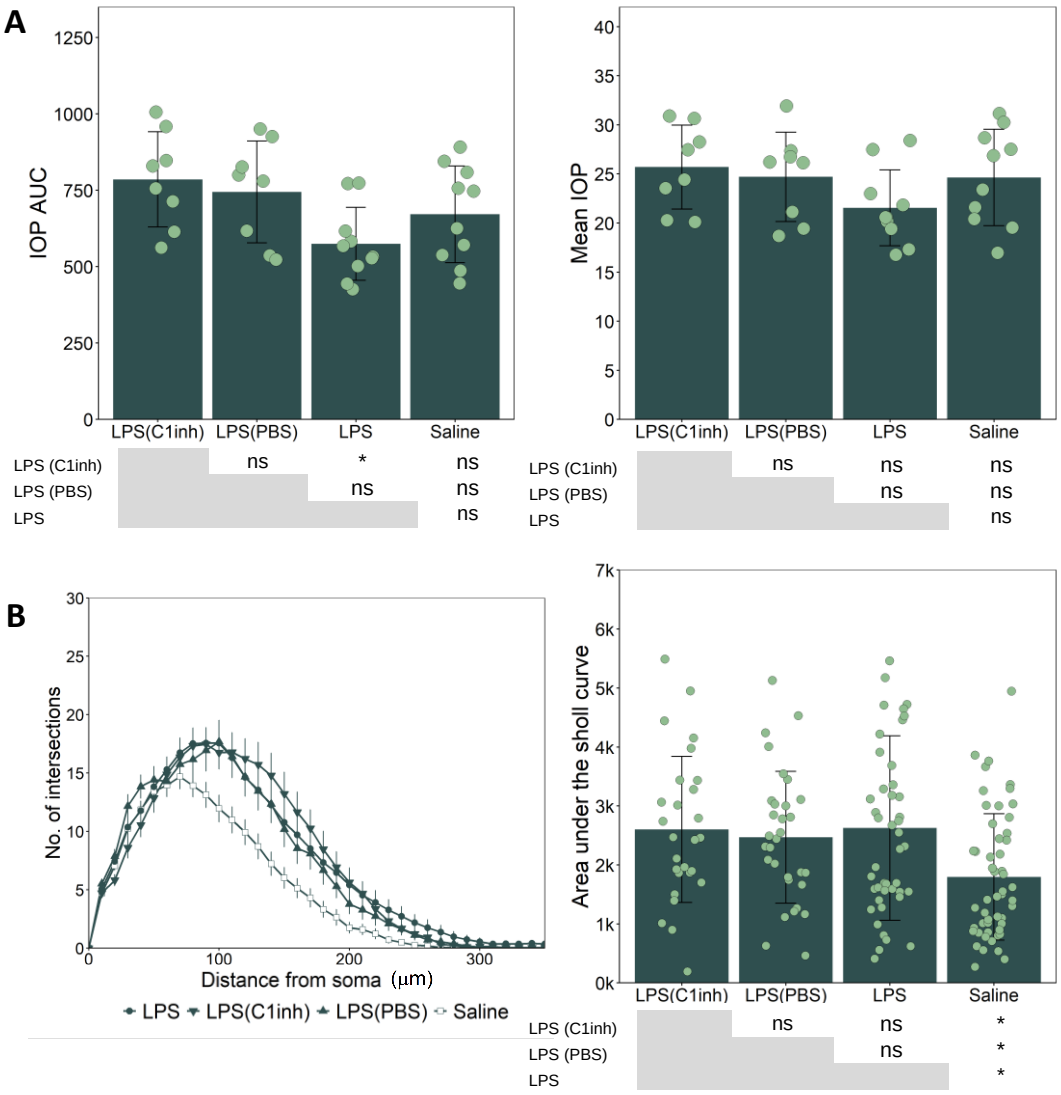

Figure 5.5 IOP and Sholl analysis comparison across OHT eyes of the LPS treated groups and OHT eyes from Saline treated controls. (A) IOP AUC and Mean IOP (mmHg) across groups from n = 8 OHT eyes for LPS(C1inh) and LPS(PBS) and n=10 OHT eyes for LPS and Saline. Error bars = SD. One-way ANOVA followed by Tukey HSD (B) Sholl profiles and Sholl AUC across the same groups. N = 28, 31, 45, 53 cells for LPS(C1inh), LPS(PBS), LPS and Saline respectively. Sholl profile error bars = SEM, Sholl AUC error bars = SD; Kruskal Wallis followed by Dunn's test with Benjamini and Hochberg corrections; $p > 0.05$ ns, $p < 0.05$ *

5.3.4 Electroretinography

Non-invasive ERG recordings were obtained before the start of the experiment as in 2.3, and repeated during the last 2 to 3 days to assess the retinal response. In some cases, there was excessive electrical noise in the

ERG signal, so it was not possible to obtain final recordings from all eyes. Out of 32 eyes, a full set of baseline and final recordings could not be obtained in 7. The analysis of the photopic response at 2.2 log cd sec/m^2, from the 25 eyes with a full set of recordings (C1inh-NT n = 8, C1inh-OHT n = 4, PBS-NT n = 8, PBS-OHT n = 5), is reported in Figure 5.6. A and B show the change in amplitude of the B-wave and PhNR, and C-D show the average waves prior to OHT induction (baseline) and after 4 weeks of OHT. The median B-wave amplitude of the NT eyes at the second recording was slightly reduced between the first and second recording. Median B-wave change: -9.1% for C1inh-NT and -16.9% for PBS-NT, p = 0.7. OHT eyes demonstrated notable loss of amplitude at the B-wave: C1inh-OHT -57.9%, PBS-OHT -40.6% (C1inh-OHT vs PBS-OHT p = 0.4), with the result being more significant at the C1inh-OHT group (C1inh-NT vs C1inh-OHT p = 0.03, PBS-NT vs PBS-OHT p = 0.2). At the PhNR level, the median amplitude difference in the C1inh-NT and PBS-NT groups was -9.4% and -16.3%, respectively (p = 0.7). Among the OHT eyes there was amplitude loss of -48.5% for C1inh-OHT and -43% for PBS-OHT (p = 0.9) (C1inh-NT vs C1inh-OHT p = 0.07, PBS-NT vs PBS-OHT p = 0.07).

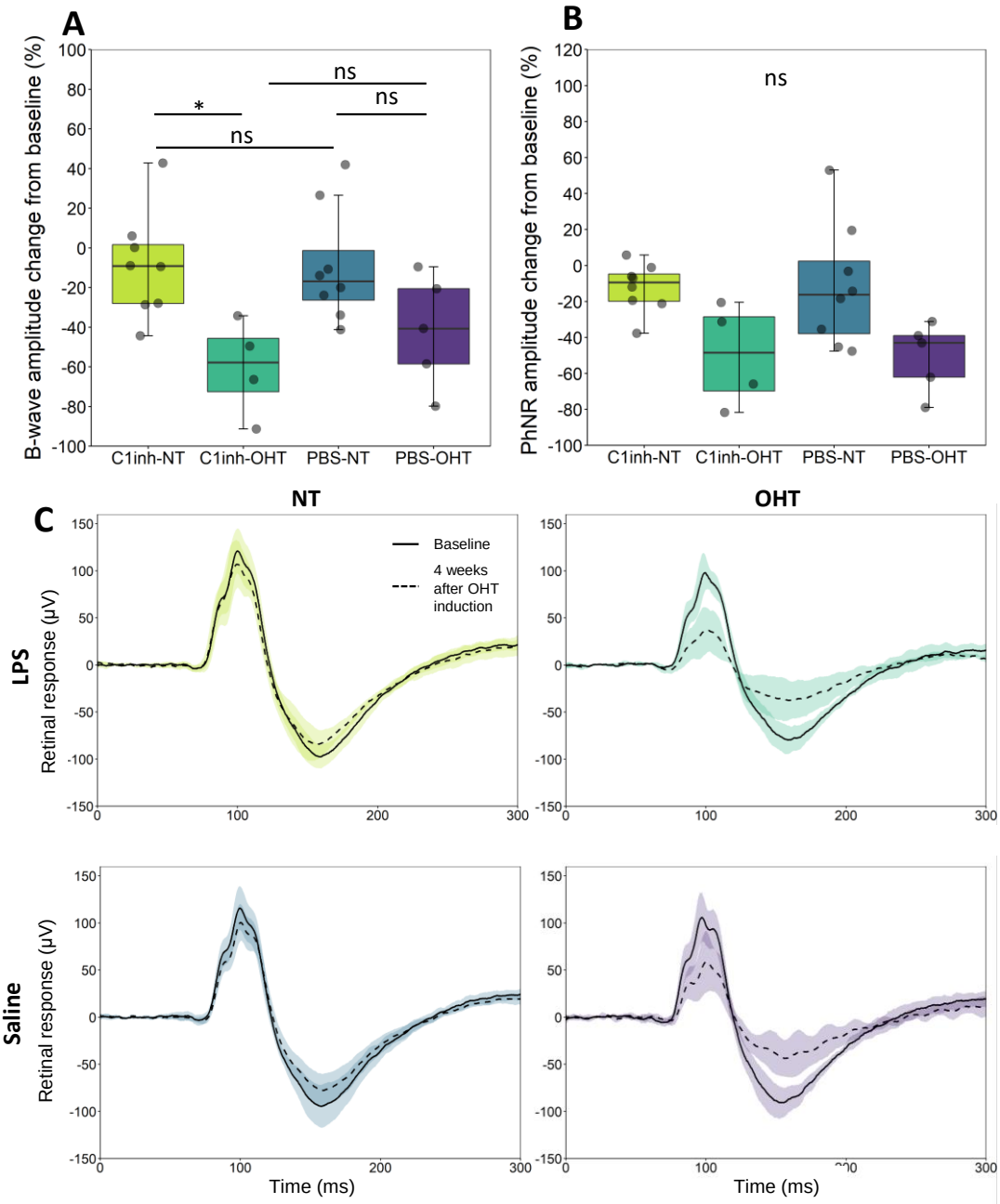

Figure 5.6 Changes in retinal response after 4 weeks of OHT in the cohort with LPS-induced inflammation and inhibition of the classical complement pathway via intravitreal injections of C1 inhibitor. (A-B) Percentage of amplitude change of B-wave and PhNR between baseline recording and recording obtained at the end of the experiment. (Boxplot middle line = median, lower hinge = 25% quartile, upper hinge =75% quartile, lower whisker = smallest observation greater than or equal to lower hinge -1.5 * IQR, upper whisker = largest observation less than or equal to upper hinge + 1.5 * IQR, * $p<0.05$, ns $p>0.05$ (Kruskal Wallis followed by Dunn's Test)). (C) Average retinal response per group before the onset of experiments and at the end of the experiment. The solid line indicates the baseline response and the dashed line the final response.

5.3.5 Microglial morphology

Half retinas (n = 4 per: C1inh-NT, C1inh-OHT, PBS-NT, PBS-OHT) were labelled with IBA1 following the protocol described in 2.9. A total of 3 images, were obtained from the mid-peripheral region of each retina as shown in Figure 2.8 (B). A total of 235 microglia, C1inh-NT n = 60, C1inh-OHT n = 61, PBS-NT n = 50, PBS-OHT n = 64 (4 to 5 cells per image), were reconstructed following the protocol described in 2.11. Figure 5.7 (A) shows representative microglia from NT and OHT retinas with resting microglia demonstrating elongated processed and activated microglia with retracted processes. Figure 5.7 shows the results of Sholl analysis and total process length analysis from microglial reconstructions. The microglia morphology of the NT retinas was similar for all metrics analysed across C1inh-NT and PBS-NT ($p > 0.05$). Microglial processes were significantly retracted in OHT retinas with C1inh-OHT demonstrating a stronger effect. The Sholl AUC was: C1inh-NT 162.5 ± 46, C1inh-OHT 72.7 ± 27, PBS-NT 166.9 ± 46.6, PBS-OHT 98.2 ± 39.4 (C1inh-NT vs C1inh-OHT $p < 0.001$, PBS-NT vs PBS-OHT $p < 0.001$, C1inh-NT vs PBS-NT $p = 0.7$, C1inh-OHT vs PBS-OHT $p = 0.005$). The total process length in µm was C1inh-NT 235 ± 65.6, C1inh-OHT 100.5 ± 40.5, PBS-NT 249.3 ± 67.4, PBS-OHT 139.7 ± 59.4 (C1inh-NT vs C1inh-OHT $p < 0.001$, PBS-NT vs PBS-OHT $p < 0.001$, C1inh-NT vs PBS-NT $p = 0.4$, C1inh-OHT vs PBS-OHT $p = 0.005$). Overall, in addition to the significant retraction of microglial processes in OHT retinas compared to NT, there was significantly more retraction in C1inh-OHT retinas compared to PBS-OHT. Examining the IOP increase in the subset of OHT retinas used for microglial staining (Figure 5.7 C) it is noticed that the IOP AUC in the C1inh-OHT group was relatively higher than in PBS-OHT (859 vs 716, $p > 0.05$), while in the whole cohort IOP increase across groups was more even across groups (Figure 5.3).

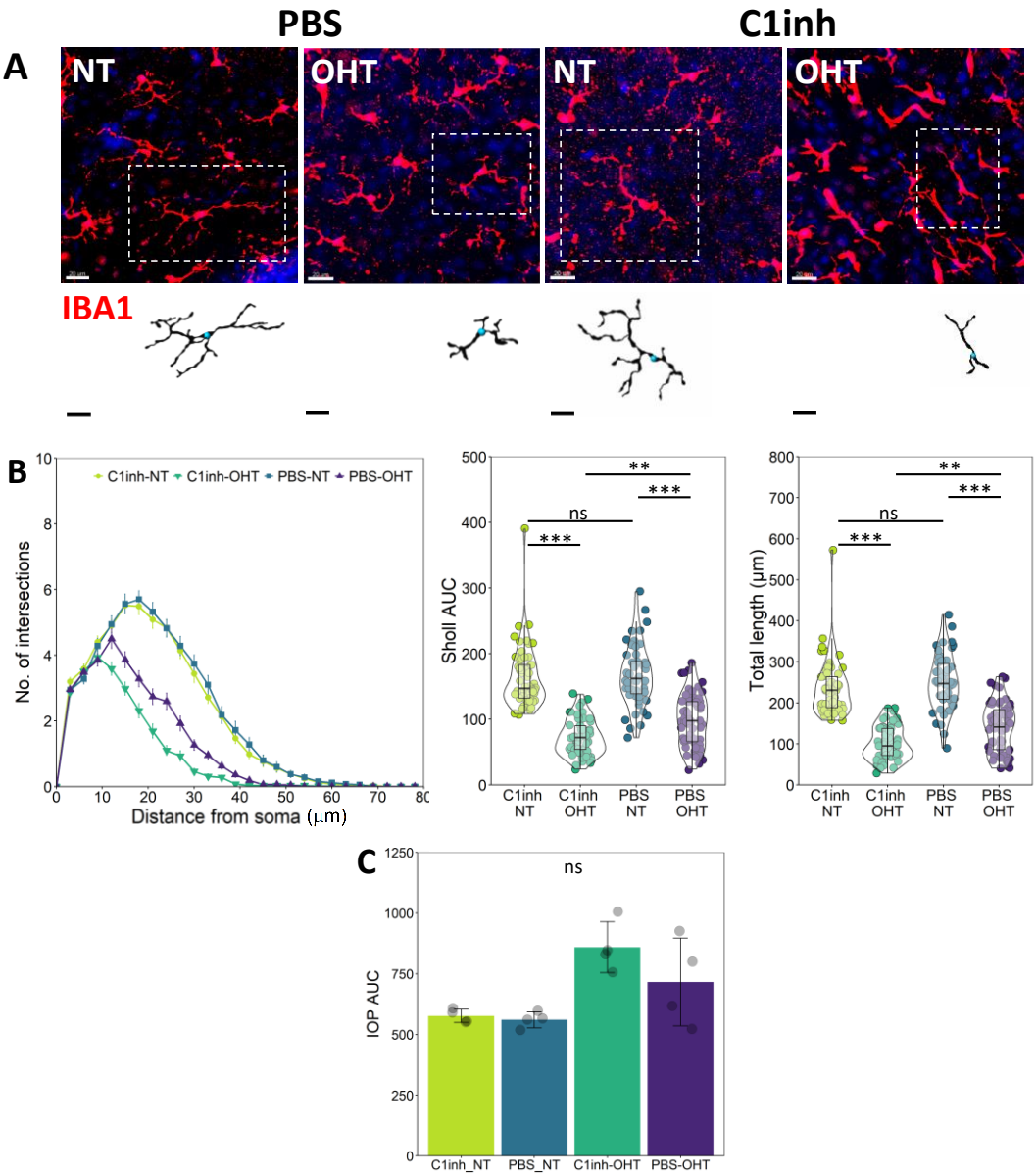

Figure 5.7 Analysis of microglial morphology from n=16 (4 per group) half retinas from the C1 inhibitor/PBS groups. A total of 235 microglia (C1inh-NT n=60, C1inh-OHT n=61, PBS-NT n=50, PBS-OHT n=64) were reconstructed and the complexity as well as total length of their processes were analysed. (A) Representative resting microglia from NT retinas and activated microglia from OHT retinas and their reconstructions. Scale bars = 20µm. (B) Average Sholl profile, Sholl AUC and total length of microglial processes (µm). (C) IOP AUC corresponding to the subset of 16 retinas used for IBA1 labelling. Sholl profile error bars = SEM. Sholl AUC, total length and IOP AUC error bars = SD. Kruskal Wallis followed by Dunn's test post hoc, ns $p > 0.05$, * $p > 0.05$ ** $p < 0.01$, *** $p < 0.001$.

5.3.6 RGC density

RGC density was examined via immunofluorescent RBPMS labelling on half retinas (n = 4 per: C1inh-NT, C1inh-OHT, PBS-NT, PBS-OHT), as described in 2.9 and 2.10. Figure 5.8 shows RBPMS+ cells density per group. Cell counts across both NT groups yielded similar results (Average ± SD per mm^2: C1inh-NT 2,107 ± 223, PBS-NT 2,213 ± 239, p = 0.6). RGC density decreased in OHT retinas with the effect being more marked in C1inh-OHT (-63% for C1inh-OHT, -36% for PBS-OHT). Mean RGC density ± SD per mm^2: C1inh-OHT 775 ± 757, PBS-OHT 1,420 ± 1,015, p = 0.4). C1inh-OHT vs C1inh-NT p = 0.1, PBS-OHT vs PBS-NT p = 0.2. However, in the subset of retinas used for RGC counts, the IOP AUC in the C1inh-OHT group was relatively higher than in PBS-OHT as shown in Figure 5.7.

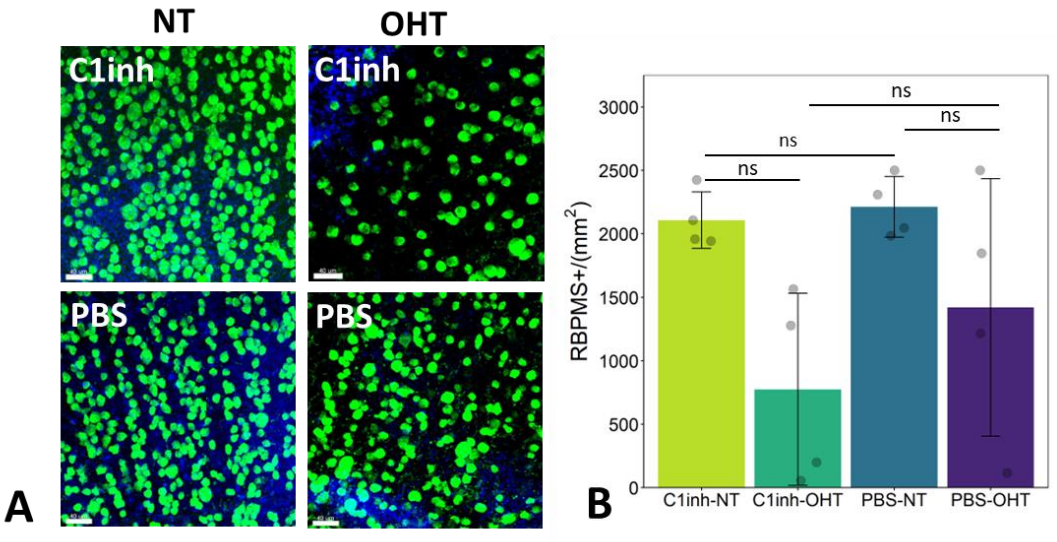

Figure 5.8 RGC density in OHT and NT contralateral controls from n=16 (4 per group) half retinas from the C1 inhibitor/PBS. (A) Representative images of RBPMS labelling of RGCs (green labelled cells). Scale bars = 40µm (B) Density of RBPMS labelled cells per mm^2. Reduced density was observed in OHT retinas. The average density in C1inh-OHT retinas was lower than PBS-OHT retinas. Error bars = DS, Kruskal Wallis with Dunn's post hoc ns p>0.05.

5.4 Discussion

In a 2016 study using a similar glaucoma model (Williams *et al.*, 2016) found that intravitreal C1 inhibition protected the dendritic and synaptic architecture of RGCs. Using the same protocol of C1 inhibition, this chapter investigates the effect of C1 inhibition in OHT retinas of immune primed animals.

The weight loss pattern observed was consistent, with the previous experiment in this thesis using the same LPS protocol and also very similar across both experimental groups in this chapter. The IOP increase induced through the bead injections was at a very similar level across both OHT groups. This reinforces the possibility that the trend observed in Chapter 4 for lower IOP in the LPS OHT group, although not statistically significant, might have been associated with the response to LPS as discussed in 4.4. The IOP in the OHT groups in this chapter was overall higher than the IOP in the LPS OHT group of Chapter 4, and was in fact at a closer level to the IOP of the Saline OHT group in Chapter 4 (see Figure 5.5). However, there is an important difference between the two experiments, which is the number of bead injections. In the experiment presented in this chapter, it was necessary to perform two to three injections as opposed to one in Chapter 4, so the IOP results are not directly comparable. However, even though OHT in this experiment was at the level of OHT in the Saline group of Chapter 4, the Sholl AUCs of RGC dendrites across all LPS receiving groups in both experiments were similar, while the OHT Saline group IOP was significantly lower compared to all LPS groups. In fact, the Saline OHT group was the only group to have statistically significant decrease of RGC Sholl AUC compared to its NT contralateral control. These results taken together raise a question regarding the role of the immune system in RGC dendritic survival observed across immune-primed animals in both experiments, and whether it should not only be attributed to IOP differences. Overall OHT-related changes on RGC dendritic complexity in this cohort were relatively modest and not statistically significant. Importantly, in this cohort, inhibition of the classical pathway of the complement system did not have an effect on RGC dendritic atrophy and retinal function on C1inhibitor treated OHT eyes vs control OHT eyes.

Similarly, to the experiments described in Chapter 4, the changes to retinal function were more notable than the morphological changes. Both the b-wave and the PhNR were affected. As discussed in Chapter 4, although the b-wave has been shown to be resistant to glaucomatous damage and is considered vulnerable to ischemia, there have been studies indicating that RGCs contribute to the photopic b-wave and that this part of the ERG can be affected during RGC degeneration independently of ischemia (Grozdanic *et al.*, 2003; Bui and Fortune, 2004). In this cohort IOP peaked between 30-50mmHg for most OHT eyes, with 4 eyes exceeding 50mmHg up and reaching up to 55mmHg. As already discussed, even though in mice it has been shown that retinal perfusion is maintained until 70mmHg (Kong *et al.*, 2012), the possibility of transient ischemic events cannot be completely excluded.

Analysis of microglial morphology showed significant process retraction typical of microglial activation. Unexpectedly, the C1inh-OHT group microglia showed significantly more process retraction compared to the PBS-OHT group. However, this analysis was conducted on half retina samples taken from every other retina during dissections for DiOlistic labelling. Looking at the IOPs of the subset of eyes corresponding to the samples, it is shown that in those samples IOP was relatively more increased in the C1inhibitor-OHT eyes compared to PBS-OHT, which may indicate the responsiveness of microglia to the degree of challenge and the sensitivity of this analysis to picking up subtle differences. The same samples were used to quantify RGCs, so this could also be the reason for the observed difference in the RGC survival rate between the two OHT groups.

Overall, the main finding of this chapter is that in this model of experimentally induced OHT in combination with systemic immune activation, inhibition of the classical pathway of the complement system in the retina did not have an effect on dendritic remodelling and functional deficits observed on those retinas, as opposed to the neuroprotective effect seen in (Williams *et al.*, 2016). In addition, the modest dendritic changes observed repeatedly in the LPS cohorts of the experiments in this chapter and in Chapter 4, as opposed to the significantly more severe dendritic loss observed in the Saline OHT controls is an interesting finding with relation to the role of the immune

activation in this observation. These findings are further discussed in context with relevant literature in Chapter 7.

Chapter 6. Microglial activation in contralateral normotensive eyes

6.1 Introduction

The effect of systemic inflammation on neuronal damage is mediated via complex processes involving inflammatory pathways such as the complement system, and glial cells. More in depth understanding of the microglial response will be needed to decipher if, and to what extent, systemic inflammation plays a role in glaucomatous progression. In experimental models of ocular diseases, including glaucoma, it is common practice to use the contralateral normotensive eyes as controls. However, there has been evidence suggesting that in those models, immune activation takes place in contralateral NT eyes. Using a mouse model of unilateral OHT, Gallego and colleagues found increased major histocompatibility complex class II expressed on microglia from NT eyes contralateral to OHT compared to naïve, and reported a qualitative increase in microglial density (Gallego *et al.*, 2012). Expanding on these findings, Rojas *et al.* reported a quantified increase in microglial density as well as a reduction in arbor area (Rojas *et al.*, 2014). In addition, Sapienza *et al*. found immune activation in sites of RGC projection at the superior colliculus (SC), of both the OHT and contralateral NT eyes, compared to naïve controls (Sapienza *et al.*, 2016). These, studies have examined the microglial population as a whole, without characterisation of microglia at an individual cell level. Microglial morphology is very diverse both in disease as well as under normal physiologic conditions, as microglial morphology dynamically changes in response to local stimuli (Kettenmann *et al.*, 2011). Morphologic characterisation of large populations of microglia could be a sensitive metric for understanding the environment that they reside in. The experiments in this chapter aim to investigate the effect of contralateral OHT on microglial morphology, both in NT eyes where the contralateral is OHT and in OHT eyes where the contralateral is also OHT (bilateral OHT).

6.2 Experimental design and methods

OHT was introduced unilaterally and bilaterally and unoperated animals were used as naïve controls. Throughout the chapter the bilateral NT naïve controls are abbreviated NT/NT. The unilateral OHT eyes and their contralateral NT are abbreviated OHT/NT and NT/OHT, respectively. The bilateral OHT eyes are abbreviated OHT/OHT (Figure 6.1).

The experiments were conducted in the Pete Williams lab in Karolinska Institutet, Sweden. All experimental procedures were undertaken in accordance with the ARVO Statement for the Use of Animals in Ophthalmic and Research. Individual study protocols were approved by Stockholm's Committee for Ethical Animal Research (10389-2018). Details of contributions to the results presented in this chapter from members of the Pete William's lab, Assistant Professor James Tribble and Dr Amin Otmani, are detailed in the Acknowledgements**.** OHT was induced following the epoxy microbead protocol described in 3.3.3. Two weeks after OHT induction rats were heavily anaesthetized with pentobarbital (75 mg/kg) and euthanized by cervical dislocation. The eyes were immediately enucleated and fixed in 3.7% PFA in 1× PBS. Fixed eyes were dissected and whole flat mount retinas were co-labelled with RBPMS and Isolectin B4 (IsoB4) (Invitrogen), which targets Poly-N-acetyllactosamine found on microglia, endothelial cells, monocytes/macrophages, using the following protocol. The tissue was permeabilized in 0.5% Triton X-100 in 1× PBS for 1 hour and blocked in 5% bovine serum albumin in 1× PBS for 1 hour. Rabbit anti RBPMS (Novus) and biotin conjugated IsoB4 (Invitrogen) were applied overnight at 4°C, 1:500 and 0.1 mg/ml in 1× PBS, respectively. The samples were washed in 1× PBS for 5 × 5 minutes and secondary antibodies goat anti rabbit AF 568 (Abcam) and strepdavidin AF 488 conjugate (Invitrogen) were applied 1:500 and 4 µg/ml in 1× PBS for 4 hours at room temperature. Samples were washed in 1× PBS for 5 × 5 minutes and stained with DAPI nuclear stain 1:500 in 1× PBS (made from 500 µg/ml stock) for 10 minutes. The samples were washed for 5 minutes in 1× PBS, dried, and mounted in Fluoromount-G (Invitrogen, Carlsbad, CA). Z-stack images were acquired on a Zeiss LSM800-Airy microscope using a 20× lens. The size of the images was 319.45 × 319.45 µm (0.312 µm/pixel)

and all imaging parameters were kept constant. For each retina 4 images were collected, each per superior, nasal, inferior and temporal quadrant, at 1500 µm from the ONH. Microglial tracing was performed manually using the Imaris Filament tracer tool with automatic depth estimation and volume filling enabled, as described in 2.11. Data of Sholl analysis, number of branches, total process length and field area were extracted from Imaris.

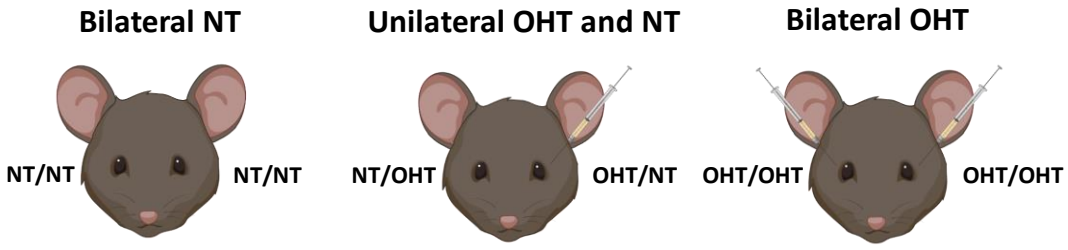

Figure 6.1 Experimental setup for morphological assessment of microglia in unilateral and bilateral OHT, as well as contralateral NT eyes. The analysis was performed on rats with unilateral OHT (n = 5 rat), bilateral OHT (n=3 rats) or bilateral NT (n = 3 rats). Operated eyes of the unilateral OHT group are abbreviated OHT/NT and unoperated contralateral controls NT/OHT. Bilateral OHT eyes are abbreviated OHT/OHT and bilateral NT eyes NT/NT.

6.3 Results

The results presented in this chapter are a part of a larger study that investigated neuroinflammation across the pathway of RGC projections, including the retina, the ON, the dorsal lateral geniculate nucleus (dLGN) and the superior colliculus (SC) (Tribble, Kokkali, *et al.*, 2021). The subset of findings presented in this chapter corresponds to parts of the study where the author had the most substantial contribution. The IOP and RGC quantification, correspond to the subset of the cohort that was used for the morphological assessment of microglia presented in this chapter.

6.3.1 IOP analysis

OHT was induced unilaterally in 5 rats (n = 5 NT/OHT and n = 5 OHT/NT eyes) and bilaterally in 3 rats (n = 6 OHT/OHT eyes); 3 unoperated rats were used as naïve controls (n = 6 NT/NT eyes). IOP increased to a similar degree in

OHT/NT and OHT/OHT and there were no significant changes to contralateral normotensive controls NT/OHT compared to naïve eyes NT/NT (Figure 6.2).

In detail, the mean IOP ± SD in mmHg per group was: NT/NT = 17 ± 1, NT/OHT = 17.4 ± 0.8, OHT/NT = 30.1 ± 2.3, OHT/OHT= 31.2 ±. 3.9. The increase in both OHT groups was significant compared to NT groups (OHT/NT vs NT/OHT p = 0.03, OHT/NT vs NT/NT p = 0.02, OHT/OHT vs NT/NT p = 0.009, OHT/OHT vs NT/OHT p = 0.01). No significant differences were seen between unilateral and bilateral OHT (p = 0.8) or normotensive contralateral controls and naïve eyes (p = 0.7). Similarly, IOP AUC was: NT/NT = 237 ± 14, NT/OHT = 244 ± 12, OHT/NT = 446 ± 36, OHT/OHT = 443 ± 58. IOP AUC was significantly increased in both OHT groups compared to NT groups (OHT/NT vs NT/OHT p = 0.03, OHT/NT vs NT/NT p = 0.01, OHT/OHT vs NT/NT p = 0.01, OHT/OHT vs NT/OHT p = 0.02). No significant differences were seen between unilateral and bilateral OHT (p = 0.9) or NT contralateral controls and naïve eyes (p = 0.7). The mean ± SD IOP peak was 48 ± 6 mmHg for OHT/NT and 42 ± 7 mmHg for OHT/OHT (p = 0.6). In NT eyes the IOP peak was 20 ± 1.8 and 19 ± 1.1 for NT/OHT and NT/NT (p = 0.6) (OHT/NT vs NT/OHT p = 0.01, OHT/NT vs NT/NT p = 0.02, OHT/OHT vs NT/NT p = 0.01, OHT/OHT vs NT/OHT p = 0.04).

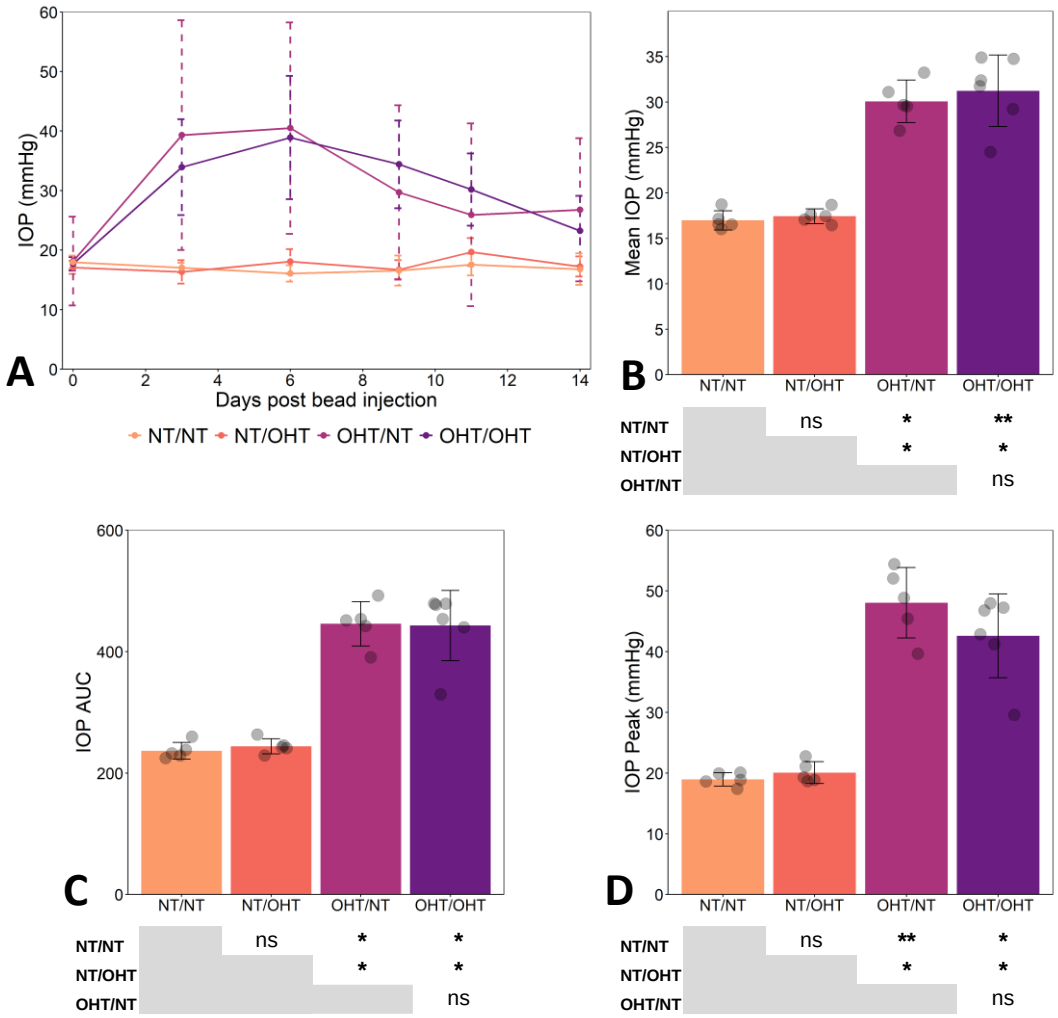

Figure 6.2 IOP results from unilateral and bilateral OHT. NT/NT n = 5, NT/OHT n = 5, OHT/NT n = 5, OHT/OHT n = 6 (n refers to eyes). (A) Average IOP profile per group. (B, C, D) Mean IOP, AUC of the IOP, Peak IOP. All metrics were significanly increased in the OHT groups, while there were no significant differences between bilateral and unilateral OHT or between naïve and contralateral NT controls. Error bars = SD, Kruskal Wallis followed by Dunn's test for multiple comparisons ns, $p > 0.05$, * $p < 0.05$, ** $p < 0.01$, *** $p < 0.001$.

6.3.2 RGC density

RBPMS labelled RGCs were counted using the semiautomated method described in 2.10, in a 319.45 × 319.45 µm area. Compared to NT/NT, RGC density in OHT/NT and OHT/OHT retinas was significantly reduced, 36% ($p = 0.004$) and 42% ($p < 0.001$), respectively. For each retina counts from 4 images were averaged. The mean ± SD RGC density per mm^2, per group, was 2494 ± 192 for NT/NT, 2864 ± 166 for NT/OHT, 1603 ± 249 for OHT/NT, 1457 ± 544 for OHT/OHT (see Figure 6.3). There were no significant

differences between NT/NT and NT/OHT (p = 0.3) or OHT/NT and OHT/OHT (p = 0.9).

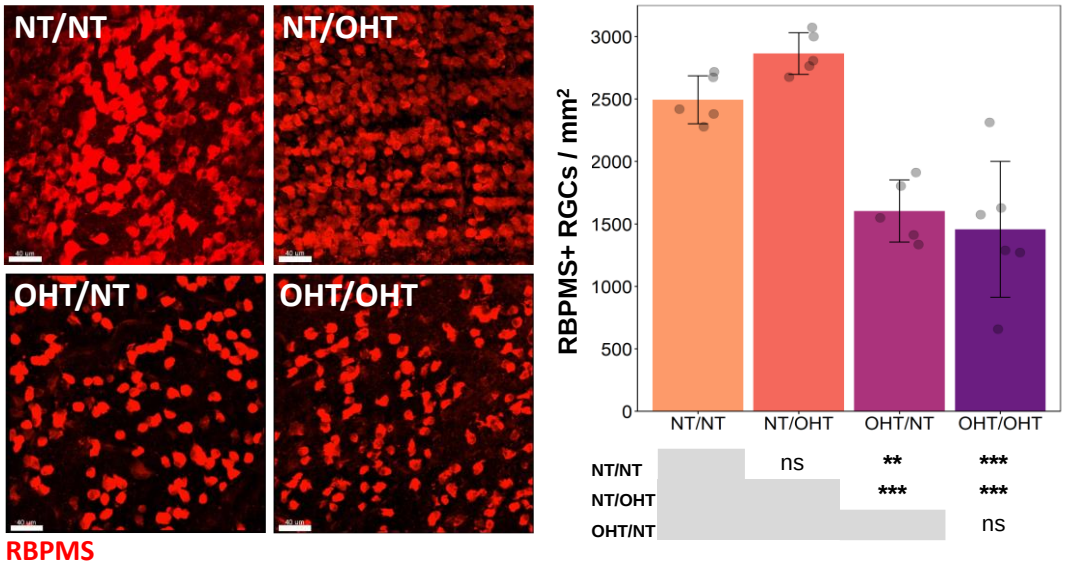

Figure 6.3 RGC density following 14 days of unilateral and bilateral OHT. (Left) Representative images of RBPMS stained RGCs. Scale bar = 40µm (Right) Density of RBPMS labelled RGCs per mm^2 from n = 5, 5, 5 and 6 retinas for NT/NT, NT/OHT, OHT/NT and OHT/OHT, respectively. RGC density was significantly reduced in OHT eyes, however there was no significant effect of bilateral or unilateral NT or OHT on RGC survival. Error bars = SD, One-way ANOVA, followed by Tukey HSD, p > 0.05 ns, p < 0.05 *, p <0.01 **, p<0.001 ***.

6.3.3 GCL microglia

Microglia positioned in the RNFL/GCL were reconstructed and assessed for branching complexity, field area, and volume. A total of n =741 individual microglia were reconstructed (n = 137 microglia in NT/NT, 185 in NT/OHT, 197 in OHT/NT, 222 in OHT/OHT, from n = 5 NT/NT eyes, n = 5 NT/OHT eyes, n = 5 OHT/NT eyes, 6 OHT/OHT eyes). A shift towards morphological features of microglial activation (shorter and thicker processes) was observed with increasing magnitude through the groups (NT/NT < NT/OHT <OHT/NT < OHT/OHT).

In detail, the mean ± SD Sholl AUC decreased to 106 ± 64 for OHT/OHT, 138 ± 74 for OHT/NT and 273 ± 99 for NT/OHT from 317 ± 103 of NT/NT. All the shifts were statistically significant compared to naïve controls (NT/NT vs NT/OHT p = 0.03, NT/NT vs OHT/NT p < 0.001, NT/NT vs OHT/OHT p <

0.001) and each step change was statistically significant compared to the one before (NT/OHT vs OHT/NT $p < 0.001$, OHT/NT vs OHT/OHT $p < 0.001$). A similar pattern was observed in branching points, total process length (μm) and field area (μm^2). The mean ± SD number of branches was 33 ± 12 for NT/NT, 29 ± 13 for NT/OHT, 13 ± 10 for OHT/NT, 10 ± 8 OHT/OHT (NT/NT vs NT/OHT $p = 0.02$, NT/NT vs OHT/NT $p < 0.001$, NT/NT vs OHT/OHT $p < 0.001$, NT/OHT vs OHT/NT $p < 0.001$, OHT/NT vs OHT/OHT $p = 0.002$). The mean ± SD total process length in μm was 494 ± 164 for NT/NT, 421 ± 156 for NT/OHT, 203 ± 115 for OHT/NT, 152 ± 98 OHT/OHT (NT/NT vs NT/OHT $p = 0.01$, NT/NT vs OHT/NT $p < 0.001$, NT/NT vs OHT/OHT $p < 0.001$, NT/OHT vs OHT/NT $p < 0.001$, OHT/NT vs OHT/OHT $p < 0.001$); mean ± SD field area in μm^2 1339 ± 425 for NT/NT, 1177 ± 452 for NT/OHT, 621 ± 341 for OHT/NT, 490±288 OHT/OHT (NT/NT vs NT/OHT $p = 0.01$, NT/NT vs OHT/NT $p < 0.001$, NT/NT vs OHT/OHT $p < 0.001$, NT/OHT vs OHT/NT $p < 0.001$, OHT/NT vs OHT/OHT $p = 0.002$). The normalized volume (μm^3/μm of length) of processes was significantly increased in microglia from OHT retinas to 0.86 ± 0.19 in OHT/NT and 1 ± 0.21 in OHT/OHT retinas, compared to 0.67 ± 0.14 in NT/NT (OHT/NT vs NT/NT $p < 0.001$,OHT/OHT vs NT/NT $p < 0.001$), and 0.68 ± 0.09 in NT/OHT (OHT/NT vs NT/OHT $p < 0.001$, OHT/OHT vs NT/OHT $p < 0.001$). There were no significant changes in volume in the NT/OHT microglia compared to NT/NT ($p = 0.9$), but OHT/OHT volume was significantly more increased compared to OHT/NT ($p < 0.001$).

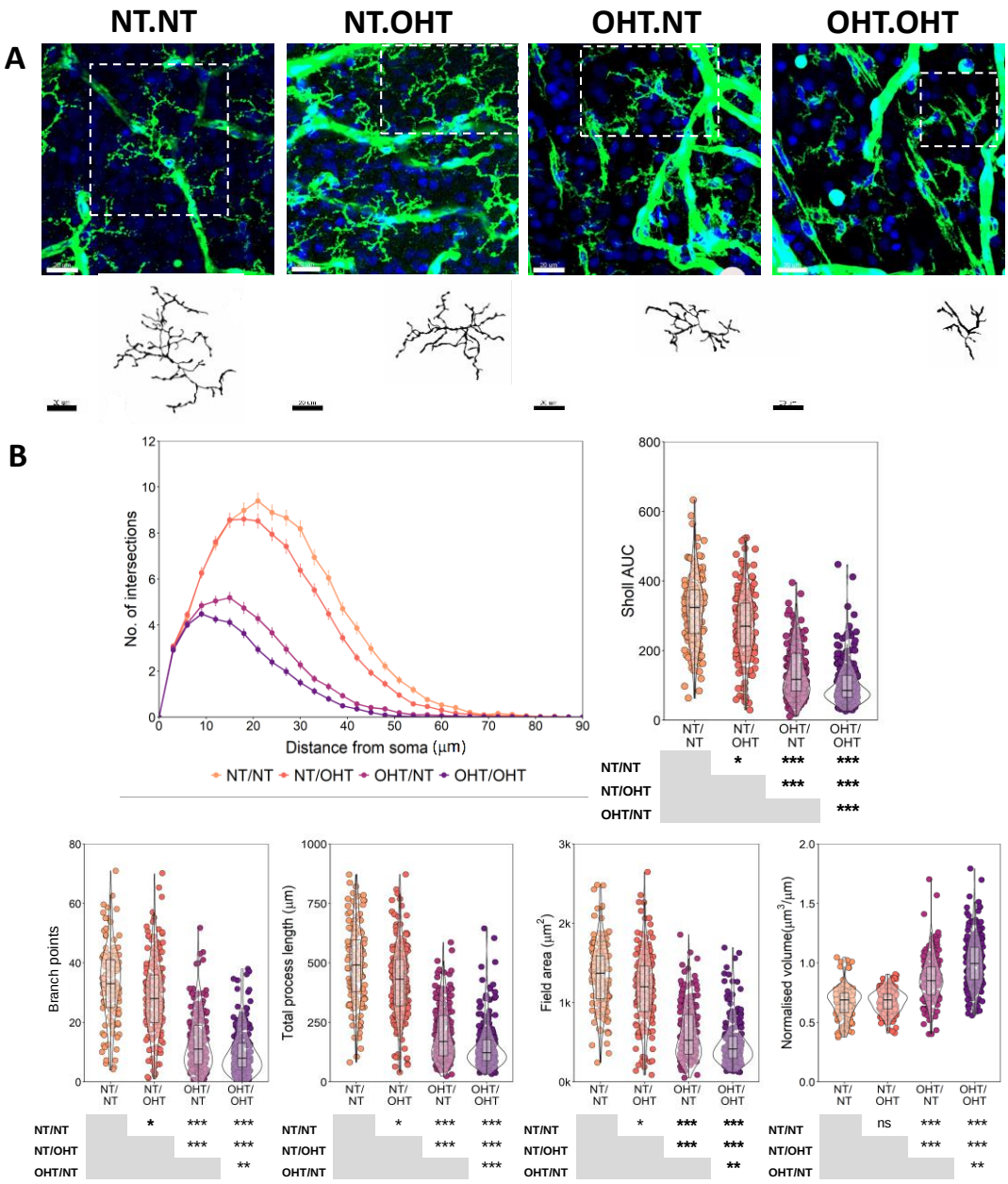

Figure 6.4 Morphological analysis of microglia in the GCL. (A) Indicative GCL microglia and their reconstructions. Scale bars = 20 µm. (B) Metrics of morphological analysis on n = 137 microglia in NT/NT, 185 in NT/OHT, 197 in OHT/NT, 222 in OHT/OHT, from n = 5 NT/NT eyes, 5 NT/OHT eyes, 5 OHT/NT eyes and 6 OHT/OHT eyes. Error bars in Sholl profiles = SEM, all other error bars = SD. Kruskal Wallis followed by Dunn's test for multiple comparisons with Benjamini and Hochberg correction, ns $p > 0.05$, *$p < 0.05$, **$p < 0.01$, ***$p < 0.001$.

6.3.4 IPL microglia

Changes to microglial morphology were seen in the IPL too, but they were more subtle, and the contralateral eye effect was reduced. In total, 556 microglia were reconstructed in the IPL (n = 92 microglia in NT/NT, 134 in NT/OHT, 160 in OHT/NT, 170 in OHT/OHT, from n = 5 NT/NT eyes, n = 5 NT/OHT eyes, n = 5 OHT/NT eyes, 6 OHT/OHT eyes). Sholl AUC, number of branches and total process length was significantly reduced in OHT retinas but not in NT/OHT; while field area had a gradual reduction throughout the groups but particularly in OHT, and volume was increased in OHT retinas to a similar degree but not in NT/OHT.

In more detail, mean Sholl AUC ± SD was in NT eyes was 346 ± 81 in NT/NT and 329 ± 86 in NT/OHT ($p = 0.16$); in OHT/NT eyes it was 253 ± 67 (OHT/NT vs NT/NT $p < 0.001$, OHT/NT vs NT/OHT $p < 0.001$, OHT/NT vs OHT/OHT $p = 0.002$); in OHT/OHT it was 226 ± 75 (OHT/OHT vs NT/NT $p < 0.001$, OHT/OHT vs NT/OHT $p < 0.001$). The mean number of branching points + SD was 37 ± 10 in NT/NT and 35 ± 10 in NT/OHT ($p = 0.18$), 27 ± 9 in OHT/NT eyes (OHT/NT vs NT/NT $p < 0.001$, OHT/NT vs NT/OHT $p < 0.001$, OHT/NT vs OHT/OHT $p < 0.001$) and 23 ± 9 in OHT/OHT (OHT/OHT vs NT/NT $p < 0.001$, OHT/OHT vs NT/OHT $p < 0.001$). The mean total process length (µm) ± SD was 538 ± 125 and 500 ± 117 in NT/NT and NT/OHT, respectively ($p = 0.09$); in OHT/NT eyes it was 377 ± 100 (OHT/NT vs NT/NT $p < 0.001$, OHT/NT vs NT/OHT $p < 0.001$, OHT/NT vs OHT/OHT $p = 0.002$), and in OHT/OHT it was 336 ± 116 (OHT/OHT vs NT/NT $p <0.001$, OHT/OHT vs NT/OHT $p < 0.001$). The mean field area (μm^2) ± SD was 1,421 ± 356 for NT/NT and 1,273 ± 320 for NT/OHT ($p = 0.01$); for OHT/NT it was 1,041 ± 394 (OHT/NT vs NT/NT $p < 0.001$, OHT/NT vs NT/OHT $p < 0.001$, OHT/NT vs OHT/OHT $p < 0.001$), and for OHT/OHT it was 922 ± 322 (OHT/OHT vs NT/NT $p <0.001$, OHT/OHT vs NT/OHT $p < 0.001$). Finally, normalized volume (µm3/µm of length) was 0.61 ± 0.11 in NT/NT and 0.56 ± 0.10 in NT/OHT ($p = 0.002$), while in OHT eyes it was 0.67 ± 0.14 for OHT/NT (OHT/NT vs NT/NT $p = 0.02$, OHT/NT vs NT/OHT $p < 0.001$, OHT/NT vs OHT/OHT $p = 0.8$) and 0.68 ± 0.16 OHT/OHT (OHT/OHT vs NT/NT $p = 0.01$, OHT/OHT vs NT/OHT $p < 0.001$).

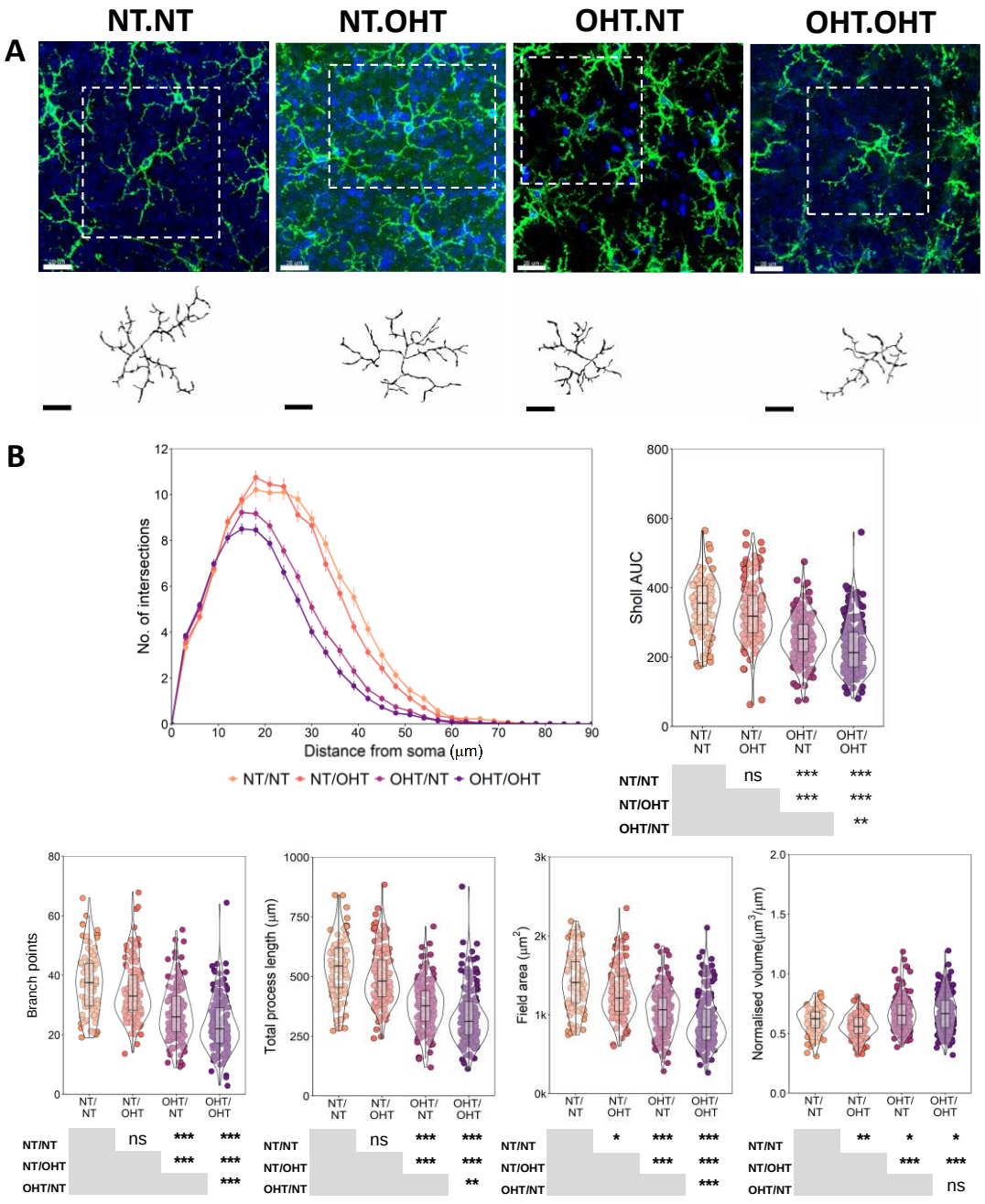

Figure 6.5 Morphological analysis of microglia in the IPL. (A) Indicative IPL microglia and their reconstructions. The arrows point to the cell soma. Scale bars = 20 µm. (B) Metrics of morphological analysis on n = 92 microglia in NT/NT, 134 in NT/OHT, 160 in OHT/NT, 170 in OHT/OHT, from n = 5 NT/NT eyes, 5 NT/OHT eyes, 5 OHT/NT eyes and 6 OHT/OHT eyes. Error bars in Sholl profiles = SEM, all other error bars = SD. Kruskal Wallis followed by Dunn's test for multiple comparisons with Benjamini and Hochberg correction, ns $p > 0.05$, *$p < 0.05$, **$p < 0.01$, ***$p < 0.001$.

6.4 Discussion

Unilateral glaucoma models are commonly used in glaucoma research, however microglial activation in the contralateral NT eye has been reported in such models (Gallego *et al.*, 2012; Rojas *et al.*, 2014; Sapienza *et al.*, 2016). In this study, detailed morphological analysis, at an individual cell level, quantitatively confirmed that retinal microglia in contralateral normotensive control eyes demonstrate a morphological phenotype typical of activation (retracted processes of increased volume), particularly in the GCL/NFL. In addition, the degree of the shift towards an activated phenotype is gradient, with the effect being subtle in the contralateral normotensive eyes, where there was no direct insult to the retina, and greatest in the bilateral OHT eyes, even though there were no significant IOP related differences between the bilateral and unilateral OHT eyes. This was most evident in the GCL/NFL, whereas in the IPL the differences between the naïve controls and the contralateral controls, as well as between the bilateral and unilateral OHT were reduced. After 14 days of OHT, the microglial activation in the contralateral controls and the amplified activation observed in bilateral OHT did not have any significant effect with regard to RGC survival.

The effect was not limited to the retina. Signs of microglial activation extended across the trajectory of RGC axons, in the ON and the brain. Data from Tribble, Kokkali, *et al.*, 2021, (not included in this thesis) showed that in OHT eyes microglial activation, as evidenced via increased microglia density, spread throughout the optic nerve and in unilateral OHT signs of activated microglia could be seen on both optic tracts after the chiasm. In contralateral NT there was no significant change in microglial density across the ON, however, morphological changes at a cell level were not assessed, because delineation of individual microglia was not possible. In fact, there was no contralateral effect to microglial density in any of the sites assessed (retina, ON, dLGN, SC), however, wherever it was possible to conduct a morphological analysis, differences were revealed. Microglial activation was observed in terminal visual thalami. In the dLGN, morphological changes, indicative of microglial activation were seen in both hemispheres of the unilateral OHT group compared to naïve NT, suggesting that microglial

activation is not proportionate to the degree of axon decussation, and in the bilateral OHT group the changes were significantly greater compared with OHT/NT. Changes were also observed in the SC, where overall all groups were significantly different compared to NT/NT, but less so between them, suggesting a more binary-like type of activation. In addition, cytokine arrays revealed upregulation of cytokines, particularly in OHT eyes, including significant upregulation of FGF-1 in contralateral NT compared to naïve NT, however whether this response is related to microglial activation and if it contributes to neuroprotection or drives inflammation, requires further exploration (Tribble, Kokkali, *et al.*, 2021).

Neuronal signalling with markers demonstrating a normal healthy state, such as CD200, CX3CL1 and CD47, or injury CCL21, defines the state of microglia, which in response either remain resting or switch to an activated phenotype (Szepesi *et al.*, 2018). Changes to CD200 expression as well as its microglial receptor CD200R have been found in early glaucoma (Taylor *et al.*, 2011), while in the DBA/2J model, loss of CX3CL1 signalling results in earlier axon transport dysfunction (Breen *et al.*, 2016). In addition, as discussed in detail in 1.6.4 complement components are upregulated in human and experimental glaucoma, and in activated microglia there is increased expression of complement receptors, as well as Toll-like receptors and proinflammatory cytokines. This responsiveness of microglia to neuronal dysfunction might explain microglial activation in NT contralateral retinas and terminal thalami in both hemispheres. In pigmented rats, approximately 10% of axons continue on the ipsilateral pathway after the chiasm (Jeffery, 1984). It is possible that in unilateral OHT these axons could carry the proinflammatory signalling to the area where healthy RGCs terminate. However, how this results in activation at the cell soma end in the contralateral eye requires further experimental investigation. In addition, the increased activation seen in the retina and the dLGN in bilateral OHT suggests that there is a cumulative effect from bilateral insult that drives further activation in both sides.

Overall, the findings in this chapter show that contralateral NT eyes in unilateral glaucoma models are not the equivalent of naïve controls.

Implications of this for glaucoma research, as well as clinical relevance are further discussed in Chapter 7.

Chapter 7. Discussion

In glaucoma, as well as other neurodegenerative diseases, there has been evidence that neuroinflammation may play a significant role, but whether it contributes to disease progression remains unclear (Williams *et al.*, 2017). This thesis investigates the effect of systemic immune activation on RGC degeneration in a rat model of experimental glaucoma. This chapter discusses the main findings and conclusions of this thesis, as well as future directions for this research.

7.1 Magnetic beads coated with functional groups are a reliable way for induction of OHT

There are many models of induced OHT using magnetic or non-magnetic microbeads to block aqueous outflow through Schlemm's canal and cause IOP elevation. A common issue of those models is the need for repeated injections (Morgan and Tribble, 2015). This problem also occurred in the initial experiments of this thesis. The use of beads coated with epoxy groups, resolved this issue, likely due to the ability of epoxy groups to bind amino and hydroxyl groups, which are present on many cell surfaces. This resulted in higher success rates and increased the duration of OHT achieved by a single injection in this model. As an average most marked OHT was observed in the first two weeks with IOP gradually dropping to basal values by the end of the four week period. Using this model, RGC dendritic atrophy, impacted retinal function, RGC loss and microglial activation were observed four weeks after OHT induction. Furthermore, characterisation of this model by (Tribble, Otmani, *et al.*, 2021) over a two week period, showed that it produces clinically relevant features, including RGC somal loss, axonal loss and dysfunction, and vascular compromise. The magnetic microbead model was first developed in 2011 in Prof Morgan's lab by Samsel *et al.* and introduced the advantage of achieving complete occlusion of the iridocorneal angle with reduced volume of microbeads, and keeping the visual axis clear for *in vivo* assessment of the retina e.g. via ERG. The amendment of using coated magnetic microbeads in this thesis further improves the model by allowing to reduce the number of

injections, thus improving the animal experience throughout the experiments, and minimising disruption in the aqueous chamber. In addition, higher success rates allow to reduce the overall number of animals required for experiments.

7.2 Systemic inflammation did not exacerbate the progress of neurodegeneration in experimental glaucoma

Systemic inflammation and periodontitis have been linked to cognitive decline in animal models and in Alzheimer's disease (Teeling *et al.*, 2007; Holmes *et al.*, 2009; Püntener *et al.*, 2012; Ide *et al.*, 2016). In addition, increased bacterial counts have been found in mouthwash specimens from patients with glaucoma (Astafurov, Elhawy, *et al.*, 2014). Recently, markers of systemic inflammation have been associated with primary angle-closure glaucoma (PACG) progression (Li *et al.*, 2021), and periodontitis with increased risk of developing POAG (Sun *et al.*, 2020). The hypothesis tested in this thesis was that systemic inflammation may exacerbate RGC neurodegeneration. This was investigated on a rat model of induced OHT via intracameral injections of magnetic microbeads, who were subsequently treated with two fortnightly doses of 500 µg/kg LPS to induce systemic inflammation. Contrary to the initial hypothesis, systemic inflammation did not exacerbate dendritic atrophy, in fact dendritic atrophy was significantly minimised compared to the control group. At first the results pointed towards this being the effect of lower IOP elevation in the LPS group (Chapter 4, 4.3.3). However, additional experiments showed that this was replicated regardless of the level of IOP (Chapter 5, 5.3.3.2). Functional deficits in LPS treated animals with OHT were detected, but they were still not more severe than in control OHT eyes. In addition, morphological changes typical of microglial activation, were even across a small sample of OHT eyes from LPS treated animals and controls treated with saline.

Studies using *in vivo* and *in vitro* models to investigate whether systemic inflammation contributes to neurodegeneration report a plethora of differential outcomes. Qin and colleagues found that a single injection of 5 mg/kg of body weight LPS induced progressive loss of dopaminergic neurons in the substantia nigra of mice, which was detectable 7 months after the LPS challenge (Qin *et al.*, 2007), and in rat models of multiple sclerosis, 500 µg/kg

of systemic LPS reactivated pre-existing inflammatory brain lesions (Serres *et al.*, 2009). In a model of prion disease, a single systemic LPS challenge of 500 µg/kg induced neuronal death in mice with ongoing brain inflammation (Cunningham *et al.*, 2005). In the DBA/2J glaucoma model, mice injected with 60µg of LPS (assuming an average mouse weight of 30 g, this equals approximately 2 mg/kg) had TLR4 upregulation in the retina and increased axonal degeneration and neuronal loss (Astafurov, Elhawy, *et al.*, 2014). By contrast, repeated LPS exposure (1.0 mg/kg for four consecutive days) was shown to be neuroprotective in a model of experimental brain injury, with microglia being primed towards the M2 phenotype that is considered to mitigate damage and promote tissue repair (Chen *et al.*, 2012). In a rat model of transient focal cerebral ischemia LPS-treated exosomes were associated with enhancing microglial polarisation to the M2 phenotype, reduced ischemic injury and improved neurological function (Zheng *et al.*, 2019). Low dose LPS pre-conditioning (200µg/kg) reduced post-injury gliosis and neurodegeneration in a rat model of experimental traumatic brain injury (TBI) (Turner *et al.*, 2017). Finally, in a rat model of experimental autoimmune encephalitis, E. coli infection did not aggravate the disease and did not induce any significant changes in the optic nerve or RGCs (Kumar *et al.*, 2015).

This diversity of outcomes highlights that the role of the immune responses in neuronal injury and neurodegeneration is multifaceted and cannot be described as a simple good *vs* bad paradigm. Early immune responses are considered part of the natural attempt to minimise damage following an initial insult, but when these responses enter a chronic phase they may contribute to further neuronal damage and disease progression (Soto and Howell, 2014). The exact nature and timing of this shift is still not clear. The role of microglia, the CNS's resident macrophage-like cells, is of particular interest in this process. As for peripheral macrophages, microglial activation has been categorised as classical, or M1, related to a pro-inflammatory phenotype with production of inflammatory cytokines and reactive oxygen species (ROS), and alternative, or M2, related to an anti-inflammatory phenotype that induces wound repair and debris clearance (Colton, 2009). However, as more is revealed about microglial activity in the CNS, models that propose phenotypes

the exists across a spectrum of activation, are gaining ground over the idea of a binary type of activation (Cherry, Olschowka and O'Banion, 2014; Jurga, Paleczna and Kuter, 2020). Microglia are highly plastic cells that are not locked in a particular state, instead they change in response to signalling from their environment. However, it has been suggested that continuous long-term activation might make them less responsive to anti-inflammatory signalling or affect their ability to perform phagocytosis (Cherry, Olschowka and O'Banion, 2014). In addition, in a study where microglial response was induced via systemic LPS in both aged (18 to 22 mo) and adult (3 to 4 mo) mice, microglia from aged mice showed exaggerated and prolonged activation, as well as impaired Interleukin 4 Receptor alpha (IL-4Ra) upregulation that inhibited their ability to switch from M1 to M2 phenotype in the presence of pro-M2 cytokine Interleukin 4 signalling (Fenn *et al.*, 2012).

Age is a major risk factor in glaucoma and in other neurodegenerative disease, such as Alzheimer's and Parkinson's diseases. The impact of age on neuronal function has been linked with altered inflammatory responses, both systemically and in the CNS, including glial activation and altered cytokine expression (Lynch, 2010; Trollor *et al.*, 2021). In a mouse model of acute OHT, aged retinas developed more severe loss of inner retinal function compared with young adult mice (Kong *et al.*, 2012), and in a rat model of acute OHT greater RGC loss was seen in aged compared to young retinas, which was associated with a more pro-inflammatory glial phenotype, increased C3 deposition and pro-inflammatory cytokine upregulation (Meng *et al.*, 2022). The studies in this thesis were conducted using young adult rats due to limitations in obtaining aged rats. Although in this thesis systemic inflammation did not result in more severe outcomes in terms of both RGC structure and function in a chronic OHT model, taking into account the combinatory effect of increased aged, raises the question of whether a differential outcome would have been seen in a more aged cohort.

Another aspect that warrants further investigation is the effect of the techniques used to assess neurodegeneration. In this study, DiOlistic labelling was used to assess RGC dendritic morphology, ERGs for retinal function and RBPMS labelling for RGC survival rate. Although the ERG and RBPMS results

are less conclusive, due to smaller sample size and variability of the data, in the LPS group there was a trend for relatively more changes observed in retinal function and RGC density compared to the more modest changes seen in dendritic morphology. Microglial phagocytosis of damaged cells and cell debris is important for maintaining tissue homeostasis and it has been shown that pharmacological reduction of microglial phagocytosis results in increased secondary cell death due to neurotoxicity after traumatic brain injury (Herzog *et al.*, 2019; Márquez-Ropero *et al.*, 2020). It is interesting to consider that well-regulated microglial activation for swift clearance of cell debris may allow the surviving neurons to maintain healthier dendritic arborisation by promoting restoration of homeostasis in their environment. Assessment of RGC survival rate, morphology and function of surviving neurons are all important in obtaining a holistic view of the state of the surviving neuronal population.

7.3 Inhibition of the C1 complex did not have an effect on glaucomatous damage

As discussed in Chapter 1 (1.6.4), many studies have shown upregulation of complement components in both animal and human ocular tissue, particularly the C1q protein of the classical pathway. The role of complement in glaucoma is not clear yet, but studies have reported neuroprotective effects from targeted inhibition of the classical pathway, MAC and C3 (Howell *et al.*, 2013; Williams *et al.*, 2016; Bosco *et al.*, 2018). In contrast, global C3 deletion via gene knock out actually increased glaucomatous damage (Harder *et al.*, 2017).

In this thesis, the C1 complex that initiates the classical pathway was inhibited in the retina via intravitreal injections of C1 inhibitor. The C1 inhibition protocol was the same as in a published study (Williams *et al.*, 2016) that found C1 inhibition protected the dendritic and synaptic architecture of RGCs on a similar experimental glaucoma model. The additional element of the study in this thesis is the systemic immune activation via LPS, as described in Chapter 5 (5.2). In this study C1 inhibition did not have an impact on dendritic survival or retinal function, in OHT eyes treated with the inhibitor, compared to control OHT eyes treated with vehicle only. RGC survival analysis was inconclusive

due to sample size and variability, but microglia from OHT eyes treated with C1 inhibitor demonstrated a morphology indicative of greater activation (fewer and shorter processes) compared to microglia from vehicle treated OHT eyes. This might have been due to the relatively higher IOP of C1 inhibitor OHT eyes compared to OHT controls, in the subset used in microglial morphological analysis. However, it is interesting to consider this from the perspective of the crosstalk that occurs between microglia and the classical pathway of the complement system (Zabel and Kirsch, 2013). During normal CNS development high levels of proteins of the classical pathway are localised on synapses and participate in synaptic pruning (Stevens *et al.*, 2007) in a process that includes tagging synapses for elimination by microglia (Paolicelli *et al.*, 2011). This natural process normally happens during a discrete window in development, but it has been shown to be reactivated during early Alzheimer's disease models and result in synaptic loss (Hong *et al.*, 2016). In addition, microglia have been identified as major sites of C1q synthesis in the CNS, which is drastically upregulated after injury and can drive microglial activation, likely resulting in an autocrine/paracrine signalling mechanism (Färber *et al.*, 2009). While the C1 inhibitor would inhibit the formation of the C1 complex by inactivating the C1r and C1s proteases to halt initiation of the complement cascade (Davis, Mejia and Lu, 2008), it would not eliminate C1q, which could still activate microglia. C1q performs a diverse range of activities extending beyond the complement pathway (Kouser *et al.*, 2015; Benavente *et al.*, 2020). At the same time, it has been reported that administration of C1 inhibitor to C1q deficient mice with brain ischemia/reperfusion injury has a neuroprotective effect independently of C1q (De Simoni *et al.*, 2004). Taken together, these findings suggest that it is worth considering the role of C1q and C1 inhibitor, in glaucoma, in the context of their activity in the complement system, as well as different pathways.

7.4 Microglia are activated in contralateral normotensive eyes in unilateral glaucoma and further activated in bilateral glaucoma

In glaucoma research, unilateral glaucoma models that use the contralateral eye as control are common, including experiments in this thesis. However,

interestingly, signs of microglial activation in contralateral NT eyes have been reported (Gallego *et al.*, 2012; Rojas *et al.*, 2014; Sapienza *et al.*, 2016). In the study presented in Chapter 6, a detailed morphological analysis at cell level quantitatively confirmed that in unilateral experimental glaucoma, retinal microglia in contralateral NT eyes demonstrate a morphological phenotype with retracted processes of increased volume, typical of activation, particularly in the GCL/NFL. In addition, morphological analysis of microglia in bilateral OHT showed that activation in those retinas was greater than in unilateral OHT retinas. As shown in Tribble, Kokkali, *et al.*, 2021, microglial activation was also observed in terminal visual thalami, dLGN and SC, in both hemispheres of animals with unilateral OHT, and in the dLGN, but not SC, with an effect that was greater in animals with bilateral OHT. As discussed in 6.4, whether the convergence of RGC terminals from healthy and injured retinas that happens after the chiasm may result in propagation of proinflammatory signalling that drives contralateral activation and produces a cumulative effect from bilateral insult, warrants further investigation.

The findings from this study show that contralateral NT eyes in unilateral glaucoma models cannot be regarded as naïve controls, and their use in glaucoma research carries the risk of obscuring subtle changes in RGC populations by minimising apparent changes in the OHT eye relative to the NT. In the investigation of the role of neuroinflammation in glaucomatous retina this is particularly relevant, as comparisons against these controls which already have underlying neuroinflammation might mask significant findings in glaucomatous eyes. At the same time understanding the effects of this mechanism, is important for the treatment of glaucoma patients. Primary glaucoma usually progresses into bilateral disease, even when initially it is presented unilaterally, and it is estimated that eventually 1 out of 6 patients will become bilaterally blind due to glaucoma (Peters, Bengtsson and Heijl, 2013). Confirming whether neuroinflammation of the contralateral visual pathway exists in human glaucoma, and whether it plays any role in the progression from unilateral to bilateral glaucoma, could have implications for the treatment of the disease and the clinical approach towards the contralateral eye. Finally, the graded pattern of microglial activation, with the

greatest effect being seen in bilateral OHT, is also of clinical relevance as it has been shown that having bilateral glaucoma increases the risk of glaucoma progression almost 2-fold compared to unilateral glaucoma (Leske *et al.*, 2003).

7.5 Conclusions and future directions

The findings of this thesis suggest that systemic inflammation does not significantly contribute to neurodegeneration in experimental glaucoma. However, in some of the LPS treated animals there was a trend for less IOP elevation and the experiments were done on adult but not aged cohorts. Indeed, age is a major risk factor for glaucoma, and it has also been associated with immune dysregulation. Therefore, future studies would need to look into the effect of systemic inflammation on aged cohorts and employ strategies to ensure even IOP elevation across groups so that the risk of the effects of neuroinflammation being masked or counteracted by differences in IOP is minimised. In addition, it is important to understand the role of microglia, as well as other glial cells, in the pathophysiology of RGC damage. Microglia play a key role in inflammation in the CNS and the spectrum of their phenotype and activity continually emphasises the versatility of those cells and the diversity of disease outcomes associated with their response. This thesis presents a useful assessment of the state of RGCs and microglia. A detailed dissection of neurodegenerative/neuroprotective mechanisms was not in the scope of this thesis, but it will be an important step to build on the findings of the studies presented here. In addition, the finding of microglial activation in the contralateral eye should warrant towards caution in the use of contralateral normotensive eyes as controls in experimental glaucoma studies. While experimental models offer valuable understanding of disease mechanisms to reveal opportunities for novel treatment strategies, translation of findings in experimental models to clinical application is challenging. More studies investigating comorbidities of glaucoma and chronic inflammation in patients, will be important to steer the direction of glaucoma research.

References

Abbott, C. J. *et al.* (2014) ‘Comparison of retinal nerve fiber layer thickness in vivo and axonal transport after chronic intraocular pressure elevation in young versus older rats’, *PLoS ONE*, 9(12), pp. 1–24. doi: 10.1371/journal.pone.0114546.

Abdul, Y., Akhter, N. and Husain, S. (2013) ‘Delta-opioid agonist SNC-121 protects retinal ganglion cell function in a chronic ocular hypertensive rat model’, *Investigative Ophthalmology and Visual Science*, 54(3), pp. 1816–1828. doi: 10.1167/iovs.12-10741.

Ahmed, F. *et al.* (2004) ‘Microarray Analysis of Changes in mRNA Levels in the Rat Retina after Experimental Elevation of Intraocular Pressure’, *Investigative Opthalmology & Visual Science*, 45(4), p. 1247. doi: 10.1167/iovs.03-1123.

Ahmed, F., Chaudhary, P. and Sharma, S. C. (2001) ‘Effects of increased intraocular pressure on rat retinal ganglion cells’, *International Journal of Developmental Neuroscience*, 19(2), pp. 209–218. doi: 10.1016/S0736-5748(00)00073-3.

Ahnelt, P. K. (1998) ‘The photoreceptor mosaic’, *Eye (Basingstoke)*, 12(3), pp. 531–540. doi: 10.1038/eye.1998.142.

Alasil, T. *et al.* (2014) ‘Correlation of retinal nerve fiber layer thickness and visual fields in glaucoma: A broken stick model’, *American Journal of Ophthalmology*. Elsevier Inc., 157(5), pp. 953-959.e2. doi: 10.1016/j.ajo.2014.01.014.

Anderson, M. G. *et al.* (2002) ‘Mutations in genes encoding melanosomal proteins cause pigmentary glaucoma in DBA/2J mice’, *Nature Genetics*, 30(1), pp. 81–85. doi: 10.1038/ng794.

Applebury, M. L. *et al.* (2000) ‘The murine cone photoreceptor: a single cone type expresses both S and M opsins with retinal spatial patterning.’, *Neuron*, 27(3), pp. 513–523. doi: 10.1016/S0896-6273(00)00062-3.

Astafurov, K., Dong, C. Q., *et al.* (2014) ‘Complement expression in the retina is not influenced by short-term pressure elevation.’, *Molecular vision*, 20(January), pp. 140–52. Available at: http://www.ncbi.nlm.nih.gov/pubmed/24505213.

Astafurov, K., Elhawy, E., *et al.* (2014) ‘Oral Microbiome Link to Neurodegeneration in Glaucoma’, *PLoS ONE*. Edited by S. Barnes, 9(9), p. e104416. doi: 10.1371/journal.pone.0104416.

Bally, I. *et al.* (2009) ‘Identification of the C1q-binding sites of human C1r and C1s. A refined three-dimensional model of the C1 complex of complement’, *Journal of Biological Chemistry*, 284(29), pp. 19340–19348. doi: 10.1074/jbc.M109.004473.

Banitt, M. R. *et al.* (2013) ‘Progressive loss of retinal ganglion cell function precedes structural loss by several years in glaucoma suspects’, *Investigative Ophthalmology and Visual Science*, 54(3), pp. 2346–2352. doi: 10.1167/iovs.12-11026.

Barkan, O. (1938) ‘Glaucoma: Classification, Causes, and Surgical Control*’, *American Journal of Ophthalmology*, 21(10), pp. 1099–1117. doi: 10.1016/S0002-9394(38)90805-0.

Bear, M. F., Connors, B. W. and Paradiso, M. A. (2016) ‘The Eye’, in Bear, M. F., Connors, B. W., and Paradiso, M. A. (eds) *Neuroscience, Exploring the Brain*. 4th edn. Philadelphia, PA: Wolters Kluwer, pp. 293–330.

Benavente, F. *et al.* (2020) ‘Novel c1q receptor-mediated signaling controls neural stem cell behavior and neurorepair’, *eLife*, 9, pp. 1–31. doi: 10.7554/ELIFE.55732.

Bhagat, P. R., Deshpande, K. V. and Natu, B. (2014) ‘Utility of Ganglion Cell Complex Analysis in Early Diagnosis and Monitoring of Glaucoma using a Different Spectral Domain Optical Coherence Tomography’, *Journal of Current Glaucoma Practice*, 8(3), pp. 101–106. doi: 10.5005/jp-journals-10008-1171.

Block, F. and Schwarz, M. (1998) ‘The b-wave of the electroretinogram as an

index of retinal ischemia', *General Pharmacology*, 30(3), pp. 281–287. doi: 10.1016/S0306-3623(97)00359-5.

Block, F., Schwarz, M. and Sontag, K. H. (1992) 'Retinal ischemia induced by occlusion of both common carotid arteries in rats as demonstrated by electroretinography', *Neuroscience Letters*, 144(1–2), pp. 124–126. doi: 10.1016/0304-3940(92)90731-L.

Boland, M. V and Quigley, H. A. (2007) 'Risk factors and open-angle glaucoma: Classification and application', *Journal of Glaucoma*, 16(4), pp. 406–418. doi: 10.1097/IJG.0b013e31806540a1.

Bosco, A. *et al.* (2008) 'Reduced retina microglial activation and improved optic nerve integrity with minocycline treatment in the DBA/2J mouse model of glaucoma', *Investigative Ophthalmology and Visual Science*, 49(4), pp. 1437–1446. doi: 10.1167/iovs.07-1337.

Bosco, A. *et al.* (2018) 'Complement C3-Targeted Gene Therapy Restricts Onset and Progression of Neurodegeneration in Chronic Mouse Glaucoma', *Molecular Therapy*. Elsevier Ltd., 26(10), pp. 2379–2396. doi: 10.1016/j.ymthe.2018.08.017.

Bosco, A., Steele, M. R. and Vetter, M. L. (2011) 'Early microglia activation in a mouse model of chronic glaucoma', *Journal of Comparative Neurology*, 519(4), pp. 599–620. doi: 10.1002/cne.22516.

Bowd, C. (2000) 'The Retinal Nerve Fiber Layer Thickness in Ocular Hypertensive, Normal, and Glaucomatous Eyes With Optical Coherence Tomography', *Arch Ophthalmol*, 118. doi: 10.1001/archopht.118.1.22.

Bowmaker, J. K. and Dartnall, H. J. (1980) 'Visual pigments of rods and cones in a human retina.', *The Journal of Physiology*, 298(1), pp. 501–511. doi: 10.1113/jphysiol.1980.sp013097.

Boycott, B. B. *et al.* (1975) 'Interplexiform cells of the mammalian retina and their comparison with catecholamine-containing retinal cells.', *Proceedings of the Royal Society of London. Series B, Containing papers of a Biological character. Royal Society (Great Britain)*, 191(1104), pp. 353–368. doi:

10.1098/rspb.1975.0133.

Boycott, B. B. and Dowling, J. E. (1969) ‘Organization of the primate retina: Light microscopy, with an appendix: A second type of midget bipolar cell in the primate retina’, *Philosophical Transactions of the Royal Society of London. Series B, Biological Sciences*, 255(799), pp. 109–184. doi: 10.1098/rstb.1969.0004.

Breen, K. T. *et al.* (2016) ‘Loss of Fractalkine Signaling Exacerbates Axon Transport Dysfunction in a Chronic Model of Glaucoma’, *Frontiers in Neuroscience*, 10(NOV), pp. 1–15. doi: 10.3389/fnins.2016.00526.

Bringmann, A. *et al.* (2006) ‘Müller cells in the healthy and diseased retina’, *Progress in Retinal and Eye Research*, 25(4), pp. 397–424. doi: 10.1016/j.preteyeres.2006.05.003.

Brooks, D. E. (1990) ‘Glaucoma in the Dog and Cat’, *Veterinary Clinics of North America: Small Animal Practice*, 20(3), pp. 775–797. doi: 10.1016/S0195-5616(90)50062-5.

Buckingham, B. P. *et al.* (2008) ‘Progressive Ganglion Cell Degeneration Precedes Neuronal Loss in a Mouse Model of Glaucoma’, *Journal of Neuroscience*, 28(11), pp. 2735–2744. doi: 10.1523/JNEUROSCI.4443-07.2008.

Bui, B. V. and Fortune, B. (2004) ‘Ganglion cell contributions to the rat full-field electroretinogram’, *Journal of Physiology*, 555(1), pp. 153–173. doi: 10.1113/jphysiol.2003.052738.

Bunker, S. *et al.* (2015) ‘Experimental Glaucoma Induced by Ocular Injection of Magnetic Microspheres’, *Journal of Visualized Experiments*, (96), pp. 1–5. doi: 10.3791/52400.

Calandrella, N. *et al.* (2007) ‘Degenerative and apoptotic events at retinal and optic nerve level after experimental induction of ocular hypertension’, *Molecular and Cellular Biochemistry*, 301(1–2), pp. 155–163. doi: 10.1007/s11010-006-9407-0.

Carter-Dawson, L. *et al.* (1998) ‘Glutamine Immunoreactivity in Müller Cells of

Monkey Eyes with Experimental Glaucoma', *Experimental Eye Research*, 66(5), pp. 537–545. doi: 10.1006/exer.1997.0447.

Chauhan, B. C. *et al.* (2002) 'Effect of intraocular pressure on optic disc topography, electroretinography, and axonal loss in a chronic pressure-induced rat model of optic nerve damage', *Investigative Ophthalmology and Visual Science*, 43(9), pp. 2969–2976.

Chen, Z. *et al.* (2012) 'Lipopolysaccharide-Induced Microglial Activation and Neuroprotection against Experimental Brain Injury Is Independent of Hematogenous TLR4', *Journal of Neuroscience*, 32(34), pp. 11706–11715. doi: 10.1523/JNEUROSCI.0730-12.2012.

Cherry, J. D., Olschowka, J. A. and O'Banion, M. K. (2014) 'Neuroinflammation and M2 microglia: The good, the bad, and the inflamed', *Journal of Neuroinflammation*, 11(1), pp. 1–15. doi: 10.1186/1742-2094-11-98.

Cho, H. and Kee, C. (2013) 'Population-based glaucoma prevalence studies in Asians', *Survey of Ophthalmology*. Mosby, Inc, pp. 1–14. doi: 10.1016/j.survophthal.2013.09.003.

Chong, R. S. and Martin, K. R. (2015) 'Glial cell interactions and glaucoma', *Current Opinion in Ophthalmology*, 26(2), pp. 73–77. doi: 10.1097/ICU.0000000000000125.

Chrysostomou, V. and Crowston, J. G. (2013) 'The photopic negative response of the mouse electroretinogram: Reduction by acute elevation of intraocular pressure', *Investigative Ophthalmology and Visual Science*, 54(7), pp. 4691–4697. doi: 10.1167/iovs.13-12415.

Colotto, A. *et al.* (2000) 'Photopic negative response of the human ERG: losses associated with glaucomatous damage.', *Investigative ophthalmology & visual science*, 41(8), pp. 2205–11. Available at: https://pubmed.ncbi.nlm.nih.gov/10892864/.

Colton, C. A. (2009) 'Heterogeneity of microglial activation in the innate immune response in the brain', *Journal of Neuroimmune Pharmacology*, 4(4),

pp. 399–418. doi: 10.1007/s11481-009-9164-4.

Cordeiro, M. F. *et al.* (2011) ‘Imaging apoptosis in the eye’, *Eye*. Nature Publishing Group, 25(5), pp. 545–553. doi: 10.1038/eye.2011.64.

Crowston, J. G. *et al.* (2015) ‘An acute intraocular pressure challenge to assess retinal ganglion cell injury and recovery in the mouse’, *Experimental Eye Research*. Elsevier Ltd, 141, pp. 3–8. doi: 10.1016/j.exer.2015.03.006.

Cull, G. A. *et al.* (2012) ‘Relationship between Orbital Optic Nerve Axon Counts and Retinal Nerve Fiber Layer Thickness Measured by Spectral Domain Optical Coherence Tomography’, *Investigative Opthalmology & Visual Science*, 53(12), p. 7766. doi: 10.1167/iovs.12-10752.

Cunningham, C. *et al.* (2005) ‘Central and systemic endotoxin challenges exacerbate the local inflammatory response and increase neuronal death during chronic neurodegeneration’, *Journal of Neuroscience*, 25(40), pp. 9275–9284. doi: 10.1523/JNEUROSCI.2614-05.2005.

Curcio, C. a *et al.* (1987) ‘Distribution of cones in human and monkey retina: individual variability and radial asymmetry.’, *Science (New York, N.Y.)*, 236(4801), pp. 579–582. doi: 10.1126/science.3576186.

Dacey, D. (1999) ‘Primate retina: cell types, circuits and color opponency’, *Progress in Retinal and Eye Research*, 18(6), pp. 737–763. doi: 10.1016/S1350-9462(98)00013-5.

Dai, C. *et al.* (2012) ‘Structural basis of glaucoma: The fortified astrocytes of the optic nerve head are the target of raised intraocular pressure’, *Glia*, 60(1), pp. 13–28. doi: 10.1002/glia.21242.

Davis, A. E., Mejia, P. and Lu, F. (2008) ‘Biological activities of C1 inhibitor’, *Molecular Immunology*, 45(16), pp. 4057–4063. doi: 10.1016/j.molimm.2008.06.028.

Dawson, W. W. *et al.* (1993) ‘Primary open angle glaucomas in the rhesus monkey.’, *British Journal of Ophthalmology*, 77(5), pp. 302–310. doi: 10.1136/bjo.77.5.302.

Detwiler, S. R. (1943) *Vertebrate photoreceptors.* New York: Macmillan

Company.

Dielemans, I. *et al.* (1994) ‘The Prevalence of Primary Open-angle Glaucoma in a Population-based Study in The Netherlands: The Rotterdam Study’, *Ophthalmology*. American Academy of Ophthalmology, Inc, 101(11), pp. 1851–1855. doi: 10.1016/S0161-6420(94)31090-6.

Dokladny, K. *et al.* (2010) ‘LPS-induced cytokine levels are repressed by elevated expression of HSP70 in rats: Possible role of NF-κB’, *Cell Stress and Chaperones*, 15(2), pp. 153–163. doi: 10.1007/s12192-009-0129-6.

Dowling, J. E. (2012) *The retina: An approachable part of the brain*. Revised ed. Edited by J. E. Downing. Cambridge (MA): Belknap Press (of Harvard University press).

Dowling, J. E. and Wald, G. (1960) ‘The Biological Function of Vitamin A Acid’, *Proceedings of the National Academy of Sciences*, 46(5), pp. 587–608. doi: 10.1073/pnas.46.5.587.

Drasdo, N. *et al.* (2002) ‘Ocular optics, electroretinography and primary open angle glaucoma’, *Ophthalmic and Physiological Optics*, 22(5), pp. 455–462. doi: 10.1046/j.1475-1313.2002.00078.x.

Dreyer, E. B. (1996) ‘Elevated Glutamate Levels in the Vitreous Body of Humans and Monkeys With Glaucoma’, *Archives of Ophthalmology*, 114(3), p. 299. doi: 10.1001/archopht.1996.01100130295012.

Dunkelberger, J. R. and Song, W. C. (2010) ‘Complement and its role in innate and adaptive immune responses’, *Cell Research*. Nature Publishing Group, 20(1), pp. 34–50. doi: 10.1038/cr.2009.139.

ElGohary, A. A. and Elshazly, L. H. M. (2015) ‘Photopic negative response in diagnosis of glaucoma: an experimental study in glaucomatous rabbit model.’, *International journal of ophthalmology*, 8(3), pp. 459–464. doi: 10.3980/j.issn.2222-3959.2015.03.05.

Ellinwood, N. M. *et al.* (2010) ‘Candidate Gene Analysis of a Feline Model of Primary Congenital Glaucoma Implicates LTBP2 as the Causative Locus’, *Investigative Ophthalmology & Visual Science*, 51(13), p. 6390.

Färber, K. *et al.* (2009) ‘C1q, the recognition subcomponent of the classical pathway of complement, drives microglial activation’, *Journal of Neuroscience Research*, 87(3), pp. 644–652. doi: 10.1002/jnr.21875.

Farkas, I. *et al.* (2002) ‘CD59 blocks not only the insertion of C9 into MAC but inhibits ion channel formation by homologous C5b-8 as well as C5b-9’, *Journal of Physiology*, 539(2), pp. 537–545. doi: 10.1113/jphysiol.2001.013381.

Feng, L. *et al.* (2013) ‘Sustained ocular hypertension induces dendritic degeneration of mouse retinal ganglion cells that depends on cell type and location’, *Investigative Ophthalmology and Visual Science*, 54(2), pp. 1106–1117. doi: 10.1167/iovs.12-10791.

Fenn, A. M. *et al.* (2012) ‘Lipopolysaccharide-induced interleukin (IL)-4 receptor-α expression and corresponding sensitivity to the M2 promoting effects of IL-4 are impaired in microglia of aged mice’, *Brain, Behavior, and Immunity*. Elsevier Inc., 26(5), pp. 766–777. doi: 10.1016/j.bbi.2011.10.003.

Forrester, J. V. *et al.* (2016) ‘Anatomy of the eye and orbit’, in Forrester, J. V. et al. (eds) *The Eye*. Fourth edi. Elsevier, pp. 1-102.e2. doi: 10.1016/B978-0-7020-5554-6.00001-0.

Forrester, J. V, Worgul, B. V and Merriam, G. R. (1980) ‘Endotoxin-induced uveitis in the rat’, *Albrecht von Graefe’s Archive for Clinical and Experimental Ophthalmology*, 213(4), pp. 221–233. doi: 10.1007/BF00417543.

Foster, P. J. *et al.* (2002) ‘The definition and classification of glaucoma in prevalence surveys’, *British Journal of Ophthalmology*, 86(2), pp. 238–242. doi: 10.1136/bjo.86.2.238.

Frishman, L. J. and Wang, M. H. (2011) ‘Electroretinogram of Human, Monkey and Mouse’, *Adler’s Physiology of the Eye*, pp. 480–501. doi: 10.1016/b978-0-323-05714-1.00024-8.

Fry, L. E. *et al.* (2018) ‘The coma in glaucoma: Retinal ganglion cell dysfunction and recovery’, *Progress in Retinal and Eye Research*. Elsevier, 65(March), pp. 77–92. doi: 10.1016/j.preteyeres.2018.04.001.

Fu, J. Y. *et al.* (1990) ‘The induction and suppression of prostaglandin H2

synthase (cyclooxygenase) in human monocytes', *Journal of Biological Chemistry*, 265(28), pp. 16737–16740. doi: 10.1016/s0021-9258(17)44821-6.

Fujita, T. *et al.* (1987) 'The mechanism of action of decay-accelerating factor (DAF). DAF inhibits the assembly of C3 convertases by dissociating C2a and Bb.', *Journal of Experimental Medicine*, 166(5), pp. 1221–1228. doi: 10.1084/jem.166.5.1221.

Fukuda, Y. (1977) 'A three-group classification of rat retinal ganglion cells: histological and physiological studies', *Brain Research*, 119(2), pp. 327–344. doi: 10.1016/0006-8993(77)90314-6.

Gaasterland, D. and Kupfer, C. (1974) 'Reports: Experimental Glaucoma in the Rhesus Monkey', *Investigative Opthalmology & Visual Science*, 13(6), pp. 455–457.

Gallego, B. I. *et al.* (2012) 'IOP induces upregulation of GFAP and MHC-II and microglia reactivity in mice retina contralateral to experimental glaucoma', *Journal of Neuroinflammation*, 9, pp. 1–18. doi: 10.1186/1742-2094-9-92.

Gelatt, K. N., Peiffer, R. L. and Gwin, R. M. (1977) 'Clinical manifestatons of inherited glaucoma in the beagle', *Investigative Ophthalmology and Visual Science*, 16(12), pp. 1135–1142.

Ginhoux, F. *et al.* (2010) 'Fate Mapping Analysis Reveals That Adult Microglia Derive from Primitive Macrophages', *Science*, 330(6005), pp. 841–845. doi: 10.1126/science.1194637.

Glovinsky, Y., Quigley, H. A. and Dunkelberger, G. R. (1991) 'Retinal ganglion cell loss is size dependent in experimental glaucoma.', *Investigative ophthalmology & visual science*, 32(3), pp. 484–91. Available at: http://www.ncbi.nlm.nih.gov/pubmed/2001923.

Glovinsky, Y., Quigley, H. A. and Pease, M. E. (1993) 'Foveal Ganglion Cell Loss Is Size Dependent in Experimental Glaucoma', *Investigative Opthalmology & Visual Science*, (2), pp. 395–400. Available at: https://iovs.arvojournals.org/article.aspx?articleid=2179177.

Gomez, C. R. *et al.* (2008) 'Diminished Acute Phase Response and Increased

Hepatic Inflammation of Aged Rats in Response to Intraperitoneal Injection of Lipopolysaccharide', *The Journals of Gerontology Series A: Biological Sciences and Medical Sciences*, 63(12), pp. 1299–1306. doi: 10.1093/gerona/63.12.1299.

Gordon, M. O. *et al.* (2002) 'The Ocular Hypertension Treatment Study: baseline factors that predict the onset of primary open-angle glaucoma.', *Archives of Ophthalmology*, 120(6), pp. 714–20; discussion 829-30. doi: 10.1001/archopht.120.6.714.

Gotoh, Y., Machida, S. and Tazawa, Y. (2004) 'Selective Loss of the Photopic Negative Response in Patients with Optic Nerve Atrophy', *Archives of Ophthalmology*, 122(3), pp. 341–346. doi: 10.1001/archopht.122.3.341.

Grozdanic, S. D. *et al.* (2003) 'Temporary elevation of the intraocular pressure by cauterization of vortex and episcleral veins in rats causes functional deficits in the retina and optic nerve', *Experimental Eye Research*, 77(1), pp. 27–33. doi: 10.1016/S0014-4835(03)00089-7.

Guo, L. *et al.* (2005) 'Retinal ganglion cell apoptosis in glaucoma is related to intraocular pressure and IOP-induced effects on extracellular matrix', *Investigative Ophthalmology and Visual Science*, 46(1), pp. 175–182. doi: 10.1167/iovs.04-0832.

Harder, J. M. *et al.* (2017) 'Early immune responses are independent of RGC dysfunction in glaucoma with complement component C3 being protective', *Proceedings of the National Academy of Sciences*, 114(19), pp. E3839–E3848. doi: 10.1073/pnas.1608769114.

Harris, C. L. *et al.* (2003) 'Characterization of the mouse analogues of CD59 using novel monoclonal antibodies: tissue distribution and functional comparison', *Immunology*, 109(1), pp. 117–126. doi: 10.1046/j.1365-2567.2003.01628.x.

Herbort, C. P., Chan, C. C. and Nussenblatt, R. B. (1990) 'Endotoxin-induced uveitis in the rat: a hypothesis for preferential involvement of the anterior uvea', *Current Eye Research*. Taylor & Francis, 9(sup1), pp. 119–124. doi: 10.3109/02713689008999430.

Hernandez, M. R., Miao, H. and Lukas, T. (2008) ‘Astrocytes in glaucomatous optic neuropathy’, *Progress in Brain Research*, 173(08), pp. 353–373. doi: 10.1016/S0079-6123(08)01125-4.

Herzog, C. *et al.* (2019) ‘Rapid clearance of cellular debris by microglia limits secondary neuronal cell death after brain injury in vivo’, *Development*, 146(9). doi: 10.1242/dev.174698.

Heywood, R. (1975) ‘Glaucoma in the Rat’, *British Veterinary Journal*, 131(2), pp. 213–221. doi: 10.1016/S0007-1935(17)35342-3.

Hoekzema, R. *et al.* (1992) ‘Endotoxin-induced uveitis in the rat. The significance of intraocular interleukin-6.’, *Investigative Ophthalmology & Visual Science*, 33(3), pp. 532–539.

Holmes, C. *et al.* (2009) ‘Systemic inflammation and disease progression in Alzheimer disease’, *Neurology*, 73(10), pp. 768 LP – 774. doi: 10.1212/WNL.0b013e3181b6bb95.

Hong, S. *et al.* (2016) ‘Complement and Microglia Mediate Early Synapse Loss in Alzheimer Mouse Models’, *Science*, 352(6286), pp. 712–716. doi: 10.1126/science.aad8373.Complement.

Howell, G. R. *et al.* (2007) ‘Axons of retinal ganglion cells are insulted in the optic nerve early in DBA/2J glaucoma’, *The Journal of Cell Biology*, 179(7), pp. 1523–1537. doi: 10.1083/jcb.200706181.

Howell, G. R. *et al.* (2011) ‘Molecular clustering identifies complement and endothelin induction as early events in a mouse model of glaucoma’, *Journal of Clinical Investigation*, 121(4), pp. 1429–1444. doi: 10.1172/JCI44646.

Howell, G. R. *et al.* (2012) ‘Radiation treatment inhibits monocyte entry into the optic nerve head and prevents neuronal damage in a mouse model of glaucoma’, *Journal of Clinical Investigation*, 122(4), pp. 1246–1261. doi: 10.1172/JCI61135.

Howell, G. R. *et al.* (2013) ‘Deficiency of complement component 5 ameliorates glaucoma in DBA/2J mice’, *Journal of Neuroinflammation*, 10(1), p. 851. doi: 10.1186/1742-2094-10-76.

Howell, G. R. *et al.* (2014) ‘Combinatorial targeting of early pathways profoundly inhibits neurodegeneration in a mouse model of glaucoma’, *Neurobiology of Disease*, 71(4), pp. 44–52. doi: 10.1016/j.nbd.2014.07.016.

Huang, W. *et al.* (2018) ‘Comparative analysis of retinal ganglion cell damage in three glaucomatous rat models’, *Experimental Eye Research*. Elsevier, 172(February), pp. 112–122. doi: 10.1016/j.exer.2018.03.019.

Huggert, A. (1957) ‘Obstruction of the outflow of aqueous humour, produced experimentally’, *Acta Ophthalmologica*, 35(1), pp. 1–11. doi: 10.1111/j.1755-3768.1957.tb05866.x.

Hughes, A. (1979) ‘A schematic eye for the rat’, *Vision Research*, 19, pp. 569–588. doi: 10.1016/0042-6989(79)90172-X.

Husain, S., Abdul, Y. and Crosson, C. E. (2012) ‘Preservation of retina ganglion cell function by morphine in a chronic ocular-hypertensive rat model’, *Investigative Ophthalmology and Visual Science*, 53(7), pp. 4289–4298. doi: 10.1167/iovs.12-946.

Huxlin, K. R. and Goodchild, A. K. (1997) ‘Retinal Ganglion Cells in the Albino Rat: Revised Morphological Classification’, *The Journal of Comparative Neurology*, 385, pp. 309–323.

Ide, M. *et al.* (2016) ‘Periodontitis and Cognitive Decline in Alzheimer’s Disease’, *PLOS ONE*. Edited by P. Garg, 11(3), p. e0151081. doi: 10.1371/journal.pone.0151081.

Ingram, G. *et al.* (2008) ‘Complement in multiple sclerosis : its role in disease and potential as a biomarker’, pp. 128–139. doi: 10.1111/j.1365-2249.2008.03830.x.

Inman, D. M. and Horner, P. J. (2007) ‘Reactive nonproliferative gliosis predominates in a chronic mouse model of glaucoma’, *Glia*, 55(9), pp. 942–953. doi: 10.1002/glia.20516.

Jacobs, G. H., Neitz, J. and Deegan, J. F. (1991) ‘Retinal receptors in rodents maximally sensitive to ultraviolet light’, *Nature*, 353(6345), pp. 655–656. doi: 10.1038/353655a0.

Java, A. *et al.* (2015) ‘Role of complement receptor 1 (CR1; CD35) on epithelial cells: A model for understanding complement-mediated damage in the kidney’, *Molecular Immunology*, 67(2), pp. 584–595. doi: 10.1016/j.molimm.2015.07.016.

Jeffery, G. (1984) ‘Retinal ganglion cell death and terminal field retraction in the developing rodent visual system’, *Developmental Brain Research*, 13(1), pp. 81–96. doi: 10.1016/0165-3806(84)90079-8.

Jha, P. *et al.* (2011) ‘Complement mediated apoptosis leads to the loss of retinal ganglion cells in animal model of glaucoma’, *Molecular Immunology*, 48(15–16), pp. 2151–2158. doi: 10.1016/j.molimm.2011.07.012.

John, S. W. M. *et al.* (1998) ‘Essential iris atrophy, pigment dispersion, and glaucoma in DBA/2J mice’, *Investigative Ophthalmology and Visual Science*, 39(6), pp. 951–962.

Johnson, M. A. *et al.* (1989) ‘Pattern-evoked potentials and optic nerve fiber loss in monocular laser-induced glaucoma’, *Investigative Ophthalmology and Visual Science*, 30(5), pp. 897–907.

Johnson, T. V. and Tomarev, S. I. (2010) ‘Rodent models of glaucoma’, *Brain Research Bulletin*, 81(2–3), pp. 349–358. doi: 10.1016/j.brainresbull.2009.04.004.

Jurga, A. M., Paleczna, M. and Kuter, K. Z. (2020) ‘Overview of General and Discriminating Markers of Differential Microglia Phenotypes’, *Frontiers in Cellular Neuroscience*, 14(August), pp. 1–18. doi: 10.3389/fncel.2020.00198.

de Kater, A. W. *et al.* (1986) ‘The Slate turkey: a model for secondary angle closure glaucoma.’, *Investigative ophthalmology & visual science*, 27(12), pp. 1751–4. Available at: http://www.ncbi.nlm.nih.gov/pubmed/3793405.

Keltner, J. L. *et al.* (2006) ‘The Association between Glaucomatous Visual Fields and Optic Nerve Head Features in the Ocular Hypertension Treatment Study’, *Ophthalmology*, 113(9), pp. 1603–1612. doi: 10.1016/j.ophtha.2006.05.061.

Kerrigan-Baumrind, L. A. *et al.* (2000) ‘Number of ganglion cells in glaucoma

eyes compared with threshold visual field tests in the same persons', *Investigative Ophthalmology and Visual Science*, 41(3), pp. 741–748.

Kerrigan, L. A. (1997) 'TUNEL-Positive Ganglion Cells in Human Primary Open-angle Glaucoma', *Archives of Ophthalmology*, 115(8), p. 1031. doi: 10.1001/archopht.1997.01100160201010.

Kettenmann, H. *et al.* (2011) 'Physiology of Microglia', *Physiological Reviews*, 91(2), pp. 461–553. doi: 10.1152/physrev.00011.2010.

Kim, Y. U. *et al.* (1995) 'Mouse complement regulatory protein Crry/p65 uses the specific mechanisms of both human decay-accelerating factor and membrane cofactor protein.', *Journal of Experimental Medicine*, 181(1), pp. 151–159. doi: 10.1084/jem.181.1.151.

Kimberley, F. C., Sivasankar, B. and Paul Morgan, B. (2007) 'Alternative roles for CD59', *Molecular Immunology*, 44(1–3), pp. 73–81. doi: 10.1016/j.molimm.2006.06.019.

Kirkiewicz, M., Lubiński, W. and Penkala, K. (2016) 'Photopic negative response of full-field electroretinography in patients with different stages of glaucomatous optic neuropathy', *Documenta Ophthalmologica*, 132(1), pp. 57–65. doi: 10.1007/s10633-016-9528-z.

Klein, B. E. K. *et al.* (1992) 'Prevalence of Glaucoma: The Beaver Dam Eye Study', *Ophthalmology*, 99(10), pp. 1499–1504. doi: 10.1016/S0161-6420(92)31774-9.

Klos, A. *et al.* (2009) 'The role of the anaphylatoxins in health and disease', *Molecular Immunology*, 46(14), pp. 2753–2766. doi: 10.1016/j.molimm.2009.04.027.

Kolker, A. E. *et al.* (1963) 'The development of glaucoma in rabbits', *Investigative ophthalmology*, 2, pp. 316–21. Available at: http://www.ncbi.nlm.nih.gov/pubmed/14090721.

Kong, Y. X. G. *et al.* (2012) 'Impact of aging and diet restriction on retinal function during and after acute intraocular pressure injury', *Neurobiology of Aging*. Elsevier Inc., 33(6), pp. 1126.e15-1126.e25. doi:

10.1016/j.neurobiolaging.2011.11.026.

Kouser, L. *et al.* (2015) ‘Emerging and novel functions of complement protein C1q’, *Frontiers in Immunology*, 6(JUN). doi: 10.3389/fimmu.2015.00317.

de Kozak, Y. *et al.* (1994) ‘Differential tumor necrosis factor expression by resident retinal cells from experimental uveitis-susceptible and -resistant rat strains’, *Journal of Neuroimmunology*, 55(1), pp. 1–9. doi: 10.1016/0165-5728(94)90141-4.

Križaj, D. (2019) ‘What is glaucoma ?’, in Kolb, H., Fernandez, E., and Nelson, R. (eds) *Webvision: The Organization of the Retina and Visual System*. Salt Lake City (UT): University of Utah Health Sciences Center.

Kuehn, M. H. *et al.* (2006) ‘Retinal synthesis and deposition of complement components induced by ocular hypertension’, *Experimental Eye Research*, 83(3), pp. 620–628. doi: 10.1016/j.exer.2006.03.002.

Kumar, P. *et al.* (2015) ‘Systemic Escherichia coli infection does not influence clinical symptoms and neurodegeneration in experimental autoimmune encephalomyelitis’, *BMC Neuroscience*, 16(1), pp. 1–9. doi: 10.1186/s12868-015-0172-4.

Kur, J., Newman, E. A. and Chan-Ling, T. (2012) ‘Cellular and physiological mechanisms underlying blood flow regulation in the retina and choroid in health and disease’, *Progress in Retinal and Eye Research*, 31(5), pp. 377–406. doi: 10.1016/j.preteyeres.2012.04.004.

Lachmann, P. J. and Müller-Eberhard, H. J. (1968) ‘The demonstration in human serum of “conglutinogen-activating factor” and its effect on the third component of complement.’, *Journal of immunology*, 100(4), pp. 691–8. Available at: http://www.ncbi.nlm.nih.gov/pubmed/5645214.

Lei, Y. *et al.* (2009) ‘Topography of neuron loss in the retinal ganglion cell layer in human glaucoma’, *British Journal of Ophthalmology*, 93(12), pp. 1676–1679. doi: 10.1136/bjo.2009.159210.

Leske, M. C. *et al.* (1995) ‘Risk factors for open-angle glaucoma. The Barbados Eye Study.’, *Archives of Ophthalmology*, 113(7), pp. 918–24.

Available at: http://www.ncbi.nlm.nih.gov/pubmed/7605285.

Leske, M. C. *et al.* (2003) 'Factors for Glaucoma Progression and the Effect of Treatment: The Early Manifest Glaucoma Trial', *Archives of Ophthalmology*, 121(1), pp. 48–56. doi: 10.1001/archopht.121.1.48.

Leung, C. K. S. *et al.* (2011) 'Long-term in vivo imaging and measurement of dendritic shrinkage of retinal ganglion cells', *Investigative Ophthalmology and Visual Science*, 52(3), pp. 1539–1547. doi: 10.1167/iovs.10-6012.

Li, B., Barnes, G. E. and Holt, W. F. (2005) 'The decline of the photopic negative response (PhNR) in the rat after optic nerve transection', *Documenta Ophthalmologica*, 111(1), pp. 23–31. doi: 10.1007/s10633-005-2629-8.

Li, S. *et al.* (2021) 'Association of systemic inflammation indices with visual field loss progression in patients with primary angle-closure glaucoma: potential biomarkers for 3P medical approaches', *EPMA Journal*, 12(4), pp. 659–675. doi: 10.1007/s13167-021-00260-3.

Libby, R. T., Anderson, M. G., *et al.* (2005) 'Inherited glaucoma in DBA/2J mice: Pertinent disease features for studying the neurodegeneration', *Visual Neuroscience*, 22(5), pp. 637–648. doi: 10.1017/S0952523805225130.

Libby, R. T., Li, Y., *et al.* (2005) 'Susceptibility to neurodegeneration in a glaucoma is modified by bax gene dosage', *PLoS Genetics*, 1(1), pp. 0017–0026. doi: 10.1371/journal.pgen.0010004.

Liszewski, M. K., Post, T. W. and Atkinson, J. P. (1991) 'Membrane Cofactor Protein (MCP or CD46): Newest Member of the Regulators of Complement Activation Gene Cluster', *Annu. Rev. Immunol*, 9, pp. 431–55. doi: 10.1146/annurev.iy.09.040191.002243.

Luo, C. *et al.* (2010) 'Glaucomatous tissue stress and the regulation of immune response through glial toll-like receptor signaling', *Investigative Ophthalmology and Visual Science*, 51(11), pp. 5697–5707. doi: 10.1167/iovs.10-5407.

Lynch, M. A. (2010) 'Age-related neuroinflammatory changes negatively impact on neuronal function', *Frontiers in Aging Neuroscience*, 1(January), pp.

1–8. doi: 10.3389/neuro.24.006.2009.

Makou, E., Herbert, A. P. and Barlow, P. N. (2013) ‘Functional anatomy of complement factor H’, *Biochemistry*, 52(23), pp. 3949–3962. doi: 10.1021/bi4003452.

Márquez-Ropero, M. *et al.* (2020) ‘Microglial Corpse Clearance: Lessons From Macrophages’, *Frontiers in Immunology*, 11(March), pp. 1–17. doi: 10.3389/fimmu.2020.00506.

Martin, P. R. (1986) ‘The projection of different retinal ganglion cell classes to the dorsal lateral geniculate nucleus in the hooded rat’, *Experimental Brain Research*, 62(1), pp. 77–88. doi: 10.1007/BF00237404.

Marx, M. S. *et al.* (1986) ‘Flash and pattern electroretinograms in normal and laser-induced glaucomatous primate eyes’, *Investigative Ophthalmology and Visual Science*, 27(3), pp. 378–386.

Marx, M. S. *et al.* (1988) ‘Signs of early damage in glaucomatous monkey eyes: Low spatial frequency losses in the pattern ERG and VEP’, *Experimental Eye Research*, 46(2), pp. 173–184. doi: 10.1016/S0014-4835(88)80075-7.

McLellan, G. J. *et al.* (2006) ‘A Feline Model of Primary Congenital Glaucoma – Histopathological and Genetic Characterization ’, *Investigative Ophthalmology & Visual Science*, 47(13), p. 175.

McLellan, G. J. and Miller, P. E. (2011) ‘Feline glaucoma-a comprehensive review’, *Veterinary Ophthalmology*, 14(SUPPL. 1), pp. 15–29. doi: 10.1111/j.1463-5224.2011.00912.x.

Medeiros, F. A. *et al.* (2013) ‘Retinal ganglion cell count estimates associated with early development of visual field defects in glaucoma’, *Ophthalmology*, 120(4), pp. 736–744. doi: 10.1016/j.ophtha.2012.09.039.

Meng, S. *et al.* (2022) ‘Age of Rats Affects the Degree of Retinal Neuroinflammatory Response Induced by High Acute Intraocular Pressure’, *Disease Markers*, 2022. doi: 10.1155/2022/9404977.

Miyahara, T. *et al.* (2003) ‘Gene microarray analysis of experimental

glaucomatous retina from cynomologous monkey', *Investigative Ophthalmology and Visual Science*, 44(10), pp. 4347–4356. doi: 10.1167/iovs.02-1032.

Miyata, K. *et al.* (2007) 'Reduction of oscillatory potentials and photopic negative response in patients with autosomal dominant optic atrophy with OPA1 mutations', *Investigative Ophthalmology and Visual Science*, 48(2), pp. 820–824. doi: 10.1167/iovs.06-0845.

Morgan, B. P. (2018) 'Complement in the pathogenesis of Alzheimer's disease', *Seminars in Immunopathology*, 40(1), pp. 113–124. doi: 10.1007/s00281-017-0662-9.

Morgan, J. E. (2000) 'Retinal ganglion cell death in experimental glaucoma', *British Journal of Ophthalmology*, 84(3), pp. 303–310. doi: 10.1136/bjo.84.3.303.

Morgan, J. E. (2002) 'Retinal Ganglion Cell Shrinkage in Glaucoma', *Journal of Glaucoma*, 11, pp. 365–370. doi: 10.1097/01.IJG.0000021803.38852.03.

Morgan, J. E. *et al.* (2006) 'Retinal Ganglion Cell Remodelling in Experimental Glaucoma', in Hollyfield, J. G., Anderson, R. E., and LaVail, M. M. (eds) *Retinal Degenerative Diseases*. Boston, MA: Springer US, pp. 397–402. doi: 10.1007/0-387-32442-9_56.

Morgan, J. E. and Tribble, J. R. (2015) 'Microbead models in glaucoma', *Experimental Eye Research*, 141, pp. 9–14. doi: 10.1016/j.exer.2015.06.020.

Morrison, J. *et al.* (1995) 'Structure and composition of the rodent lamina cribrosa', *Experimental Eye Research*, 60(2), pp. 127–135. doi: 10.1016/S0014-4835(95)80002-6.

Morrison, J. C. *et al.* (1997) 'A rat model of chronic pressure-induced optic nerve damage.', *Experimental Eye Research*, 64, pp. 85–96. doi: 10.1006/exer.1996.0184.

Morrison, J. C. *et al.* (2005) 'Understanding mechanisms of pressure-induced optic nerve damage', *Progress in Retinal and Eye Research*, 24(2), pp. 217–240. doi: 10.1016/j.preteyeres.2004.08.003.

Morrison, J. C. *et al.* (2016) ‘A period of controlled elevation of IOP (CEI) produces the specific gene expression responses and focal injury pattern of experimental rat glaucoma’, *Investigative Ophthalmology and Visual Science*, 57(15), pp. 6700–6711. doi: 10.1167/iovs.16-20573.

Morrison, J. C., Cepurna Ying Guo, W. O. and Johnson, E. C. (2011) ‘Pathophysiology of human glaucomatous optic nerve damage: Insights from rodent models of glaucoma’, *Experimental Eye Research*, 93(2), pp. 156–164. doi: 10.1016/j.exer.2010.08.005.

Naskar, R., Wissing, M. and Thanos, S. (2002) ‘Detection of Early Neuron Degeneration and Accompanying Microglial Responses in the Retina of a Rat Model of Glaucoma’, *Investigative Ophthalmology & Visual Science*, 43(9), pp. 2962–2968.

Nelson, R. (1995) ‘Visual Responses of Ganglion Cells’, in *Webvision:The Organisation of the Retina and Visual System*. Salt Lake City (UT): University of Utah Health Sciences Center. Available at: https://www.ncbi.nlm.nih.gov/books/NBK11550/.

Nelson, R., Famiglietti, E. V and Kolb, H. (1978) ‘Intracellular staining reveals different levels of stratification for on- and off-center ganglion cells in cat retina’, *Journal of Neurophysiology*, 41(2), pp. 472–483. doi: 10.1152/jn.1978.41.2.472.

Neufeld, A. H. (1999) ‘Microglia in the Optic Nerve Head and the Region of Parapapillary Chorioretinal Atrophy in Glaucoma’, *Archives of Ophthalmology*, 117(8), pp. 1050–1056. doi: 10.1001/archopht.117.8.1050.

Niyadurupola, N. *et al.* (2013) ‘Intraocular pressure lowering is associated with an increase in the photopic negative response (PhNR) amplitude in glaucoma and ocular hypertensive eyes’, *Investigative Ophthalmology and Visual Science*, 54(3), pp. 1913–1919. doi: 10.1167/iovs.12-10869.

Noris, M. and Remuzzi, G. (2013) ‘Overview of Complement Activation and Regulation’, *Seminars in Nephrology*, 33(6), pp. 479–492. doi: 10.1016/j.semnephrol.2013.08.001.

Okisaka, S. *et al.* (1997) ‘Apoptosis in retinal ganglion cell decrease in human glaucomatous eyes’, *Japanese Journal of Ophthalmology*, 41(2), pp. 84–88. doi: 10.1016/S0021-5155(97)00013-0.

Orihuela, R., McPherson, C. A. and Harry, G. J. (2016) ‘Microglial M1/M2 polarization and metabolic states’, *British Journal of Pharmacology*, 173(4), pp. 649–665. doi: 10.1111/bph.13139.

Oyster, C. W. (1999) *The human eye: structure and function*. Sunderland; Basingstoke: Sinauer Associates; Macmillan.

Panda-Jonas, S. *et al.* (1993) ‘Retinal Photoreceptor Count , Retinal Surface Area , and Optic Disc Size in Normal Human Eyes’, *Ophthalmology*. American Academy of Ophthalmology, Inc, 101(3), pp. 519–523. doi: 10.1016/S0161-6420(94)31305-4.

Paolicelli, R. C. *et al.* (2011) ‘Synaptic pruning by microglia is necessary for normal brain development’, *Science*, 333(6048), pp. 1456–1458. doi: 10.1126/science.1202529.

Pavlidis, M. *et al.* (2003) ‘Retinal Ganglion Cells Resistant to Advanced Glaucoma: A Postmortem Study of Human Retinas with the Carbocyanine Dye DiI’, *Investigative Ophthalmology and Visual Science*, 44(12), pp. 5196–5205. doi: 10.1167/iovs.03-0614.

Pederson, J. E. and Anderson, D. R. (1980) ‘The Mode of Progressive Disc Cupping in Ocular Hypertension and Glaucoma’, *Archives of Ophthalmology*, 98(3), pp. 490–495. doi: 10.1001/archopht.1980.01020030486010.

Perry, V. H. (1979) ‘The Ganglion Cell Layer of the Retina of the Rat : A Golgi Study’, *Proceedings of the Royal Society of London*, 204, pp. 363–375. doi: 10.1098/rspb.1979.0033.

Perry, V. H., Oehler, R. and Cowey, A. (1984) ‘Retinal ganglion cells that project to the dorsal lateral geniculate nucleus in the macaque monkey’, *Neuroscience*, 12(4), pp. 1101–1123. doi: 10.1016/0306-4522(84)90006-X.

Perry, V. H. and Walker, M. (1980) ‘Amacrine cells, displaced amacrine cells and interplexiform cells in the retina of the rat.’, *Proceedings of the Royal*

Society of London. Series B, Containing papers of a Biological character. Royal Society (Great Britain), 208(1173), pp. 415–431. doi: 10.1098/rspb.1980.0060.

Peters, D., Bengtsson, B. and Heijl, A. (2013) 'Lifetime risk of blindness in open-angle glaucoma', *American Journal of Ophthalmology*. The Authors, 156(4), pp. 724–730. doi: 10.1016/j.ajo.2013.05.027.

Polyak, S. L. (1942) 'The Retina: The Anatomy and the Histology of the Retina in Man, Ape and Monkey, Including the Consideration of Visual Functions, the History of Physiological Optics and the Histological Laboratory Technique', *JAMA: The Journal of the American Medical Association*, 118(15), p. 1337. doi: 10.1001/jama.1942.02830150073033.

Porciatti, V. (2015) 'Electrophysiological assessment of retinal ganglion cell function', *Experimental Eye Research*, 141, pp. 164–170. doi: 10.1016/j.exer.2015.05.008.

Prashar, A. *et al.* (2007) 'Measurement of intraocular pressure (IOP) in chickens using a rebound tonometer: Quantitative evaluation of variance due to position inaccuracies', *Experimental Eye Research*, 85(4), pp. 563–571. doi: 10.1016/j.exer.2007.07.010.

Preiser, D. *et al.* (2013) 'Photopic negative response versus pattern electroretinogram in early glaucoma', *Investigative Ophthalmology and Visual Science*, 54(2), pp. 1182–1191. doi: 10.1167/iovs.12-11201.

Püntener, U. *et al.* (2012) 'Long-term impact of systemic bacterial infection on the cerebral vasculature and microglia', *Journal of Neuroinflammation*, 9, pp. 1–13. doi: 10.1186/1742-2094-9-146.

Purves, D., Augustine, G. J. and Fitzpatrick, D. (2001) 'The Retina', in Purves, D., Augustine, G. J., and Fitzpatrick, D. (eds) *Neuroscience*. 2nd edn. Sunderland: Sinauer Associates.

Qin, L. *et al.* (2007) 'Systemic LPS causes chronic neuroinflammation and progressive neurodegeneration', *Glia*, 55(5), pp. 453–462. doi: 10.1002/glia.20467.

Quigley, H. A. *et al.* (1987) ‘Chronic glaucoma selectively damages large optic nerve fibers.’, *Investigative Ophthalmology and Visual Science*, 28(6), pp. 913–20.

Quigley, H. A. *et al.* (1995) ‘Retinal ganglion cell death in experimental glaucoma and after axotomy occurs by apoptosis’, *Investigative Ophthalmology and Visual Science*, 36(5), pp. 774–786.

Quigley, H. A., Addicks, E. and Green, R. W. (1982) ‘Optic Nerve Damage in Human Glaucoma in Glaucoma , Ischemic Neuropathy , Papilledema , and Toxic Neuropathy’, *Archives of Ophthalmology*, 100, p. 135.

Quigley, H. A., Dunkelberger, G. R. and Green, W. R. (1989) ‘Retinal Ganglion Cell Atrophy Correlated With Automated Perimetry in Human Eyes With Glaucoma’, *American Journal of Ophthalmology*, 107(5), pp. 453–464. doi: 10.1016/0002-9394(89)90488-1.

Quigley, H. a and Addicks, E. M. (1980) ‘Chronic experimental glaucoma in primates. II. Effect of extended intraocular pressure elevation on optic nerve head and axonal transport.’, *Investigative ophthalmology & visual science*, 19(2), pp. 137–52.

R Core Team (2019) ‘R: A language and environment for statistical computing.’ Vienna, Austria: R Foundation for Statistical Computing. Available at: https://www.r-project.org/.

Raetz, C. R. H. and Whitfield, C. (2002) ‘Lipopolysaccharide Endotoxins’, *Annual Review of Biochemistry*, 71(1), pp. 635–700. doi: 10.1146/annurev.biochem.71.110601.135414.

Rangaswamy, N. V. *et al.* (2004) ‘Photopic ERGs in patients with optic neuropathies: Comparison with primate ERGs after pharmacologic blockade of inner retina’, *Investigative Ophthalmology and Visual Science*, 45(10), pp. 3827–3837. doi: 10.1167/iovs.04-0458.

Ransohoff, R. M. and Cardona, A. E. (2010) ‘The myeloid cells of the central nervous system parenchyma.’, *Nature*, 468(7321), pp. 253–62. doi: 10.1038/nature09615.

Ricklin, D. and Lambris, J. D. (2007) ‘Complement-targeted therapeutics’, *Nature Biotechnology*, 25(11), pp. 1265–1275. doi: 10.1038/nbt1342.

Riggs, L. A. (1986) ‘Electroretinography’, *Vision Research*, 26(9), pp. 1443–1459. doi: 10.1016/0042-6989(86)90167-7.

Rodriguez, A. R., de Sevilla Müller, L. P. and Brecha, N. C. (2014) *The RNA binding protein RBPMS is a selective marker of ganglion cells in the mammalian retina*, *Journal of Comparative Neurology*. doi: 10.1002/cne.23521.

Rojas, B. *et al.* (2014) ‘Microglia in mouse retina contralateral to experimental glaucoma exhibit multiple signs of activation in all retinal layers’, *Journal of Neuroinflammation*, 11(1), pp. 1–24. doi: 10.1186/1742-2094-11-133.

Rollins, S. A. and Sims, P. J. (1990) ‘The complement-inhibitory activity of CD59 resides in its capacity to block incorporation of C9 into membrane C5b-9.’, *The Journal of Immunology*, 144(9), pp. 3478–3483. doi: 10.4049/jimmunol.144.9.3478.

Rosenbaum, J. T. *et al.* (1980) ‘Endotoxin-induced uveitis in rats as a model for human disease’, *Nature*, 286(5773), pp. 611–613. doi: 10.1038/286611a0.

Rotchford, A. P. and Johnson, G. J. (2002) ‘Glaucoma in Zulus: A Population-Based Cross-sectional Survey in a Rural District in South Africa’, *Archives of Ophthalmology*, 120(4), pp. 471–478. doi: 10.1001/archopht.120.4.471.

Roversi, P. *et al.* (2011) ‘Structural basis for complement factor I control and its disease-associated sequence polymorphisms’, *Proceedings of the National Academy of Sciences*, 108(31), pp. 12839–12844. doi: 10.1073/pnas.1102167108.

Saleh, M., Nagaraju, M. and Porciatti, V. (2007) ‘Longitudinal evaluation of retinal ganglion cell function and IOP in the DBA/2J mouse model of glaucoma’, *Investigative Ophthalmology and Visual Science*, 48(10), pp. 4564–4572. doi: 10.1167/iovs.07-0483.

Samsel, P. A. *et al.* (2011) ‘A Novel Method for the Induction of Experimental Glaucoma Using Magnetic Microspheres’, *Investigative Opthalmology &*

Visual Science, 52(3), p. 1671. doi: 10.1167/iovs.09-3921.

Sanchez-Cantu, L., Rode, H. N. and Christou, N. V (1989) 'Endotoxin Tolerance Is Associated With Reduced Secretion of Tumor Necrosis Factor', *Archives of Surgery*, 124(12), pp. 1432–1436. doi: 10.1001/archsurg.1989.01410120082016.

Sapienza, A. *et al.* (2016) 'Bilateral neuroinflammatory processes in visual pathways induced by unilateral ocular hypertension in the rat', *Journal of Neuroinflammation*. Journal of Neuroinflammation, 13(1), pp. 1–16. doi: 10.1186/s12974-016-0509-7.

Sarma, J. V. and Ward, P. A. (2011) 'The complement system', *Cell and Tissue Research*, 343(1), pp. 227–235. doi: 10.1007/s00441-010-1034-0.

Schlamp, C. L. *et al.* (2006) 'Progressive ganglion cell loss and optic nerve degeneration in DBA/2J mice is variable and asymmetric', *BMC Neuroscience*, 7, pp. 1–14. doi: 10.1186/1471-2202-7-66.

Schneider, M. and Fuchshofer, R. (2015) 'The role of astrocytes in optic nerve head fibrosis in glaucoma', *Experimental Eye Research*. Elsevier Ltd, 142, pp. 49–55. doi: 10.1016/j.exer.2015.08.014.

Schnitzer, J. (1988) 'Chapter 7 Astrocytes in mammalian retina', *Progress in Retinal Research*, 7(C), pp. 209–231. doi: 10.1016/0278-4327(88)90009-0.

Sefton, A. J., Dreher, B. and Harvey, A. (2004) *The Rat Nervous System*. third edit, *The rat nervous system*. third edit. Edited by G. Paxinos. Elsevier. doi: 10.1016/B978-0-12-547638-6.X5000-7.

Serna, M. *et al.* (2016) 'Structural basis of complement membrane attack complex formation', *Nature Communications*. Nature Publishing Group, 7, pp. 1–7. doi: 10.1038/ncomms10587.

Serres, S. *et al.* (2009) 'Systemic inflammatory response reactivates immune-mediated lesions in rat brain', *Journal of Neuroscience*, 29(15), pp. 4820–4828. doi: 10.1523/JNEUROSCI.0406-09.2009.

Sholl, D. A. (1953) 'Dendritic organization in the neurons of the visual and motor cortices of the cat.', *Journal of anatomy*, 87(4), pp. 387–406.

Shou, T. *et al.* (2003) ‘Differential dendritic shrinkage of α and β retinal ganglion cells in cats with chronic glaucoma’, *Investigative Ophthalmology and Visual Science*, 44(7), pp. 3005–3010. doi: 10.1167/iovs.02-0620.

Al Shoyaib, A., Archie, S. R. and Karamyan, V. T. (2020) ‘Intraperitoneal Route of Drug Administration: Should it Be Used in Experimental Animal Studies?’, *Pharmaceutical Research*. Pharmaceutical Research, 37(1). doi: 10.1007/s11095-019-2745-x.

Silveira, L. C. L. and Perry, V. H. (1991) ‘The topography of magnocellular projecting ganglion cells (M-ganglion cells) in the primate retina’, *Neuroscience*, 40(1), pp. 217–237. doi: 10.1016/0306-4522(91)90186-R.

De Simoni, M. G. *et al.* (2004) ‘The Powerful Neuroprotective Action of C1-Inhibitor on Brain Ischemia-Reperfusion Injury Does Not Require C1q’, *American Journal of Pathology*. American Society for Investigative Pathology, 164(5), pp. 1857–1863. doi: 10.1016/S0002-9440(10)63744-3.

Singer, M. and Jones, A. M. (2011) ‘Bench-to-bedside review: the role of C1-esterase inhibitor in sepsis and other critical illnesses.’, *Critical care (London, England)*, 15(1), p. 203. doi: 10.1186/cc9304.

Smedowski, A. *et al.* (2014) ‘A rat experimental model of glaucoma incorporating rapid-onset elevation of intraocular pressure’, *Scientific Reports*, 4, pp. 1–11. doi: 10.1038/srep05910.

Soto, I. *et al.* (2011) ‘Retinal ganglion cell loss in a rat ocular hypertension model is sectorial and involves early optic nerve axon loss’, *Investigative Ophthalmology and Visual Science*, 52(1), pp. 434–441. doi: 10.1167/iovs.10-5856.

Soto, I. and Howell, G. R. (2014) ‘The Complex Role of Neuroinflammation in Glaucoma’, *Cold Spring Harbor Perspectives in Medicine*, 4(8), pp. a017269–a017269. doi: 10.1101/cshperspect.a017269.

Stasi, K. *et al.* (2006) ‘Complement component 1Q (C1Q) upregulation in retina of murine, primate, and human glaucomatous eyes’, *Investigative Ophthalmology and Visual Science*, 47(3), pp. 1024–1029. doi:

10.1167/iovs.05-0830.

Stephan, A. H. *et al.* (2013) ‘A Dramatic Increase of C1q Protein in the CNS during Normal Aging’, 33(33), pp. 13460–13474. doi: 10.1523/JNEUROSCI.1333-13.2013.

Stevens, B. *et al.* (2007) ‘The Classical Complement Cascade Mediates CNS Synapse Elimination’, *Cell*, 131(6), pp. 1164–1178. doi: 10.1016/j.cell.2007.10.036.

Stewart, W. C. *et al.* (2000) ‘Factors associated with long-term progression or stability in primary open-angle glaucoma’, *American Journal of Ophthalmology*, 130(3), pp. 274–279. doi: 10.1016/S0002-9394(00)00487-6.

Sun, K. T. *et al.* (2020) ‘Periodontitis and the subsequent risk of glaucoma: results from the real-world practice’, *Scientific Reports*. Nature Publishing Group UK, 10(1), pp. 1–8. doi: 10.1038/s41598-020-74589-6.

Sun, W., Li, N. and He, S. (2002) ‘Large-scale morophological survey of rat retinal ganglion cells’, *Visual Neuroscience*, 19(4), pp. 483–493. doi: 10.1017/S0952523802194107.

Swindale, N. V. *et al.* (1996) ‘Contrast Sensitivity for Flickering and Static Letters and Visual Avuity at Isoluminance in Glaucoma’, *Journal of Glaucoma*, 5, pp. 156–169.

Szel, A. and Rohlich, P. (1992) ‘Tow Cone Types of Rat Retina Detected by Anti-visual Pigment Antibodies’, *Exp Eye Res*, 55, pp. 47–55.

Szepesi, Z. *et al.* (2018) ‘Bidirectional Microglia–Neuron Communication in Health and Disease’, *Frontiers in Cellular Neuroscience*, 12(September), pp. 1–26. doi: 10.3389/fncel.2018.00323.

Tansley, K. (1956) ‘Comparison of the lamina cribrosa in mammalian species with good and with indifferent vision’, *British Journal of Ophthalmology*, 40(3), pp. 178–182. doi: 10.1136/bjo.40.3.178.

Taylor, S. *et al.* (2011) ‘Involvement of the CD200 receptor complex in microglia activation in experimental glaucoma’, *Experimental Eye Research*, 92(5), pp. 338–343. doi: 10.1016/j.exer.2011.01.012.

Teeling, J. L. *et al.* (2007) ‘Sub-pyrogenic systemic inflammation impacts on brain and behavior, independent of cytokines’, *Brain, Behavior, and Immunity*, 21(6), pp. 836–850. doi: 10.1016/j.bbi.2007.01.012.

Tezel, G. *et al.* (2010) ‘Oxidative stress and the regulation of complement activation in human glaucoma’, *Investigative Ophthalmology and Visual Science*, 51(10), pp. 5071–5082. doi: 10.1167/iovs.10-5289.

Tezel, G., Yang, J. and Wax, M. B. (2004) ‘Heat shock proteins, immunity and glaucoma’, *Brain Research Bulletin*, 62(6), pp. 473–480. doi: 10.1016/S0361-9230(03)00074-1.

Tham, Y. *et al.* (2020) ‘Global Prevalence of Glaucoma and Projections of Glaucoma Burden through 2040 A Systematic Review and Meta-Analysis’, *Ophthalmology*, 121(11), pp. 2081–2090. doi: 10.1016/j.ophtha.2014.05.013.

Tielsch, J. M. (1994) ‘Family History and Risk of Primary Open Angle Glaucoma’, *Archives of Ophthalmology*, 112(1), p. 69. doi: 10.1001/archopht.1994.01090130079022.

Tribble, J. R., Otmani, A., *et al.* (2021) ‘Retinal ganglion cell degeneration in a rat magnetic bead model of ocular hypertensive glaucoma’, *Translational Vision Science and Technology*, 10(1), pp. 1–16. doi: 10.1167/tvst.10.1.21.

Tribble, J. R., Kokkali, E., *et al.* (2021) ‘When is a control not a control? Reactive microglia occur throughout the control contralateral pathway of retinal ganglion cell projections in experimental glaucoma’, *Translational Vision Science and Technology*, 10(1), pp. 1–23. doi: 10.1167/tvst.10.1.22.

Trollor, J. N. *et al.* (2021) ‘The association between systemic inflammation and cognitive performance in the elderly : the Sydney Memory and Ageing Study’. doi: 10.1007/s11357-011-9301-x.

Turner, R. C. *et al.* (2017) ‘Single low-dose lipopolysaccharide preconditioning: neuroprotective against axonal injury and modulates glial cells’, *Neuroimmunology and Neuroinflammation*, 4(1), p. 6. doi: 10.20517/2347-8659.2016.40.

Ueno, R., Narumiya, S. and Ogorochi, T. (1982) ‘Role of prostaglandin D2 in

the hypothermia of rats caused by bacterial lipopolysaccharide', *Proceedings of the National Academy of Sciences of the United States of America*, 79(19 I), pp. 6093–6097. doi: 10.1073/pnas.79.19.6093.

Urcola, J. H., Hernández, M. and Vecino, E. (2006) 'Three experimental glaucoma models in rats: Comparison of the effects of intraocular pressure elevation on retinal ganglion cell size and death', *Experimental Eye Research*, 83(2), pp. 429–437. doi: 10.1016/j.exer.2006.01.025.

Viswanathan, S. *et al.* (1999) 'The photopic negative response of the macaque electroretinogram: Reduction by experimental glaucoma', *Investigative Ophthalmology and Visual Science*, 40(6), pp. 1124–1136. doi: 10.1167/iovs.11-8461.

Viswanathan, S. *et al.* (2001) 'The photopic negative response of the flash electroretinogram in primary open angle glaucoma', *Investigative Ophthalmology and Visual Science*, 42(2), pp. 514–522. doi: 10.1167/iovs.11-8461.

Viswanathan, S., Frishman, L. J. and Robson, J. G. (2000) 'The uniform field and pattern ERG in macaques with experimental glaucoma: Removal of spiking activity', *Investigative Ophthalmology and Visual Science*, 41(9), pp. 2797–2810.

Wald, G. (1935) 'Vitamin A in eye tissues', *Journal of General Physiology*, 18(6), pp. 905–915. doi: 10.1085/jgp.18.6.905.

Wang, M. *et al.* (2011) 'Adaptive Müller cell responses to microglial activation mediate neuroprotection and coordinate inflammation in the retina', *Journal of Neuroinflammation*. BioMed Central Ltd, 8(1), p. 173. doi: 10.1186/1742-2094-8-173.

Wang, X., Tay, S. S. W. and Ng, Y. K. (2000) 'An immunohistochemical study of neuronal and glial cell reactions in retinae of rats with experimental glaucoma', *Experimental Brain Research*, 132(4), pp. 476–484. doi: 10.1007/s002210000360.

Weber, A. (1877) 'Die Ursache des Gaucoms.', *Graefe's Archive for*

Ophthalmology, 23, pp. 1–91.

Weber, A. J., Kaufman, P. L. and Hubbard, W. C. (1998) ‘Morphology of single ganglion cells in the glaucomatous primate retina’, *Investigative Ophthalmology and Visual Science*, 39(12), pp. 2304–2320.

Weber, A. J. and Zelenak, D. (2001) ‘Experimental glaucoma in the primate induced by latex microspheres’, *Journal of Neuroscience Methods*, 111(1), pp. 39–48. doi: 10.1016/S0165-0270(01)00443-5.

West, M. A. and Heagy, W. (2002) ‘Endotoxin tolerance: A review’, *Critical Care Medicine*, 30(1).

Whitmore, A. V., Libby, R. T. and John, S. W. M. (2005) ‘Glaucoma: Thinking in new ways - A rôle for autonomous axonal self-destruction and other compartmentalised processes?’, *Progress in Retinal and Eye Research*, 24(6), pp. 639–662. doi: 10.1016/j.preteyeres.2005.04.004.

Wilks, T. A., Harvey, A. R. and Rodger, J. (2013) ‘Seeing with Two Eyes: Integration of Binocular Retinal Projections in the Brain’, *Intech*. doi: dx.doi.org/10.5772/56491.

Williams, P. A. *et al.* (2013) ‘Retinal ganglion cell dendritic atrophy in DBA/2J glaucoma’, *PLoS ONE*, 8(8), pp. 1–10. doi: 10.1371/journal.pone.0072282.

Williams, P. A. *et al.* (2016) ‘Inhibition of the classical pathway of the complement cascade prevents early dendritic and synaptic degeneration in glaucoma’, *Molecular Neurodegeneration*. Molecular Neurodegeneration, 11(1), p. 26. doi: 10.1186/s13024-016-0091-6.

Williams, P. A. *et al.* (2017) ‘Neuroinflammation in glaucoma: A new opportunity’, *Experimental Eye Research*, 157(10), pp. 20–27. doi: 10.1016/j.exer.2017.02.014.

Williams, P. A., Morgan, J. E. and Votruba, M. (2010) ‘Opa1 deficiency in a mouse model of dominant optic atrophy leads to retinal ganglion cell dendropathy’, *Brain*, 133(10), pp. 2942–2951. doi: 10.1093/brain/awq218.

Winkler, N. S. and Fautsch, M. P. (2014) ‘Effects of prostaglandin analogues on aqueous humor outflow pathways’, *Journal of Ocular Pharmacology and*

Therapeutics, 30(2–3), pp. 102–109. doi: 10.1089/jop.2013.0179.

Woldemussie, E., Wijono, M. and Ruiz, G. (2004) 'Müller cell response to laser-induced increase in intraocular pressure in rats', *Glia*, 47(2), pp. 109–119. doi: 10.1002/glia.20000.

Zabel, M. K. and Kirsch, W. M. (2013) 'From development to dysfunction: Microglia and the complement cascade in CNS homeostasis', *Ageing Research Reviews*, 12(3), pp. 749–756. doi: 10.1016/j.arr.2013.02.001.

Zhang, Q. *et al.* (2010) 'Circulating mitochondrial DAMPs cause inflammatory responses to injury', *Nature*, 464(7285), pp. 104–107. doi: 10.1038/nature08780.

Zheng, Y. *et al.* (2019) 'Exosomes from LPS-stimulated macrophages induce neuroprotection and functional improvement after ischemic stroke by modulating microglial polarization', *Biomaterials Science*. Royal Society of Chemistry, 7(5), pp. 2037–2049. doi: 10.1039/c8bm01449c.

Ziegler-Heitbrock, H. W. L. (1995) 'Molecular mechanism in tolerance to lipopolysaccharide', *Journal of Inflammation*, 45(1), pp. 13–26.

Appendix A: Animal health score sheet

General health indicators (Wolfensohn and Lloyd)

Parameter	Animal ID:	Score	Date: Time:	Date: Time:	Date: Time:
Appearance	Normal	0			
	General Lack of grooming	1			
	Staring coat, ocular, nasal discharges	2 each			
	Piloerection, hunched up	4 each			
Weight Loss	Normal	0			
	5% weight loss	1			
	Up to 15% weight loss	2			
	Over 15% weight loss	4			
Natural Behaviour	Normal	0			
	Minor changes e.g. Lack of nest	1			
	Less mobile and alert, isolated	2			
	Vocalisation, self-mutilation, restless or inactive, cold	4 each			
Provoked Behaviour	Normal	0			
	Less active and/or slow movement	1			
	Only moves when directly provoked	4			
	Does not move, even when provoked or displays hyperactivity when provoked	9			
		Total:			

Specific Research Parameter

Parameter	Animal ID:	Score	Date: Time:	Date: Time:	Date: Time:
Post-surgical Wound (following intracameral or intravitreal injections)	Normal	0			
	Slight redness	1 each			
	Redness, inflammation, swelling	2 each			
	Unresolved signs of inflammation after a week at site of infection e.g. hypopyon	5			
		Total:			

Score Key

Score	
0	Normal
1-3	Use observation card
4-8	Monitor carefully, seek advice from NACWO
9-12	Observe regularly, NACWO must be involved to discuss whether end-points have been reached. ***Advice may need to be sought from the NVS regarding ongoing treatment e.g. antibiotics, analgesia, fluid therapy***
13-15	Euthanise by an appropriate method

Note: The clinical signs outlined in the score sheet will be used to assess the health of experimental animals. However, the judgement and experience of the licensee may necessitate actions at earlier time points, as appropriate.

Additional Guidance
Clear humane endpoints:

- After a procedure requiring anaesthesia, animals showing signs of breathing difficulty or failure to recover properly within the expected time frame (of less than 1 hour) will be euthanised by a schedule 1 method
- Animals that lose 20% of body weight at any time of the experiments will be euthanised by a Schedule 1 method.

Appendix B: Intraocular pressure profiles

Subcutaneous LPS cohort (Chapter 4)

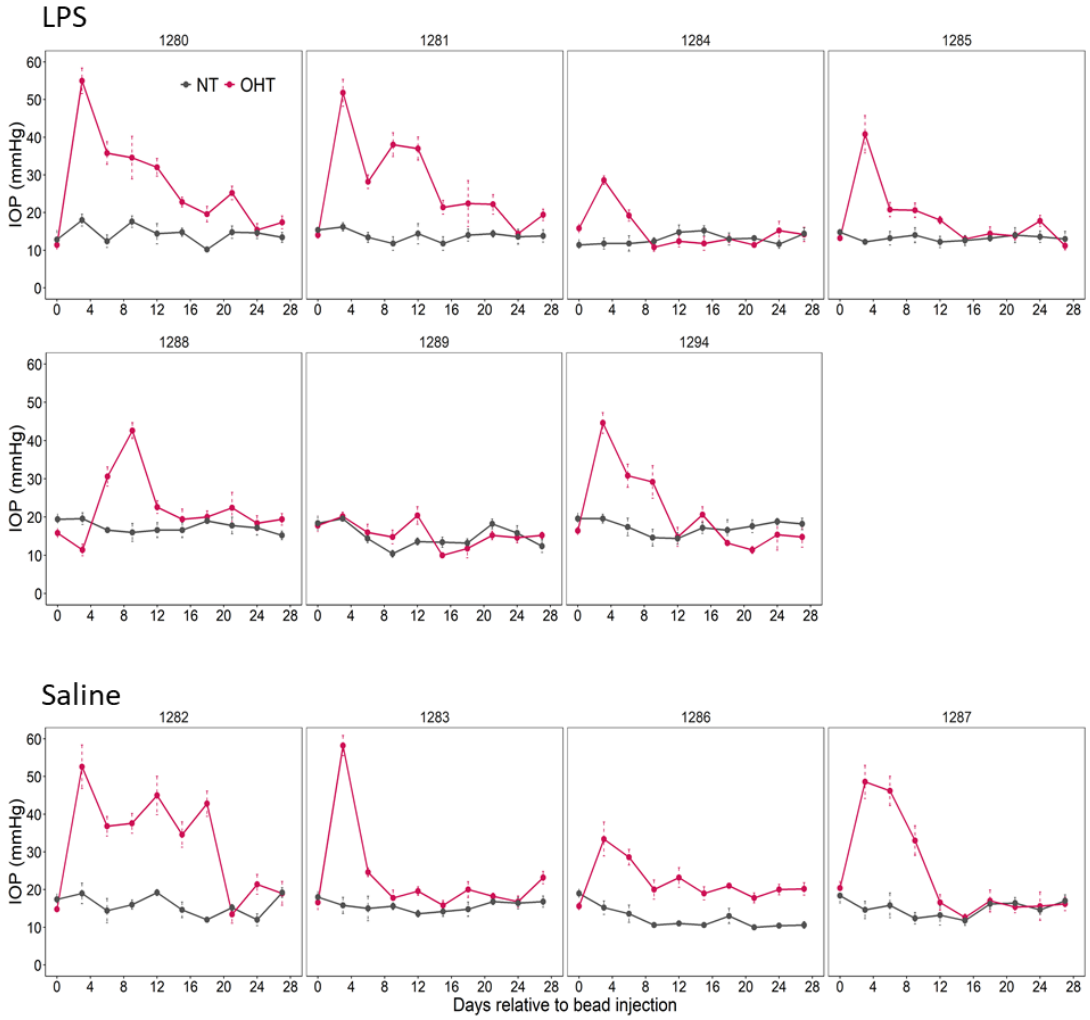

Appendix B – Figure 1: Individual IOP profiles following induction of OHT. Fuchsia = OHT eye, black = NT eye. Error bars = SD.

Intraperitoneal LPS cohort (Chapter 4)

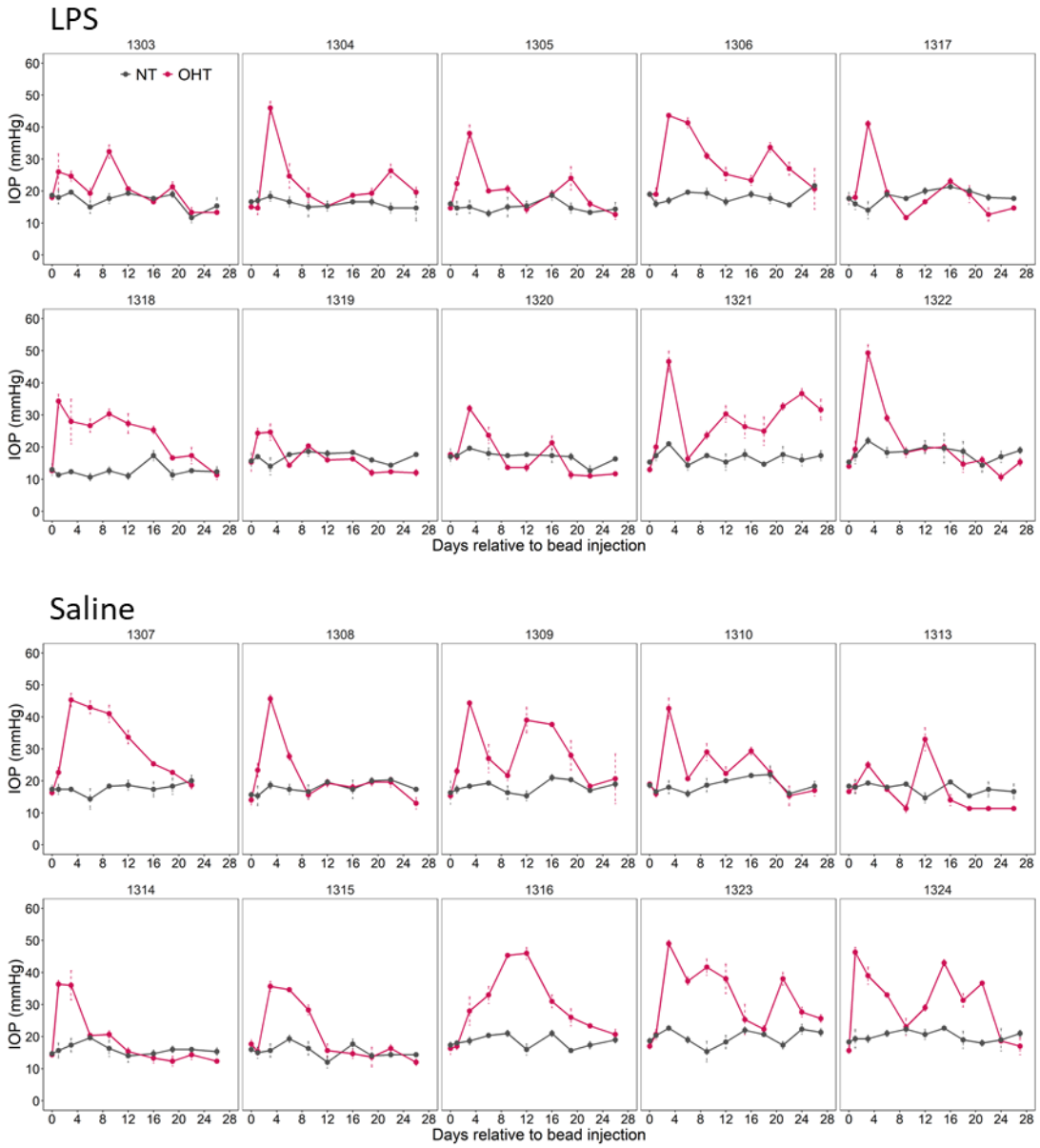

Appendix B – Figure 2: Individual IOP profiles following induction of OHT. Fuchsia = OHT eye, black = NT eye. Error bars = SD.

Intraperitoneal LPS + C1 inhibitor cohort (Chapter 5)

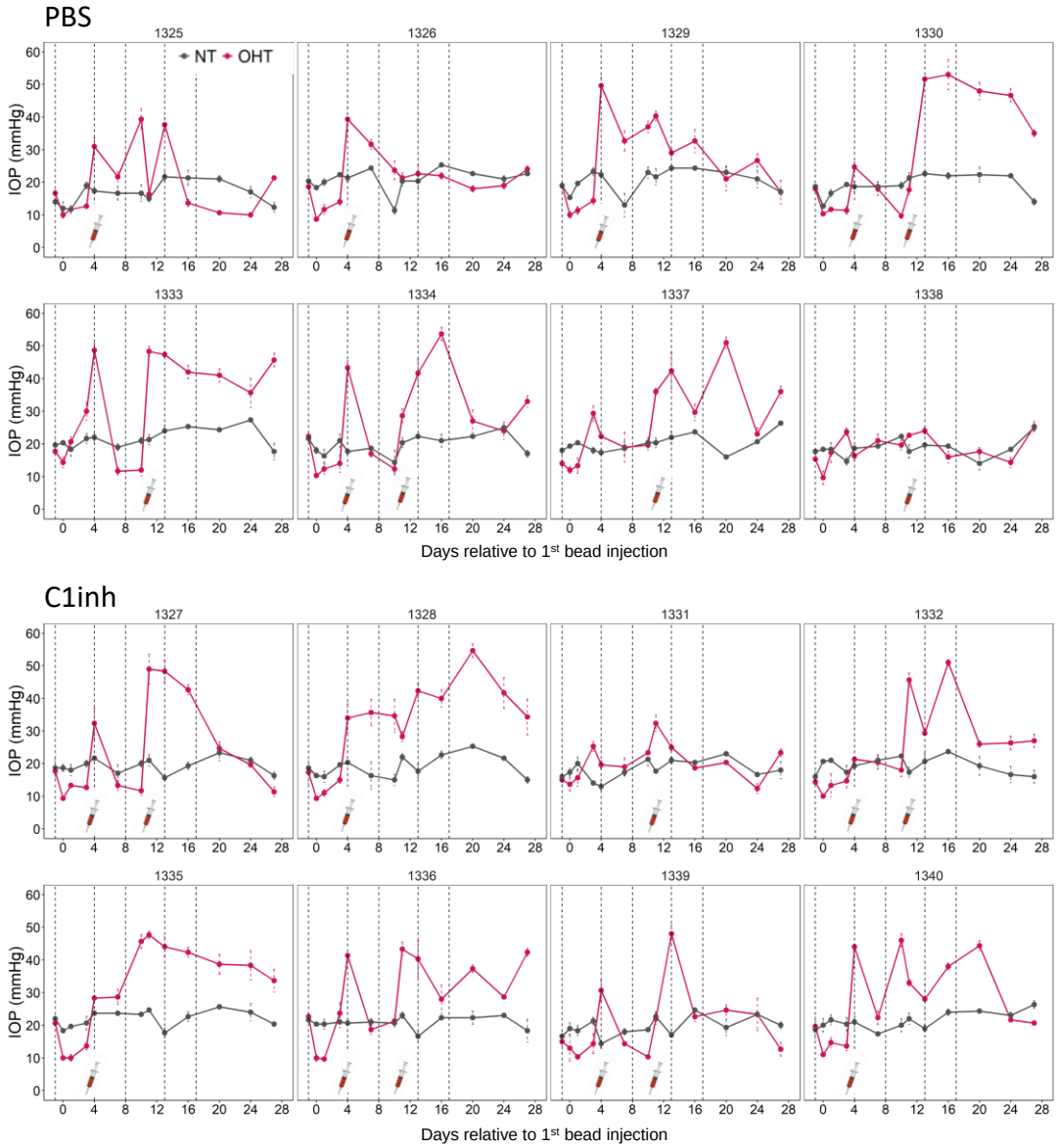

Appendix B – Figure 3: Individual IOP profiles following induction of OHT. Fuchsia = OHT eye, black = NT eye. Error bars = SD. Dashed vertical lines indicate the time point of C1 inhibitor or PBS injection. Syringe icon indicates the time point of repeated bead injections.